ulm university universität uulm

Fakultät für Naturwissenschaften
Institut für Quantenphysik

Theoretical approach to high-precision atom interferometry

Particle-particle interaction and the influence of gravity

Dissertation
zur Erlangung des Doktorgrades
Dr. rer. nat.
der Fakultät für Naturwissenschaften der
Universität Ulm

vorgelegt von
Christian Ufrecht
aus Stuttgart

Ulm 2019

Contents

Introduction

The wave properties of matter in quantum mechanics first postulated by de Broglie in 1923 [1] as well as Einstein's theory of general relativity [2] have radically changed our perception of the world at the beginning of the twentieth century. While each theory is extremely successful and well tested within its range of validity, a unification of both theories has so far resisted any attempt.

However, the advances in precision of modern matter-wave interferometers have paved the way to designing experiments at the interface of gravity and quantum mechanics. Indeed, quantum mechanical devices are on the brink of becoming sensitive enough to challenge predictions of general relativity such as the weak equivalence principle or set bounds on alternative gravitational theories.

Reaching sensitivities required for these experiments necessitates a careful assessment of deleterious effects some of which might be atom-atom interactions or the influence of the gravitational potential of the laboratory setup itself. Estimation of the size of such effects calls for refined theoretical tools for the description of light-pulse atom interferometry which is the subject of the present thesis.

Early development

Today's atom interferometers are based on almost a century of theoretical and experimental research. The first evidence for the wave properties of electrons by Davisson and Germer in 1927 [3] as well as of molecules [4] and of neutrons [5] opened up the possibility to design matter-wave interferometers. Profiting from an increased coherence in neutron interferometers made out of perfect synthetic nickel crystals [6], Colella, Overhauser and Werner first measured the phase induced by the linear gravitational field in Ref. [7] and by the rotation of the Earth [8]. See Ref. [9] for a general review on neutron interferometry.

Since atoms have a larger mass than neutrons and consequently a shorter de Broglie wave length and are moreover less sensitive to electric stray fields compared to electrons because they do not carry a charge [10], attention turned towards interferometry with neutral atoms. The first interferometer was realized by Carnal and Mlynek in a double-slit configuration [11] but it was soon pointed out that laser light provides more controllability thanks to the internal structure of the atoms. In addition, internal state labeling [12] allows for a simplified read out at the exit ports.

In contrast to a conventional light interferometer, in matter-wave interferometers in which the atoms are coherently manipulated with laser beams, the atoms take the role of the light while lasers act as mirrors. Diffraction of atoms on standing laser beams was utilized in a measurement of the Sagnac effect [13]. In contrast, Kasevich and Chu

resolved the gravitational acceleration in Ref. [14] employing short laser pulses. These light-pulse interferometers constitute the main focus of this thesis. For a general review on atom interferometry we refer to the Refs. [15, 16].

High-precision atom interferometry
Benefiting from these pioneering experiments, large amounts of effort were spent in the following years on the development of refined setups, which resulted in a tremendous increase in accuracy. Alternative diffraction mechanisms to Raman scattering like Bragg diffraction [17–20] and double Bragg diffraction [21] were developed which render the interferometer phase less sensitive to state-dependent influences since only one internal state is occupied during the whole interferometer time.

Modern light-pulse interferometers are high-precision inertial sensors when used as gyroscopes to measure rotations [22–24], as accelerometer to measure absolute accelerations [14, 25–30], or as gradiometers to resolve tidal effects of the gravitational field [31–34]. The best absolute gravimeter currently reaches impressing accuracies of $\Delta g/g = 7 \cdot 10^{-12}$, where g is the linear gravitational acceleration.

Apart from applications in navigation and geodesy, atom light-pulse interferometers have opened perspectives for probing fundamental constants such as the Newton gravitational constant [33, 35–38], where atom interferometers can already compete with classical tests [33], and the fine-structure constant [39–42] for which the currently best determined value was obtained in Ref. [42].

The weak equivalence principle
Matter-wave interferometers also allow precise tests of fundamental physics, as for example the weak equivalence principle [43, 44] which states that a non-self gravitating test particle should experience the same gravitational acceleration irrespectively of its mass and internal composition. As a cornerstone of general relativity, violations would directly hint towards unknown physics [45]. Experimentally possible violations can be parameterized by

$$\eta(A, B) = 2\frac{a(A) - a(B)}{a(A) + a(B)} \tag{1}$$

where a is the acceleration of two test masses A and B, respectively. The seminal experiments conducted by Eötvös [46] at the end of the nineteenth century yielded a value of $\eta = 10^{-8}$. Further classical tests with torsion balances [47], lunar laser ranging [48] and in the MICROSCOPE satellite [49] have so far increased the accuracy to the $\eta = 10^{-13}$ level.

The advance in sensitivity of matter-wave interferometers in recent years provided a promising technique to extend the tests to the quantum domain. Differential acceleration measurements known as common-mode rejection [50, 51] between the two species employed results in a high degree of immunity with respect to vibration noise. Up to now these dual-species interferometers have reached sensitivities of about $\eta \sim 10^{-8}$ in experiments with two different rubidium isotopes [52–55], two different atomic species [56] and in a differential acceleration measurement between bosonic and fermionic atoms [52, 57].

In order to reach sensitivities in quantum tests of the weak equivalence principle below

the current $\eta = 10^{-13}$ level where violations might appear, further advances in accuracy are required. The differential phase due to linear gravitation in a Mach-Zehnder interferometer is given by the celebrated formula

$$\phi = -\boldsymbol{k}\boldsymbol{g}T^2 \tag{2}$$

where $\hbar\boldsymbol{k}$ is the effective momentum transfer of the laser pulses on the atoms and T is half of the total interrogation time. Consequently, further enhancement of sensitivity can be achieved by large-momentum-transfer techniques [58–61], that is, by increasing $\boldsymbol{k}$, or by longer interrogation times T, which enters Eq. (2) quadratically. However, the free-fall time on Earth is limited to about a second by the size of the laboratory [29, 61]. This problem can be circumvented by relocating the experiments to microgravity environments.

The Quantus project
Supported by the German Aerospace Center (DLR), the QUANTUS project aims at developing compact and robust devices for long-time interferometry in microgravity. Miniaturized laser systems and on-chip production of Bose-Einstein condensates [62, 63] have led to remarkable robustness of setups surviving accelerations of up to $50g$ in the Bremen drop tower [64] which serves as a test bed for future high-precision measurements. Experiments in microgravity on parabola flights [65], in the drop tower [66, 67] and in sounding rockets [68] laid the foundation for future dedicated space missions on the international space station (ISS) [69, 70] or in satellites [71, 72] to probe the weak equivalence principle below the 10^{-15} level.
The huge advance in precision also requires refined theoretical tools as more and more formerly neglected effects like stray fields, gravitational effects of the laboratory setup itself, black-body radiation etc. become relevant. The insight that all these influences are extremely small but important to be taken into account calls for the development of a consistent perturbative description. In addition, to compare the sizes of influences of different origin and to check to which order each effect must be taken into account, the method should be simple and straightforward.
In chapter 1 we present a new approach to calculate phase and contrast of light-pulse interferometers which satisfies all these requirements. After deriving the formalism, we apply it to a number of examples to illustrate its mechanism.

Interferometry with Bose-Einstein condensates
Employing Bose-Einstein condensates as high-flux atom sources for interferometry [19, 20, 26] considerably enhances coherence properties of an interferometer compared to, for instance, a noncondensed thermal input state. Furthermore, the small momentum width of an ultracold Bose-Einstein condensate directly translates into smaller expansion rates of the atomic clouds during the interferometer sequence, in particular when combined with delta-kick collimation [73, 74].
Bose-Einstein condensation is a fascinating phenomenon, however, intricate from a fundamental point of view. In chapter 2 we review the mathematical tools necessary for a profound understanding, required for both experimentalists and theorists who work in this field. Subsequently, we contrast number-conserving to spontaneous symmetry-

breaking approaches in respect of an application to atom interferometry with Bose-Einstein condensates.

Despite the numerous merits of Bose-Einstein condensates as atom sources, these systems are intrinsically self interacting. Atom-atom interactions, however, bring about new detrimental effects which are difficult to control. Even though some salient features like mean-field shifts due to imperfect laser pulses can be assessed to some extent, analytic descriptions are in general unsatisfactory and one cannot refrain from numerical simulations. However, naive implementations on a grid of the extent of the interferometer are generally numerical intractable. Hence, in chapter 3 we develop a description in terms of comoving frames with each interferometer branch in a general second-quantized description and derive validity conditions for this approach. Working in second quantization further enables future work that builds on our results to include thermal and quantum fluctuations in a description beyond mean-field.

Particle-particle interactions not only introduce mean-field effects but also result in phase diffusion [75, 76] which derogates the phase relation between the interferometer arms and limits the accuracy to which the relative phase can be determined. In chapter 4 we derive a two-mode approximation from the general framework presented in chapter 3 and show that phase diffusion also takes a prominent role in long-time interferometry with Bose-Einstein condensates even when the wave packets are allowed to expand considerably prior to the first laser pulse in order to decrease the effect of interactions.

Chapter 1

Light-pulse atom interferometry with noninteracting particles

Light-pulse atom interferometers [12–14] consist of a series of light pulses that coherently drive transitions between motional states which establish different interferometer arms. After some interrogation time the atoms are redirected and finally recombined. The probability of finding an atom in one of the exit ports forms an interference pattern which is dependent on the relative phase accumulated between the interferometer arms.

In this chapter we will address the theoretical description of light-pulse interferometers. In recent years, a large number of different methods have been proposed to calculate phase and contrast of atom interferometers. Pioneered by Storey and Cohen-Tannoudji [77], path-integral methods have become a powerful tool in the context of atom interferometry [78–80]. In a seminal series of papers [81–84] Bordé and coworkers pursued an approach borrowed from the theory of optics. To illustrate how the interpretation of phases based on these approaches might be misleading, Schleich et al. developed a representation-free approach [85] which purely relies on operator algebra. It was further advanced by Kleinert et al. in Ref. [86] to treat path-independent harmonic potentials. Other representation-free descriptions that describe the motion along the interferometer arms from the perspective of comoving frames were developed in Refs. [87–90]. Finally, we mention a description in phase space put forward in Ref. [91].

Clearly, all these descriptions are equivalent within their range of validity but, depending on the problem, one or the other method might be more suited to streamline calculations or to arrange the result in a particularly transparent form.

After a brief introduction into the underlying theory of light-pulse interferometry in Sec. 1.1, we will present two formalisms for the calculation of phase and contrast. In Sec. 1.2 we transform into the comoving frames associated with each trajectory of the interferometer. In Sec. 1.3 we will develop a perturbative approach which will prove to be highly efficient in case of small perturbing effects on the interferometer.

1.1. Descriptions of light-pulse atom interferometers

In this section we will first describe all tools necessary to describe light-pulse atom interferometry. This includes the concept of internal and external states, the definition of the Hamiltonian, a discussion of light-matter interaction, and the introduction of particular geometries like the Mach-Zehnder interferometer.

1.1.1. Internal and external degrees of freedom

Mathematically, an atom interferometer requires at least two linearly independent states. In a superposition, each of the states acquires a different phase during the free evolution time. After mixing the states and projecting onto one of them, the phase difference can be read out. More generally we assume a Hilbert space $\mathcal{H} = \mathcal{H}_\text{e} \otimes \mathcal{H}_\text{i}$, which is the tensor product of an infinite dimensional *external* Hilbert space $\mathcal{H}_\text{e}$ and a finite dimensional *internal* Hilbert space $\mathcal{H}_\text{i}$ with dimension N_i. The most general wave function then takes the form

$$|\psi(t)\rangle = \sum_{j=1}^{N_\text{i}} c_j(t) \, |\psi_j(t)\rangle \otimes |j\rangle \; . \tag{1.1}$$

The ket $|j\rangle$ denotes the internal state and $|\psi_j\rangle$ is the *external wave function*. Note that the internal Hilbert space is not necessarily spanned by the energy levels of an atom, as e.g. in the case for Raman diffraction, but can also correspond to states which label a momentum ladder in the case of Bragg or double-Bragg diffraction. This subtlety will be discussed in much more detail in chapter 3.

1.1.2. Hamiltonian

Next, we turn to the Hamiltonian describing an interferometer. Throughout this chapter it will be given by sum

$$\hat{H} = \hat{H}_\text{e} + \hat{H}_\text{L} \tag{1.2}$$

where $\hat{H}_\text{L}$ is the laser-atom interaction Hamiltonian which drives transitions between internal states whereas the *external* Hamiltonian $\hat{H}_\text{e}$ is diagonal in this basis, consequently does not mix internal states. More specifically

$$\hat{U}_\text{e}(t_\text{d}, t_\text{i}) \, |\psi_j(t_\text{i})\rangle \otimes |j\rangle = \hat{U}_{\text{e},j}(t_\text{d}, t_\text{i}) \, |\psi_j(t_\text{i})\rangle \otimes |j\rangle = |\psi_j(t_\text{d})\rangle \otimes |j\rangle \tag{1.3}$$

where t_i denotes the initial time, t_d the *detection* time or final time and $\hat{U}_\text{e}$ is the time-evolution operator with respect to $\hat{H}_\text{e}$. At this stage the explicit form of the Hamiltonians is not required to understand the underlying principles, therefore the specification will be postponed to later sections. In chapter 3, in the context of a description in the language of second quantization, we will additionally add particle-particle interaction.

1.1.3. General interferometer sequence

In the sum, Eq. (1.2), the laser-atom interaction Hamiltonian is only nonvanishing during the short laser pulses and mirrors of duration Δt_j during the intervals $[t_j, t_j + \Delta t_j]$ where the laser is turned on. In the time between the pulses the time-evolution is solely determined by the external Hamiltonian such that a general interferometer sequence can be cast into the form

$$
\hat{U}(t_{\mathrm{d}}, t_{\mathrm{i}}) = \hat{U}_{\mathrm{e}}(t_{\mathrm{d}}, t_n + \Delta t_n) \hat{U}(t_n + \Delta t_n, t_n) \hat{U}_{\mathrm{e}}(t_n, t_{n-1} + \Delta t_{n-1}) \ \ldots \ \hat{U}_{\mathrm{e}}(t_1, t_{\mathrm{i}})
$$
$$
= \hat{U}_{\mathrm{e}}(t_{\mathrm{d}}, t_n) \hat{S}(t_n) \hat{U}_{\mathrm{e}}(t_n, t_{n-1}) \ \ldots \ \hat{U}_{\mathrm{e}}(t_1, t_{\mathrm{i}}) . \tag{1.4}
$$

In the second line we changed to the interaction picture with respect to $\hat{H}_{\mathrm{e}}$ and defined

$$
\hat{S}(t_j) = \mathcal{T} \exp \left\{ -\frac{\mathrm{i}}{\hbar} \int_{t_j}^{t_j + \Delta t_j} \mathrm{d}t \, \hat{U}_{\mathrm{e}}^\dagger(t, t_j) \hat{H}_{\mathrm{L}}(t) \hat{U}_{\mathrm{e}}(t, t_j) \right\} , \tag{1.5}
$$

which we will refer to as *beam-splitter operator*. At first glance, in the second line of Eq. (1.4) this operator seems to act for an infinitely short time since the intervals Δt_j do not appear explicitly. Inspection of Eq. (1.5) reveals that the integral still extends over the interaction zones and time ordering cannot be disregarded. The replacement of the operator in the integral by an effective Hamiltonian times a delta function in time which obviates the time-ordering operator will be referred to as *delta-pulse approximation*. Formally, this can always be achieved by e.g. resorting to the Magnus expansion [92], which, however, leads practically to an infinite series if even convergence can be achieved. We will learn about more viable methods to derive the delta-pulse approximation in chapter 3.

1.1.4. Light-matter interaction

Before evaluating sequences like the one from Eq. (1.4) in more detail, we need to further specify the atom-light interaction. In the simplest case, the atoms interact with two counterpropagating laser beams that have a frequency difference $\Delta \omega = \omega_b - \omega_a$, where ω_a and ω_b are the frequencies of the two beams. The lasers drive a two-photon process via an ancillary state within the same internal state in the case of Bragg diffraction, Fig. 1.1.a, or between two states in case of Raman diffraction, Fig. 1.1.b. In the latter, the atoms are put into a superposition of the internal states. As the absorption and emission of a photon is associated with the momentum transfer $\hbar k = \hbar(k_a + k_b)$, where k_a and k_b are the respective wave numbers of the lasers, the external wave function corresponding to each internal state will subsequently separate spatially leading to different interferometer branches. Similarly, in the case of Bragg diffraction the lasers drive transitions between momentum states which again establish the interferometer branches. For the sake of a simple discussion in this section we focus on Raman diffraction. As the lasers are strongly detuned with respect to the ancillary state, it can be adiabatically eliminated [85] and we obtain an effective two-level description. Thus, the internal Hilbert space consists of the two internal states $|1\rangle$ and $|2\rangle$. Within the
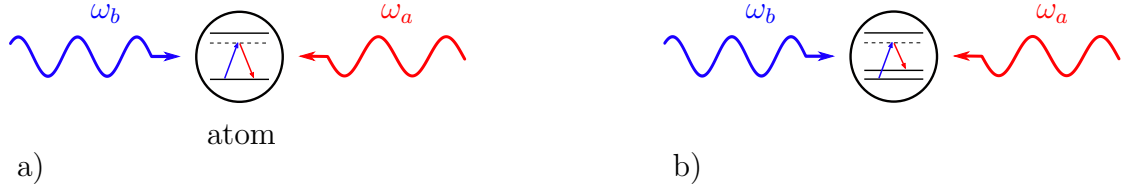
Figure 1.1.: Different diffraction schemes for atom interferometry. a) Bragg diffraction. A two-level atom interacts with two counterpropagating laser beams. The absorption of a "blue" photon is associated with a momentum transfer in positive momentum direction (the arrows depicted in the atoms are understood as drawn in an energy-momentum diagram). Since the laser frequencies are strongly detuned with respect to the atomic transition, the atom undergoes a two-photon process back to the initial internal state. b) Raman diffraction. Contrary to a), the laser beams are incident on a three-level atom and the frequencies are chosen such that the transition to a different internal state is resonant.

simple delta-pulse approximation the action of the beam-splitter operators take the form [93]

$$\hat{S}_{\theta_j}(t_j)\,|\psi_1\rangle \otimes |1\rangle = \cos(\theta_j/2)\,|\psi_1\rangle \otimes |1\rangle + \mathrm{i}\sin(\theta_j/2)\mathrm{e}^{+\mathrm{i}k\hat{z}+\mathrm{i}\varphi_\mathrm{L}(t_j)}\,|\psi_1\rangle \otimes |2\rangle$$

$$\hat{S}_{\theta_j}(t_j)\,|\psi_2\rangle \otimes |2\rangle = \cos(\theta_j/2)\,|\psi_2\rangle \otimes |2\rangle + \mathrm{i}\sin(\theta_j/2)\mathrm{e}^{-\mathrm{i}k\hat{z}-\mathrm{i}\varphi_\mathrm{L}(t_j)}\,|\psi_2\rangle \otimes |1\rangle \ . \qquad (1.6)$$

Each laser-pulse imprints the laser phase $\varphi_\mathrm{L}(t_j)$, the phase difference of the lasers at $t = t_j$. In Eq. (1.6) a $\theta_j = \pi/2$ pulse sets the atoms in an equal superposition of the internal states, while a $\theta_j = \pi$ pulse inverts the internal states. The multiplication with the exponential $\exp(\pm\mathrm{i}k\hat{z})$ implies the momentum transfer $\pm\hbar k$.

A more detailed analysis of the diffraction process can be found in Refs. [94–103], just to name a few.

The method of adiabatic elimination and the application to Bragg and other diffraction schemes in the context of second quantization will be investigated more rigorously in chapter 3.

1.1.5. Mach-Zehnder Interferometer

We now turn to the Mach-Zehnder (MZ) interferometer sequence [14] and explicitly calculate its phase. As schematically depicted in Fig. 1.2, it consists of the pulse sequence $\pi/2$-π-$\pi/2$, thus the total time-evolution operator is

$$\hat{U}(t_\mathrm{d}, t_\mathrm{i}) = \hat{U}_\mathrm{e}(t_\mathrm{d}, t_3)\hat{S}_{\pi/2}(t_3)\hat{U}_\mathrm{e}(t_3, t_2)\hat{S}_\pi(t_2)\hat{U}_\mathrm{e}(t_2, t_1)\hat{S}_{\pi/2}(t_1)\hat{U}_\mathrm{e}(t_1, t_\mathrm{i}) \qquad (1.7)$$

with the initial state $|\psi(t_\mathrm{i})\rangle = |\psi_1(t_\mathrm{i})\rangle \otimes |1\rangle$. Using Eq. (1.3) and Eq. (1.6), we obtain the probability of finding an atom in $|2\rangle$ at the end of the sequence

$$P_{|2\rangle} = |\,\langle 2|\,\hat{U}(t_\mathrm{d}, t_\mathrm{i})\,|\psi(t_\mathrm{i})\rangle\,|^2 = \frac{1}{2}\left(1 - \Re\left[\langle\hat{U}_1^\dagger(t_\mathrm{d}, t_\mathrm{i})\hat{U}_2(t_\mathrm{d}, t_\mathrm{i})\rangle\mathrm{e}^{\mathrm{i}\varphi_\mathrm{L}}\right]\right) . \qquad (1.8)$$
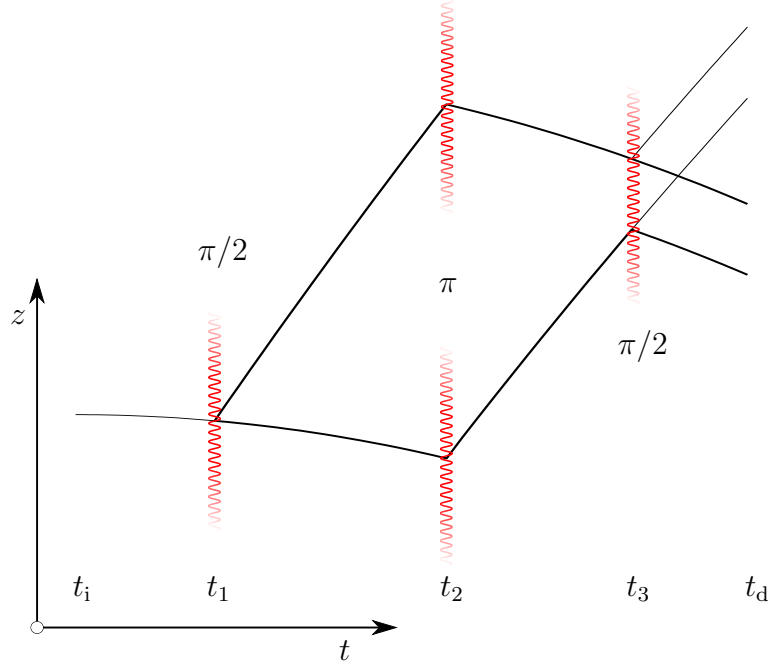
Figure 1.2.: Schematic picture of a Mach-Zehnder geometry. The initial wave function is put into an equal superposition of the internal states by a $\pi/2$ pulse at $t = t_1$. As a result of the momentum transfer, the two parts of the wave function corresponding to the internal states subsequently separate spatially, are redirected by a π pulse at $t = t_2$, which inverses the internal states. Finally, a second $\pi/2$ pulse at $t = t_3$ mixes the states and the relative phase accumulated along the two interferometer branches is read out by measuring the number of particles in one of the internal states.

In Eq. (1.8) the expectation value is understood to be taken with respect to the initial external state $|\psi_1(t_i)\rangle$ and

$$\varphi_L = \varphi_L(t_1) - 2\varphi_L(t_2) + \varphi_L(t_3) \tag{1.9}$$

collects the phases imprinted by the laser pulses. In this work the product $\hat{U}_1^\dagger \hat{U}_2$ will be referred to as *overlap operator* since it encodes all the information about the time evolution along the interferometer branches needed for the calculation of phase and contrast. In the case of the MZ geometry it abbreviates the operators

$$\hat{U}_2(t_d, t_i) \equiv \hat{U}_{e,2}(t_d, t_3) e^{ik\hat{z}} \hat{U}_{e,1}(t_3, t_2) e^{-ik\hat{z}} \hat{U}_{e,2}(t_2, t_1) e^{ik\hat{z}} \hat{U}_{e,1}(t_1, t_i)$$
$$\hat{U}_1(t_d, t_i) \equiv \hat{U}_{e,2}(t_d, t_2) e^{ik\hat{z}} \hat{U}_{e,1}(t_2, t_i) \,, \tag{1.10}$$

which correspond to the motion along the two paths in the MZ interferometer. With the help of the overlap operator we changed to a branch-dependent description which is solely expressed in terms of the diagonal elements of the external time-evolution operator and the momentum kicks. It will be the main topic of the present chapter to bring the overlap operator into a more accessible form. To this end, we first combine each

operator product in Eq. (1.10) to one time-evolution operator by simply incorporating the exponentials $\exp(\pm \mathrm{i}k\hat{z})$ into the external Hamiltonian and by redefining

$$\hat{H}(t) = \hat{H}_\mathrm{e} + \hat{H}_\mathrm{L}(t) \tag{1.11}$$

for each interferometer branch separately with the effective laser-atom interaction Hamiltonian

$$\hat{H}_\mathrm{L} = -\sum_j \hbar k_j \hat{z}\delta(t - t_j) \tag{1.12}$$

within the delta-pulse approximation. Due to the delta function in Eq. (1.12), the time ordering of the time-evolution operator will automatically put the exponential at the right position. As we will show later in this chapter, for a particle in a linear gravitational field with the external Hamiltonian

$$\hat{H}_\mathrm{e} = \frac{\hat{\boldsymbol{p}}^2}{2m} + m\boldsymbol{g}\hat{\boldsymbol{r}} \tag{1.13}$$

where m is the mass of the particle and $\boldsymbol{g}$ the linear gravitational acceleration, and equal interrogation times $t_2 - t_1 = t_3 - t_2 \equiv T$, the overlap operator reduces to a c-number $\hat{U}_1^\dagger \hat{U}_2 = \mathrm{e}^{\mathrm{i}\varphi}$ and we find the relation [104]

$$\varphi = -\boldsymbol{k}\boldsymbol{g}T^2 \,. \tag{1.14}$$

For this simple form of the overlap operator we further obtain

$$P_{|2\rangle} = \frac{1}{2}\left[1 - \cos(\varphi + \varphi_\mathrm{L})\right] \,, \tag{1.15}$$

which displays an interference pattern. In the more general case

$$\langle \hat{U}_1^\dagger \hat{U}_2 \rangle = C\mathrm{e}^{\mathrm{i}\varphi} \,. \tag{1.16}$$

The real number $C \leq 1$ is called *contrast* or *visibility* of the interferometer. If $C = 1$ the interferometer is referred to as *closed*, otherwise as *open*.

1.1.6. Laser phases and gravimetry

Light-pulse atom interferometers are high-precision inertial sensors. As such, they can be employed to measure the absolute value of the gravitational acceleration [14, 25, 28, 29] with high precision. In Sec. 1.1.4 we introduced the laser phase $\varphi_\mathrm{L}(t_j)$. It takes an important role in the context of gravimetry, which will be discussed in the following. The atoms moving along the two interferometer arms of an MZ interferometer accumulate the relative phase $\varphi = -\boldsymbol{k}\boldsymbol{g}T^2$ induced by the linear gravitational potential. Between the laser pulses the atoms fall freely and gain velocity. Consequently, the lasers which are supported to defy gravity need to be *chirped* [105], that is, the frequency difference must be dynamically modulated to compensate for the Doppler-shifted atomic resonance. This time-dependence of the phase can be achieved by an acousto-optic modulator. In the previous section we saw from Eq. (1.8) that the laser phase contributes to the total phase of the interferometer, which makes a precise control

absolutely crucial. Contrary to the optical frequencies of the lasers, the much smaller frequency difference $\Delta\omega$ can experimentally be well controlled by comparing to an rf reference source [78, 106]. For the linear chirp

$$\Delta\omega(t) = \alpha t \tag{1.17}$$

in addition to compensation of the Doppler shift due to linear motion and internal-state-energy differences we find the total interferometer phase

$$\varphi + \varphi_{\mathrm{L}} = -(\boldsymbol{k}\boldsymbol{g} + 2\alpha)T^2\,, \tag{1.18}$$

which exactly vanishes for $\alpha = -1/2\boldsymbol{k}\boldsymbol{g}$. Leaving the total interferometer time T unchanged, one scans the phase by varying the chirping rate of the lasers [25]. From the common minimum of Eq. (1.15) for at least two different interferometer times [63] we infer $g = -2\alpha/k$ in the case of laser pulses aligned with the direction of the linear gravitational field.

1.2. Transformation to comoving frames

In the previous section we defined the overlap operator and showed how it connects to the paths of an interferometer. In this section we will derive a formalism to access this operator by transforming into *comoving frames* attached to each *local wave packet* moving along the arms of the interferometer. This method has already been used in the literature in similar forms in Refs. [87, 107–111], was put in modern form in Refs. [88, 89], and was recently generalized to interferometry in curved space time [90].
This section serves mainly as a revision of this formalism, but it will be rederived in the following by using a particularly simple notation and by relying solely on operator algebra. This derivation will serve as a starting point for a generalization of the formalism to atom interferometers with interacting particles within a second-quantized approach in chapter 3.

Displacement operators

The formalism in this section as well as in chapter 3 relies on the concept of *displacement operators*. This operator has already been extensively used in the context of atom interferometry, for instance in Refs. [86–90, 107, 108, 111]. In this work, we closely follow the notation of [86] and define a displacement operator as

$$\hat{D}(\boldsymbol{\chi}) = \mathrm{e}^{-\frac{\mathrm{i}}{\hbar}\boldsymbol{\chi}^{\mathrm{T}}\boldsymbol{\mathcal{J}}\hat{\boldsymbol{\xi}}} \tag{1.19}$$

where

$$\boldsymbol{\chi} = (\boldsymbol{\chi}^r, \boldsymbol{\chi}^p)^{\mathrm{T}} \tag{1.20}$$

is a six-dimensional, possibly time-dependent vector which denotes the position and, respectively, momentum displacement. Note that with the notation in Eq. (1.20) we defined a column vector even though both $\boldsymbol{\chi}^r$ and $\boldsymbol{\chi}^p$ are already three-dimensional column vectors. In the same spirit we define the six-dimensional phase-space operator

$$\hat{\boldsymbol{\xi}} = (\hat{\boldsymbol{r}}, \hat{\boldsymbol{p}})^{\mathrm{T}} \tag{1.21}$$

and introduced the matrix

$$\boldsymbol{\mathcal{J}} = \begin{pmatrix} 0 & \mathbb{1} \\ -\mathbb{1} & 0 \end{pmatrix} \tag{1.22}$$

with $\mathbb{1}$ being the three-dimensional identity matrix. The definition, Eq. (1.19), appears to be most useful when we calculate the action of a displacement operator on a quantum state in position representation

$$\langle \boldsymbol{r} | \, \hat{D}(\boldsymbol{\chi}) \, | \psi \rangle = \mathrm{e}^{-\frac{\mathrm{i}}{2\hbar} \boldsymbol{\chi}^p \boldsymbol{\chi}^r} \, \mathrm{e}^{\frac{\mathrm{i}}{\hbar} \boldsymbol{\chi}^p \boldsymbol{r}} \, \psi \left(\boldsymbol{r} - \boldsymbol{\chi}^r \right) , \tag{1.23}$$

which is, apart from an additional phase factor, a translation by $\boldsymbol{\chi}^p$ in momentum and by $\boldsymbol{\chi}^r$ in position space. A proof of Eq. (1.23) can be found in App. A where we review and prove some of the most important properties and identities of displacement operators.

Hamiltonian

As outlined in Sec. 1.1.5, after finding the overlap operator for a specific interferometer geometry we define a Hamiltonian

$$\hat{H} = H(\hat{\boldsymbol{\xi}}, t) \tag{1.24}$$

for each interferometer path. This Hamiltonian contains the atom-laser interaction in the form

$$\hat{H}_{\mathrm{L}} = -\sum_n \hbar \boldsymbol{k}_n \hat{\boldsymbol{r}} \, \delta(t - t_n) , \tag{1.25}$$

which we generalized to describe laser pulses pointing in arbitrary directions. Note that the laser-atom interaction Hamiltonian is in general different for each interferometer branch. Furthermore, we disregard trivial phases due to the energies of the internal states.

1.2.1. Outline of the method

In many cases the separation of the interferometer branches, induced by the laser pulses, is much larger than the size of the local wave packets moving along the interferometer arms [89]. Thus, it is easily recognized that a description in comoving frames attached to each local wave packet is much more convenient. The transformation to these frames will remove all linear contributions to the Hamiltonian including the laser-atom interaction. Guided by this insight, we transform a general external time-evolution operator according to

$$\hat{U}(t, t_{\mathrm{i}}) = \mathrm{e}^{\mathrm{i}\phi} \hat{D}(\boldsymbol{\chi}) \, \hat{U}_{\mathrm{R}}(t, t_{\mathrm{i}}) \hat{D}^{\dagger}(\boldsymbol{\chi}_{\mathrm{i}}) \tag{1.26}$$

where $\hat{U}_{\mathrm{R}}$ is the time-evolution operator with respect to the *reduced Hamiltonian*

$$\hat{H}_{\mathrm{R}} = H(\hat{\boldsymbol{\xi}} + \boldsymbol{\chi}) - \frac{\partial H(\boldsymbol{\chi})}{\partial \boldsymbol{\chi}}^{\mathrm{T}} \hat{\boldsymbol{\xi}} - H(\boldsymbol{\chi}) , \tag{1.27}$$

which generates the time evolution in the comoving frame. To simplify notation, we omitted the explicit time dependence of ϕ, $\boldsymbol{\chi}$ and H. The six-dimensional displacement vector $\boldsymbol{\chi}$ satisfies the equations of motion

$$\dot{\boldsymbol{\chi}} = \boldsymbol{\mathcal{J}} \frac{\partial H(\boldsymbol{\chi})}{\partial \boldsymbol{\chi}}, \qquad \boldsymbol{\chi}(t_\mathrm{i}) = \boldsymbol{\chi}_\mathrm{i} \tag{1.28}$$

and the symplectic matrix $\boldsymbol{\mathcal{J}}$ was defined in Eq. (1.22). For a proof of Eq. (1.26) we evaluate the derivative of the displacement operator in Eq. (A.15) and furthermore use Eq. (A.14). The ordinary differential equation, Eq. (1.28), constitutes the set of the classical Hamilton equations of motion

$$\dot{\boldsymbol{\chi}}^r = \frac{\partial H(\boldsymbol{\chi})}{\partial \boldsymbol{\chi}^p} \quad \text{and} \quad \dot{\boldsymbol{\chi}}^p = -\frac{\partial H(\boldsymbol{\chi})}{\partial \boldsymbol{\chi}^r} \tag{1.29}$$

with the initial conditions $\boldsymbol{\chi}^r(t_\mathrm{i}) = \boldsymbol{\chi}_\mathrm{i}^r$ and $\boldsymbol{\chi}^p(t_\mathrm{i}) = \boldsymbol{\chi}_\mathrm{i}^p$. The additional phase in Eq. (1.26) is calculated from the differential equation

$$\hbar\dot{\phi} = \frac{1}{2}\left(\dot{\boldsymbol{\chi}}^r \boldsymbol{\chi}^p - \dot{\boldsymbol{\chi}}^p \boldsymbol{\chi}^r\right) - H(\boldsymbol{\chi}), \tag{1.30}$$

which becomes after partial integration and with the help of Eq. (1.29)

$$\phi = \frac{1}{\hbar}\int_{t_\mathrm{i}}^{t} \mathrm{d}t' \left(\frac{\partial H(\boldsymbol{\chi})}{\partial \boldsymbol{\chi}^p}\boldsymbol{\chi}^p - H(\boldsymbol{\chi})\right) - \frac{1}{2\hbar}\left(\boldsymbol{\chi}^p\boldsymbol{\chi}^r - \boldsymbol{\chi}_\mathrm{i}^p\boldsymbol{\chi}_\mathrm{i}^r\right). \tag{1.31}$$

The expression within the parenthesis looks very familiar. Indeed, it is the classical Lagrange function, the integral over it the classical action S. This insight allows us to obtain the simple result

$$\hat{U}(t, t_\mathrm{i}) = \mathrm{e}^{\frac{\mathrm{i}}{\hbar}S - \frac{\mathrm{i}}{2\hbar}\left(\boldsymbol{\chi}^p\boldsymbol{\chi}^r - \boldsymbol{\chi}_\mathrm{i}^p\boldsymbol{\chi}_\mathrm{i}^r\right)} \hat{D}(\boldsymbol{\chi})\,\hat{U}_R\hat{D}^\dagger(\boldsymbol{\chi}_\mathrm{i}). \tag{1.32}$$

It is important to note that so far we have not made any restrictions, that is, the Hamiltonian can be of any possible nonlinear form in $\hat{\boldsymbol{\xi}}$. When we now apply Eq. (1.32) to the overlap operator which is the product of the two branch-dependent time-evolution operators, we obtain

$$\hat{U}_1^\dagger\hat{U}_2 = \mathrm{e}^{\frac{\mathrm{i}}{\hbar}\Delta S - \frac{\mathrm{i}}{2\hbar}\Delta\boldsymbol{\chi}^r\left(\boldsymbol{\chi}_1^p + \boldsymbol{\chi}_2^p\right)} \hat{D}(\boldsymbol{\chi}_\mathrm{i})\hat{U}_{R,1}^\dagger\hat{D}(\Delta\boldsymbol{\chi})\hat{U}_{R,2}\hat{D}^\dagger(\boldsymbol{\chi}_\mathrm{i}) \tag{1.33}$$

by combining the two displacement operators with the help of the "composition rule", Eq. (A.10). The relative phase-space displacement is denoted by

$$\Delta\boldsymbol{\chi} = \boldsymbol{\chi}_2 - \boldsymbol{\chi}_1 \tag{1.34}$$

and

$$\Delta S = S_2 - S_1 \tag{1.35}$$

is the classical action difference along the two paths. The contribution to the phase in addition to the classical action difference was termed *separation phase* in Refs. [87, 112].

Interpretation of the transformation

In the introduction to this section we claimed that transformation, Eq. (1.26), removes the linear part of the Hamiltonian. This becomes most evident when we Taylor expand around $\boldsymbol{\chi}$

$$H(\hat{\boldsymbol{\xi}} + \boldsymbol{\chi}) = H(\boldsymbol{\chi}) + \frac{\partial H(\boldsymbol{\chi})}{\partial \boldsymbol{\chi}}^{\mathrm{T}} \hat{\boldsymbol{\xi}} + \frac{1}{2} \hat{\boldsymbol{\xi}}^{\mathrm{T}} \frac{\partial^2 H(\boldsymbol{\chi})}{\partial \boldsymbol{\chi}^2} \hat{\boldsymbol{\xi}} + \Delta \hat{H} \tag{1.36}$$

where $\Delta \hat{H}$ includes all the terms higher than second order. When we substitute this expansion into Eq. (1.27), the reduced Hamiltonian becomes

$$\hat{H}_{\mathrm{R}} = \frac{1}{2} \hat{\boldsymbol{\xi}}^{\mathrm{T}} \frac{\partial^2 H(\boldsymbol{\chi})}{\partial \boldsymbol{\chi}^2} \hat{\boldsymbol{\xi}} + \Delta \hat{H} \,, \tag{1.37}$$

where the linear terms of the Taylor expansion are now compensated. It is important to stress that so far we allowed general anharmonic Hamiltonians. One might object that in this case the notion of classical paths is of no physical relevance since the Ehrenfest theorem is only valid for at most harmonic Hamiltonians. While this statement is true, if H is a smooth function of $\boldsymbol{\chi}$ over the size the local wave packets in each interferometer arm, the effects of the higher-order derivatives decrease order by order. In this case, the Ehrenfest theorem is still approximately valid and $\boldsymbol{\chi}$ can be interpreted as classical trajectory. However, it is important to note that even for strong anharmonicities the transformation is exact and might still simplify calculations. Only the paths $\boldsymbol{\chi}$ do not allow for an interpretation as classical trajectories.

Initial conditions

In the derivation above, the initial condition $\boldsymbol{\chi}_{\mathrm{i}}$ could be chosen completely arbitrarily. However, the choice

$$\boldsymbol{\chi}_{\mathrm{i}} = \langle \hat{\boldsymbol{\xi}} \rangle \tag{1.38}$$

where the expectation value is with respect to the initial state $|\psi(t_{\mathrm{i}})\rangle$ is particularly useful. In this case we can shift the initial wave function as

$$|\psi\rangle = \hat{D}(\boldsymbol{\chi}_{\mathrm{i}}) |\tilde{\psi}\rangle \,, \tag{1.39}$$

where now $\langle \tilde{\psi} | \hat{\boldsymbol{\xi}} | \tilde{\psi} \rangle = 0$ as can be easily seen by applying Eq. (A.14). When we now wish to calculate the expectation value of Eq. (1.33), the displacement operators with respect to the initial position in phase space cancel, hence

$$\langle \hat{U}_1^\dagger \hat{U}_2 \rangle = \mathrm{e}^{\frac{\mathrm{i}}{\hbar} \Delta S - \frac{\mathrm{i}}{2\hbar} \Delta \boldsymbol{\chi}^r \left(\boldsymbol{\chi}_1^p + \boldsymbol{\chi}_2^p \right)} \langle \tilde{\psi} | \hat{U}_{R,1}^\dagger \hat{D}(\Delta \boldsymbol{\chi}) \hat{U}_{R,2} | \tilde{\psi} \rangle \,. \tag{1.40}$$

During the evolution with respect to $\hat{H}_{\mathrm{R}}$, the wave function $|\tilde{\psi}\rangle$ will approximately rest at the minimum of the reduced potential and its evolution is determined solely by harmonic and higher-order contributions to the potentials.

Closed interferometer

The interferometer is closed if in Eq. (1.33) the displacement $\Delta\boldsymbol{\chi} = 0$, which corresponds to a closed trajectory in phase space, and furthermore $\hat{U}_{R,1}^{\dagger}\hat{U}_{R,2} = 1$ due to perfect overlap. For this case we arrive at the celebrated formula

$$\hat{U}_1^{\dagger}\hat{U}_2 = \mathrm{e}^{\frac{\mathrm{i}}{\hbar}\Delta S}\,, \tag{1.41}$$

which follows from the Feynman path-integral formalism in [77]. In the framework of the formalism described in this section, Eq. (1.41) follows from Schrödinger quantum mechanics in a very simple fashion.

The formula, Eq. (1.40), is the main result of this section. It will be further investigated in the following in the context of the local linear and local harmonic approximation.

1.2.2. Local linear approximation

In Sec. 1.2.1 we showed by Taylor expansion that only terms of second and higher order in position and momentum operators appear in the reduced time-evolution operator. Given the Hamiltonian

$$\hat{H} = \frac{\hat{\boldsymbol{p}}^2}{2m} + V(\hat{\boldsymbol{r}}) \tag{1.42}$$

with a smooth potential $\hat{V}$, we now neglect second-and higher-order derivatives of $\hat{V}$. Thus, the time evolution of the wave packets in the two comoving frames is determined by the same reduced Hamiltonian

$$\hat{U}_R = \exp\left\{-\frac{\mathrm{i}}{\hbar}\frac{\hat{\boldsymbol{p}}^2}{2m}(t - t_{\mathrm{i}})\right\} \tag{1.43}$$

for every path. When we recall the definition of the displacement operator and the identity

$$\hat{U}_R^{\dagger}\hat{\boldsymbol{r}}\hat{U}_R = \hat{\boldsymbol{r}} + \frac{\hat{\boldsymbol{p}}}{m}(t - t_{\mathrm{i}})\,, \tag{1.44}$$

it is straightforward to show that

$$\hat{U}_R^{\dagger}\hat{D}(\Delta\boldsymbol{\chi})\hat{U}_R = \hat{D}(\Delta\tilde{\boldsymbol{\chi}}) \tag{1.45}$$

where we introduced the abbreviation

$$\Delta\tilde{\boldsymbol{\chi}} = \left(\Delta\boldsymbol{\chi}^r - \frac{\Delta\boldsymbol{\chi}^p}{m}(t - t_{\mathrm{i}}), \Delta\boldsymbol{\chi}^p\right)^{\mathrm{T}}\,. \tag{1.46}$$

These considerations help us arrive at the final result for the overlap operator in the *local linear approximation*

$$\hat{U}_1^{\dagger}\hat{U}_2 = \mathrm{e}^{\frac{\mathrm{i}}{\hbar}\Delta S - \frac{\mathrm{i}}{2\hbar}\Delta\boldsymbol{\chi}^r\left(\boldsymbol{\chi}_1^p + \boldsymbol{\chi}_2^p\right)}\hat{D}(\Delta\tilde{\boldsymbol{\chi}})\,, \tag{1.47}$$

where we employed Eq. (1.33).

Before we turn to the local harmonic approximation a few remarks are in order. First, we note that Eq. (1.47) is exact for linear potentials. In the case of small nonlinear

contributions to the Hamiltonian one is soon confronted with consistency issues and one should be careful with this approximation.

It is important to point out that the displacement operator in the overlap operator in Eq. (1.47) is not with respect to the classical trajectories, given by $\Delta\boldsymbol{\chi}$, as one could expect naively, but rather with respect to Eq. (1.46). This takes into account the expansion dynamics of the wave packet, when we evaluate the expectation value of the overlap operator with respect to the initial state.

1.2.3. Local harmonic approximation

In this section we proceed to the next-order approximation known as *local harmonic approximation*. We neglect all derivatives higher than second order in Eq. (1.37), hence only keep harmonic contributions so that with Eq. (1.33) the overlap operator becomes

$$\hat{U}_1^\dagger \hat{U}_2 = e^{\frac{i}{\hbar}\Delta S - \frac{i}{2\hbar}\Delta\boldsymbol{\chi}^r\left(\boldsymbol{\chi}_1^p + \boldsymbol{\chi}_2^p\right)} \hat{U}_{R,1}^\dagger \hat{D}(\Delta\boldsymbol{\chi}) \hat{U}_{R,2} \tag{1.48}$$

where

$$\hat{U}_{R,j} = \mathcal{T}\exp\left\{ -\frac{i}{\hbar}\int_{t_i}^t \mathrm{d}t' \, \frac{1}{2}\hat{\boldsymbol{\xi}}^{\mathrm{T}} \mathcal{A}_j \hat{\boldsymbol{\xi}} \right\} \tag{1.49}$$

with the abbreviation

$$\mathcal{A}_j = \frac{\partial^2 H(\boldsymbol{\chi}_j)}{\partial \boldsymbol{\chi}_j^2} \, . \tag{1.50}$$

Note that $\mathcal{A}$ is in general time dependent. The index j labels the two different paths. The meaning of Eq. (1.48) is obvious. In order to calculate the expectation value of the overlap operator take the initial wave function and propagate it with Eq. (1.49) individually for each branch. Think e.g. of the standard Hamiltonian

$$\hat{H} = \frac{\hat{\boldsymbol{p}}^2}{2m} + \frac{1}{2}m\,\hat{\boldsymbol{r}}^{\mathrm{T}}\Gamma\hat{\boldsymbol{r}} \, , \tag{1.51}$$

then the initial wave function only experiences an expansion (contraction, rotation) in position space due to the Gaussian Hamiltonian. As a second step use these wave functions to calculate the expectation value of the displacement operator. Alternatively, we can again commute the reduced time-evolution operators with the displacement operator

$$\hat{U}_{R,1}^\dagger(t,t_i) \hat{D}(\Delta\boldsymbol{\chi}) \hat{U}_{R,2}(t,t_i) = \hat{D}(T_1^{-1}(t,t_i)\Delta\boldsymbol{\chi}) \hat{U}_{R,1}^\dagger(t,t_i) \hat{U}_{R,2}(t,t_i) \tag{1.52}$$

with the time-evolution matrix

$$T_j(t,t_i) = \mathcal{T}\exp\left\{ \int_{t_i}^t \mathrm{d}t' \, \boldsymbol{\mathcal{J}}\mathcal{A}_j(t') \right\} \, . \tag{1.53}$$

With the help of Eq. (1.52) we rewrite Eq. (1.48) as

$$\hat{U}_1^\dagger \hat{U}_2 = e^{\frac{i}{\hbar}\Delta S - \frac{i}{2\hbar}\Delta\boldsymbol{\chi}^r\left(\boldsymbol{\chi}_1^p + \boldsymbol{\chi}_2^p\right)} \hat{D}(T_1^{-1}\Delta\boldsymbol{\chi}) \hat{U}_{R,1}^\dagger \hat{U}_{R,2} \, . \tag{1.54}$$

Thus, for arbitrary time-dependent quadratic Hamiltonians, however, the same on both interferometer branches, the two reduced-time evolution operators cancel and Eq. (1.54) reduces to

$$\hat{U}_1^\dagger \hat{U}_2 = \mathrm{e}^{\frac{\mathrm{i}}{\hbar}\Delta S - \frac{\mathrm{i}}{2\hbar}\Delta \boldsymbol{\chi}^r \left(\boldsymbol{\chi}_1^p + \boldsymbol{\chi}_2^p \right)} \hat{D}(T^{-1}\Delta\boldsymbol{\chi}) \,. \tag{1.55}$$

In this case the calculation shows that it is sufficient to solve a set of ordinary differential equations instead of propagating an infinite dimensional Schrödinger equation in position space. When we consider general potentials, the local harmonic potentials are always different at different positions, so that the two reduced time-evolution operators do not cancel. One now either has to evaluate the actual time evolution of the initial state due to $\hat{U}_{\mathrm{R},1}$ and $\hat{U}_{\mathrm{R},2}$, or resort to the approximative methods discussed in Sec. 1.3.

1.2.4. Beyond harmonic approximation: Numerical simulation

Even in the most general case of Eq. (1.37) the transformation is still useful, when we assume that the evolution through the interferometer is mainly due to the linear potential (including the laser pulses) and the effect of the harmonic and higher-order contributions is significant to some extent but does not completely alter the overall displacement of the local wave packets. In this case eliminating the linear part of the potential allows one to numerically simulate the evolution for both wave packets on a grid of the spatial extent of the wave packet rather than the extent of the interferometer.

1.3. Perturbative methods

In the previous section we described a method to calculate phase and contrast of an interferometer. Even though the formalism allows the intuitive interpretation in terms of comoving frames, it entails the following problems: For general anharmonic perturbing potentials, one first has to solve the full classical equations of motion, in general numerically. After the transformation, Eq. (1.26), the Hamiltonian in the comoving frames still contains the complicated perturbing potentials for which an analytic solution is generally not known. We can now either numerically simulate the Schrödinger equation in the comoving frames or further proceed perturbatively if the perturbation is small. Since we calculate the dynamical phase, proportional to the classical action, to all orders in the perturbation potential, we have to check carefully for consistency in order to take into account the effect of the perturbing potential in the reduced time-evolution operator to the correct order.

Realizing that the perturbations are usually small, when for example resulting from gravity gradients or the gravitational potential caused by the laboratory setup, a perturbative treatment that allows for direct access to the overlap operator would be much more transparent. The new method derived in this section provides a consistent perturbative expansion of phase and contrast in powers of the perturbing potentials. Apart from a treatment of quite general anharmonic Hamiltonians, the method is also capable of dealing with time-dependent perturbations. The aim of this section is to develop this formalism.

Let the Hamiltonian be given by the sum

$$\hat{H}_j(t) = H_{0,j}(\hat{\boldsymbol{\xi}}, t) + \epsilon H_j'(\hat{\boldsymbol{\xi}}, t) \tag{1.56}$$

where $j = 1, 2$ label the possibly time-dependent Hamiltonians along the paths of an atom interferometer. In this section all Hamiltonians are path dependent. This will only be explicitly indicated by an index when it is necessary and otherwise might lead to confusion. The Hamiltonian in Eq. (1.56) separates into two parts. The first, $\hat{H}_0$, is a simple Hamiltonian that allows an analytic solution of the Heisenberg equations of motion, that is, it contains at most harmonic potentials. A typical form of the unperturbed Hamiltonian for one of the branches is

$$\hat{H}_0 = \frac{\hat{\boldsymbol{p}}^2}{2m} + m\boldsymbol{g}\hat{\boldsymbol{r}} - \sum_n \hbar\boldsymbol{k}_n\hat{\boldsymbol{r}}\,\delta(t - t_n) \tag{1.57}$$

even though the following discussion is more general. The second part, $\epsilon\hat{H}'$, contains e.g. anharmonic potentials, which will be treated perturbatively, since it is proportional to ϵ which is supposed to be small.

The calculation now aims at contrast C and phase φ, defined by Eq. (1.16), as a power series in terms of ϵ. In order to obtain a representation-free description of the MZ interferometer, Schleich et al. [85] proceeded the following way: Because an interferometer can be described by a sequence of time-evolution operators intersected by the exponentials $\exp(\pm \mathrm{i}k\hat{z})$, these can be combined to one exponential in the case of time-independent Hamiltonians with the help of the Baker-Campbell-Hausdorff (BCH) series

$$\mathrm{e}^{-\frac{\mathrm{i}}{\hbar}\hat{H}_1 T}\mathrm{e}^{-\frac{\mathrm{i}}{\hbar}\hat{H}_2 T} = \mathrm{e}^{-\frac{\mathrm{i}}{\hbar}\hat{H}_1 T - \frac{\mathrm{i}}{\hbar}\hat{H}_2 T - \frac{1}{2\hbar^2}\left[\hat{H}_1, \hat{H}_2\right]T^2 + \cdots}. \tag{1.58}$$

When trying to adapt this method to Hamiltonians like Eq. (1.56), the following problems arise. Apart from being only valid for time-independent Hamiltonians, Eq. (1.58) is an expansion in powers of T, thus only valid for small T. Since the Hamiltonian is the sum of $\hat{H}_0$ and $\epsilon\hat{H}'$, even the nth-order commutator involves first-order terms in ϵ. One way to circumvent this problem would be a change into the interaction picture with respect to $\hat{H}_0$. Then, however, $\hat{H}'$ becomes time dependent and Eq. (1.58) is not valid anymore.

We therefore need to pursue an alternative perturbation method which can be viewed as a generalization of the BCH series for time-dependent Hamiltonians.

1.3.1. Path ordering

We gain deeper insight into the problem when we consider the sequence

$$\hat{U}_1^{\dagger}(t, t_{\mathrm{i}})\hat{U}_2(t, t_{\mathrm{i}}) = \overline{\mathcal{T}}\exp\left\{\frac{\mathrm{i}}{\hbar}\int_{t_{\mathrm{i}}}^{t}\mathrm{d}t\,\hat{H}_1(t)\right\}\mathcal{T}\exp\left\{-\frac{\mathrm{i}}{\hbar}\int_{t_{\mathrm{i}}}^{t}\mathrm{d}t\,\hat{H}_2(t)\right\} \tag{1.59}$$

where $\overline{\mathcal{T}}$ denotes the anti time-ordering operator and the Hamiltonians are completely arbitrary. Realizing that the time-ordering operator on the right-hand side orders - reading from right to left - from t_{i} to t, the anti time-ordering operator subsequently

orders from t back to t_i. We can combine the product by introducing a time contour γ and the path-ordering operator $\mathcal{T}_\gamma$ which orders time along this contour. With this concept Eq. (1.59) is rewritten as

$$\hat{U}_1^\dagger(t, t_\mathrm{i})\hat{U}_2(t, t_\mathrm{i}) = \mathcal{T}_\gamma \exp\left\{ -\frac{\mathrm{i}}{\hbar} \int_\gamma \mathrm{d}t\, \hat{H}(t) \right\} \tag{1.60}$$

where we defined the Hamiltonians on the contour depicted in Fig. 1.3.

It was Schwinger [113] and Keldysh [114] who first introduced this method in the context of thermal quantum field theory.

$$\hat{H}(t) = \hat{H}_2(t) \quad \text{for } t \text{ on } \gamma_2\,,$$
$$\hat{H}(t) = \hat{H}_1(t) \quad \text{for } t \text{ on } \gamma_1\,.$$
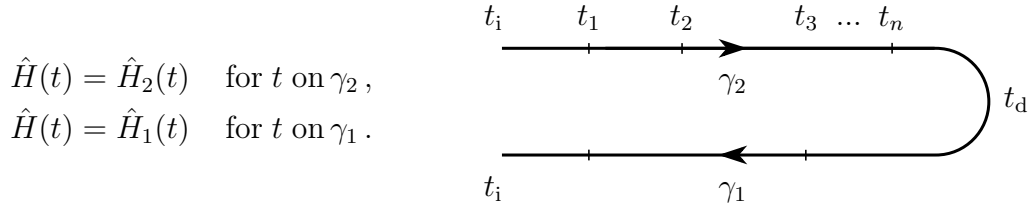
Figure 1.3.: Sketch of the integration path. In order to combine Eq. (1.60) to one time-ordered exponential, we formally introduce a path-ordering operator. The integral runs over γ_2, where $\hat{H}(t) = \hat{H}_2(t)$ from $t = t_\mathrm{i}$ to the final interferometer time t_d and then returns back to t_i over γ_1, where $\hat{H}(t) = \hat{H}_1(t)$. At times $t = t_1, ..., t_n$ laser pulses affect the wave packets on γ_1 or γ_2.

An excellent introduction into this concept can be found in the textbook [115] and the references therein. At first sight this method does not seem very helpful since Eq. (1.60) still involves the rather formal path-ordering operator. However, the Magnus expansion [92] helps us get rid of $\mathcal{T}_\gamma$ and we write

$$\hat{U}_1^\dagger(t, t_\mathrm{i})\hat{U}_2(t, t_\mathrm{i}) = \exp\left\{ -\frac{\mathrm{i}}{\hbar} \int_\gamma \mathrm{d}t\, \hat{H}(t) \right.$$
$$\left. -\frac{1}{2\hbar^2} \int_\gamma \mathrm{d}t \int_\gamma^t \mathrm{d}t'\, \left[\hat{H}(t), \hat{H}(t')\right] + ... \right\}\,. \tag{1.61}$$

The Magnus expansion is a formal series to write a time-ordered exponential as the exponential of an operator without time ordering. Unlike the Dyson expansion, it is performed in the exponent, which makes this method particularly useful for the case considered here.

1.3.2. Closed unperturbed interferometer

In the previous section we discussed the concept of path ordering and the Magnus expansion. We are now in the position to formulate the perturbation expansion for the Hamiltonian given by Eq. (1.56). Let us for simplicity first turn to a closed interferometer with respect to the unperturbed Hamiltonian. Note that even if the unperturbed interferometer is closed, the perturbing Hamiltonian will not only introduce a correction

to the phase but also - among other effects - slightly perturb the trajectories, resulting in open interferometers. The assumption of a closed unperturbed interferometer allows us to write

$$\hat{U}_1^\dagger(t_\mathrm{d}, t_\mathrm{i})\hat{U}_2(t_\mathrm{d}, t_\mathrm{i}) = \mathrm{e}^{\mathrm{i}\phi_0}\,\mathcal{T}_\gamma \exp\left\{-\frac{\mathrm{i}}{\hbar}\epsilon \int_\gamma \mathrm{d}t\, H'(\hat{\boldsymbol{\xi}}(t), t)\right\}. \tag{1.62}$$

First, we transformed into the interaction picture with respect to $\hat{H}_{0,j}$ and used the fact that the unperturbed interferometer is closed, that is,

$$\hat{U}_{0,1}^\dagger(t_\mathrm{d}, t_\mathrm{i})\hat{U}_{0,2}(t_\mathrm{d}, t_\mathrm{i}) = \mathrm{e}^{\mathrm{i}\phi_0} \tag{1.63}$$

where $\hat{U}_{0,j}$ are the time-evolution operators for path j with respect to the unperturbed Hamiltonians. The phase in Eq. (1.63) is related to the classical action difference, ΔS_0, with respect to the unperturbed Hamiltonian, as was shown in Sec. 1.2, or can be calculated by the method which will be derived in example 1. By changing to the interaction picture, we also have to transform the perturbing Hamiltonian according to

$$\hat{H}_j'(t) \rightarrow \hat{U}_{0,j}^\dagger(t, t_\mathrm{i})H_j'(\hat{\boldsymbol{\xi}}, t)\hat{U}_{0,j}(t, t_\mathrm{i}) = H_j'(\hat{\boldsymbol{\xi}}(t), t) \tag{1.64}$$

where

$$\hat{U}_{0,j}^\dagger(t, t_\mathrm{i})\hat{\boldsymbol{\xi}}\hat{U}_{0,j}(t, t_\mathrm{i}) = \hat{\boldsymbol{\xi}}(t) \tag{1.65}$$

are the solutions of the Heisenberg equations of motion. Since the unperturbed Hamiltonian is at most quadratic in $\hat{\boldsymbol{\xi}}$, explicit expressions can be obtained for $\hat{\boldsymbol{\xi}}(t)$. For the unperturbed Hamiltonian, Eq. (1.57), we obtain

$$\hat{\boldsymbol{r}}(t) = \hat{\boldsymbol{r}} + \frac{\hat{\boldsymbol{p}}}{m}t + \boldsymbol{r}_\mathrm{c}(t)\,,$$
$$\hat{\boldsymbol{p}}(t) = \hat{\boldsymbol{p}} + \boldsymbol{p}_\mathrm{c}(t) \tag{1.66}$$

where $\boldsymbol{r}_\mathrm{c}(t)$ and $\boldsymbol{p}_\mathrm{c}(t)$ are determined by the classical trajectories. For an open MZ interferometer in a linear potential in z direction the solutions can be inferred from Fig. 1.4.

Transforming into the interaction picture, the path-ordered exponential in Eq. (1.62) has become proportional to ϵ. Consequently, with the help of the Magnus expansion we arrive at a perturbation expansion in powers of ϵ

$$\hat{U}_1^\dagger(t_\mathrm{d}, t_\mathrm{i})\hat{U}_2(t_\mathrm{d}, t_\mathrm{i}) = \exp\left\{\mathrm{i}\sum_{n=0}^\infty \epsilon^n \hat{\phi}_n\right\}. \tag{1.67}$$

Comparing with Eq. (1.61), we obtain the first-and second-order contributions

$$\hat{\phi}_1 = -\frac{1}{\hbar}\int_\gamma \mathrm{d}t\, H'(\hat{\boldsymbol{\xi}}(t), t) \tag{1.68}$$

$$\hat{\phi}_2 = \frac{\mathrm{i}}{2\hbar^2}\int_\gamma \mathrm{d}t \int_\gamma^t \mathrm{d}t'\, \left[H'(\hat{\boldsymbol{\xi}}(t), t), H'(\hat{\boldsymbol{\xi}}(t'), t')\right]. \tag{1.69}$$

In general the expansion, Eq. (1.67), does not terminate. The nth-order term involves combinations of nth-order nested contour integrals over nested commutators as given by the Magnus expansion. Depending on the problem, the evaluation of the nested contour integrals can be rather involved. It is therefore desirable to obtain expressions with integrals extending only over the interval $[t_\mathrm{i}, t_\mathrm{d}]$. For that reason we derive an alternative form of the standard Magnus expansion in App. B.1 and provide explicit expressions up to third order. The first two terms of the infinite series are

$$\hat{\phi}_1 = -\frac{1}{\hbar} \oint \mathrm{d}t\, \hat{H}'(t)\,, \tag{1.70}$$

$$\hat{\phi}_2 = -\frac{\mathrm{i}}{2\hbar^2} \int_{t_\mathrm{i}}^{t_\mathrm{d}} \mathrm{d}t \int_t^{t_\mathrm{d}} \mathrm{d}t'\, [\hat{H}'_+(t), \hat{H}'_-(t')] \tag{1.71}$$

with $\hat{H}'_+ = \hat{H}'_2 + \hat{H}'_1$ and $\hat{H}'_- = \hat{H}'_2 - \hat{H}'_1$.

Connection to the previous section

Suppose the Hamiltonian

$$\hat{H} = \hat{H}_0 + \epsilon V'(\hat{\boldsymbol{r}}, t) \tag{1.72}$$

where H_0 is again given by Eq. (1.57) and V' is supposed to be smooth around the unperturbed trajectories. After changing into the interacting picture with respect to the unperturbed Hamiltonian, we Taylor-expand the potential around the unperturbed trajectories of the interferometer

$$V'(\boldsymbol{r}_\mathrm{c}(t)+\hat{\bar{\boldsymbol{r}}}, t) = V'(\boldsymbol{r}_\mathrm{c}(t))+\partial_i V'(\boldsymbol{r})|_{\boldsymbol{r}=\boldsymbol{r}_\mathrm{c}(t)}\hat{\bar{x}}_i(t)+\frac{1}{2}\partial_i\partial_j V'(\boldsymbol{r})|_{\boldsymbol{r}=\boldsymbol{r}_\mathrm{c}(t)}\hat{\bar{x}}_i(t)\hat{\bar{x}}_j(t)\,... \tag{1.73}$$

where $\hat{\boldsymbol{r}} = (\hat{x}_1, \hat{x}_2, \hat{x}_3)^\mathrm{T}$ and $\hat{\bar{\boldsymbol{r}}} = \hat{\boldsymbol{r}} + \frac{\hat{\boldsymbol{p}}}{m}t$. The variance of $\hat{\bar{\boldsymbol{r}}}$ is related to the size of the wave packet. Thus, Eq. (1.73) is an expansion in the ratio of the width of the local wave function to the change of the potential. If the potential is sufficiently smooth, we neglect all terms but the first in Eq. (1.73) to obtain a first-order correction of the phase in ϵ

$$\varphi = \phi_0 - \frac{1}{\hbar}\epsilon \oint \mathrm{d}t\, V'(\hat{\boldsymbol{\xi}}(t), t) = \frac{1}{\hbar} \oint \mathrm{d}t\, \{\mathscr{L}_0(t) - \epsilon V'(\boldsymbol{r}_\mathrm{c}(t))\}\,, \tag{1.74}$$

where we made use of Eq. (1.41) to relate the unperturbed phase to the Lagrange function $\mathscr{L}_0$ corresponding to the Hamiltonian $\hat{H}_0$. Hence, for smooth potentials and ϵ small it is sufficient to integrate the perturbing potential along the unperturbed trajectories. Note the key difference compared to Eq. (1.33) in which we have to integrate the Lagrange function with respect to the perturbed trajectories which is much more involved since the trajectories itself first must be determined either numerically or perturbatively. It is therefore worthwhile realizing that Eq. (1.33) and Eq. (1.41) yield identical results for a closed unperturbed interferometer, when neglecting wave-packet effects, and to first order in ϵ.

Expectation value of exponential operators

Before we turn to a few examples, it is important to mention that we still need to evaluate the expectation value of the exponential of operators. For small values of ϵ the cumulant expansion [116, p. 928] can be extremely helpful. For an operator $\hat{A}$ it states

$$\langle e^{\hat{A}} \rangle = \exp\left(\sum_{n=1}^{\infty} \frac{\kappa_n}{n!} \right) \tag{1.75}$$

if existent, where the cumulants are defined by

$$\kappa_n = \frac{d^n}{dt^n} \ln\langle e^{\hat{A}t} \rangle \Big|_{t=0} . \tag{1.76}$$

Applying the cumulant expansion to Eq. (1.67), we obtain to third order in ϵ

$$\varphi = \phi_0 + \epsilon\langle\hat{\phi}_1\rangle + \epsilon^2\langle\hat{\phi}_2\rangle + \epsilon^3\left(-\frac{1}{6}\langle\hat{\phi}_1^3\rangle + \frac{1}{2}\langle\hat{\phi}_1^2\rangle\langle\hat{\phi}_1\rangle - \frac{1}{3}\langle\hat{\phi}_1\rangle^3 + \langle\hat{\phi}_3\rangle \right) + ... \tag{1.77}$$

and

$$\ln(C) = -\frac{1}{2}\epsilon^2\left(\langle\hat{\phi}_1^2\rangle - \langle\hat{\phi}_1\rangle^2 \right) - \epsilon^3\left(\frac{1}{2}\langle\hat{\phi}_1\hat{\phi}_2 + \hat{\phi}_2\hat{\phi}_1\rangle - \langle\hat{\phi}_1\rangle\langle\hat{\phi}_2\rangle \right) + ... \tag{1.78}$$

for phase and contrast by separating complex and real parts. We now invoke the following argument. When we are only interested in the lowest-order contribution to phase and contrast we can neglect the influence of $\hat{\phi}_2$ since it only enters as a correction to the phase. In this sense the expansion is still consistent after neglecting $\langle\hat{\phi}_2\rangle$ even though ϵ^2 appears in the contrast.

It is important to note that truncating Eq. (1.75) at a certain order does not necessarily lead to good approximations. Depending on the size of ϵ and the perturbation Hamiltonian, there might, however, exist an optimal number of terms one takes into account which need to be estimated individually for every situation.

Initial conditions

The Magnus expansion of the overlap operator is completely independent of the initial wave function. Let us again assume a state

$$|\psi\rangle = \hat{D}(\boldsymbol{\chi}_i)|\tilde{\psi}\rangle \tag{1.79}$$

with $\langle\tilde{\psi}|\hat{\boldsymbol{\xi}}|\tilde{\psi}\rangle = 0$.

In the following we will present two equivalent approaches to include the initial conditions into the calculation. Depending on the aim of the calculation, one or the other method might provide more insight.

In the first method we calculate the overlap operator as a function of $\hat{\boldsymbol{\xi}}$. In order to obtain its expectation value with respect to $|\psi\rangle$, we use Eq. (A.14), thus replace

$$\hat{\boldsymbol{\xi}} \to \hat{\boldsymbol{\xi}} + \boldsymbol{\chi}_i \tag{1.80}$$

everywhere in the overlap operator to subsequently calculate its expectation value with respect to $|\tilde{\psi}\rangle$. Performing the calculation this way highlights that, independent of the geometry, the phase of a closed interferometer is independent of the initial velocity and position of the wave packet. Note that the reverse statement is also true. The phase of an open interferometer necessarily depends on the initial conditions. It was pointed out in Ref. [117] that this fact limits the accuracy of tests of the equivalence principle. The nonclosure of the interferometer resulting for instance from gravity gradients introduces a phase dependent on the initial relative position and velocity of the atomic clouds of the two atomic species employed, which cannot be controlled accurately enough. A solution to this problem was provided in Ref. [118] and will be discussed and generalized in Sec. 1.3.4.

In the second method we substitute the operators according to Eq. (1.80) before we perform the Magnus expansion. This results in the replacement

$$\begin{aligned} \boldsymbol{r}_{\mathrm{c}}(t) &\to \boldsymbol{r}_0 + \boldsymbol{v}_0 t + \boldsymbol{r}_{\mathrm{c}}(t) \\ \boldsymbol{p}_{\mathrm{c}}(t) &\to m\boldsymbol{v}_0 + \boldsymbol{p}_{\mathrm{c}}(t) \end{aligned} \tag{1.81}$$

in the classical trajectories.

Independent of the method used, the expectation value of functions of $\hat{\boldsymbol{r}}$ and $\hat{\boldsymbol{p}}$ with respect to $|\tilde{\psi}\rangle$ becomes particularly simple since all moments of these operators are automatically centered.

1.3.3. Examples

After developing the perturbation theory in the previous sections, we apply the method to a number of examples. First, we present a fast calculation of a general interferometer sequence in the linear gravitational potential. This example is followed by an analysis of the leading-order perturbation effects on phase and contrast by a harmonic potential. The subsequent example will extend the discussion to a second-order description of the gravitational potential including cubic anharmonicities.

Example 1: General interferometer sequence in the linear gravitational potential

In this example we present a fast way to obtain an explicit expression for the overlap operator of a light-pulse interferometer in a linear gravitational field. The Hamiltonian reads

$$\hat{H}_j(t) = \frac{\hat{\boldsymbol{p}}^2}{2m} + mg\hat{z} - f_{\mathrm{L}}^{(j)}(t)\hat{z}\,, \tag{1.82}$$

where the function $f_{\mathrm{L}}^{(j)}(t)$ is branch dependent in the sense

$$f_{\mathrm{L}}^{(j)}(t) = \sum_n \hbar k_n^{(j)}\,\delta(t - t_n)\,. \tag{1.83}$$

Here, j labels the path and n the laser pulses. Note that this notation assumes that each laser pulse acts simultaneously on both interferometer arms. In case a laser pulse acts exclusively on one branch, simply choose the respective $k_n^{(j)} = 0$ on the other

$$\hat{z}(t) = \hat{z} + \tfrac{\hat{p}}{m}t + v_{\mathrm{r}}T - \tfrac{1}{2}gt^2$$
$$\hat{p}(t) = \hat{p} - mgt$$

Exit port 2

②b

$$\hat{z}(t) = \hat{z} + \tfrac{\hat{p}}{m}t + v_{\mathrm{r}}(t - T_0) - \tfrac{1}{2}gt^2$$
$$\hat{p}(t) = \hat{p} + mv_{\mathrm{r}} - mgt$$

②a

Exit port 1

①b

$$\hat{z}(t) = \hat{z} + \tfrac{\hat{p}}{m}t - \tfrac{1}{2}gt^2$$
$$\hat{p}(t) = \hat{p} - mgt$$

$$\hat{z}(t) = \hat{z} + \tfrac{\hat{p}}{m}t + v_{\mathrm{r}}(t - T - T_0) - \tfrac{1}{2}gt^2$$
$$\hat{p}(t) = \hat{p} + mv_{\mathrm{r}} - mgt$$

①a

$$\hat{z}(t) = \hat{z} + \tfrac{\hat{p}}{m}t - \tfrac{1}{2}gt^2$$
$$\hat{p}(t) = \hat{p} - mgt$$
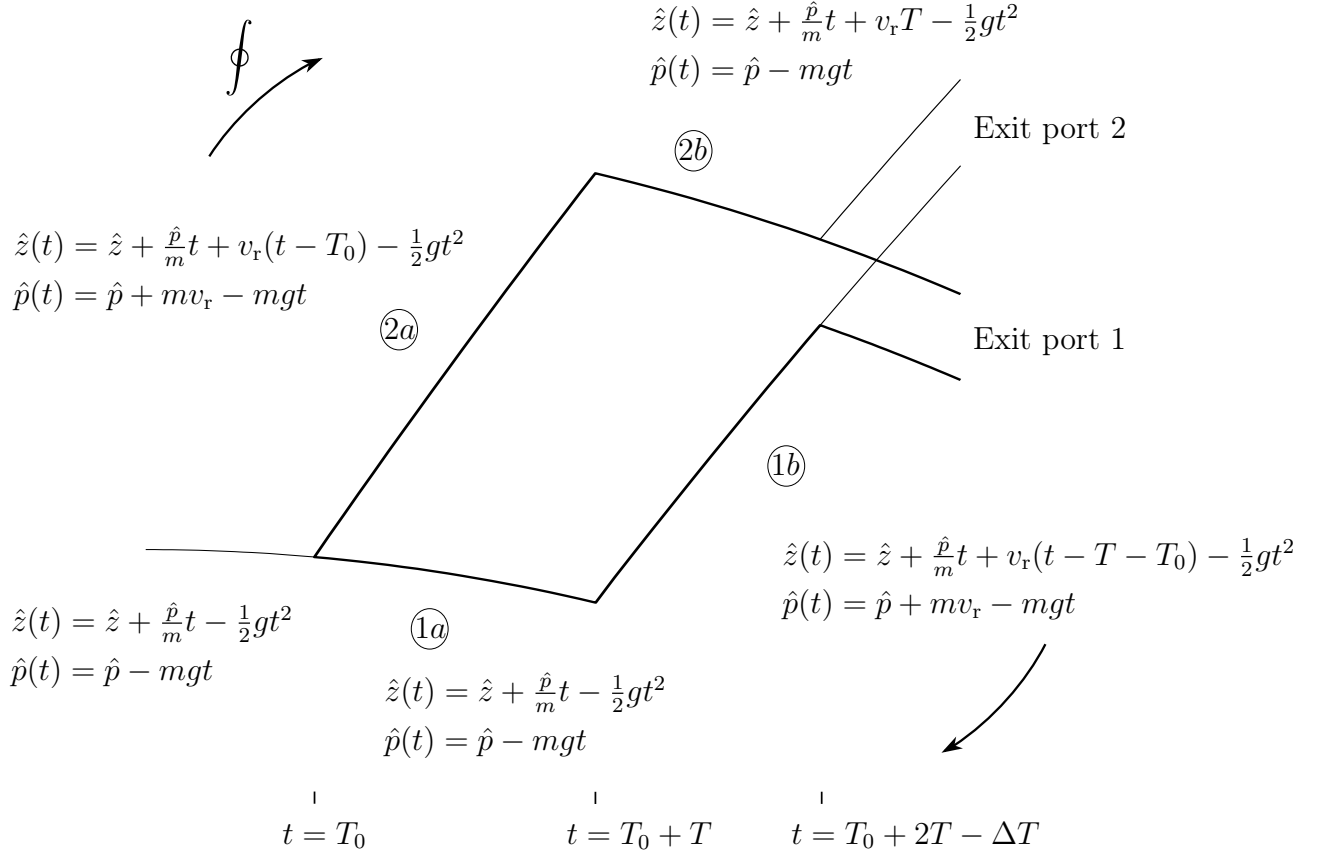
$$t = T_0 \qquad\qquad t = T_0 + T \qquad t = T_0 + 2T - \Delta T$$

Figure 1.4.: Sketch of a Mach-Zehnder in the linear gravitational field. After an initial free fall time T_0 the interferometer sequence is generated by three laser pulses at $t = T_0$, $t = T + T_0$ and $t = T_0 + 2T - \Delta T$. Next to the interferometer paths the Heisenberg equations of motions with respect to the unperturbed Hamiltonian, Eq. (1.82), are depicted, where $v_{\mathrm{r}} = \tfrac{\hbar k}{m}$ is the recoil velocity. The arrows define the integration direction over the contour γ.

without loss of generality. In order to apply the perturbation formula we must specify the unperturbed Hamiltonian and choose

$$\hat{H}_0 = \frac{\hat{\boldsymbol{p}}^2}{2m} + mg\hat{z} \,. \tag{1.84}$$

Even though the perturbation by the laser pulses is far from being small, we can still apply the above perturbation formula since, as we will recognize, the Magnus expansion terminates at second order. For this reason a calculation with the help of the BCH series as shortly described in the beginning of this section was also possible [85]. The interaction picture with respect to Hamiltonian, Eq. (1.84), is readily calculated. It results in the transformation

$$\hat{z} \rightarrow \hat{z} + \frac{\hat{p}_z}{m}t - \frac{1}{2}gt^2 \,. \tag{1.85}$$

We now apply Eq. (1.67) together with Eq. (1.70) and Eq. (1.71). Since the unperturbed Hamiltonian is branch independent, we find $\phi_0 = 0$. With $f_{L-} = f_L^{(2)} - f_L^{(1)}$ the first-order contribution is calculated as

$$\hat{\phi}_1 = -\frac{1}{\hbar}\int_{t_i}^{t_d} dt\, H'_-(\hat{\boldsymbol{\xi}}(t), t) = \frac{1}{\hbar}\int_{t_i}^{t_d} dt\, f_{L-}(t)\left(\hat{z} + \frac{\hat{p}_z}{m}t - \frac{1}{2}gt^2\right)$$
$$= \frac{1}{\hbar}\left(\Delta\chi^p\hat{z} - \Delta\chi^z\hat{p}_z\right) + \phi_g \tag{1.86}$$

where we defined the relative momentum and position displacement

$$\Delta\chi^p = \hbar\sum_n k_n^{(-)}, \qquad\qquad \Delta\chi^z = -\frac{\hbar}{m}\sum_n k_n^{(-)}t_n, \tag{1.87}$$

in the case of an open geometry and the gravitational phase

$$\phi_g = -\frac{1}{2}g\sum_n k_n^{(-)}t_n^2 \tag{1.88}$$

due to the motion in the gravitational field. We furthermore introduced the notation $k_n^{(\pm)} = k_n^{(2)} \pm k_n^{(1)}$. Finally, we evaluate the second-order contribution which we define as *kinetic phase*

$$\phi_k \equiv \hat{\phi}_2 = -\frac{i}{2\hbar^2}\int_{t_i}^{t_d} dt\int_t^{t_d} dt'\left[H'_+(\hat{\boldsymbol{\xi}}(t), t), H'_-(\hat{\boldsymbol{\xi}}(t'), t')\right]$$
$$= \frac{1}{2m\hbar}\int_{t_i}^{t_d} dt\int_t^{t_d} dt'\, f_{L+}(t)f_{L-}(t')(t' - t)$$
$$= \frac{1}{2m}\int_{t_i}^{t_d} dt\, f_{L+}(t)\sum_{j=1}^N k_j^{(-)}(t_j - t)\Theta(t < t_j)$$
$$= \frac{\hbar}{2m}\sum_{j=2}^N\sum_{n=1}^{j-1} k_j^{(-)}k_n^{(+)}(t_j - t_n), \tag{1.89}$$

where we introduced the Heaviside function $\int_t^{t_d} dt'\,\delta(t' - t_j) = \Theta(t < t_j)$ and N is the total number of laser pulses. This phase can be employed in recoil measurements to infer $\hbar/m$ in order to determine the fine-structure constant [39]. In summary, we can write

$$\hat{U}_1^\dagger(t_d, t_i)\hat{U}_2(t_d, t_i) = \hat{D}(\Delta\chi)e^{i\phi_g + i\phi_k}. \tag{1.90}$$

The momentum and, respectively, position displacement is determined by Eq. (1.87), the gravitational phase by Eq. (1.88) and the kinetic phase by Eq. (1.89).

As an example we now consider an MZ interferometer with the laser pulses at $t_0 = 0$, $t_1 = T$, and $t_2 = 2T$. We slightly modify the momentum transfer of the laser pulses by replacing $\boldsymbol{k} \to \boldsymbol{k} + \Delta\boldsymbol{k}_1$ at t_1 and $\boldsymbol{k} \to \boldsymbol{k} + \Delta\boldsymbol{k}_2$ at t_2 and generalize the discussion above to nonaligned laser pulses. The result of this example will be needed for the discussion of open interferometers in Sec. 1.3.4. We find

$$\hat{U}_1^\dagger(t_d, t_i)\hat{U}_2(t_d, t_i) = \exp\left\{-i(\boldsymbol{k} - \Delta\boldsymbol{k}_1 + 2\Delta\boldsymbol{k}_2)\boldsymbol{g}T^2 + i\boldsymbol{v}_r(\Delta\boldsymbol{k}_2 - \Delta\boldsymbol{k}_1)T - \frac{i}{\hbar}\Delta\boldsymbol{\chi}^T\boldsymbol{\mathcal{J}}\hat{\boldsymbol{\xi}}\right\} \tag{1.91}$$

with

$$\Delta \boldsymbol{\chi}^r = -2(\Delta \boldsymbol{v}_{\mathrm{r2}} - \Delta \boldsymbol{v}_{\mathrm{r1}})T$$
$$\Delta \boldsymbol{\chi}^p = m(\Delta \boldsymbol{v}_{\mathrm{r2}} - 2\Delta \boldsymbol{v}_{\mathrm{r1}}) \tag{1.92}$$

and the recoil velocities are related to the wave numbers by $\Delta \boldsymbol{v}_{\mathrm{r}j} = \hbar \Delta \boldsymbol{k}_j / m$.
The result of this example can be easily generalized to branch-independent harmonic potentials. One then recovers the formalism of Ref. [86].

Example 2: Harmonic potential

In this example we discuss the impact of gravity gradients or, in general, harmonic potentials on phase and contrast of an interferometer. While these results have been known for many years, we show how straightforward the calculation becomes with our method. We will furthermore generalize the following calculation to include anharmonicities in the subsequent example.

Experimentally, the insensitivity to linear accelerations of *double-loop* also known as *butterfly geometries* (see for instance Fig. 2 in Ref. [10]) offers a possibility to measure gravity gradients. The advantage of the dual-cloud set up in Refs. [31, 51] is the immunity to spurious effects like platform vibrations due to the differential measurement known as *common-mode rejection*. These gradiometers have important applications for testing fundamental physical constants [33] and future perspectives in geodesy [32]. An increase in the accuracy of gradiometers [50] allows to measure gradient effects in Ref. [34], which are related to proper-time differences [118], by using a coherent superposition of two interferometers rather than two independent ensembles.

In App. B.3 we expand the gravitational potential of the Earth on the surface to third order in the inverse of its radius. The z axis is chosen in direction of the linear acceleration g and we disregard the zero-order term as it only introduces an irrelevant global phase. To second order, the perturbation reads

$$V(\hat{\boldsymbol{r}}) = mg\hat{z} + \frac{1}{2}m\Gamma_{ij}^{(1)}\,\hat{x}_i\hat{x}_j\,, \tag{1.93}$$

where repeated indices are summed over and $\boldsymbol{\Gamma}^{(1)}$ symmetric. We furthermore identify the local acceleration $g \cong 9.81\mathrm{m/s}^2$. We now consider a closed interferometer with respect to the linear Hamiltonian, Eq. (1.82), and calculate the first-order contribution. From the discussion in Eq. (1.66) we obtain for the Heisenberg equations of motion

$$\hat{x}_j(t) = \hat{\bar{x}}_j(t) + z_{\mathrm{c}}(t)\delta_{jz} \tag{1.94}$$

with

$$\hat{\bar{x}}_j(t) = \hat{x}_j + \frac{\hat{p}_j}{m}t\,. \tag{1.95}$$

Note again that the path-dependent classical trajectory z_{c} is calculated with respect to the unperturbed Hamiltonian without the perturbing harmonic potential. According to Eq. (1.68) the first order is obtained as the integral over the perturbation potential

evaluated at the Heisenberg equations of motion. This results in

$$\hat{\phi}_1 = -\frac{m}{2\hbar} \oint dt \left\{ 2\Gamma_{zj}^{(1)} z_c(t)\hat{\bar{x}}_j(t) + \Gamma_{zz}^{(1)} z_c(t)^2 \right\}$$
$$= \varphi_1 - \frac{1}{\hbar}\boldsymbol{\chi}^{\mathrm{T}}\boldsymbol{\mathcal{J}}\hat{\boldsymbol{\xi}}. \tag{1.96}$$

The integral over the term quadratic in $\hat{\bar{x}}(t)$ is zero since it is path independent since it does not contain z_c. The fact that also higher-order nested contour integrals over path-independent functions vanish is further investigated in App. B.2. In Eq. (1.96),

$$\varphi_1 = -\frac{m}{2\hbar}\Gamma_{zz}^{(1)} f_{\varphi 1} \tag{1.97}$$

is the first-order correction to the phase and the displacement is given as

$$\chi_j^p = -m\Gamma_{zj}^{(1)} f_{\chi_p 1}$$
$$\chi_p^r = \Gamma_{zj}^{(1)} f_{\chi_r 1}. \tag{1.98}$$

The functions f only depend on the interferometer geometry. The explicit expressions are collected in App. B.3 where we also calculate them exemplarily for an MZ interferometer. Thus, we obtain with the cumulant expansion, Eq. (1.77) and (1.78), exemplarily for an MZ interferometer with initial velocity $v_0 = 0$ of the atomic cloud

$$\varphi = \phi_0 + \langle\hat{\phi}_1\rangle = -kgT^2 + \frac{7}{12}\Gamma_{zz}^{(1)} gkT^4 - \Gamma_{zz}^{(1)}\frac{\hbar k^2}{2m}T^3 \tag{1.99}$$

and

$$\ln(C) = -\frac{1}{2}\mathrm{Var}(\hat{\phi}_1) = -\frac{1}{2\hbar^2}\left(\boldsymbol{\chi}^{p\mathrm{T}}\boldsymbol{\Sigma}_{rr}\boldsymbol{\chi}^p + \boldsymbol{\chi}^{r\mathrm{T}}\boldsymbol{\Sigma}_{pp}\boldsymbol{\chi}^r\right) \tag{1.100}$$

where we introduced the covariance matrix

$$\boldsymbol{\Sigma} = \begin{pmatrix} \boldsymbol{\Sigma}^{rr} & \boldsymbol{\Sigma}^{rp} \\ (\boldsymbol{\Sigma}^{rp})^{\mathrm{T}} & \boldsymbol{\Sigma}^{pp} \end{pmatrix} \tag{1.101}$$

defined by

$$\Sigma_{jk} = \frac{1}{2}\langle\hat{\xi}_j\hat{\xi}_k + \hat{\xi}_k\hat{\xi}_j\rangle - \langle\hat{\xi}_j\rangle\langle\hat{\xi}_k\rangle. \tag{1.102}$$

Furthermore we set the cross correlations $\boldsymbol{\Sigma}^{rp} = 0$ for an initial state which is supposed to be the ground-state of some potential. Note that $\langle\hat{\boldsymbol{\xi}}\rangle = 0$ in general as we included the initial conditions into the classical equations of motion.

The expression for the contrast, Eq. (1.100), is valid for a wide range of input states but generally only for $C \approx 1$, otherwise the cumulant expansion cannot guarantee an accurate approximation. In the case of the Gaussian input state [119], in position representation

$$\psi(\boldsymbol{r}) = \frac{1}{(2\pi)^{3/4}\left(\det\Sigma_{rr}\right)^{1/4}} \exp\left\{-\frac{1}{4}\boldsymbol{r}^{\mathrm{T}}\boldsymbol{\Sigma}_{rr}^{-1}\boldsymbol{r}\right\}, \tag{1.103}$$

the cumulant expansion terminates at second order and Eq. (1.100) is exact. For this state, we find additionally $\boldsymbol{\Sigma}_{pp} = \frac{\hbar^2}{4}\boldsymbol{\Sigma}_{rr}^{-1}$. Due to the influence of the perturbing

potential, the interferometer is not closed, and the contrast drops to zero at the moment the terms in Eq. (1.100) become of the order of one. In Sec. 1.3.4 we will discuss open interferometers and generalize mitigation strategies for the loss of contrast.

There are multiple ways to obtain the above results. Here, we presented a straightforward derivation by means of the path-dependent perturbation theory. Of course, the results can be easily extended to include non-aligned momentum transfers and $\hat{p}_j \hat{x}_k$ terms resulting e.g. from Coriolis forces in rotating coordinate systems.

Example 3: Gravitational potential to second order in R^{-1}

In the previous example we calculated the influence of the gravitational potential of the Earth to first order in the inverse of its radius on a closed interferometer. Now we extend the discussion to second order. For this calculation it is important to realize that we cannot simply apply Eq. (1.71) to the potential, Eq. (1.93). Since the third derivative of the gravitational potential also scales with $1/R^2$, we need to include the cubic correction into the potential in the form

$$V(\hat{\boldsymbol{r}}) = \frac{1}{2}m\Gamma_{ij}^{(1)}\,\hat{x}_i\hat{x}_j + \frac{1}{2}m\Gamma_{ijk}^{(2)}\,\hat{x}_i\hat{x}_j\hat{x}_k \qquad (1.104)$$

with $\Gamma^{(1)} \sim R^{-1}$ and $\Gamma^{(2)} \sim R^{-2}$. For the derivation and the explicit values of $\Gamma_{ij}^{(1)}$ and $\Gamma_{ijk}^{(2)}$ we again refer to App. B.3.1. In the following calculation we will denote the origin of terms by a subscript on the functions f. The application of Eq. (1.70) to the perturbing potential, Eq. (1.104), results in the first-order terms calculated in the previous example (labeled by subscript 1) and a second-order contribution (in R^{-1}) from the anharmonicities (labeled by subscript 2). Additionally, second-order terms arise from Eq. (1.71) applied to the harmonic part of the potential (labeled by subscript 3). The latter terms will be calculated next. Evaluating the commutator

$$\left[\hat{H}_+(t), \hat{H}_-(t')\right] = \mathrm{i}m\hbar\Big\{2[\Gamma^{(1)}]_{iz}^2\,z_{c-}(t')\,\hat{\bar{x}}_i(t) \\ + [\Gamma^{(1)}]_{zz}^2\,z_{c+}(t)z_{c-}(t')\Big\}(t'-t) + \mathcal{O}(1/R^3)\,, \qquad (1.105)$$

with $z_{c\pm} = z_c^{(2)} \pm z_c^{(1)}$, where again the superscript denotes the path, and with the help of the relation

$$\left[\hat{\bar{x}}_i(t), \hat{\bar{x}}_j(t')\right] = \frac{\mathrm{i}\hbar}{m}(t'-t)\delta_{ij}\,, \qquad (1.106)$$

we arrive at

$$\hat{\phi}_2 = -\frac{m}{2\hbar}[\Gamma^{(1)}]_{zz}^2 f_{\varphi 3} - \frac{m}{\hbar}[\Gamma^{(1)}]_{jz}^2\left(m\,\hat{x}_j f_{\chi_p 3} + \hat{p}_j f_{\chi_r 3}\right)\,. \qquad (1.107)$$

The calculation of contributions stemming from the cubic terms to first order in the Magnus expansion is straightforward and left to the reader. Collecting all terms, we arrive at the final result

$$\hat{U}_1^\dagger(t_\mathrm{d}, t_\mathrm{i})\hat{U}_\mathrm{d}(t_\mathrm{d}, t_\mathrm{i}) = \exp\left\{\mathrm{i}\left(\phi_0 + \varphi_1 - \frac{1}{\hbar}\boldsymbol{\chi}^\mathrm{T}\boldsymbol{\mathcal{J}}\hat{\boldsymbol{\xi}} - \frac{1}{2\hbar}\hat{\boldsymbol{\xi}}^\mathrm{T}\boldsymbol{A}\hat{\boldsymbol{\xi}}\right)\right\}\,. \qquad (1.108)$$

The first term is the phase of the unperturbed interferometer, e.g. $\phi_0 = -kgT^2$ for an MZ interferometer. The next term provides a correction to the phase

$$\varphi_1 = -\frac{m}{2\hbar}\left(\Gamma^{(1)}_{zz}f_{\varphi 1} + \Gamma^{(2)}_{zzz}f_{\varphi 2} + [\Gamma^{(1)}]^2_{zz}f_{\varphi 3}\right).\tag{1.109}$$

The functions f are again listed in App. B.3.2. The coefficients for the linear terms in $\hat{\boldsymbol{\xi}}$ are

$$\chi_{p,j} = -m\left\{\Gamma^{(1)}_{zj}f_{\chi_p 1} + \frac{3}{2}\Gamma^{(2)}_{zzj}f_{\chi_p 2} + [\Gamma^{(1)}]^2_{jz}f_{\chi_p 3}\right\}$$

$$\chi_{r,j} = \Gamma^{(1)}_{zj}f_{\chi_r 1} + \frac{3}{2}\Gamma^{(2)}_{zzj}f_{\chi_r 2} + [\Gamma^{(1)}]^2_{jz}f_{\chi_r 3}.\tag{1.110}$$

The matrix

$$\boldsymbol{A} = \begin{pmatrix} \boldsymbol{A}^{rr} & \boldsymbol{A}^{rp} \\ (\boldsymbol{A}^{rp})^{\mathrm{T}} & \boldsymbol{A}^{pp} \end{pmatrix}\tag{1.111}$$

consists of four blocks. Each element is proportional to $\Gamma^{(2)}_{zjk}$ and defined by

$$A^{rr}_{jk} = 3m\Gamma^{(2)}_{zjk}f_{A1}, \qquad A^{rp}_{jk} = 3\Gamma^{(2)}_{zjk}f_{A2}, \qquad A^{pp}_{jk} = 3\frac{1}{m}\Gamma^{(2)}_{zjk}f_{A3}.\tag{1.112}$$

The terms quadratic in $\hat{\boldsymbol{\xi}}$ account for distortion effects due to different expansion dynamics of the wave packet in the cubic potential along different paths. This effect goes beyond the formalism [86] developed for path independent harmonic potentials.

Application to an atomic-fountain experiment

In order to get a feeling for the size of the contributions, we apply the results to an atomic fountain experiment [61, 120] which is depicted in Fig. 1.5. For the initial velocity

$$v_0 = gT - \frac{v_{\mathrm{r}}}{2}\tag{1.113}$$

in z direction of the atomic cloud it is a symmetric MZ setup. The wave packet is accelerated to this velocity by a launching pulse at $t = 0$ right after the release from the trap. Again, the unperturbed interferometer is closed and we obtain the familiar result

$$\phi_0 = -kgT^2\tag{1.114}$$

for the phase, independent of the initial velocity v_0. Next, we calculate the Heisenberg equations of motions. As before, they are read off Fig. 1.4 with $T_0 = \Delta T = 0$.

For interferometer times of about $1.5\,\mathrm{s}$ corresponding to the free-fall time in a $10\,\mathrm{m}$ tower, the corrections from the gravitational field are extremely small so that an approximate treatment in the form of the expansion, Eq. (1.75), is valid. The exponent in Eq. (1.108) is correct to order $1/R^2$ and it is therefore sufficient to truncate the cumulant expansion at the variance.

We obtain the phase to order R^{-2} by the expectation value of Eq. (1.108) as

$$\varphi = \phi_0 + \varphi_1 + \frac{1}{2\hbar}\mathrm{tr}(\boldsymbol{A}\boldsymbol{\Sigma}),\tag{1.115}$$
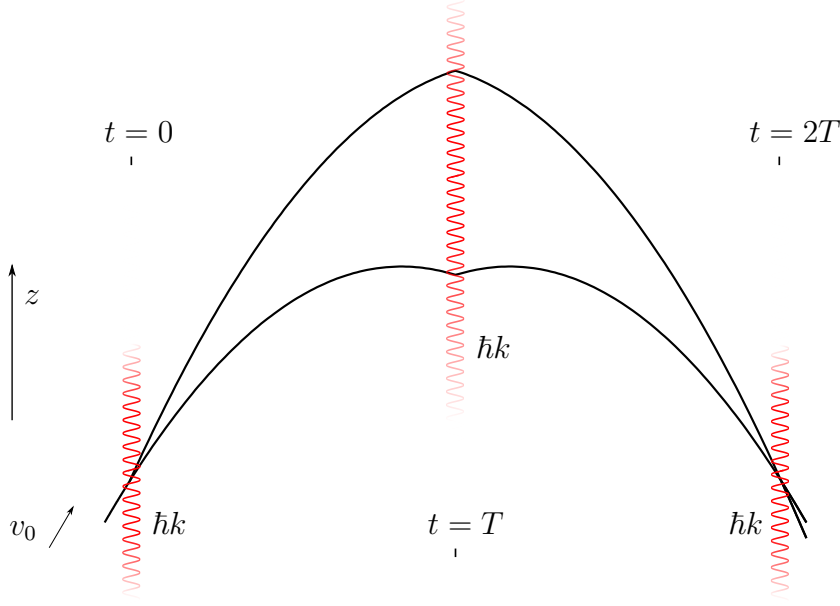
Figure 1.5.: Atomic fountain setup. After switching off the trap, the atoms are accelerated and enter the MZ configuration with initial mean velocity v_0. If the half interferometer time T is chosen according to Eq. (1.113), the interferometer is symmetric to $t = T$.

where we used

$$\langle 2\boldsymbol{\chi}^{\mathrm{T}}\boldsymbol{\mathcal{J}}\hat{\boldsymbol{\xi}} + \hat{\boldsymbol{\xi}}^{\mathrm{T}}\boldsymbol{A}\hat{\boldsymbol{\xi}}\rangle = \mathrm{tr}(\boldsymbol{A}\boldsymbol{\Sigma}) \tag{1.116}$$

with the covariance matrix $\boldsymbol{\Sigma}$. This expression can be further simplified with the help of Eq. (1.112) to

$$\mathrm{tr}(\boldsymbol{A}\boldsymbol{\Sigma}) = 3\mathrm{tr}\left\{\boldsymbol{\Gamma}_z^{(2)}\left(\boldsymbol{\Sigma}^{rr}mf_{A1} + 2\boldsymbol{\Sigma}^{rp}f_{A1} + \boldsymbol{\Sigma}^{pp}\frac{1}{m}f_{A3}\right)\right\} \tag{1.117}$$

with $\Gamma_{zjk}^{(2)} = (\Gamma_z^{(2)})_{jk}$. Inserting the explicit form of $\boldsymbol{\Gamma}^{(1)}$ and $\boldsymbol{\Gamma}^{(2)}$ from App. B.3 into Eq. (1.117), the final expression for the phase reads

$$\varphi = \phi_0 + R^{-1}\frac{mg}{\hbar}f_{\varphi 1} - R^{-2}\frac{mg}{\hbar}\left(2gf_{\varphi 3} + f_{\varphi 2} - \frac{3}{2}\Delta_r^2 f_{A1} - \frac{3}{2m^2}\Delta_p^2 f_{A3}\right) \tag{1.118}$$

with

$$\Delta_r^2 = \Delta x^2 + \Delta y^2 - 2\Delta z^2 \quad \text{and} \quad \Delta_p^2 = \Delta p_x^2 + \Delta p_y^2 - 2\Delta p_z^2 \tag{1.119}$$

where $\Delta\mathcal{O} = \langle\hat{\mathcal{O}}^2\rangle^{\frac{1}{2}}$ denotes the standard deviation of the operator $\hat{\mathcal{O}}$ and we assumed $\boldsymbol{\Sigma}^{rp} = 0$ for the initial state. Remarkably, as can be inferred from Eq. (1.119), the phase due to the different expansion dynamics along the paths cancels for a symmetric initial state.

Next, we calculate the contrast by evaluating the variance

$$\mathrm{Var}\left\{-\mathrm{i}\left(\frac{1}{\hbar}\boldsymbol{\chi}^{\mathrm{T}}\boldsymbol{\mathcal{J}}\hat{\boldsymbol{\xi}} + \frac{1}{2\hbar}\hat{\boldsymbol{\xi}}^{\mathrm{T}}\boldsymbol{A}\hat{\boldsymbol{\xi}}\right)\right\} = -\frac{1}{\hbar^2}\boldsymbol{\chi}^{\mathrm{T}}\boldsymbol{\mathcal{J}}\boldsymbol{\Sigma}\boldsymbol{\mathcal{J}}^{\mathrm{T}}\boldsymbol{\chi} + \mathcal{O}\left(R^{-3}\right), \qquad (1.120)$$

which is independent of $\boldsymbol{A}$ since it is already of the order of $1/R^2$. The result in Eq. (1.120) was already obtained in Eq. (1.100), consequently the contrast for the Gaussian initial state, Eq. (1.103), with $\boldsymbol{\Sigma}_{pp} = \frac{\hbar^2}{4}\boldsymbol{\Sigma}_{rr}^{-1}$ reads

$$\ln(C) = -\frac{1}{2\hbar^2}\boldsymbol{\chi}^{p\mathrm{T}}\boldsymbol{\Sigma}_{rr}\boldsymbol{\chi}^{p} - \frac{1}{8}\boldsymbol{\chi}^{r\mathrm{T}}\boldsymbol{\Sigma}_{rr}^{-1}\boldsymbol{\chi}^{r}. \qquad (1.121)$$

This expression contains terms of $\mathcal{O}(1/R^3)$, but we emphasize that the result is only correct to second order and higher-order terms need to be neglected consistently.

So far the calculation applies to general interferometer geometries via the functions f which are defined in App. B.3. Apart from the general definition we also state in this appendix the explicit values for an MZ interferometer with general initial velocity. For the special choice, Eq. (1.113), we obtain

$$f_{\varphi 1} = \frac{5}{6}gv_{\mathrm{r}}T^4, \qquad f_{\varphi 2} = \frac{11}{20}g^2v_{\mathrm{r}}T^6 + \frac{1}{8}v_{\mathrm{r}}^3T^4, \qquad f_{\varphi 3} = -\frac{59}{180}gv_{\mathrm{r}}T^6$$

$$f_{A1} = v_{\mathrm{r}}T^2, \qquad f_{A3} = \frac{7}{6}v_{\mathrm{r}}T^4. \qquad (1.122)$$

In Fig. 1.6 we compare the different contributions to the phase for a factorizing Gaussian input state with $\Delta x_j \Delta p_j = \hbar/2$. Furthermore, we choose a disk-shaped state with $\Delta x = \Delta y = 2\Delta z$ for a nonvanishing Δ_r and Δ_p to get a feeling for the size of distortion effects.

Discussion

We conclude this example by the following remarks. In Eq. (1.118) the first term within the parenthesis stems from the second-order treatment in the Magnus expansion with respect to the harmonic part of the potential, whereas the second term is the first-order result of the cubic part. A comparison for the considered interferometer shows that the terms are of the same order of magnitude, the presumption at the beginning of this example was therefore correct. For a consistent calculation to second order in the radius of the Earth one needs to include the cubic terms in the expansion of the gravitational potential.

It is interesting to note that in Eq. (1.118) the specific form of the interferometer sequence enters the equations only through the functions f. Therefore, Eq. (1.118) is valid for general sequences. One simply needs to calculate the functions f defined in App. B.3.

The Taylor expansion of the gravitational potential and the Magnus expansion of the overlap operator are effectively an expansion in the ratio of $l/R \ll 1$, where l is the characteristic size of the interferometer. For $l \approx 10\,\mathrm{m}$ this parameter is smaller than 10^{-5}.
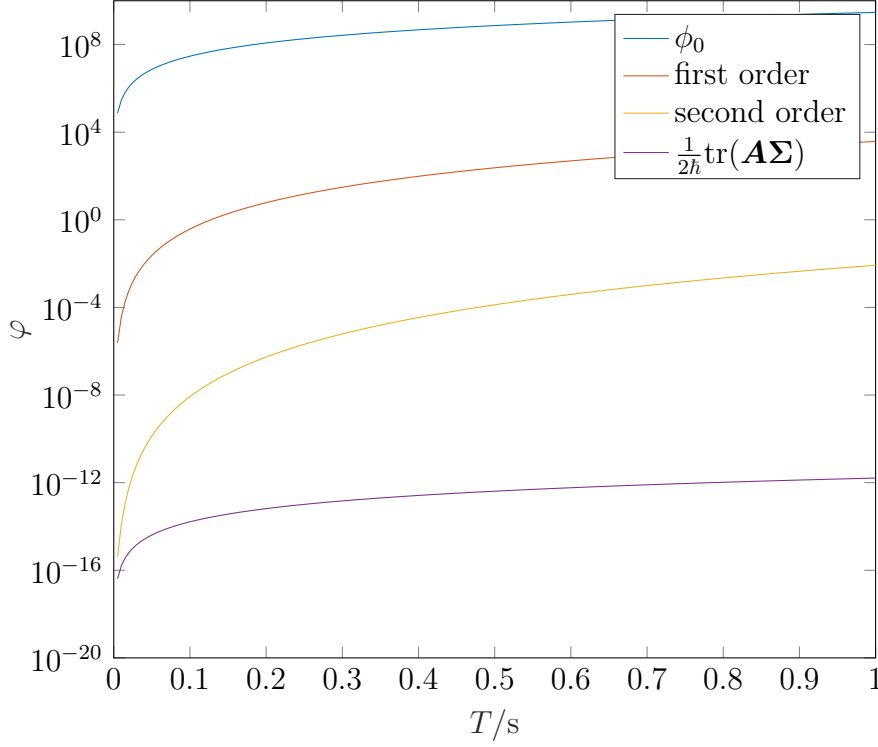
Figure 1.6.: Atomic-fountain experiment in the gravitational potential. The figure shows the absolute values of the phase contributions up to second order in the inverse of the Earth's radius. The phase of the unperturbed interferometer is $\phi_0 = -kgT^2$ and first-and second-order contributions are stated in Eq. (1.118). The purple line shows the phase $\frac{1}{2\hbar}\mathrm{tr}(\boldsymbol{A\Sigma})$ emergent from non-perfect overlap of the wave packets due to different expansion dynamics with respect to different local harmonic potentials. Even the second-order contributions, apart from phases due to distortion effects, will become relevant in near-future applications for example in a setup to determine influences of relativistic effects. The numerical values are obtained for ^{87}Rb with $k \approx 3{\cdot}10^8 \,\mathrm{m}^{-1}$, $\Delta x = \Delta y = 2\Delta z = 100\mu\mathrm{m}$ and $\Delta p_i = \hbar/(2\Delta x_i)$, valid for an initial Gaussian state.

Although we restricted the discussion to the simple case of laser pulses aligned with $\boldsymbol{g}$, a generalization is straightforward and will be done in example 4. Furthermore, velocity-dependent forces appearing in rotating coordinate systems can be easily included.

One can again observe the advantage of the expansion in ϵ over the expansion in T as done in Eq. (1.58). Terms of the order of T^6 appear in $f_{\varphi 3}$, that is, already at second order in R^{-1} one would have to apply the BCH series to at least 6th order, which seems quite impossible.

Finally, we note again that it is particularly easy to calculate the expectation value of the overlap operator since this must be done with respect to the initial state. In addition to that, when the cumulant expansion is valid, it is even sufficient to know only the first few moments of the initial wave function.

1.3.4. Open unperturbed interferometers

In the previous section we realized that, although the unperturbed interferometer is closed, a perturbation may lead to open interferometers. Experimentally, nonclosure is sometimes introduced deliberately by a slight asymmetry in the laser-pulse timing to extract the quantity to be measured by a phase shear [67, 121]. However, open interferometers arising from gravity gradients [88] or rotations [29] in general introduce an undesirable dependence of the interferometer phase on the initial conditions of the wave packet and to a loss of contrast.

One way to overcome this problem is to slightly open the unperturbed interferometer to exactly compensate for these effects. Such mitigation strategies have been proposed for rotations by using tip-tilt mirrors [122] and for gravity gradients by varying the pulse timing [88, 89] or by slightly changing the momentum transfer of the π pulse in an MZ interferometer [118]. Recently, these methods have been implemented successfully [123, 124].

Motivated by these ideas, we aim at a generalization to include anharmonicities into the method. This will be done in detail in example 4 for the case of the anharmonic Hamiltonian, Eq. (1.104), and additional gravitational potentials stemming from the mass distribution of the laboratory setup.

But let us first discuss the general formalism for open unperturbed interferometers. The Hamiltonian is again the sum

$$\hat{H}_j(t) = \hat{H}_{0,j}(t) + \epsilon \hat{H}'_j(t) \tag{1.123}$$

of a simple $\hat{H}_0$, given by Eq. (1.57), and a complicated but small $\epsilon\hat{H}'$. In order to calculate the overlap operator, we transform as before into the interaction picture with respect to the unperturbed Hamiltonian

$$\hat{U}_1^\dagger(t_\mathrm{d}, t_\mathrm{i})\hat{U}_2(t_\mathrm{d}, t_\mathrm{i}) = \mathrm{e}^{\mathrm{i}\phi_0}\hat{U}_{1,\mathrm{H}}^\dagger(t_\mathrm{d}, t_\mathrm{i})\hat{D}(\Delta\boldsymbol{\chi}_0)\hat{U}_{2,\mathrm{H}}(t_\mathrm{d}, t_\mathrm{i}) \tag{1.124}$$

Here, we used the fact that the overlap operator with respect to Eq. (1.57) can always be cast as a phase and a displacement operator

$$\hat{U}_{0,1}^\dagger(t_\mathrm{d}, t_\mathrm{i})\hat{U}_{0,2}(t_\mathrm{d}, t_\mathrm{i}) = \mathrm{e}^{\mathrm{i}\phi_0}\hat{D}(\Delta\boldsymbol{\chi}_0)\,. \tag{1.125}$$

When we change into the interaction picture we also need to replace the momentum and position operators in the perturbation Hamiltonian by the solution of the Heisenberg equations of motion, generated by $\hat{H}_0$, which, as before, take the form given in Eq. (1.66). This is denoted by the subscript H on the time-evolution operators.

Next, we interchange the displacement operator with the time-evolution operator to its left. Since $\hat{D}$ is unitary, we need to replace

$$H'_1(\hat{\boldsymbol{\xi}}(t), t) \rightarrow \hat{D}^\dagger(\Delta\boldsymbol{\chi}_0)H'_1(\hat{\boldsymbol{\xi}}(t), t)\hat{D}(\Delta\boldsymbol{\chi}_0)\,, \tag{1.126}$$

that is, by using Eq. (A.14), we substitute

$$\boldsymbol{r}_\mathrm{c}(t) \rightarrow \Delta\boldsymbol{\chi}_0^r + \frac{\Delta\boldsymbol{\chi}_0^p}{m}t + \boldsymbol{r}_\mathrm{c}(t)$$
$$\boldsymbol{p}_\mathrm{c}(t) \rightarrow \Delta\boldsymbol{\chi}_0^p + \boldsymbol{p}_\mathrm{c}(t) \tag{1.127}$$

in the equations of motion for $\hat{H}_1'$. We are now in the position to apply the Magnus expansion to the product $\hat{U}_{1,\mathrm{H}}^\dagger \hat{U}_{2,\mathrm{H}}$ in exact correspondence to the discussion of the closed unperturbed interferometer. This results in the general expression

$$\hat{U}_1^\dagger(t_\mathrm{d}, t_\mathrm{i})\hat{U}_2(t_\mathrm{d}, t_\mathrm{i}) = \hat{D}(\Delta\boldsymbol{\chi}_0)\exp\left\{\sum_{n=0}^\infty \epsilon^n \hat{\phi}_n\right\}, \qquad (1.128)$$

which consists of a displacement operator multiplied by the exponential of the infinite series obtained by the Magnus expansion of the overlap operator. One could argue that it would be advantageous to combine the product to one exponential. However, in case $\Delta\boldsymbol{\chi}_0$ is large, the expectation value of Eq. (1.128) is simpler to calculate. In contrast, if $\Delta\boldsymbol{\chi}_0$ scales with ϵ, we can combine the product of the displacement operator and the exponential using the BCH formula to the desired order. In conclusion, we reduced the problem of an open interferometer to the closed situation already discussed in the previous sections.

Example 4: Generalized mitigation strategy for open interferometers

In example 3 we considered an MZ interferometer in the gravitational field up to second order in the inverse of the Earth's radius. As manifested by the nonvanishing operator-valued terms in the overlap operator, this interferometer does not close. It was shown in Ref. [118] that by a slight modification of the momentum transfer in the π pulse, the interferometer can be forced to close again. We will show that this result can be generalized to mitigate also the effect of the cubic contributions in the Taylor expansion of the gravitational potential of the Earth as well as the influence of nearby mass distributions by modifying additionally the momentum transfer of the last laser pulse.

Gravitational potential of the earth

We first consider the gravitational potential of the Earth. As was discussed in example 3, it is characterized by its smoothness, meaning that each term in the Taylor expansion decreases by another factor of $1/R$. Let the perturbing potential again be given by

$$V(\hat{\boldsymbol{r}}) = \frac{1}{2}m\Gamma_{ij}^{(1)}\,\hat{x}_i\hat{x}_j + \frac{1}{2}m\Gamma_{ijk}^{(2)}\,\hat{x}_i\hat{x}_j\hat{x}_k \qquad (1.129)$$

where $\boldsymbol{\Gamma}^{(1)}$ and $\boldsymbol{\Gamma}^{(2)}$ are chosen fully symmetric. We calculate the overlap operator in the following up to second order in $\Gamma^{(1)}$ and to first order in $\Gamma^{(2)}$. Consistency conditions will be derived at the end of this example but for the gravitational potential of the Earth they will be well satisfied.

The overlap operator for the open unperturbed interferometer with $\boldsymbol{k} \to \boldsymbol{k} + \Delta\boldsymbol{k}_1$ for the middle π pulse and $\boldsymbol{k} \to \boldsymbol{k} + \Delta\boldsymbol{k}_2$ for the third $\pi/2$ pulse has been calculated already in example 1. In Eq. (1.92) we found explicit expressions for the displacements, which we provide again here,

$$\begin{aligned}
\Delta\boldsymbol{\chi}_0^r &= -2(\Delta\boldsymbol{v}_{\mathrm{r}2} - \Delta\boldsymbol{v}_{\mathrm{r}1})T \\
\Delta\boldsymbol{\chi}_0^p &= m(\Delta\boldsymbol{v}_{\mathrm{r}2} - 2\Delta\boldsymbol{v}_{\mathrm{r}1})\,.
\end{aligned} \qquad (1.130)$$

Next, we repeat the calculation performed for the gravitational potential with harmonic and cubic perturbations but in contrast to example 3 we need to account for the open unperturbed interferometer. In this calculation we will not specify the phase, but rather focus on the operator-valued terms. To close again the interferometer, $\Delta\boldsymbol{\chi}_0$ obviously must be chosen of the order of $\mathcal{O}(\Gamma^{(1)}, \Gamma^{(2)})$. Thus, we combine the two exponentials in Eq. (1.128) to a single one with the help of the BCH series. Comparison with the calculation in example 3 shows that $\hat{\phi}_1 \sim \Gamma^{(1)}\hat{\xi} + \Gamma^{(2)}\hat{\xi} + \Gamma^{(2)}\hat{\xi}\hat{\xi}$ and $\hat{\phi}_2 \sim [\Gamma^{(1)}]^2\hat{\xi}$. Consequently, all commutators in the BCH either result in c-numbers, thus phases which are not discussed in the present consideration, or lead to terms which scale beyond the order considered here. In conclusion we can write the result as

$$\hat{U}_1^\dagger(t_{\mathrm{d}}, t_{\mathrm{i}})\hat{U}_{\mathrm{d}}(t_{\mathrm{d}}, t_{\mathrm{i}}) = \exp\left\{\mathrm{i}\left(\varphi - \frac{1}{\hbar}\Delta\boldsymbol{\chi}^{\mathrm{T}}\boldsymbol{\mathcal{J}}\hat{\boldsymbol{\xi}} - \frac{1}{2\hbar}\hat{\boldsymbol{\xi}}^{\mathrm{T}}\boldsymbol{A}\hat{\boldsymbol{\xi}}\right)\right\} \tag{1.131}$$

where φ is some phase and

$$\Delta\boldsymbol{\chi} = \Delta\boldsymbol{\chi}_0 + \Delta\boldsymbol{\chi}_1 + \Delta\boldsymbol{\chi}_2 + \Delta\boldsymbol{\chi}_3\,. \tag{1.132}$$

The displacements are defined in App. B.3.3 and calculated for the MZ interferometer with well defined launching velocity $\boldsymbol{v}_0$, not to be confused with the small uncontrollable initial velocity, whose influence will be discussed at the end of this example. It is important to recall that for the calculation in App. B.3.3 we not only have to consider the modified trajectories (due to the modified laser pulses), but also need to take into account the fact that the unperturbed interferometer is open. At the beginning of this section we showed that this is done by changing the classical trajectories according to Eq. (1.127) on path 1. Note that $\Delta\boldsymbol{\chi}_0 \sim \Gamma^{(1)}$, thus to the order considered here this modification is only necessary for $\Delta\boldsymbol{\chi}_1$, for the other displacements it is even sufficient to integrate along the trajectories of the standard closed MZ interferometer. Furthermore, we introduce the notation

$$(\boldsymbol{\Gamma}^{(2)}\boldsymbol{a})_{ij} = \Gamma^{(2)}_{ijk}a_k \quad \text{and} \quad (\boldsymbol{b}^{\mathrm{T}}\boldsymbol{\Gamma}^{(2)}\boldsymbol{a})_i = \Gamma^{(2)}_{ijk}b_j a_k \tag{1.133}$$

for vectors $\boldsymbol{a}$ and $\boldsymbol{b}$ and recall that $\boldsymbol{\Gamma}^{(2)}$ is fully symmetric. In order to remove the operator-valued terms linear in $\hat{\boldsymbol{\xi}}$, we solve for $\Delta\boldsymbol{\chi} = 0$ with the result

$$\Delta\boldsymbol{v}_{\mathrm{r}1} = -\frac{1}{2}\boldsymbol{\Gamma}^{(1)}\boldsymbol{v}_{\mathrm{r}}T^2 + \frac{1}{24}[\boldsymbol{\Gamma}^{(1)}]^2\boldsymbol{v}_{\mathrm{r}}T^4 + \frac{5}{8}\boldsymbol{v}_{\mathrm{r}}^{\mathrm{T}}\boldsymbol{\Gamma}^{(2)}(\boldsymbol{g}T - 2\boldsymbol{v}_0 - \boldsymbol{v}_{\mathrm{r}})T^3$$

$$\Delta\boldsymbol{v}_{\mathrm{r}2} = -\frac{1}{4}\boldsymbol{v}_{\mathrm{r}}^{\mathrm{T}}\boldsymbol{\Gamma}^{(2)}(2\boldsymbol{g}T - 2\boldsymbol{v}_0 - \boldsymbol{v}_{\mathrm{r}})T^3\,, \tag{1.134}$$

which can easily be verified by substituting Eq. (1.134) together with the expressions calculated in App. B.3.3 back into Eq. (1.132). Remarkably for a symmetric atomic fountain experiment as depicted in Fig. 1.5 with $\boldsymbol{v}_0 = \boldsymbol{g}T - \boldsymbol{v}_{\mathrm{r}}/2$ we find $\Delta\boldsymbol{v}_{\mathrm{r}2} = 0$, thus it is sufficient to only modify the momentum transfer of the π pulse.
For the validity of the perturbative approach some conditions have to be fulfilled which we discuss next. By comparing the sizes of the terms in the Hamiltonian together with a dimension analysis, we conclude

$$\Gamma^{(1)}T^2 \ll 1\,, \qquad \Gamma^{(2)}gT^4 \ll 1\,, \qquad \Gamma^{(2)}gT^2 \ll \Gamma^{(1)}\,, \tag{1.135}$$

and we used $v_{\mathrm{r}} \ll gT$. The first two conditions ensure that the perturbative treatment of harmonic and cubic terms is valid individually, the third makes sure that a treatment to first order in $\Gamma^{(2)}$ and to second order in $\Gamma^{(1)}$ is consistent. For the gravitational potential of the Earth all these conditions are satisfied, in particular we even showed in example 3 that the second-order terms in $\Gamma^{(1)}$ are of the same size as the first-order terms in $\Gamma^{(2)}$.

Gravitational potential of nearby mass distributions

In the case of nearby mass distributions, however, the situation can become quite different. The potential is in general not sufficiently smooth so that a Taylor expansion of the potential over the size of the interferometer is not valid anymore. Instead, we employ the local harmonic approximation, which was introduced in Eq. (1.73), that is, we expand the potential locally around the trajectories of the wave packets up to second order. For the gravitational potential $V = m\Phi^{(\mathrm{s})}$ which we add to the perturbing potential, Eq. (1.129), we obtain the first-order expression

$$\hat{\phi}_1^{(\mathrm{s})} = \varphi^{(\mathrm{s})} - \frac{\mathrm{i}}{\hbar}m \oint \mathrm{d}t\, \boldsymbol{g}^{(\mathrm{s})}(t)\hat{\bar{\boldsymbol{r}}}(t) - \frac{\mathrm{i}}{2\hbar}m \oint \mathrm{d}t\, \hat{\bar{\boldsymbol{r}}}(t)^{\mathrm{T}}\boldsymbol{\Gamma}^{(\mathrm{s})}(t)\hat{\bar{\boldsymbol{r}}}(t) \qquad (1.136)$$

where $g_i^{(\mathrm{s})}(t) = \partial_i\Phi^{(\mathrm{s})}(\boldsymbol{r})|_{\boldsymbol{r}=\boldsymbol{r}_{\mathrm{c}}(t)}$ and $\Gamma_{ij}^{(\mathrm{s})}(t) = \partial_i\partial_j\Phi^{(\mathrm{s})}(\boldsymbol{r})|_{\boldsymbol{r}=\boldsymbol{r}_{\mathrm{c}}(t)}$. This results in the displacements

$$\Delta\boldsymbol{\chi}_{(\mathrm{s})}^p = -m \oint \mathrm{d}t\, \boldsymbol{g}^{(\mathrm{s})}(t)$$

$$\Delta\boldsymbol{\chi}_{(\mathrm{s})}^r = \oint \mathrm{d}t\, \boldsymbol{g}^{(\mathrm{s})}(t)t\,. \qquad (1.137)$$

Since the absolute value of the gravitational potential of the nearby mass distributions is extremely small compared to the gravitational potential of the Earth, a first-order calculation (in the Magnus expansion) is sufficient. Furthermore, we can again evaluate all functions at the trajectories of the standard MZ interferometer. Choosing the recoil velocities in Eq. (1.130) to compensate the expressions in Eq. (1.137) results in the additional recoil velocities

$$\Delta\boldsymbol{v}_{\mathrm{r}1}^{(\mathrm{s})} = \oint \mathrm{d}t\, \boldsymbol{g}^{(\mathrm{s})}(t)\left(\frac{t}{2T} - 1\right)$$

$$\Delta\boldsymbol{v}_{\mathrm{r}2}^{(\mathrm{s})} = \oint \mathrm{d}t\, \boldsymbol{g}^{(\mathrm{s})}(t)\left(\frac{t}{T} - 1\right), \qquad (1.138)$$

which can simply be added to the expressions in Eq. (1.134) to the order considered here. For completeness we also state the contributions quadratic in $\hat{\boldsymbol{\xi}}$

$$\boldsymbol{A}_{(\mathrm{s})}^{rr} = m \oint \mathrm{d}t\, \boldsymbol{\Gamma}^{(\mathrm{s})}(t), \quad \boldsymbol{A}_{(\mathrm{s})}^{rp} = \oint \mathrm{d}t\, \boldsymbol{\Gamma}^{(\mathrm{s})}(t)t, \quad \boldsymbol{A}_{(\mathrm{s})}^{pp} = \frac{1}{m} \oint \mathrm{d}t\, \boldsymbol{\Gamma}^{(\mathrm{s})}(t)t^2\,. \qquad (1.139)$$

With Eq. (1.138) we found two simple expressions for how we should change the momentum transfer of the laser pulses in an experiment to close the interferometer trajectories. Note that $\boldsymbol{g}^{(s)}$ in general is not aligned with the z axis so that also the direction

of the momentum transfer must be slightly changed. This should be experimentally achievable using tip-tilt mirrors [118].

Initial conditions

With Eq. (1.134) and Eq. (1.138) we found a way to eliminate all terms linear in $\hat{\boldsymbol{\xi}}$. However, the overlap operator still contains quadratic terms. Fortunately, phase contributions dependent on the initial conditions originating from these terms are small as we will show in the following. To this end, we write as in Eq. (1.79)

$$|\psi\rangle = \hat{D}(\boldsymbol{\chi}_\mathrm{i})|\tilde{\psi}\rangle \tag{1.140}$$

where $\boldsymbol{\chi}_\mathrm{i} = (\boldsymbol{r}_\mathrm{i}, m\boldsymbol{v}_\mathrm{i})^\mathrm{T}$ describes the small uncontrollable initial condition of the state and $\langle\tilde{\psi}|\hat{\boldsymbol{\xi}}|\tilde{\psi}\rangle = 0$. Using Eq. (A.14) for the expectation value of the overlap operator introduces the additional phase $\varphi_\mathrm{i} = -\boldsymbol{\chi}_\mathrm{i}^\mathrm{T}\boldsymbol{A}\boldsymbol{\chi}_\mathrm{i}/2\hbar$. With the help of the explicit expressions derived in App. B.3.3, this phase can be shown to be additionally suppressed by the factor $v_\mathrm{i}/v_\mathrm{r} \ll 1$ compared to those contributions which would arise without employing the compensation technique.

Contrast

Finally, we calculate the contrast after employing the elimination technique. With the help of the cumulant expansion we obtain

$$C = \exp\left\{-\frac{1}{2}\mathrm{Var}\left(\frac{1}{2\hbar}\hat{\boldsymbol{\xi}}^\mathrm{T}\boldsymbol{A}\hat{\boldsymbol{\xi}}\right)\right\}. \tag{1.141}$$

The variance is most easily calculated in Wigner representation for a general Gaussian input state [125]

$$W(\boldsymbol{r}, \boldsymbol{p}) = \frac{1}{\sqrt{(2\pi)^6\det(\boldsymbol{\Sigma})}}\exp\left\{-\frac{1}{2}\boldsymbol{\xi}^\mathrm{T}\boldsymbol{\Sigma}^{-1}\boldsymbol{\xi}\right\} \tag{1.142}$$

by using the Wigner-Weyl representation [126] of the operator in Eq. (1.141), with the result

$$\ln(C) = -\frac{1}{4\hbar^2}\mathrm{tr}\left(\boldsymbol{A}\overline{\boldsymbol{\Sigma}}\boldsymbol{A}\overline{\boldsymbol{\Sigma}}^*\right). \tag{1.143}$$

In Eq. (1.143) we introduced the abbreviation

$$\overline{\boldsymbol{\Sigma}} = \boldsymbol{\Sigma} + \frac{\mathrm{i}\hbar}{2}\boldsymbol{\mathcal{J}}, \tag{1.144}$$

which is a positive semidefinite matrix [127]. The trace in Eq. (1.143) is always larger than or equal to zero, consequently $C \leq 0$ as it should. Typically, this loss of contrast which results from the diminished overlap due to different expansion dynamics along the paths of the interferometer is small and can be disregarded.

1.3.5. Particle-particle interaction

When Bose-Einstein condensates are used as highly-coherent atom sources one needs to account for the mutual interaction between the particles. Fortunately, in many cases the wave function is initially allowed to expand (in position space) before the first laser pulse is applied, which significantly reduces the strength of the particle-particle interaction. It is often sufficient to treat the BEC on a mean-field level, thus one propagates the order parameter with the Gross-Pitaevskii equation until right before the first laser pulse. From that point on one neglects interactions and the Schrödinger equations provides a sufficiently accurate description. For that reason, the theory of this chapter can still be employed when this propagated GP state is used as initial input state. Note that this is only true for perfect laser pulses so that the number of particles on each branch is perfectly balanced and mean-field phases cancel. Furthermore, one has to make sure that distortion effects and phases can be neglected that arise from the split of the order parameter in two wave packets.

In the next chapter we will discuss the impact of particle-particle interactions in much more detail by starting from a second-quantized treatment. This will help us assess interaction effects, some of which are spurious, others might even be used to increase the performance of an atom interferometer.

1.4. Summary

In this chapter we considered two powerful formalisms to calculate phase and contrast of atom light-pulse interferometers.

The first method, which has already been used by several authors, simplifies the theoretical treatment of an interferometer by describing the evolution in comoving frames. The transformation to these frames removes the motion due to linear potentials and the laser pulses, hence the local wave packets only evolve according to residual nonlinear potentials. We first provided a straightforward derivation in which we obtained the result by mere operator algebra. Furthermore, we derived an exact formula for general potentials which does not rely on the local harmonic approximation. This method is particularly suited to be applied in the case of potentials smooth in a neighborhood of the local wave packets but possibly strongly anharmonic over the extent of the interferometer. Even in the case of completely general potentials, the formalism extremely decreases the computational effort in numerically exact simulations.

In the second part of this chapter we presented a new approach which is able to account for arbitrary perturbation Hamiltonians, however, proportional to a small factor ϵ. By deriving a generalization of the Magnus expansion, we arrived at an elegant perturbative expansion of phase and contrast in powers of ϵ. In a number of examples we illustrated the method and showed to what extent even complicated calculations are streamlined within this formalism. Finally, we discussed mitigation strategies for gravity gradients and generalized the methods to take into account the effect of anharmonicities in the gravitational potential of the Earth as well as the influence of nearby mass sources.

Chapter 2

Bose-Einstein condensation

Bose-Einstein condensation (BEC) was first proposed by Einstein, when he extended the ideas of the Indian physicist Bose [128], who investigated photons at thermal equilibrium, to massive noninteracting particles [129] which are nowadays called bosons. As a result of the exchange symmetry of the bosonic wave function, all particles should occupy the lowest energy eigenfunction at ultralow temperatures, leading to a macroscopic matter wave.

Intensive work was required on the theoretical side [130, 131] and sophisticated cooling techniques had to be developed until 70 years later BEC was for the first time experimentally discovered in dilute alkali gases in 1995 by Cornell, Wieman, and Ketterle [132, 133]. They were awarded the Nobel Prize only six years later [134, 135].

Ultracold quantum gases offer remarkable controllability. Not only parameters like particle number or the trap frequency can be experimentally well controlled but even interactions among the particles can be tuned via Feshbach resonances [136] from attractive to strongly repulsive, thus providing unique possibilities to study many-body effects.

A Bose-Einstein condensate can be viewed as a coherent nonlinear matter wave which gives rise to phenomena like solitons [137] or the formation of vortices [138]. The extraordinary coherence properties also make BECs a preferable source for atom interferometry.

Nowadays, Bose-Einstein condensates are routinely produced in many laboratories for many types of atomic species all over the world.

In this chapter we will shortly review the theoretical framework of Bose-Einstein condensation. Starting with the mathematical definition of BEC in Sec. 2.1, we will revisit the question of relative phase between two BECs which have never "seen" each other in Sec. 2.2. The answer to this question will guide us to the philosophical perspective on Bose-Einstein condensation which is suited best for the description of atom interferometry. Finally, in Sec. 2.3 we will briefly discuss the stationary and time-dependent Thomas-Fermi approximation.

2.1. Definition of Bose-Einstein condensation

What is Bose-Einstein condensation? At first sight the answer seems to be straightforward. A system is Bose-Einstein condensed if there exists a macroscopically occupied energy eigenstate. This definition, however, becomes highly nontrivial in interacting systems, where single-particle states are not defined anymore and the idea of BEC becomes obscure.

2.1.1. Penrose-Onsager criterion

These problems where resolved in the seminal work by Penrose and Onsager [139] in which they resorted to the (time-dependent) reduced one-particle density matrix

$$\rho\left(\boldsymbol{r}, \boldsymbol{r}', t\right) = \langle \hat{\Psi}^\dagger(\boldsymbol{r}')\hat{\Psi}(\boldsymbol{r})\rangle. \tag{2.1}$$

Here, $\hat{\Psi}(\boldsymbol{r})$ is the field operator in second quantization that annihilates a particle in the state $|\boldsymbol{r}\rangle$ and satisfies the well-known bosonic commutation relations

$$\left[\hat{\Psi}(\boldsymbol{r}), \hat{\Psi}^\dagger(\boldsymbol{r}')\right] = \delta(\boldsymbol{r} - \boldsymbol{r}') \qquad \text{and} \qquad \left[\hat{\Psi}(\boldsymbol{r}), \hat{\Psi}(\boldsymbol{r}')\right] = 0, \tag{2.2}$$

reflecting the symmetry of the many-particle wave function under exchange of two particles.

A system is Bose-Einstein condensed if the one-particle density matrix shows exactly one macroscopic eigenvalue N_0, that is,

$$\int \mathrm{d}^3\boldsymbol{r}'\, \rho\left(\boldsymbol{r}, \boldsymbol{r}', t\right)\phi_j(\boldsymbol{r}', t) = N_j\phi_j(\boldsymbol{r}, t) \quad \text{with one } N_0 \sim \mathcal{O}(N) \tag{2.3}$$

in the thermodynamic limit and all others $N_j \sim \mathcal{O}(1)$ for $j \neq 0$, where N is the total number of particles in the system. The eigenfunctions $\phi_j(\boldsymbol{r}, t)$ are referred to as *natural orbitals*. They constitute a complete set of orthogonal functions as the one-particle density matrix is hermitian. The criterion in Eq. (2.3) serves as a very general definition of Bose-Einstein condensation, valid for interacting systems even out of equilibrium. For mesoscopic systems the Penrose-Onsager criterion is applicable in the form that one N_0 must exist which is large compared to all other eigenvalues.

We are able to reconcile this rather mathematical definition with the intuitive one stated at the beginning of this section when we represent the Schrödinger-picture field operator in the unambiguous basis of natural orbits

$$\hat{\Psi}(\boldsymbol{r}) = \sum_j \hat{a}_j(t)\phi_j(\boldsymbol{r}, t), \tag{2.4}$$

where the annihilation operator $\hat{a}_j(t)$ satisfies the standard commutation relations

$$\left[\hat{a}_n(t), \hat{a}_m^\dagger(t)\right] = \delta_{nm}. \tag{2.5}$$

A system is said to have undergone Bose-Einstein condensation when one mode function of the field operator represented in the basis of natural orbitals is occupied by a

macroscopic fraction of the total particle number. This function is called *condensate mode*.

At first sight, the Penrose-Onsager criterion might not seem helpful as it cannot predict the existence of BEC for a given Hamiltonian. However, it does not only serve as a stringent mathematical definition of Bose-Einstein condensation but is also the starting point for the construction of modern number-conserving theories which will be discussed in Sec. 2.2.2.

Finally, we mention that the concept of *off-diagonal long-range order* [140] is also closely related to the definition of Bose-Einstein condensation in the case of homogeneous systems.

2.1.2. Hamiltonian

In the previous section we discussed the Penrose-Onsager criterion as a definition of Bose-Einstein condensation. We now specify the Hamiltonian of an interacting BEC which again is most easily done in second quantization. For bosons of mass m subjected to an external potential $V(\boldsymbol{r}, t)$ the Hamiltonian reads

$$\hat{H} = \int \mathrm{d}^3\boldsymbol{r}\ \hat{\Psi}^\dagger(\boldsymbol{r})\mathcal{H}(\boldsymbol{r}, t)\hat{\Psi}(\boldsymbol{r}) + \frac{g}{2}\int \mathrm{d}^3\boldsymbol{r}\ \hat{\Psi}^\dagger(\boldsymbol{r})\hat{\Psi}^\dagger(\boldsymbol{r})\hat{\Psi}(\boldsymbol{r})\hat{\Psi}(\boldsymbol{r}) \tag{2.6}$$

with the single-particle operator

$$\mathcal{H}(\boldsymbol{r}, t) = -\frac{\hbar^2}{2m}\Delta + V(\boldsymbol{r}, t)\,. \tag{2.7}$$

In addition, we replaced the general two-body interaction potential by a contact potential

$$U(\boldsymbol{r} - \boldsymbol{r}') = g\,\delta(\boldsymbol{r} - \boldsymbol{r}') \tag{2.8}$$

where $g = 4\pi\hbar^2 a_s/m$ and the parameter a_s is the s-wave scattering length. This substitution is generally a good approximation for weakly interacting, dilute samples and short-range interactions [141]. Note that we did not include three- and higher-order interaction terms. These can be neglected in most cases, where the samples are dilute enough [142].

With the help of the Heisenberg equation of motion

$$\mathrm{i}\hbar\frac{\mathrm{d}}{\mathrm{d}t}\hat{\Psi}(\boldsymbol{r}, t) = \left[\hat{\Psi}(\boldsymbol{r}, t), \hat{H}\right] \tag{2.9}$$

we arrive at the dynamical equation for the field operator $\hat{\Psi}(\boldsymbol{r}, t)$

$$\mathrm{i}\hbar\frac{\mathrm{d}}{\mathrm{d}t}\hat{\Psi}(\boldsymbol{r}, t) = \left(-\frac{\hbar^2}{2m}\Delta + V(\boldsymbol{r}) + g\,\hat{\Psi}^\dagger(\boldsymbol{r}, t)\hat{\Psi}(\boldsymbol{r}, t)\right)\hat{\Psi}(\boldsymbol{r}, t)\,, \tag{2.10}$$

where we used the relations in Eq. (2.2). This equation accounts for the full quantum behavior of the system. In the next section we will discuss the conceptual background of Bose-Einstein condensation, which eventually leads to the Gross-Pitaevskii equation and its generalizations as an approximate solution to Eq. (2.10) for a Bose-Einstein condensed system.

2.2. Conceptual background of Bose-Einstein condensation

We begin by revisiting the question raised by Anderson in Ref. [143] if two Bose-Einstein condensates which have never "seen" each other exhibit a well defined relative phase. On a fundamental level this breaks down to the question whether the quantum state for the two condensates (for simplicity we only consider two modes) is more like $|\Psi\rangle = \left|\overline{N}/2, \overline{N}/2\right\rangle$ or $|\Psi\rangle = |N/2, N/2\rangle$. In the former case each condensate is in a coherent state which consists of a superposition of Fock states with only on average $\overline{N}$ particles but a well defined relative phase. In the latter case the system is described by a twin-Fock state with exactly N particles and there is no predetermined phase relation.

In Ref. [144] it was pointed out that the question is only meaningful when a measurement is performed. After some numerical work done in Ref. [145], it was shown in Ref. [146] that a definite relative phase between two twin-Fock states with initially ill-defined phase relation builds up in the measurement process. In each run of the experiment the phase is completely random and unpredictable. Thus, the two states cannot be distinguished experimentally. Furthermore, a dynamical spread of the relative phase was predicted in Ref. [144], which quickly removes any predetermined phase relation.

In fact both philosophical perspectives can be used to construct successful formalisms for the description of Bose-Einstein condensates, namely $U(1)$ symmetry-breaking methods as opposed to number-conserving theories. In the following we will therefore compare both methods with the aim to understand which of them is better suited for the description of atom interferometry.

2.2.1. $U(1)$ symmetry-breaking methods

The Hamiltonian in Eq. (2.6) is invariant under global $U(1)$ transformations. We can break this symmetry by adding the infinitesimal sources [147]

$$\hat{H}_{\mathrm{S}} = \epsilon \int \mathrm{d}^3\boldsymbol{r} \, \left(\eta^*(\boldsymbol{r})\hat{\Psi}(\boldsymbol{r}) + \eta(\boldsymbol{r})\hat{\Psi}^\dagger(\boldsymbol{r}) \right) \tag{2.11}$$

to the Hamiltonian. A system is then said to exhibit spontaneous symmetry breaking (SSB) if

$$\lim_{\epsilon \to 0} \lim_{N \to \infty} \langle \hat{\Psi}(\boldsymbol{r}) \rangle_\epsilon = \psi(\boldsymbol{r}, t) \neq 0 \tag{2.12}$$

where $N \to \infty$ denotes the appropriate thermodynamic limit. The spatial- and time-dependent function ψ is called the *order parameter* of the system. The average in Eq. (2.12) is understood as *Bogoliubov quasi average* [147] which implicitly includes the symmetry-breaking term, Eq. (2.11). Note that spontaneous symmetry breaking is always defined in the thermodynamic limit. For mesoscopic systems or if we interchanged the limits in Eq. (2.12), the result would always be zero.

Showing that SSB implies BEC, one furthermore realizes that the order parameter is equivalent to the condensate mode function in the thermodynamic limit defined via the

Penrose-Onsager criterion. Assuming spontaneous symmetry breaking, we separate the Schrödinger-picture-field operator

$$\hat{\Psi}(\boldsymbol{r}) = \psi(\boldsymbol{r}, t) + \delta\hat{\Psi}(\boldsymbol{r}, t) \tag{2.13}$$

into the order parameter and the fluctuation operator $\delta\hat{\Psi}(\boldsymbol{r}, t)$ with, by definition, zero expectation value. Bogoliubov showed [148] that adding infinitesimal sources and this *Bogoliubov operator shift* becomes asymptotically equivalent inside all correlation functions. The fluctuation operator then attains bosonic commutation relations.

We will explain in Sec. 2.2.2 that not only SSB implies BEC but that Bose-Einstein condensation is also sufficient for spontaneous symmetry breaking. Thus, we conclude that if a system exhibits BEC, an infinitesimal perturbation of the form Eq. (2.11) is enough to render the replacement, Eq. (2.13), asymptotically exact with a nonvanishing order parameter inside all correlation functions.

The philosophy behind the $U(1)$ symmetry-breaking approach to BEC is the assumption that it is justified to follow the same concept for mesoscopic systems with finite particle number [149]. In this sense the approach is an extrapolation from the thermodynamic limit to finite systems. It is important to keep in mind that this assumption leads to the problems discussed later in this section. However, if carefully addressed, the $U(1)$ symmetry-breaking approach has proven to be a viable method for the description of Bose-Einstein condensates. Guided by these insights, we will derive the Gross-Pitaevskii equation and its generalization in the following.

Gross-Pitaevskii equation

When we substitute Eq. (2.13) into Eq. (2.10) and assume a negligible fraction of noncondensate atoms, that is, one neglects the fluctuation operator, we arrive at the celebrated Gross-Pitaevskii equation (GPE)

$$i\hbar\frac{\partial}{\partial t}\psi(\boldsymbol{r}, t) = \left(-\frac{\hbar^2}{2m}\Delta + V(\boldsymbol{r}) + g\left|\psi(\boldsymbol{r}, t)\right|^2\right)\psi(\boldsymbol{r}, t)\,, \tag{2.14}$$

first derived by Gross and Pitaevskii [150, 151] to study qualitatively the behavior of superfluid helium. Since the discovery of Bose-Einstein condensation in dilute, weakly interacting gases this equation has been applied with enormous success as a description for the ground state and the dynamical properties like the existence and structure of vortices.

Because of the similarity to the Schrödinger equation in position representation, Eq. (2.14) is sometimes referred to as *nonlinear Schrödinger equation*.

Beyond the Gross-Pitaevskii approximation

For completeness we shortly comment upon methods which generalize the Gross-Pitaevskii equation to include condensate, thermal effects, quantum fluctuations, as well as their mutual interaction. For a comprehensive review on Bose-Einstein condensates at finite temperature we refer the reader to Ref. [152].

In the *Hartree-Fock Bogoliubov approach* [112, 148, 153] one substitutes the decomposition, Eq. (2.13), into the Hamiltonian, Eq. (2.6), retains all products of the fluctuation

operator, but performs decoupling approximations motivated by Wick's theorem [154, 155]. By this procedure the Hamiltonian becomes quadratic and can be diagonalized with the help of the Bogoliubov transformation. The result is a dynamical equation, similar to the Gross-Pitaevskii equation, however, coupled to a system of Bogoliubov-de Gennes equations for each noncondensate mode. Note that the *anomalous average* $m(\boldsymbol{r}) = \langle \delta \hat{\Psi}(\boldsymbol{r}) \delta \hat{\Psi}(\boldsymbol{r}) \rangle$ needs to be appropriately renormalized [156]. Even though successfully applied to various situations, e.g. in the self-consistent simulation of the ground state of a BEC interacting with a thermal cloud [157], one problem is the enormous computational effort needed to propagate a large number of Bogoliubov modes for time-dependent situations. Furthermore, as a result of the decoupling approximation, the interaction between condensate and thermal cloud are only taken into account at a mean-field level.

These problems were solved within the *ZNG* theory named after Zaremba, Nikuni and Griffin [158], see also the excellent book [159] and the references therein. In this approach the generalized Gross-Pitaevskii equation which describes the condensate is coupled to a dynamical equation in phase space similar to the Boltzmann equation. The interaction between condensate and thermal cloud as well as among noncondensate atoms is accounted for by collision integrals. Note, however, that this theory is only valid when thermal effects are large compared to quantum fluctuations, that is, for sufficiently high temperatures.

Semiclassical field simulations [160] and *projected GPE methods* [161, 162] generalize the ZNG formalism. At sufficiently high temperatures the set of modes which are considerably occupied define an energy cut-off which is important to choose correctly. The respective annihilation operators are then replaced by c-numbers. Time- and spatial averaging over the nonlinear interplay between the modes allows to compare the simulation to the outcome of experiments. These methods were reviewed in Ref. [163]. The *truncated Wigner approximation* [164] additionally accounts for the quantum fluctuations of the modes by deriving a phase-space-distribution equation for the field operator, followed by the truncation at second-order derivatives. Finally, one converts the equation into a stochastic equation of a form similar to the Gross-Pitaevskii equation.

Problems of the $U(1)$ symmetry-breaking methods

There are several severe problems associated with the notion of spontaneous $U(1)$ symmetry-breaking in the context of Bose-Einstein condensation.

First, when we substitute Eq. (2.13) into Eq. (2.3), the order parameter $\psi(\boldsymbol{r}, t)$ can only be identified as the condensate mode when

$$\int \mathrm{d}^3 \boldsymbol{r} \, \delta \hat{\Psi}^\dagger(\boldsymbol{r}, t) \psi(\boldsymbol{r}, t) = 0 \qquad (2.15)$$

during the time-evolution. This is, however, not the case in mesoscopic systems.

Second, when we substitute the decomposition, Eq. (2.13), into the Hamiltonian, Eq. (2.6), and keep terms to second order in the fluctuation operator, it turns out that the resulting Hamiltonian cannot be diagonalized. This problem, also referred to as the "problem of the missing eigenvector", was solved in Ref. [165] by complementing

the incomplete set of eigenvectors to a full basis. This leads to a linear divergence of fluctuations which is interpreted as phase diffusion [75] but quickly renders the Bogoliubov approximation inconsistent.

Third, we assumed a nonvanishing expectation value of the field operator. This requires that the system is in a superposition of different particle-number states. However, an ultracold gas, i.e. a Bose-Einstein condensate *plus* the thermal cloud, should be considered a closed system [166] with a definite number of particles.

Motivated by these problems Castin, Dum and Gardiner proposed *number-conserving methods* which are discussed in the next section. These approaches are much more intuitive, however, mathematically more cumbersome.

2.2.2. Number-conserving approaches: Theory of Castin, Dum and Gardiner

In these theories, put forward in Refs. [167, 168], one explicitly enforces the orthogonality between condensate mode and fluctuation operator by using the Penrose-Onsager criterion as a starting point for the construction of the theory. This leads to a non-local Bogoliubov Hamiltonian which, as opposed to the symmetry-breaking approach, can now be diagonalized. Furthermore, we note that in this approach the number of particles is conserved by construction. In Ref. [169, 170] this method was further advanced to allow a self-consistent treatment of condensate and noncondensate dynamics and was generalized to describe n-component condensates in Ref. [171]. The number-conserving Bogoliubov groundstate was investigated in Refs. [172, 173]. We also refer the reader to the overview of number-conserving theories in Ref. [174]. In the following brief discussion of this approach we mainly follow Ref. [169].

To this end, we assume a definite number of N particles in a closed system and write the Schrödinger-picture field operator as

$$\hat{\Psi}(\boldsymbol{r}) = \hat{a}_0(t)\phi_0(\boldsymbol{r}, t) + \delta\hat{\psi}(\boldsymbol{r}, t)\,. \tag{2.16}$$

Here, the condensate mode is identified by the Penrose-Onsager criterion. In mesoscopic systems it is the eigenvector of the reduced density matrix with the largest eigenvalue. Note the main difference between the Eqs. (2.16) and (2.13). In the number-conserving approach we do not replace the annihilation operator of the condensate mode function by a c-number. Since we are not adding symmetry-breaking terms, the $U(1)$ symmetry and the number of particles are preserved.

In the next step we have to find a fluctuation operator. One possible choice is

$$\hat{\Lambda}(\boldsymbol{r}, t) = \frac{1}{\sqrt{N_0(t)}}\hat{a}_0^\dagger(t)\delta\hat{\psi}(\boldsymbol{r}, t)\,. \tag{2.17}$$

This definition qualifies as a suitable fluctuation operator for the following reasons. First, it has zero expectation value in a nontrivial manner, which can easily be proved with the help of the Penrose-Onsager criterion. Second, it scales with the number of noncondensed atoms and can therefore be used as parameter for a perturbative expansion in the ratio of noncondensed to condensed atoms.

When we express the Hamiltonian in terms of the condensate annihilation operator and this fluctuation operator and calculate the Heisenberg equations of motion of the field operator, we obtain the standard time-dependent GPE for the condensate mode function. Truncating the Hamiltonian at second order in the fluctuation operator, results in a Bogoliubov Hamiltonian, which in contrast to the symmetry-breaking standard form contains a nonlocal projection operator. This operator ensures explicitly the orthogonality between condensate and Bogoliubov modes. For that reason, the second-order Hamiltonian can be diagonalized, thereby solving the "problem of the missing eigenvector", discussed in the previous section. The result is a set of generalized Bogoliubov-de Gennes equations for the dynamical evolution of the noncondensate atoms.

Thus, the number-conserving approach solves all the problems of the $U(1)$ symmetry-breaking formalism. However, the nonlocality of the Bogoliubov de-Gennes equations requires large computational effort when e.g. the time evolution of a large number of modes is simulated in real 3D situations.

Relation between the $U(1)$ symmetry-breaking and number-conserving methods

Finally, we comment upon the relation between the $U(1)$ symmetry-breaking and number-conserving approach. Recently Lieb et al. showed in Refs. [175, 176] that $U(1)$ symmetry breaking is necessary *and* sufficient for Bose-Einstein condensation, see also the comprehensive reviews of the proof in Refs. [177, 178]. But how do we reconcile this result with the fact that we have nowhere broken the symmetry in the number-conserving approach? For this purpose one must simply realize that the concept of SSB is defined in the thermodynamic limit, for which both approaches coincide. The proof by Lieb et al. simply states that given a system with one macroscopic eigenvalue of the reduced density matrix, we will always obtain a nonvanishing expectation value of the field operator according to Eq. (2.12) when we add the symmetry-breaking terms to the Hamiltonian. Thus, there is no contradiction whatsoever. Still, the notion of spontaneous symmetry breaking in the context of Bose-Einstein condensation remains controversial.

2.2.3. Describing atom interferometry

In the previous section we realized that the symmetry-breaking and number-conserving approach as a description for Bose-Einstein condensates lead to identical results in the thermodynamic limit. But which method is better suited for the description of atom interferometry with a finite number of particles? In order to address this question, we rewrite the field operator as

$$\hat{\Psi}(\boldsymbol{r}) = \langle \hat{a}_0 \rangle \phi_0(\boldsymbol{r}) + (\hat{a}_0 - \langle \hat{a}_0 \rangle)\phi_0(\boldsymbol{r}) + \delta\Psi(\boldsymbol{r}) \equiv \langle \hat{a}_0 \rangle \phi_0(\boldsymbol{r}) + \delta\Psi'(\boldsymbol{r}), \qquad (2.18)$$

where we omitted all time arguments for the sake of simplicity. Thus, in the symmetry-breaking approach, where $\langle \hat{a}_0 \rangle \neq 0$, fluctuations in the number of condensate atoms are incorporated in the fluctuation operator. When we discuss interferometry with different internal states, we will realize in chapter 3 that a beam-splitting process sets the condensate in a coherent superposition of the two internal states. As a result, the

number fluctuations of each state are of the order of $\sqrt{N_0}$. In the symmetry-breaking approach this fact is taken into account by complementing the eigenvectors of the nondiagonalizable Bogoliubov Hamiltonian to a complete basis [165] leading to phase diffusion as was discussed in Sec. 2.2.1.

In the number-conserving theory these fluctuations are already incorporated at the Gross-Pitaevskii level in form of a set of Gross-Pitaevskii equations for each particle-number eigenstate [167]. This set can be solved perturbatively and naturally reduced to the two mode approximation. For a more detailed discussion we refer to chapter 4. A numerical analysis together with a semianalytical treatment of the Bogoliubov-de Gennes equations for the release of a BEC out of a spherical symmetric harmonic trap reveals that the fraction of noncondensed atoms is of the order 10^{-3} so that their influence can be neglected at leading order.

Finally, we mention that the calculations are often performed within the grand-canonical ensemble even for a closed system. This should be seen as a mathematical trick which extremely simplifies calculations but is also a good approximation for the closed system [179].

In summary, we conclude that the number-conserving approach is better suited for the description of atom interferometry since it allows for a much more intuitive treatment of leading-order interaction effects.

2.3. Thomas-Fermi approximation

In this final section we briefly address an approximate analytical solution to the GPE known as Thomas-Fermi approximation [130].

2.3.1. Groundstate

First we derive the time-independent Gross-Pitaevskii equation

$$\mu\psi(\boldsymbol{r}) = \left(-\frac{\hbar^2}{2m}\Delta + V(\boldsymbol{r}) + g|\psi(\boldsymbol{r})|^2 \right)\psi(\boldsymbol{r}) \tag{2.19}$$

by substituting the separation ansatz

$$\psi(\boldsymbol{r},t) = \psi(\boldsymbol{r})\mathrm{e}^{-\mathrm{i}\mu\, t/\hbar} \tag{2.20}$$

into Eq. (2.14). Here, in contrast to the Schrödinger equation, the nonlinear eigenvalue μ is the chemical potential and not the energy [130]. Suppose that the potential in Eq. (2.19) is smooth so that the ground-state density will behave smoothly as well. This assumption helps us recognize that the second derivative of the ground-state wave function is small compared to the other terms and we will therefore neglect the Laplace operator in Eq. (2.19). Thus, we obtain to a good approximation

$$n(\boldsymbol{r}) = \frac{1}{g}\left[\mu - V(\boldsymbol{r})\right]_+ \tag{2.21}$$

where n is the particle density and the $+$ indicates that Eq. (2.21) must be set to zero where the density would otherwise be negative. The simple solution, Eq. (2.21), allows

us to explicitly determine the relation $\mu = \mu(N)$ between the chemical potential and the number of particles for a harmonic potential $V(\boldsymbol{r}) = \frac{1}{2}m\sum_i \omega_i^2 x_i^2$ to be

$$\mu = \frac{\hbar\omega_{\mathrm{ho}}}{2}\left(\frac{15Na_s}{a_{\mathrm{ho}}}\right)^{\frac{2}{5}} \tag{2.22}$$

with the harmonic oscillator length $a_{\mathrm{ho}} = \sqrt{\hbar/mw_{\mathrm{ho}}}$ and the averaged trap frequency $\omega_{\mathrm{ho}} = (\omega_x\omega_y\omega_z)^{\frac{1}{3}}$. For the validity of the Thomas-Fermi approximation the condition

$$\frac{\omega_{\mathrm{ho}}}{\omega_i}\left(\frac{15Na_s}{a_{\mathrm{ho}}}\right)^{\frac{2}{5}} \gg 1 \tag{2.23}$$

needs to be satisfied [142].

We conclude this section with a numerical comparison between the solution of Eq. (2.19) and the Thomas-Fermi approximation for a spherically symmetric, harmonic potential for different numbers of ^{87}Rb atoms. The result is depicted in Fig. 2.1. We observe how the Thomas-Fermi approximation (red line) better approximates the exact solution (blue curve), the better the Thomas-Fermi condition in Eq. (2.23) is satisfied. For $N = 10^5$ particles, which is comparable to the particle numbers in typical experiments [63], there is almost no difference. The approximation fails only close to the edge of the cloud, where the density reaches zero. Nevertheless, Fig. 2.1 shows that the Thomas-Fermi approximation accurately describes the ground-state wave function for typical parameter ranges.

2.3.2. Scaling approach

In the previous section we discussed the stationary case. In the case of harmonic trapping by the potential

$$V = \frac{1}{2}m\sum_j \omega_j(t)^2 x_j^2 \tag{2.24}$$

the Thomas-Fermi approximation allows for a generalization to dynamical situations by making use of a scaling ansatz [180–182]

$$\psi(\boldsymbol{r},t) = \frac{1}{\sqrt{\Pi_j\lambda_j(t)}}\,\mathrm{e}^{-\mathrm{i}\beta(t)}\mathrm{e}^{\mathrm{i}\frac{m}{2\hbar}\sum_j \frac{\dot{\lambda}_j(t)}{\lambda_j(t)}x_j^2}\,\psi(x_i/\lambda_i(t),0) \tag{2.25}$$

if the initial state is described by the Thomas-Fermi-ground state $\psi(\boldsymbol{r},0)$. Substituting Eq. (2.25) into the time-dependent Gross-Pitaevskii equation, this leads to

$$\hbar\dot{\beta}(t) = \frac{\mu}{\Pi_j\lambda_j(t)} \tag{2.26}$$

and to the ordinary differential equations for the scaling parameters

$$\ddot{\lambda}_k(t) = \frac{\omega_k(0)^2}{\lambda_k(t)\Pi_j\lambda_j(t)} - \omega_k(t)^2\lambda_k(t) \tag{2.27}$$
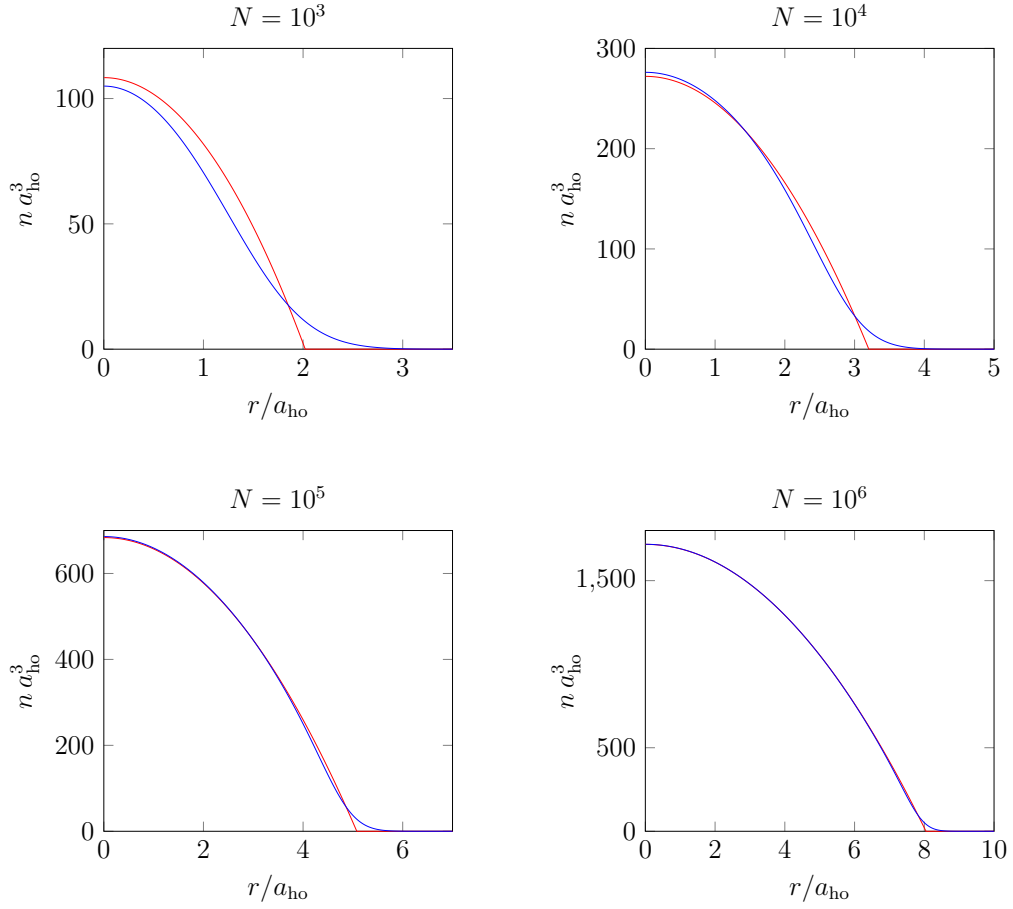
Figure 2.1.: Ground-state density distribution of a Bose-Einstein condensate in an
isotropic harmonic trap. The red line is determined by the analytic Thomas-
Fermi approximation, the blue line corresponds to the result of the numerical
simulation of the time-independent Gross-Pitaevskii equation, Eq. (2.19). The
simulation has been performed for different numbers of ^{87}Rb atoms. The pa-
rameters are $m = 1.44 \cdot 10^{-25}$kg, $\omega_{\mathrm{ho}} = 90$Hz, $a = 98.98 a_0$ with the Bohr radius
$a_0 = 5.29 \cdot 10^{-11}$m. Thus, $a/a_{\mathrm{ho}} \approx 1.8 \cdot 10^{-3}$.

with the initial conditions $\lambda_j(0) = 1$ and $\dot{\lambda}_j(0) = 0$.

Recently, the scaling approach was generalized to rotating traps in Ref. [183], where it
was pointed out that the scaling transformation is also useful for numerical simulations.
Rescaling the Gross-Pitaevskii equation reduces the computational effort dramatically,
for example when simulating the expansion dynamics of a BEC after the release from
a trap.

The formalism can be generalized further by including linear potentials [184–186]. It is
interesting to notice that the scaling transformations can be obtained by mere operator
algebra. One defines an appropriate scaling operator which allows then to include linear
potentials as well as $\hat{p}\hat{r}$ terms present in rotating coordinate systems.

Finally we note that one can even treat small time-dependent modulations of the
Thomas-Fermi profile analytically for example due to weak anharmonic potentials. To

this end, one expands the perturbations into the complete set of *collective oscillations* [187–189] thereby reducing the problem to a set of ordinary differential equations for the time dependence of the expansion parameters. For an isotropic trap these can be solved analytically as a function of the scaling parameter.

2.4. Summary

In summary, we reviewed some technical aspects of the modern understanding of Bose-Einstein condensation.

Starting from the definition of BEC according to Penrose and Onsager, we shed some light at two different philosophical points of view on Bose-Einstein condensation, namely whether one should describe it as a closed system with a definite number of particles or one should break the $U(1)$ symmetry, which violates the conservation of the particle number. These two perspectives lead to the two competing theories, namely the $U(1)$ symmetry-breaking method and the number-conserving approaches. As was shown by Lieb et al., in the thermodynamic limit Bose-Einstein condensation and spontaneous $U(1)$-symmetry breaking are equivalent. However, in mesoscopic systems, which real physical systems always are, differences appear and we concluded that the number-conserving approach is better suited for the description of atom interferometry for the following reasons. First, it is more intuitive and second, it allows to describe phase diffusion due to superpositions of particle-number states already at Gross-Pitaevskii level. It then naturally reduces to the two-mode approximation.

In the last part of this chapter we introduced the stationary and time-dependent Thomas-Fermi approximation which will be needed in chapter 4 and discussed its range of validity.

Chapter 3

Interferometry and second quantization

So far, the description of atom interferometry has been in first quantization. But for large numbers of particles, in particular when we want to assess the effects of particle-particle interaction, this description soon becomes impractical if not impossible. Also, for a discussion of particle-number fluctuations over the exit ports, spin and momentum-state squeezing or the accuracy of a measurement, we have to consider the exchange statistics of the particles. These problems are automatically taken into account when working in second quantization [190, 191].

The influence of particle-particle interaction on atom interferometers, which is intrinsic to Bose-Einstein condensates, is manifold and must be carefully considered. Mean-field induced phase shifts during the separation of the wave packets have been considered within an effective 1D model in Refs. [192–195]. The main contribution was found to originate from asymmetries in the atomic population of interferometer branches, resulting from imperfect laser pulses or the effect of interactions during the pulses [196]. Moreover, it was realized in [192] that interaction effects during the separation lead to small additional velocities of the atomic clouds, which lead to phase shifts and to a loss of contrast.

A second important impact is a derogation of the phase, known as phase diffusion, which afflicts the accuracy of phase measurements. A thorough discussion of this effect will be found in chapter 4.

The aim of the present chapter, however, is not to asses the different possible effects due to interactions but rather to provide a general framework of atom interferometry in second quantization in which it will turn out to be possible to extremely reduce the computational effort of numerical simulations and to set the stage for a deeper discussion of phase diffusion in chapter 4. We will translate the results of chapter 1 into this language, thereby generalizing the formalism to include particle-particle interaction and superpositions of particle-number states.

After a brief discussion of the method of second quantization in Sec. 3.1, we will adapt the formalism of adiabatic elimination to this language in Sec. 3.2 and derive effective laser-atom coupling schemes. Next, we will discuss the MZ interferometer with Raman diffraction in Sec. 3.3. The generalization to multiple-path geometries

and other diffraction schemes is presented in Sec. 3.4 and constitutes the main result of this chapter.

3.1. Second quantization

The start of this chapter is a brief review of the formalism of second quantization. For each internal state j we introduce the field operator $\hat{\Psi}_j(\boldsymbol{r})$. Every pair of field operators satisfies the bosonic commutation relations

$$\left[\hat{\Psi}_i(\boldsymbol{r}), \hat{\Psi}_j^\dagger(\boldsymbol{r}')\right] = \delta_{ij}\delta(\boldsymbol{r} - \boldsymbol{r}') \qquad \text{and} \qquad \left[\hat{\Psi}_i(\boldsymbol{r}), \hat{\Psi}_j(\boldsymbol{r}')\right] = 0\,, \qquad (3.1)$$

which generalize Eq. (2.2) to the case of different internal states. The field operators can be expanded into a complete set of *mode functions* or *orbitals*

$$\hat{\Psi}_j(\boldsymbol{r}) = \sum_k \left\langle \boldsymbol{r} \,|\varphi_k\rangle \, \hat{a}_k^j \right. \tag{3.2}$$

where j labels the internal and $\boldsymbol{r}$ the external degree of freedom. The set $\{|\varphi_k\rangle\}_{k=0}^\infty$ can be chosen arbitrarily as long as it is orthogonal and complete. The index k signifies the mode function, with respect to which the creation and annihilation operators are defined. These operators satisfy the well-known relations

$$\left[\hat{a}_k^j, \hat{a}_m^{n\dagger}\right] = \delta_{km}\delta_{jn}, \tag{3.3}$$

all other possible combinations like $\left[\hat{a}_k^j, \hat{a}_m^n\right]$ are zero. As the mode functions can be chosen quite generally, they do not necessarily have to be the energy eigenfunctions of some one-particle Hamiltonian. It is particularly helpful to pick the Gross-Pitaevskii ground state as the first element of the set of mode functions, when Bose-Einstein condensates are described. The other modes are then chosen to create a complete and orthogonal set.

3.1.1. Notation

In this chapter we will denote the action of a first-quantized operator $\hat{A}$ on a field by a calligraphic letter without hat

$$\mathcal{A}\hat{\Psi}(\boldsymbol{r}) \equiv \int \mathrm{d}^3\boldsymbol{r}' \, \langle \boldsymbol{r}| \, \hat{A} \, |\boldsymbol{r}'\rangle \, \hat{\Psi}(\boldsymbol{r}')\,. \tag{3.4}$$

For example the action of a displacement operator on a field operator reads within this convention

$$\mathcal{D}\hat{\Psi}_j(\boldsymbol{r}) = \int \mathrm{d}^3\boldsymbol{r}' \, \langle \boldsymbol{r}| \, \hat{D} \, |\boldsymbol{r}'\rangle \, \hat{\Psi}(\boldsymbol{r}') = \mathrm{e}^{-\frac{\mathrm{i}}{2\hbar}\boldsymbol{\chi}^p\boldsymbol{\chi}^r} \, \mathrm{e}^{\frac{\mathrm{i}}{\hbar}\boldsymbol{\chi}^p\boldsymbol{r}} \, \hat{\Psi}_j(\boldsymbol{r} - \boldsymbol{\chi}^r)\,. \tag{3.5}$$

For detailed properties of displacement operators we refer to App. A and C.1.2. In order to avoid confusion, we will always denote first-quantized time-evolution operators and Hamilton operators by the calligraphic letters $\hat{\mathcal{U}}$ and $\hat{\mathcal{H}}$, respectively.

3.1.2. Expansion in mode functions

We now consider the many-body state $|\Psi\rangle$ with its phase-space distribution centered in phase space and the set of mode functions $\{\langle \boldsymbol{r} \, | \varphi_k\rangle\}_{k=0}^{\infty}$ with respect to which the field operator $\hat{\Psi}(\boldsymbol{r})$ is expressed. We furthermore suppose that this set of mode functions is particularly suited in the sense that for example only a few modes are occupied. Now we assume the same state but displaced by $\boldsymbol{\chi} = (\boldsymbol{\chi}^r, \boldsymbol{\chi}^p)^{\mathrm{T}}$. In this case it will prove useful to expand the field operator with respect to the displaced mode functions $\langle \boldsymbol{r} \, | \varphi_k'\rangle = \langle \boldsymbol{r}| \, \hat{D} \, |\varphi_k\rangle$. Hence, we introduce a new field operator $\hat{\Psi}'(\boldsymbol{r})$ by writing

$$\hat{\Psi}(\boldsymbol{r}) = \sum_k \langle \boldsymbol{r} \, | \varphi_k'\rangle \, \hat{a}_k' \equiv \mathcal{D}\hat{\Psi}'(\boldsymbol{r}) \tag{3.6}$$

where

$$\hat{\Psi}'(\boldsymbol{r}) = \sum_k \langle \boldsymbol{r} \, | \varphi_k\rangle \, \hat{a}_k' \, . \tag{3.7}$$

Thus, expressing all observables in terms of $\hat{\Psi}(\boldsymbol{r}) = \mathcal{D}\hat{\Psi}'(\boldsymbol{r})$ effectively corresponds to a transformation into the center of the state in phase space. In the same way we can include arbitrary phase factors in the field operator. After clarifying the underlying principle in Eq. (3.6), we henceforth disregard the prime on the field operator when performing this replacement. Finally, we note that the commutation relations are left invariant under this transformation.

3.2. Hamiltonian

In this section we introduce the Hamiltonian in second quantization. It is represented by the sum

$$\hat{H} = \hat{H}_{\mathrm{e}} + \hat{H}_{\mathrm{L}} \tag{3.8}$$

where $\hat{H}_{\mathrm{L}}$ accounts for the light-matter interaction and $\hat{H}_{\mathrm{e}}$ is the *external* Hamiltonian which conserves the number of particles in each internal state. Thus it commutes with $\int \mathrm{d}^3\boldsymbol{r} \, \hat{\Psi}_j^\dagger(\boldsymbol{r})\hat{\Psi}_j(\boldsymbol{r})$. It can be further decomposed into

$$\hat{H}_{\mathrm{e}} = \hat{H}_{\mathrm{F}} + \hat{H}_{\mathrm{I}} \tag{3.9}$$

with the *free* Hamiltonian $\hat{H}_{\mathrm{F}}$ consisting only of one-body operators and the particle-particle interaction Hamiltonian $\hat{H}_{\mathrm{I}}$, which includes two-body and in principle higher-order operators. In the following three sections we will define and analyze these Hamiltonians in more detail.

3.2.1. The free part of the Hamiltonian

The free part of the external Hamiltonian is simply a standard first-quantized one-body Hamiltonian in second quantized form, that is,

$$\hat{H}_{\mathrm{F}} = \sum_j \int \mathrm{d}^3\boldsymbol{r} \, \hat{\Psi}_j^\dagger(\boldsymbol{r})\mathcal{H}_j(t)\hat{\Psi}_j(\boldsymbol{r}) \tag{3.10}$$

where $\hat{\mathcal{H}}_j(t)$ typically is

$$\hat{\mathcal{H}}_j(t) = \frac{\hat{\boldsymbol{p}}^2}{2m} + V_j(\hat{\boldsymbol{r}}, t) \, . \tag{3.11}$$

Note again that in Eq. (3.10) the notation defined in Eq. (3.4) has been employed. Within this convention we abbreviated

$$\mathcal{H}_j(t)\hat{\Psi}(\boldsymbol{r}) = \int \mathrm{d}^3 \boldsymbol{r}' \, \langle \boldsymbol{r} | \hat{\mathcal{H}}_j(t) | \boldsymbol{r}' \rangle \, \hat{\Psi}(\boldsymbol{r}') \, . \tag{3.12}$$

The action of the time-evolution operator with respect to Eq. (3.10) on a field operator can be expressed in terms of the first-quantized operator

$$\hat{\mathcal{U}}_j(t, t_\mathrm{i}) = \mathcal{T} \exp \left\{ -\frac{\mathrm{i}}{\hbar} \int_{t_\mathrm{i}}^t \mathrm{d}t' \, \hat{\mathcal{H}}_j(t') \right\} \tag{3.13}$$

as

$$\hat{U}_\mathrm{F}^\dagger(t, t_\mathrm{i}) \hat{\Psi}_j(\boldsymbol{r}) \hat{U}_\mathrm{F}(t, t_\mathrm{i}) = \mathcal{U}_j(t, t_\mathrm{i}) \hat{\Psi}_j(\boldsymbol{r}) \, , \tag{3.14}$$

which is verified in App. C.1. The reason why we chose to work in second quantization was the straightforward way to include interactions. Thus, in the next section we state and motivate the explicit form of the interaction Hamiltonians used in this work.

3.2.2. The interaction Hamiltonian

For nonrelativistic systems the second quantized particle-particle interaction Hamiltonian is of the form [142]

$$\hat{H}_\mathrm{I} = \frac{1}{2} \sum_{j,k,n,l} \int \mathrm{d}^3 \boldsymbol{r} \, \mathrm{d}^3 \boldsymbol{r}' \, \hat{\Psi}_j^\dagger(\boldsymbol{r}) \hat{\Psi}_k^\dagger(\boldsymbol{r}') V_{jknl}(\boldsymbol{r} - \boldsymbol{r}') \hat{\Psi}_n(\boldsymbol{r}) \hat{\Psi}_l(\boldsymbol{r}') \, . \tag{3.15}$$

When we neglect spin-changing processes and furthermore replace the exact interaction potential by an effective contact potential [141], which is generally a good approximation for ultracold, dilute and weakly interacting samples, the interaction Hamiltonian becomes

$$\hat{H}_\mathrm{I} = \frac{1}{2} \int \mathrm{d}^3 \boldsymbol{r} \left\{ \sum_n g_n \hat{\Psi}_n^\dagger(\boldsymbol{r}) \hat{\Psi}_n^\dagger(\boldsymbol{r}) \hat{\Psi}_n(\boldsymbol{r}) \hat{\Psi}_n(\boldsymbol{r}) + \sum_{n \neq l} g_{nl} \hat{\Psi}_n^\dagger(\boldsymbol{r}) \hat{\Psi}_n(\boldsymbol{r}) \hat{\Psi}_l^\dagger(\boldsymbol{r}) \hat{\Psi}_l(\boldsymbol{r}) \right\} \tag{3.16}$$

with symmetric $g_{nl} = g_{ln}$. Hamiltonian, Eq. (3.16), will be further particularized in later sections to Bragg diffraction

$$\hat{H}_\mathrm{I} = \frac{g}{2} \int \mathrm{d}^3 \boldsymbol{r} \, \hat{\Psi}^\dagger(\boldsymbol{r}) \hat{\Psi}^\dagger(\boldsymbol{r}) \hat{\Psi}(\boldsymbol{r}) \hat{\Psi}(\boldsymbol{r}) \tag{3.17}$$

where only one internal state is important and to Raman diffraction

$$\hat{H}_\mathrm{I} = \int \mathrm{d}^3 \boldsymbol{r} \left(\frac{g_1}{2} \hat{\Psi}_1^\dagger(\boldsymbol{r}) \hat{\Psi}_1^\dagger(\boldsymbol{r}) \hat{\Psi}_1(\boldsymbol{r}) \hat{\Psi}_1(\boldsymbol{r}) + \frac{g_2}{2} \hat{\Psi}_2^\dagger(\boldsymbol{r}) \hat{\Psi}_2^\dagger(\boldsymbol{r}) \hat{\Psi}_2(\boldsymbol{r}) \hat{\Psi}_2(\boldsymbol{r}) \right.$$
$$\left. + g_{12} \hat{\Psi}_1^\dagger(\boldsymbol{r}) \hat{\Psi}_1(\boldsymbol{r}) \hat{\Psi}_2^\dagger(\boldsymbol{r}) \hat{\Psi}_2(\boldsymbol{r}) \right) \tag{3.18}$$

where an additional excited state takes part in the dynamics. So far we have considered the free and the interaction Hamiltonian. In the next section we will turn to the light-matter interaction and derive a simple formalism to perform adiabatic elimination of ancillary states in second quantization to obtain effective coupling schemes.

3.2.3. Light-matter interaction and adiabatic elimination

In the present section we will introduce the last part of the Hamiltonian, the semiclassical laser-atom interaction. Starting from a general coupling scheme, we will derive a powerful method to obtain effective Hamiltonians capable of describing a large variety of different processes such as Raman-, Bragg-, and double-Bragg diffraction. In order to obtain effective equations one ordinarily applies the so called adiabatic elimination [85]. In this approach, one first derives the equations of motion for the wave functions corresponding to each internal state. Only integrating the fast oscillating terms allows one to approximately integrate these equations, eliminate the ancillary states and reduce the problem to smaller time scales. This at first sight very simple procedure, however, involves the following subtleties. Since one needs to perform the calculation in the interaction picture with respect to $\hat{H}_e$ as the full evolution is generated by the sum, Eq. (3.8), how to include the quartic interaction into this formalism? How to proceed when the coupling scheme involves many different internal states? Moreover, it is a priori unclear how to generalize the procedure to include higher-order contributions. We answer these questions in the formalism presented here by treating the problem on a more general level. This leads to at first sight cumbersome expressions, however, the careful bookkeeping of relevant time scales, ranging from kHz to THz, essential for the adiabatic elimination, is most easily done for a general Hamiltonian. Furthermore, it allows us to treat the three different coupling schemes discussed in this work with the same formalism and the underlying processes stand out most clearly. We show how to consistently neglect potentials and particle-particle interaction and in principle to include higher-order contributions.

We assume two manifolds of states as depicted in Fig. 3.1. The transition frequencies ω_{ij} between states in different manifolds are supposed to be much larger than the characteristic transition frequencies $\Delta\omega_i$ within each manifold. The system is driven by lasers with frequency ω_L of the order of ω_{ij}, however strongly detuned by Δ with respect to the atomic transition frequencies. The sizes of the parameters are listed in Table 3.1. In the dipole approximation [197] after application of the rotating-wave approximation the laser-atom interaction Hamiltonian can be cast in the form

$$\hat{H}_L = \int \mathrm{d}^3\boldsymbol{r} \sum_j \hbar\omega_j \hat{\Psi}_j^\dagger(\boldsymbol{r})\hat{\Psi}_j(\boldsymbol{r}) + \int \mathrm{d}^3\boldsymbol{r} \left(\sum_{j,k} \hbar\lambda_{jk}(\boldsymbol{r},t)\mathrm{e}^{-\mathrm{i}\omega_L t}\hat{\Psi}_j^\dagger(\boldsymbol{r})\hat{\Psi}_k(\boldsymbol{r}) + \mathrm{H.c.} \right).$$

(3.19)

The first contribution describes the energy of the internal states which we keep in $\hat{H}_L$ rather than in the free Hamiltonian for reasons which will become clear further below. The second contribution accounts for coupling between the states due to the lasers. Note that coupling only appears between states of different manifolds. The spatial- and time-dependent functions $\lambda_{jk}(\boldsymbol{r},t)$ oscillate only with frequencies of the order of
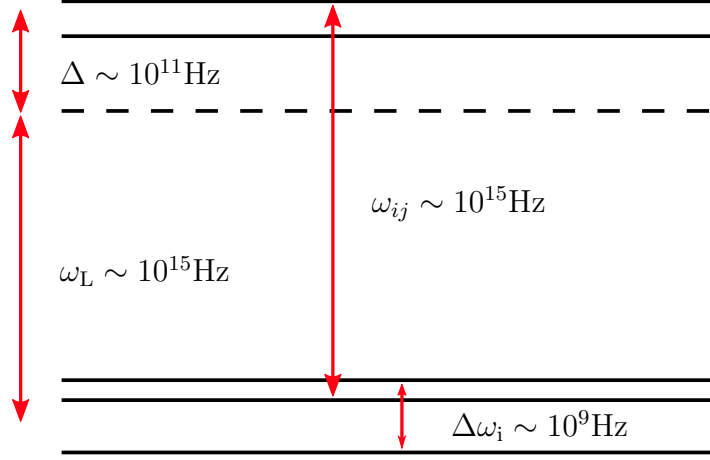
Figure 3.1.: General level scheme discussed in this section. Two manifolds of closely
lying states with frequency difference $\Delta\omega_\mathrm{i}$ within the manifolds are coupled
by a characteristic laser frequency ω_L, which is strongly detuned by Δ with
respect to the transition frequencies ω_{ij} between the two manifolds.

$\Delta\omega_\mathrm{i}$ as we extracted a characteristic laser frequency ω_L in Eq. (3.19). The modulation
of the electric fields due to the switching of the lasers, which leads to an additional time
dependence of λ, is supposed to happen on much smaller time scales. Transforming
to the interaction picture with respect to the first term in Eq. (3.19) results in the
replacement

$$\hat{\Psi}_j^\mathrm{I}(\boldsymbol{r}) = \hat{\Psi}_j(\boldsymbol{r})\mathrm{e}^{-\mathrm{i}\omega_j t} \, . \tag{3.20}$$

The external Hamiltonian $\hat{H}_\mathrm{e}$ is invariant under the above transformation per defini-
tion since it conserves the number of particles in each internal state from which the
invariance under the above transformation follows immediately. Thus, Eq. (3.20) only
affects the laser-atom interaction Hamiltonian for which we obtain

$$\hat{H}_\mathrm{L}^\mathrm{I} = \int \mathrm{d}^3\boldsymbol{r} \left(\sum_{j,k} \hbar\lambda_{jk}(\boldsymbol{r},t)\mathrm{e}^{\mathrm{i}\Delta_{jk}t}\hat{\Psi}_j^\dagger(\boldsymbol{r})\hat{\Psi}_k(\boldsymbol{r}) + \mathrm{H.c.} \right) \tag{3.21}$$

where we defined the detuning $\Delta_{jk} = \omega_{jk} - \omega_\mathrm{L}$ between the characteristic laser frequency
and $\omega_{jk} = \omega_j - \omega_k$ is the atomic transition frequency. From now on we will always
assume that transformation, Eq. (3.20), has been made and disregard the superscript
"I". As we show in App. C.2, we can replace Eq. (3.21) by the effective Hamiltonian

$$\hat{H}_\mathrm{L}^\mathrm{eff} = \frac{1}{2} \left[\hat{F}(t), \hat{H}_\mathrm{L}(t) \right] \tag{3.22}$$

with

$$\hat{F} = \int \mathrm{d}^3\boldsymbol{r} \left(\sum_{j,k} \frac{\lambda_{jk}(\boldsymbol{r},t)}{\Delta_{jk}}\mathrm{e}^{\mathrm{i}\Delta_{jk}t}\hat{\Psi}_j^\dagger(\boldsymbol{r})\hat{\Psi}_k(\boldsymbol{r}) - \mathrm{H.c.} \right) \, . \tag{3.23}$$

For a given laser-atom interaction Hamiltonian all what is left to do is to calculate the commutator, Eq. (3.22). Before we elucidate in three examples how powerful this method is, let us comment on its validity. In App. C.2 we show that as a main condition $\lambda/\Delta \ll 1$ needs to be true. A comparison with Table 3.1 and Fig. 3.2 shows that this is indeed true for the experimental parameters discussed in this work. Furthermore, the rate of change of the field operators in the interaction picture with respect to the external Hamiltonian as well as the rate of change of λ have to be much smaller than Δ. As we discuss in App. C.2, these conditions are well satisfied.

Bragg diffraction

As a first example we study Bragg-diffraction [198, 199]. Consider a two-level atom exposed to two counterpropagating laser beams as depicted in Fig. 3.2.a. The frequencies are far detuned from atomic resonance and the electric field is given by

$$\hat{\boldsymbol{\mathcal{E}}} = \boldsymbol{E}_b(t)\mathrm{e}^{\mathrm{i}\left(k_b\hat{z}-\omega_b t+\varphi_{\mathrm{L},b}\right)} + \boldsymbol{E}_a(t)\mathrm{e}^{\mathrm{i}\left(-k_a\hat{z}-\omega_a t+\varphi_{\mathrm{L},a}\right)} + \mathrm{H.c.} . \tag{3.24}$$

In the language of this section this corresponds to one state in each manifold. Moreover, the experimental parameters are supposed to resemble those given in Table 3.1. In the dipole approximation, the Hamiltonian reads

$$\hat{\mathcal{H}}_{\mathrm{L}} = \hbar\omega_e \, |e\rangle\langle e| + \hbar\left\{\left[\Omega_b(t)\mathrm{e}^{\mathrm{i}\left(k_b\hat{z}-\omega_b t+\varphi_{\mathrm{L},b}\right)} + \Omega_a(t)\mathrm{e}^{\mathrm{i}\left(-k_a\hat{z}-\omega_a t+\varphi_{\mathrm{L},a}\right)}\right]|e\rangle\langle g| + \mathrm{H.c.}\right\} . \tag{3.25}$$

The Rabi frequencies are defined as $\Omega_j = -\langle e|\, \hat{\boldsymbol{d}}\boldsymbol{E}_j\, |g\rangle\, /\hbar$ with the atomic dipole operator $\hat{\boldsymbol{d}}$. Translating this Hamiltonian to second quantization, performing the transformation Eq. (3.20) and defining the characteristic laser frequency, $\omega_{\mathrm{L}} \equiv \omega_a$, the second-quantized Hamiltonian assumes the form

$$\hat{H}_{\mathrm{L}} = \hbar \int \mathrm{d}^3\boldsymbol{r}\, \left(\hat{\Psi}_e^\dagger(\boldsymbol{r})\lambda(\boldsymbol{r},t)\mathrm{e}^{\mathrm{i}\Delta t}\hat{\Psi}_g(\boldsymbol{r}) + \mathrm{H.c.}\right) \tag{3.26}$$

with $\Delta = \omega_e - \omega_a$ and the abbreviation

$$\lambda(t,\boldsymbol{r}) = \Omega_b \mathrm{e}^{\mathrm{i}\left(k_b z-\Delta\omega t+\varphi_{\mathrm{L},b}\right)} + \Omega_a \mathrm{e}^{\mathrm{i}\left(-k_a z+\varphi_{\mathrm{L},a}\right)} \tag{3.27}$$

where $\Delta\omega = \omega_b - \omega_a \ll \Delta$. Note that we omit the implicit time dependence of the Rabi frequencies from now on for better readability. With the help of Eq. (3.22) and Eq. (3.23) we arrive at the effective Bragg-diffraction Hamiltonian

$$\hat{H}_{\mathrm{L}}^{\mathrm{eff}} = \hbar \int \mathrm{d}^3\boldsymbol{r}\, \left\{\frac{|\Omega_a|^2 + |\Omega_b|^2}{\Delta} + \left[\Omega\mathrm{e}^{\mathrm{i}(kz-\Delta\omega t+\varphi_{\mathrm{L}})} + \mathrm{H.c.}\right]\right\}\left[\hat{\Psi}_e^\dagger(\boldsymbol{r})\hat{\Psi}_e(\boldsymbol{r}) - \hat{\Psi}_g^\dagger(\boldsymbol{r})\hat{\Psi}_g(\boldsymbol{r})\right] \tag{3.28}$$

where we defined $\varphi_{\mathrm{L}} = \varphi_{\mathrm{L},b} - \varphi_{\mathrm{L},a}$ and $k = k_a + k_b$ as well as the effective Rabi frequency $\Omega = \frac{\Omega_b\Omega_a^*}{\Delta}$. Assuming an initial occupation only of the groundstate, all field operators corresponding to the upper state can be omitted since all transition elements of the Hamiltonian were eliminated. Restricting the discussion only on this subspace of the

full Hilbert space, the first term in the first brackets only leads to a global phase and can therefore be disregarded. Thus, we find the simple result

$$\hat{H}_{\mathrm{L}}^{\mathrm{eff}} = -\hbar\Omega(t) \int \mathrm{d}^3\boldsymbol{r} \, \hat{\Psi}_g^\dagger(\boldsymbol{r})\hat{\Psi}_g(\boldsymbol{r}) \, \mathrm{e}^{\mathrm{i}kz + \mathrm{i}\varphi_{\mathrm{L}}(t)} + \mathrm{H.c.} \tag{3.29}$$

and we redefined the laser phase $\varphi_{\mathrm{L}}(t) \equiv \varphi_{\mathrm{L}} - \Delta\omega t$.
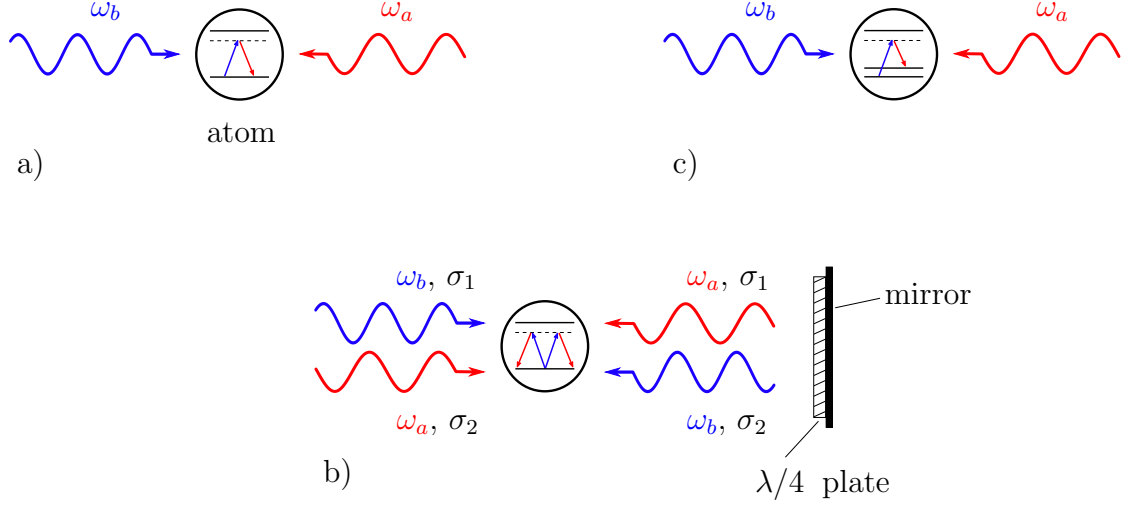
Figure 3.2.: Schematic picture of the three diffraction processes described in this work. a) Bragg diffraction. A two-level atom is exposed to two counterpropagating laser beams. The absorption of a "blue" photon is associated with a momentum transfer in positive momentum direction (the arrows depicted in the atoms are understood as drawn in an energy momentum diagram). Since the laser frequencies are strongly detuned with respect to the atomic transition, the atom undergoes a two-photon process back to the initial internal state together with the stimulated emission of a "red" photon in negative direction, leading to an additional momentum kick in positive direction. Therefore the total momentum transfer is $\hbar(k_a + k_b)$. b) Raman diffraction. Contrary to a), the laser beams are incident on a three-level atom and the frequencies are chosen such that only the transition to a different internal state is resonant. c) Double-Bragg diffraction. The atom is exposed to two pairs of counterpropagating laser beams. Due to the orthogonal polarizations σ_1 and σ_2 spurious transitions are suppressed, leading to the diffraction process of a) but in positive and negative momentum direction, simultaneously.

Double-Bragg diffraction

In this laser-atom coupling scheme, which was developed in Ref. [21] and experimentally realized in [202], two light fields of orthogonal polarization are incident from the same direction. Having passed the atom, the light beams are retro reflected and

Table 3.1.: This table shows the different frequency scales relevant for the description of the diffraction processes. It is important to carefully take into account the different scales ranging from kHz to THz. We emphasize that the numbers below should be understood as rough order-of-magnitude estimates. They are typical values for the ^{87}Rb D$_2$-transition hyperfine structure found in Ref. [200]. We also refer the reader to Ref. [201].

ω_{jk}	Frequency difference between manifolds	$10^{15}/\mathrm{s}$
ω_L	Characteristic laser frequency	$10^{15}/\mathrm{s}$
Δ	Detuning	$10^{11}/\mathrm{s}$
$\Delta\omega_\mathrm{i}$	Frequency difference within one manifold	$10^{10}/\mathrm{s}$
$\Omega_a, \Omega_b \quad (\sim \lambda)$	Single-photon Rabi frequency	$10^8/\mathrm{s}$
$\Delta\omega$	Laser frequency difference	$10^4/\mathrm{s}$ - $10^{10}/\mathrm{s}$
Ω	Effective Rabi frequency	$10^5/\mathrm{s}$
ω_r	Recoil frequency	$10^4/\mathrm{s}$ (cf. Sec. 3.5.4)
ν	Velocity selectivity	$10^3/\mathrm{s}$ (cf. Sec. 3.5.4)

the polarization is rotated by a $\lambda/4$ plate. The process is depicted schematically in Fig. 3.2.b. In this setup one state in the lower manifold is coupled to two states in the upper manifold. The first-quantization Hamiltonian then reads [21]

$$
\begin{aligned}
\hat{\mathcal{H}} =&\, \hbar\omega_{e_+} \left|e_+\right\rangle \left\langle e_+\right| + \hbar\omega_{e_-} \left|e_-\right\rangle \left\langle e_-\right| \\
&+ \hbar\left\{\Omega_+ \left[\mathrm{e}^{\mathrm{i}(k_a\hat{z}-\omega_a t+\varphi_{\mathrm{L},a}^+)} + \mathrm{e}^{\mathrm{i}(-k_b\hat{z}-\omega_b t+\varphi_{\mathrm{L},b}^+)}\right] \left|e_+\right\rangle \left\langle g\right| \right. \\
&\left. + \Omega_- \left[\mathrm{e}^{\mathrm{i}(-k_a\hat{z}-\omega_a t+\varphi_{\mathrm{L},a}^-)} + \mathrm{e}^{\mathrm{i}(k_b\hat{z}-\omega_b t+\varphi_{\mathrm{L},b}^-)}\right] \left|e_-\right\rangle \left\langle g\right| + \mathrm{H.c.}\right\} .
\end{aligned}
\tag{3.30}
$$

Following Eq. (3.20)-(3.23), we first transform into the interaction picture with respect to the level energies. Defining again the characteristic laser frequency $\omega_\mathrm{L} \equiv \omega_a$, the second-quantized Hamiltonian becomes with $\Delta_+ = \omega_{e_+} - \omega_a$ and $\Delta_- = \omega_{e_-} - \omega_a$

$$
\hat{H}_\mathrm{L} = \hbar \int \mathrm{d}^3\boldsymbol{r} \left(\lambda_+ \mathrm{e}^{\mathrm{i}\Delta_+ t} \hat{\Psi}_{e_+}^\dagger(\boldsymbol{r}) \hat{\Psi}_g(\boldsymbol{r}) + \lambda_- \mathrm{e}^{\mathrm{i}\Delta_- t} \hat{\Psi}_{e_-}^\dagger(\boldsymbol{r}) \hat{\Psi}_g(\boldsymbol{r}) + \mathrm{H.c.}\right) .
\tag{3.31}
$$

In Eq. (3.31) we furthermore introduced the abbreviations

$$
\lambda_\pm = \Omega_\pm \left(\mathrm{e}^{\mathrm{i}(\pm k_a z+\varphi_{\mathrm{L},a}^\pm)} + \mathrm{e}^{\mathrm{i}(\mp k_b z-\Delta\omega t+\varphi_{\mathrm{L},b}^\pm)}\right)
\tag{3.32}
$$

where the laser frequency difference is $\Delta\omega = \omega_b - \omega_a$ as before. Hamiltonian, Eq. (3.31), is of the form, Eq. (3.21), it is therefore straightforward to perform the adiabatic elimination. This yields

$$
\hat{H}_\mathrm{L}^\mathrm{eff} = -\hbar \int \mathrm{d}^3\boldsymbol{r} \left\{\frac{|\lambda_+|^2}{\Delta_+} + \frac{|\lambda_-|^2}{\Delta_-}\right\} \hat{\Psi}_g^\dagger(\boldsymbol{r}) \hat{\Psi}_g(\boldsymbol{r}) .
\tag{3.33}
$$

Setting $\Delta_+ \approx \Delta_-$ and $\Omega_+ = \Omega_-$, Eq. (3.33) reduces to

$$
\hat{H}_\mathrm{L}^\mathrm{eff} = -\hbar\Omega \int \mathrm{d}^3\boldsymbol{r} \left\{\mathrm{e}^{-\mathrm{i}kz+\mathrm{i}\varphi_\mathrm{L}^+(t)} + \mathrm{e}^{\mathrm{i}kz+\mathrm{i}\varphi_\mathrm{L}^-(t)} + \mathrm{H.c.}\right\} \hat{\Psi}_g^\dagger(\boldsymbol{r}) \hat{\Psi}_g(\boldsymbol{r})
\tag{3.34}
$$

with $\varphi_{\mathrm{L}}^{\pm} = \varphi_{\mathrm{L},b}^{\pm} - \varphi_{\mathrm{L},a}^{\pm} - \Delta\omega t$ and $k = k_a + k_b$ as before. Moreover, we omitted constant terms as in the case of Bragg diffraction since they only lead to a global phase. Furthermore, we defined the effective Rabi frequency $\Omega = \frac{|\Omega_{\pm}|^2}{\Delta_{\pm}}$.

Raman diffraction

In the third example we will derive the effective Hamiltonian for Raman diffraction [12, 203]. Therefore, we assume two counterpropagating laser beams with the electric field identical to the one in Eq. (3.24). In contrast to Bragg diffraction we now consider a three-level atom with two states, $|g_1\rangle$ and $|g_2\rangle$ in the lower and one state $|e\rangle$ in the upper manifold. A schematic picture of this setup can be seen in Fig. 3.2.c. We furthermore assume that there is no coupling within the lower manifold. The second-quantized Hamiltonian then becomes

$$\hat{H}_{\mathrm{L}} = \hbar \int \mathrm{d}^3\boldsymbol{r} \left\{ \lambda(\boldsymbol{r},t)\mathrm{e}^{\mathrm{i}\Delta_{eg_1}t}\hat{\Psi}_e^\dagger(\boldsymbol{r})\hat{\Psi}_{g_1}(\boldsymbol{r}) + \lambda(\boldsymbol{r},t)\mathrm{e}^{\mathrm{i}\Delta_{eg_2}t}\hat{\Psi}_e^\dagger(\boldsymbol{r})\hat{\Psi}_{g_2}(\boldsymbol{r}) + \mathrm{H.c.} \right\} . \quad (3.35)$$

As before, we defined ω_a as the characteristic laser frequency and introduced λ as in Eq. (3.27). Moreover, for the sake of simplicity we assumed that the dipole-matrix elements of the coupling between the pair of states $|e\rangle$ and $|g_1\rangle$ as well as $|e\rangle$ and $|g_2\rangle$ are the same. In addition to that we transformed into the interaction picture according to Eq. (3.20) and defined $\Delta_{eg_1} = \omega_e - \omega_{g_1} - \omega_a$ and $\Delta_{eg_2} = \omega_e - \omega_{g_2} - \omega_a$. With the help of Eq. (3.22) and Eq. (3.23), the effective Hamiltonian for Raman diffraction becomes

$$\hat{H}_{\mathrm{L}}^{\mathrm{eff}} = -\frac{\hbar}{2} \int \mathrm{d}^3\boldsymbol{r} \left\{ \frac{|\lambda|^2}{\Delta_{eg_1}}\hat{\Psi}_{g_1}^\dagger(\boldsymbol{r})\hat{\Psi}_{g_1}(\boldsymbol{r}) + \frac{|\lambda|^2}{\Delta_{eg_2}}\hat{\Psi}_{g_2}^\dagger(\boldsymbol{r})\hat{\Psi}_{g_2}(\boldsymbol{r}) \right.$$
$$\left. + \frac{|\lambda|^2}{\Delta_{eg_1}}\mathrm{e}^{\mathrm{i}(\Delta_{eg_1}-\Delta_{eg_2})t}\hat{\Psi}_{g_2}^\dagger(\boldsymbol{r})\hat{\Psi}_{g_1}(\boldsymbol{r}) + \frac{|\lambda|^2}{\Delta_{eg_2}}\mathrm{e}^{-\mathrm{i}(\Delta_{eg_1}-\Delta_{eg_2})t}\hat{\Psi}_{g_1}^\dagger(\boldsymbol{r})\hat{\Psi}_{g_2}(\boldsymbol{r}) + \mathrm{H.c.} \right\} .$$
$$(3.36)$$

In deriving Eq. (3.36) we already omitted terms of the form $\hat{\Psi}_e^\dagger(\boldsymbol{r})\hat{\Psi}_e(\boldsymbol{r})$ since no coupling elements between the exited state and the two lower states appear. If initially all particles reside in $|g_1\rangle$ or $|g_2\rangle$, the transition to $|e\rangle$ will be strongly suppressed. Depending on the choice of $\Delta\omega$, one can now either drive Bragg diffraction, that is, transitions between the same internal states, or - what we want to do here - induce transitions between $|g_1\rangle$ and $|g_2\rangle$. For that purpose one proceeds as follows. First, we expand $|\lambda|^2$ as in Eq. (3.28). The result consists of a constant term and an oscillating one with $\Delta\omega$. When we recall that $\Delta\omega_{\mathrm{i}} \equiv \Delta_{eg_1} - \Delta_{eg_2} = \omega_{g_2} - \omega_{g_1} \approx 10^9$ from Table 3.1 and choose $\Delta\omega \sim \Delta\omega_{\mathrm{i}}$, we are able to neglect all the rapidly oscillating terms in Eq. (3.36). The remaining constant terms constitute the AC Stark shift. It can be compensated for by modulating the laser intensities of the counterpropagating laser beams. Then Eq. (3.36) takes the simple form

$$\hat{H}_{\mathrm{L}}^{\mathrm{eff}} = -\hbar\Omega(t) \int \mathrm{d}^3\boldsymbol{r}\, \mathrm{e}^{\mathrm{i}kz+\mathrm{i}\varphi_{\mathrm{L}}(t)}\, \hat{\Psi}_{g_2}^\dagger(\boldsymbol{r})\hat{\Psi}_{g_1}(\boldsymbol{r}) + \mathrm{H.c.} \quad (3.37)$$

with the laser phase $\varphi_{\mathrm{L}}(t) = \varphi_{\mathrm{L}} - \Delta\omega t + \Delta\omega_{\mathrm{i}}$. Note that we also included $\Delta\omega_{\mathrm{i}}$ into the laser phase. With Eq. (3.22) and Eq. (3.23) we found a simple way to perform

adiabatic elimination within our second-quantized framework. Now that we have at hand this formalism we will try to calculate the MZ sequence in second quantization in the following sections.

3.3. Mach-Zehnder interferometer with Raman diffraction

In the previous section we eliminated the ancillary states and derived effective laser-atom interaction Hamiltonians for Bragg, double Bragg and Raman diffraction.
In the case of weak coupling between the atom and the light field it is in a wide field of experimental cases a well-established approximation to assume infinitely short laser pulses and replace the atom-light interaction by effective two-level systems (or three-level systems in the case of double-Bragg diffraction). Invoking this so called delta-pulse approximation, we will also include the external dynamics between the pulses into the consideration and study interferometers with noninteracting particles in Sec. 3.3.4 as a warm-up exercise. As it will turn out, it is straightforward to transfer the formalism derived in Sec. 1.3 to this situation. This method, however, fails when we include interactions in Sec. 3.3.5. We will then realize that the transformation to the comoving frames which was presented in Sec. 1.2 serves as an effective guide also in the interacting case. However, it will turn out to be only applicable to interferometer sequences with exactly two interferometer paths. This conjuncture reflects the two commuting field operators corresponding to the two internal states in the case of Raman diffraction. Thus, to highlight the essential features, we start by discussing the Mach-Zehnder interferometer employing Raman diffraction in Sec. 3.3.5, where this requirement is fulfilled. A generalization of this formalism capable of treating arbitrary interferometer geometries as well as the application to Bragg- and double-Bragg diffraction will be presented in Sec. 3.4.

3.3.1. Delta pulses

In Sec. 1.1.3 we already mentioned the concept of delta pulses. For the discussion in this section we assume that this approximation is valid, thus we replace the Raman atom-light interaction Hamiltonian, Eq. (3.37) by

$$\hat{H}_{\mathrm{L}}(t) = -\frac{\hbar\theta_j}{2}\delta(t - t_j)\int \mathrm{d}^3\boldsymbol{r}\,\left(\hat{\Psi}_2^{\dagger}(\boldsymbol{r})\mathrm{e}^{\mathrm{i}\boldsymbol{k}_j\boldsymbol{r}+\mathrm{i}\varphi_{\mathrm{L},j}}\hat{\Psi}_1(\boldsymbol{r}) + \mathrm{H.c.}\right) \qquad (3.38)$$

for a laser pulse at $t = t_j$, where $\varphi_{\mathrm{L},j} = \varphi_{\mathrm{L}}(t_j)$ is the laser phase at this instant of time. The *pulse area* is defined as $\theta_j = 2\int_{t_j}^{t_j+\Delta t_j}\mathrm{d}t\,\Omega(t)$, where Δt_j is the duration of the jth pulse. Furthermore, we generalized the Hamiltonian to the case of nonaligned laser pulses and changed the labeling of the states. In Sec. 3.5.3 and Sec. 3.5.4 we will reassess the delta-pulse approximation, present a rigorous derivation, and show how to consistently take into account higher-order corrections.

The time-evolution operator with respect to Eq. (3.38) is readily calculated. For a pulse at t_j we define the delta-pulse beam splitter as

$$\hat{S}_{\theta_j}(t_j) \equiv \hat{U}(t_j^+, t_j^-) = \exp\left\{ i\frac{\theta_j}{2} \int d^3\boldsymbol{r} \left(\hat{\Psi}_2^\dagger(\boldsymbol{r}) e^{i\boldsymbol{k}_j\boldsymbol{r} + i\varphi_{L,j}} \hat{\Psi}_1(\boldsymbol{r}) + \text{H.c.} \right) \right\} \qquad (3.39)$$

where t_j^- (t_j^+) denotes two points of time slightly before (after) t_j. The time integral over the delta function collapses and no time-ordering operator is necessary.

3.3.2. Beam splitter

The action of the delta-pulse beam-splitter operator on a field operator can now easily be calculated. Here, we only state the results

$$\hat{S}_\theta^\dagger \hat{\Psi}_2(\boldsymbol{r}) \hat{S}_\theta = \cos(\theta/2)\, \hat{\Psi}_2(\boldsymbol{r}) + i\sin(\theta/2)\, e^{i\boldsymbol{k}\boldsymbol{r} + i\varphi_{L}} \hat{\Psi}_1(\boldsymbol{r})$$

and

$$\hat{S}_\theta^\dagger \hat{\Psi}_1(\boldsymbol{r}) \hat{S}_\theta = \cos(\theta/2)\, \hat{\Psi}_1(\boldsymbol{r}) + i\sin(\theta/2)\, e^{-i\boldsymbol{k}\boldsymbol{r} - i\varphi_{L}} \hat{\Psi}_2(\boldsymbol{r}) . \qquad (3.40)$$

The expressions in Eq. (3.40) are most easily proved by treating θ as a dynamical variable and solving the corresponding equations of motion for the field operators. A $\pi/2$-pulse sets the atoms in an equal superposition of the internal states, that is,

$$\hat{S}_{\pi/2}^\dagger \hat{\Psi}_2(\boldsymbol{r}) \hat{S}_{\pi/2} = \frac{1}{\sqrt{2}} \left[\hat{\Psi}_2(\boldsymbol{r}) + i e^{i\boldsymbol{k}\boldsymbol{r} + i\varphi_{L}} \hat{\Psi}_1(\boldsymbol{r}) \right] ,$$

$$\hat{S}_{\pi/2}^\dagger \hat{\Psi}_1(\boldsymbol{r}) \hat{S}_{\pi/2} = \frac{1}{\sqrt{2}} \left[\hat{\Psi}_1(\boldsymbol{r}) + i e^{-i\boldsymbol{k}\boldsymbol{r} - i\varphi_{L}} \hat{\Psi}_2(\boldsymbol{r}) \right] . \qquad (3.41)$$

In the same spirit, a π-pulse

$$\hat{S}_\pi^\dagger \hat{\Psi}_2(\boldsymbol{r}) \hat{S}_\pi = i e^{i\boldsymbol{k}\boldsymbol{r} + i\varphi_{L}} \hat{\Psi}_1(\boldsymbol{r}) ,$$

$$\hat{S}_\pi^\dagger \hat{\Psi}_1(\boldsymbol{r}) \hat{S}_\pi = i e^{-i\boldsymbol{k}\boldsymbol{r} - i\varphi_{L}} \hat{\Psi}_2(\boldsymbol{r}) \qquad (3.42)$$

inverses the internal states. For general interferometer sequences with many pulses all quantities need to be additionally indexed, as done in Eq. (3.39), i.e. we label $\boldsymbol{k}_j$, θ_j and $\varphi_{L,j}$ for a laser pulse at t_j.

3.3.3. Full interferometer sequence

Having derived explicit expressions for the beam-splitter operators in the previous section, we now turn to the most general interferometer sequence

$$\hat{U}(t_d, t_i) = \hat{U}_e(t_d, t_n) \hat{S}_{\theta_n}(t_n) \hat{U}_e(t_n, t_{n-1}) \hat{S}_{\theta_{n-1}}(t_{n-1}) \; ... \; \hat{S}_{\theta_1}(t_1) \hat{U}_e(t_1, t_i) . \qquad (3.43)$$

As before, $\hat{U}_e$ is the time-evolution operator with respect to the sum of the free and the interaction Hamiltonian. We are now in the position to calculate for instance the

number difference between the two exit ports which is given by the action of the total time-evolution operator, Eq. (3.43), on the operator

$$\delta\hat{N} = \hat{N}_1 - \hat{N}_2 = \int \mathrm{d}^3\boldsymbol{r}\,\left(\hat{\Psi}_1^\dagger(\boldsymbol{r})\hat{\Psi}_1(\boldsymbol{r}) - \hat{\Psi}_2^\dagger(\boldsymbol{r})\hat{\Psi}_2(\boldsymbol{r}) \right) . \qquad (3.44)$$

Note that $\hat{U}_\mathrm{e}$ commutes with $\delta\hat{N}$ since both the free and the interaction Hamiltonian are internal-state preserving.

3.3.4. No interactions

To gain an elementary understanding of sequence, Eq. (3.43), we first set the interaction equal to zero, that is, $\hat{H}_\mathrm{e} = \hat{H}_\mathrm{F}$ and assume for simplicity the same free Hamiltonian for both internal states. This helps us show the identity

$$\hat{U}_\mathrm{F}^\dagger \mathrm{e}^{\mathrm{i}\boldsymbol{k}\boldsymbol{r}}\hat{\Psi}(\boldsymbol{r})\hat{U}_\mathrm{F} = \mathrm{e}^{\mathrm{i}\boldsymbol{k}\boldsymbol{r}}\hat{U}_\mathrm{F}^\dagger\hat{\Psi}(\boldsymbol{r})\hat{U}_\mathrm{F} = \int \mathrm{d}^3\boldsymbol{r}'\,\mathrm{e}^{\mathrm{i}\boldsymbol{k}\boldsymbol{r}}\,\langle \boldsymbol{r}|\hat{\mathcal{U}}|\boldsymbol{r}'\rangle\,\hat{\Psi}(\boldsymbol{r}') = \mathrm{e}^{\mathrm{i}\boldsymbol{k}\boldsymbol{r}}\mathcal{U}\hat{\Psi}(\boldsymbol{r}) \qquad (3.45)$$

and similarly for the action of a beam splitter, e.g. a $\pi/2$ pulse,

$$\hat{S}_{\pi/2}^\dagger \mathcal{U}\hat{\Psi}_2(\boldsymbol{r})\hat{S}_{\pi/2} = \int \mathrm{d}^3\boldsymbol{r}'\,\langle \boldsymbol{r}|\hat{\mathcal{U}}|\boldsymbol{r}'\rangle\,\hat{S}_{\pi/2}^\dagger\hat{\Psi}_2(\boldsymbol{r}')\hat{S}_{\pi/2}$$

$$= \frac{1}{\sqrt{2}}\left(\mathcal{U}\hat{\Psi}_2(\boldsymbol{r}) + \mathrm{i}\mathcal{U}\mathrm{e}^{\mathrm{i}\boldsymbol{k}\boldsymbol{r}}\hat{\Psi}_1(\boldsymbol{r}) \right) . \qquad (3.46)$$

Note the different ordering of $\mathcal{U}$ and the exponential of $\mathrm{i}\boldsymbol{k}\boldsymbol{r}$ in Eq. (3.45) compared to the second term in Eq. (3.46). The attentive reader will already have realized where the discussion leads to. Every laser pulse splits the field operator and creates a new interferometer path by the multiplication with the operator $\mathrm{e}^{\mathrm{i}\boldsymbol{k}\hat{\boldsymbol{r}}}$ which corresponds to the momentum imprint of $\hbar\boldsymbol{k}$. In contrast, for the free evolution the field operators are simply propagated by the first-quantized time-evolution operator $\hat{\mathcal{U}}$. With the help of this insight the calculation of the action of a sequence like Eq. (3.43) on an operator $\mathcal{O}(\hat{\Psi}^\dagger(\boldsymbol{r}), \hat{\Psi}(\boldsymbol{r}))$ becomes a straightforward exercise. One simply exploits Eqs. (3.45) and (3.46) to obtain the transformation of the field operators and subsequently substitutes the result in $\mathcal{O}$. All what is left to do is the manipulation of first-quantized operators.

As an example let us discuss the Mach-Zehnder interferometer in more detail. It corresponds to the sequence

$$\hat{U}(t_\mathrm{d}, t_1) = \hat{S}_{\pi/2}(t_3)\hat{U}_\mathrm{e}(t_3, t_2)\hat{S}_\pi(t_2)\hat{U}_\mathrm{e}(t_2, t_1)\hat{S}_{\pi/2}(t_1) \qquad (3.47)$$

and we measure the number-difference operator, Eq. (3.44). Note that we disregarded the external time-evolution operator from t_3 to t_d at the very left of the sequence in Eq. (3.47) since it commutes with $\delta\hat{N}$. In the following calculation we disregard all laser phases for the sake of clarity. We will include them again below by replacing $\boldsymbol{k}_j\hat{\boldsymbol{r}} \to \boldsymbol{k}_j\hat{\boldsymbol{r}} + \varphi_{\mathrm{L},j}$. We obtain for the MZ sequence

$$\hat{U}^\dagger\hat{\Psi}_1(\boldsymbol{r})\hat{U} = \frac{\mathrm{i}}{2}\left[\mathcal{U}_2 - \mathcal{U}_1\right]\mathrm{e}^{-\mathrm{i}\boldsymbol{k}_1\boldsymbol{r}}\hat{\Psi}_2(\boldsymbol{r}) - \frac{1}{2}\left[\mathcal{U}_1 + \mathcal{U}_2\right]\hat{\Psi}_1(\boldsymbol{r}) \qquad (3.48)$$

and

$$\hat{U}^\dagger \hat{\Psi}_2(\boldsymbol{r})\hat{U} = \frac{\mathrm{i}}{2}\mathrm{e}^{\mathrm{i}\boldsymbol{k}_3\boldsymbol{r}}\left[\mathcal{U}_1 - \mathcal{U}_2\right]\hat{\Psi}_1(\boldsymbol{r}) - \frac{1}{2}\mathrm{e}^{\mathrm{i}\boldsymbol{k}_3\boldsymbol{r}}\left[\mathcal{U}_1 + \mathcal{U}_2\right]\mathrm{e}^{-\mathrm{i}\boldsymbol{k}_1\boldsymbol{r}}\hat{\Psi}_2(\boldsymbol{r}) \tag{3.49}$$

where we defined the time-evolution operators

$$\hat{\mathcal{U}}_2(t_3,t_1) = \hat{\mathcal{U}}(t_3,t_2)\mathrm{e}^{-\mathrm{i}\boldsymbol{k}_2\hat{\boldsymbol{r}}}\hat{\mathcal{U}}(t_2,t_1)\mathrm{e}^{\mathrm{i}\boldsymbol{k}_1\hat{\boldsymbol{r}}} \tag{3.50}$$

and

$$\hat{\mathcal{U}}_1(t_3,t_1) = \mathrm{e}^{-\mathrm{i}\boldsymbol{k}_3\hat{\boldsymbol{r}}}\hat{\mathcal{U}}(t_3,t_2)\mathrm{e}^{\mathrm{i}\boldsymbol{k}_2\hat{\boldsymbol{r}}}\hat{\mathcal{U}}(t_2,t_1) \tag{3.51}$$

along the two paths of an MZ interferometer. If initially all particles occupy state $|1\rangle$, we obtain

$$\delta N \equiv \langle\delta\hat{N}\rangle = \int \mathrm{d}^3\boldsymbol{r}\,\mathfrak{R}\left(\langle\hat{\Psi}_1^\dagger(\boldsymbol{r})\mathcal{U}_1^\dagger\mathcal{U}_2\hat{\Psi}_1(\boldsymbol{r})\rangle\mathrm{e}^{\mathrm{i}\varphi_\mathrm{L}}\right)\,. \tag{3.52}$$

The expectation value is understood to be taken with respect to the initial state and we again included the laser phase $\varphi_\mathrm{L} = \varphi_{\mathrm{L},1} - 2\varphi_{\mathrm{L},2} + \varphi_{\mathrm{L},3}$. In the case of a closed interferometer we find $\hat{\mathcal{U}}_1^\dagger\hat{\mathcal{U}}_2 = \mathrm{e}^{\mathrm{i}\varphi}$ and Eq. (3.52) further simplifies to

$$\delta N = N\cos(\varphi + \varphi_\mathrm{L}) \tag{3.53}$$

where N is the total number of particles. Even for the general case of an open interferometer we reduced the problem to the calculation of the first quantized overlap operator which was done in chapter 1.

3.3.5. Interactions - Transformation to the comoving frames

In the previous section we translated the results of chapter 1 into the language of second quantization. We still need to perform a deeper analysis of the delta-pulse approximation but this will not lead to any major issues. The main reason for discussing the theory in second quantization is of course the straightforward way to include atom-atom interactions. However, apart from formally writing down the sequence as in Eq. (3.43) there seems to be no way for a further simplification since a first-quantized $\hat{\mathcal{U}}$ with

$$\hat{U}_\mathrm{e}^\dagger\hat{\Psi}(\boldsymbol{r})\hat{U}_\mathrm{e} = \mathcal{U}\hat{\Psi}(\boldsymbol{r}) \tag{3.54}$$

when $\hat{H}_\mathrm{e}$ contains a quartic interaction term does not exist. We showed in a direct approach, which is not detailed here, how to find subtle ways to represent the total time-evolution operator as the product of one operator which reproduces the noninteracting result and a second one which contains lengthy terms stemming from transformations of the interaction Hamiltonian. However, these hideous terms are hard to interpret and one does not get deeper insight into the problem.

There is another possible approach, which is a straightforward generalization of the formalism presented in Sec. 1.2. By transforming into the comoving frame of each local atomic cloud, we eliminate the linear potential as well as the linear motion generated by the laser pulses. This transformation is advantageous for the following reasons: For weak interactions and anharmonic potentials the time evolution of the clouds in

these frames is governed, apart from small corrections, by their free expansion. Thus, the interferometer can be numerically simulated on a grid of the size of the atomic wave packets rather than the separation of the arms. Moreover, from the theoretical perspective, the phases accumulated due to the motion along the interferometer paths can be clearly separated from those due to additional effects like atom-atom interaction. Suppose that an atomic cloud is initially located around $\boldsymbol{\chi}_j$ in phase space. As described in Sec. 3.1.2, we transform to the initial comoving frames by replacing the field operators

$$\hat{\Psi}_j(\boldsymbol{r}) \to \mathrm{e}^{\mathrm{i}\phi_j} \mathcal{D}_j \hat{\Psi}_j(\boldsymbol{r}) \tag{3.55}$$

where j labels the internal state and ϕ_j is some initial phase. A note about convention: For the sake of better readability we will abbreviate the displacement operator at initial time $\hat{D}(\boldsymbol{\chi})$ by simply $\hat{D}$, if dependent on time we write $\hat{D}(t)$ instead of $\hat{D}(\boldsymbol{\chi}(t))$. In this section the Hamiltonian will again be given by the sum

$$\hat{H} = \hat{H}_\mathrm{F} + \hat{H}_\mathrm{I} + \hat{H}_\mathrm{L} . \tag{3.56}$$

But how does the transformation into the comoving frames affect the Hamiltonian and the time evolution? In order to address this question we first express the Hamiltonian in terms of the displaced field operators according to Eq. (3.55). The free Hamiltonian becomes

$$\hat{H}_\mathrm{F} = \sum_j \int \mathrm{d}^3\boldsymbol{r} \, \left[\mathcal{D}_j \hat{\Psi}_j(\boldsymbol{r}) \right]^\dagger \mathcal{H}_j(t) \mathcal{D}_j \hat{\Psi}_j(\boldsymbol{r}) . \tag{3.57}$$

For the transformation to the comoving frames we need to replace Eq. (3.57) by the reduced Hamiltonian

$$\hat{H}_\mathrm{R} = \sum_j \int \mathrm{d}^3\boldsymbol{r} \, \hat{\Psi}_j^\dagger(\boldsymbol{r}) \mathcal{H}_j^\mathrm{R}(\boldsymbol{r},t) \hat{\Psi}_j(\boldsymbol{r}) . \tag{3.58}$$

The explicit form of this Hamiltonian will be specified further below, of course it will closely resemble the reduced Hamiltonian, Eq. (1.27). The replacement can easily be achieved by first transforming the time-evolution operator with respect Eq. (3.56) into the interaction picture with respect to $\hat{H}_\mathrm{F}$. Secondly, we reverse the interaction picture with respect to $\hat{H}_\mathrm{R}$

$$
\begin{aligned}
\hat{U}(t, t_\mathrm{i}) =& \mathcal{T} \exp\left\{ -\frac{\mathrm{i}}{\hbar} \int_{t_\mathrm{i}}^t \mathrm{d}t' \left(\hat{H}_\mathrm{F} + \hat{H}_\mathrm{I} + \hat{H}_\mathrm{L} \right) \right\} \\
=& \hat{U}_\mathrm{F}(t, t_\mathrm{i}) \mathcal{T} \exp\left\{ -\frac{\mathrm{i}}{\hbar} \int_{t_\mathrm{i}}^t \mathrm{d}t' \, \hat{U}_\mathrm{F}^\dagger(t', t_\mathrm{i}) \left(\hat{H}_\mathrm{I} + \hat{H}_\mathrm{L} \right) \hat{U}_\mathrm{F}(t', t_\mathrm{i}) \right\} \\
=& \hat{U}_\mathcal{D}(t, t_\mathrm{i}) \mathcal{T} \exp\left\{ -\frac{\mathrm{i}}{\hbar} \int_{t_\mathrm{i}}^t \mathrm{d}t' \left(\hat{H}_\mathrm{R} + \hat{U}_\mathcal{D}^\dagger(t', t_\mathrm{i}) \left[\hat{H}_\mathrm{I} + \hat{H}_\mathrm{L} \right] \hat{U}_\mathcal{D}(t', t_\mathrm{i}) \right) \right\} . \tag{3.59}
\end{aligned}
$$

In the third line we defined

$$\hat{U}_\mathcal{D} = \hat{U}_\mathrm{F} \hat{U}_\mathrm{R}^\dagger . \tag{3.60}$$

When we calculate the action of $\hat{U}_\mathcal{D}$ on the shifted field operators $\mathcal{D}_j \hat{\Psi}_j(\boldsymbol{r})$, we use

$$\exp(\hat{D}_j^\dagger \hat{H} \hat{D}_j) = \hat{D}_j^\dagger \exp(\hat{H}) \hat{D}_j \tag{3.61}$$

to remove the unitary displacement operators from the exponent in the free time-evolution operator and subsequently make use of transformation, Eq. (1.26),

$$\hat{U}_{\mathcal{D}}^{\dagger}\mathcal{D}_j\hat{\Psi}_j(\boldsymbol{r})\hat{U}_{\mathcal{D}} = \mathcal{D}_j\,\mathcal{U}_{\mathrm{F},j}\mathcal{U}_{\mathrm{R},j}^{\dagger}\hat{\Psi}_j(\boldsymbol{r}) = \mathrm{e}^{\mathrm{i}\phi_j(t)}\mathcal{D}_j(t)\hat{\Psi}_j(\boldsymbol{r}) \tag{3.62}$$

where $\hat{\mathcal{U}}_{\mathrm{F},j}$ and $\hat{\mathcal{U}}_{\mathrm{R},j}$ are the respective first-quantized time-evolution operators. The reduced Hamiltonian hence reads

$$\hat{\mathcal{H}}_j^{\mathrm{R}}(t) = \mathcal{H}_j[\hat{\boldsymbol{\xi}} + \boldsymbol{\chi}_j(t)] - \frac{\partial\mathcal{H}_j[\boldsymbol{\chi}_j(t)]^{\mathrm{T}}}{\partial\boldsymbol{\chi}_j(t)}\hat{\boldsymbol{\xi}} - \mathcal{H}_j[\boldsymbol{\chi}_j(t)]. \tag{3.63}$$

Recall the definition $\hat{\boldsymbol{\xi}} = (\hat{\boldsymbol{r}}, \hat{\boldsymbol{p}})^{\mathrm{T}}$ of the six-dimensional phase-space operator from chapter 1. As was shown in Sec. 1.2, the evolution of $\boldsymbol{\chi}_j(t)$ is determined by the classical Hamilton equations of motion with the initial condition $\boldsymbol{\chi}_j(t_{\mathrm{i}}) = \boldsymbol{\chi}_j$ and the phase is calculated as

$$\phi_j(t) = \phi_j(t_{\mathrm{i}}) + \frac{1}{\hbar}S_j(t) - \frac{1}{2\hbar}\left(\boldsymbol{\chi}_j^p(t)\boldsymbol{\chi}_j^r(t) - \boldsymbol{\chi}_j^p(t_{\mathrm{i}})\boldsymbol{\chi}_j^r(t_{\mathrm{i}})\right) \tag{3.64}$$

with the classical action S_j along path j. The initial phase $\phi_j = \phi_j(t_{\mathrm{i}})$ can be freely chosen. Before we apply this formalism to a Raman interferometer, we summarize the main result of this section. It states:

First, express every operator in terms of the displaced field operators $\mathcal{D}_j\hat{\Psi}_j(\boldsymbol{r})$. Second, replace the free Hamiltonian, given by Eq. (3.57) by the reduced Hamiltonian, Eq. (3.63). Third, substitute everywhere in the calculation $\hat{D}_j \to \mathrm{e}^{\mathrm{i}\phi_j(t)}\hat{D}_j(t)$.

3.3.6. The Raman-MZ interferometer with interactions

We now return to the MZ sequence and put our newly acquired knowledge into practical use. In Eq. (3.43) we already discussed a general interferometer sequence. In the case of an MZ interferometer it becomes

$$\hat{U}(t_{\mathrm{d}}, t_{\mathrm{i}}) = \hat{U}_{\mathrm{e}}(t_{\mathrm{d}}, t_3)\hat{S}_{\pi/2}(t_3)\hat{U}_{\mathrm{e}}(t_3, t_2)\hat{S}_{\pi}(t_2)\hat{U}_{\mathrm{e}}(t_2, t_1)\hat{S}_{\pi/2}(t_1)\hat{U}_{\mathrm{e}}(t_1, t_{\mathrm{i}}) \tag{3.65}$$

where $\hat{H}_{\mathrm{e}}$, in contrast to Sec. 3.3.4, now includes the interaction Hamiltonian, Eq. (3.18). For simplicity we shall assume that initially all particles occupy state $|1\rangle$ and the observable to be measured is again the number-difference operator, Eq. (3.52). First, we note that the time-evolution operator on the very left in Eq. (3.65) commutes with this operator, hence it is sufficient to only consider the evolution until $t = t_3$. Second, we interchange the π-pulse beam splitter with the external time-evolution operator to its left. Since the two operators do not commute, this is achieved by inserting $\hat{S}_{\pi}(t_2)\hat{S}_{\pi}^{\dagger}(t_2) = 1$. Subsequently, we act with $\hat{S}_{\pi/2}(t_3)$ and $\hat{S}_{\pi}(t_2)$ on the number-difference operator

$$\hat{S}_{\pi}^{\dagger}(t_2)\hat{S}_{\pi/2}^{\dagger}(t_3)\delta\hat{N}\hat{S}_{\pi/2}(t_3)\hat{S}_{\pi}(t_2) = -\mathrm{i}\int\mathrm{d}^3\boldsymbol{r}\left(\hat{\Psi}_1^{\dagger}(\boldsymbol{r})\hat{\Psi}_2(\boldsymbol{r})\mathrm{e}^{-\mathrm{i}(2\boldsymbol{k}_2\boldsymbol{r}-\boldsymbol{k}_3\boldsymbol{r})} - \mathrm{H.c.}\right), \tag{3.66}$$

where we made use of the beam-splitter transformations, Eq. (3.41) and Eq. (3.42). Note that we again omitted the laser phases for the sake of simple expressions, we will

again include them at the end of the calculation. By inserting unity as explained, the expression $\hat{S}_\pi^\dagger(t_2)\hat{U}_{\mathrm{e}}(t_3,t_2)\hat{S}_\pi(t_2)$ appears. Since the beam splitter operator is unitary, we can raise it in the exponent and define the new free Hamiltonian for $t \in [t_2,t_3]$

$$\tilde{\tilde{\mathcal{H}}}_1 = \mathrm{e}^{-\mathrm{i}\boldsymbol{k}_2\hat{\boldsymbol{r}}}\hat{\mathcal{H}}_2\mathrm{e}^{\mathrm{i}\boldsymbol{k}_2\hat{\boldsymbol{r}}} \qquad \text{and} \qquad \tilde{\tilde{\mathcal{H}}}_2 = \mathrm{e}^{\mathrm{i}\boldsymbol{k}_2\hat{\boldsymbol{r}}}\hat{\mathcal{H}}_1\mathrm{e}^{-\mathrm{i}\boldsymbol{k}_2\hat{\boldsymbol{r}}} \,. \tag{3.67}$$

Moreover, we need to replace

$$g_{11} \leftrightarrow g_{22} \tag{3.68}$$

in the interaction Hamiltonian. Commuting the π-pulse beam splitter to the left and defining new Hamiltonians between t_2 and t_3 has effectively removed the beam splitter at t_2. Thus, the field operators now rather describe the interferometer paths than the internal state. This interpretation together with the interferometer geometry is depicted in Fig. 3.3. Next, in the spirit of the previous section, we transform to the comoving frames, which are carried along the two paths. For that we replace

$$\hat{\Psi}_2(\boldsymbol{r}) \to \mathrm{e}^{\mathrm{i}\phi_2}\mathcal{D}_2\hat{\Psi}_2(\boldsymbol{r}) \,, \tag{3.69}$$

where $\boldsymbol{\chi}_2$ will be chosen later such that $\hat{\Psi}_2(\boldsymbol{r})$ exactly matches $\hat{\Psi}_1(\boldsymbol{r})$ at t_1. The dashed line in Fig. 3.3 shows the path of $\hat{\Psi}_2(\boldsymbol{r})$ before t_1. Since initially only path 1 is occupied, we will refer to the dashed line in Fig. 3.3 as *fictitious input port*. Path 1 starts at $\boldsymbol{\chi}_1 = 0$, hence no replacement of $\hat{\Psi}_1(\boldsymbol{r})$ is necessary.

Transformation to the comoving frames

Having realized that after moving the π-pulse beam splitter to the left, the field operators correspond to the two paths in the MZ interferometer, we define the free evolution operator along path 1

$$\bar{\hat{\mathcal{U}}}_{\mathrm{F},1}(t_3,t_{\mathrm{i}}) = \hat{\mathcal{U}}_{\mathrm{F},2}(t_3,t_2)\mathrm{e}^{\mathrm{i}\boldsymbol{k}_2\hat{\boldsymbol{r}}}\hat{\mathcal{U}}_{\mathrm{F},1}(t_2,t_{\mathrm{i}}) \,. \tag{3.70}$$

Following Sec. 3.3.5, we obtain by using Eq. (3.62) with $\boldsymbol{\chi}_1(t_{\mathrm{i}}) = 0$ and $\phi_1 = 0$

$$\begin{aligned}
\hat{U}_\mathcal{D}^\dagger(t_3,t_{\mathrm{i}})\hat{\Psi}_1(\boldsymbol{r})\hat{U}_\mathcal{D}(t_3,t_{\mathrm{i}}) &= \widetilde{\mathcal{U}}_{\mathrm{F},1}(t_3,t_2)\mathcal{U}_{\mathrm{F},1}(t_2,t_{\mathrm{i}})\mathcal{U}_{\mathrm{R},1}^\dagger(t_3,t_{\mathrm{i}})\hat{\Psi}_1(\boldsymbol{r}) \\
&= \mathrm{e}^{-\mathrm{i}\boldsymbol{k}_2\boldsymbol{r}}\overline{\mathcal{U}}_{\mathrm{F},1}(t_3,t_{\mathrm{i}})\mathcal{U}_{\mathrm{R},1}^\dagger(t_3,t_{\mathrm{i}})\hat{\Psi}_1(\boldsymbol{r}) \\
&= \mathrm{e}^{-\mathrm{i}\boldsymbol{k}_2\boldsymbol{r}}\mathrm{e}^{\mathrm{i}\phi_1(t_3)}\mathcal{D}_1(t_3)\hat{\Psi}_1(\boldsymbol{r})
\end{aligned} \tag{3.71}$$

and we furthermore recalled Eq. (3.67). Combining Eq. (3.70) to one time-evolution operator by including the laser pulse again in the form of a delta function in time, the reduced Hamiltonian after the transformation to the comoving frame is with respect to $\hat{\mathcal{H}}_1$ for $t \in [t_{\mathrm{i}},t_2]$ and with respect to $\hat{\mathcal{H}}_2$ for $t \in [t_2,t_3]$. Furthermore, the laser pulse vanishes in the comoving frame as before. The trajectory $\boldsymbol{\chi}_1(t)$ is determined by the classical Hamilton equations of motion and the phase $\phi_1(t)$ is calculated using Eq. (3.64).
Similarly, we define

$$\bar{\hat{\mathcal{U}}}_{\mathrm{F},2}(t_3,t_{\mathrm{i}}) = \mathrm{e}^{\mathrm{i}\boldsymbol{k}_3\hat{\boldsymbol{r}}}\hat{\mathcal{U}}_{\mathrm{F},1}(t_3,t_2)\mathrm{e}^{-\mathrm{i}\boldsymbol{k}_2\hat{\boldsymbol{r}}}\hat{\mathcal{U}}_{\mathrm{F},2}(t_2,t_{\mathrm{i}}) \,, \tag{3.72}$$

the free time-evolution operator along path 2. With this definition we obtain

$$
\begin{aligned}
\hat{U}_{\mathcal{D}}^{\dagger}(t_3, t_\mathrm{i}) \mathrm{e}^{\mathrm{i}\phi_2} \mathcal{D}_2 \hat{\Psi}_2(\boldsymbol{r}) \hat{U}_{\mathcal{D}}(t_3, t_\mathrm{i}) &= \widetilde{\mathcal{U}}_{\mathrm{F},2}(t_3, t_2) \mathcal{U}_{\mathrm{F},2}(t_2, t_\mathrm{i}) \mathcal{D}_2 \mathrm{e}^{\mathrm{i}\phi_2} \mathcal{U}_{\mathrm{R},2}^{\dagger}(t_3, t_\mathrm{i}) \hat{\Psi}_2(\boldsymbol{r}) \\
&= \mathrm{e}^{\mathrm{i}(\boldsymbol{k}_2 - \boldsymbol{k}_3)\boldsymbol{r}} \, \overline{\mathcal{U}}_{\mathrm{F},2}(t_3, t_\mathrm{i}) \mathcal{D}_2 \mathrm{e}^{\mathrm{i}\phi_2} \mathcal{U}_{\mathrm{R},2}^{\dagger}(t_3, t_\mathrm{i}) \hat{\Psi}_2(\boldsymbol{r}) \\
&= \mathrm{e}^{\mathrm{i}(\boldsymbol{k}_2 - \boldsymbol{k}_3)\boldsymbol{r}} \mathrm{e}^{\mathrm{i}\phi_2(t_3)} \mathcal{D}_2(t_3) \hat{\Psi}_2(\boldsymbol{r})
\end{aligned}
\tag{3.73}
$$

in the same spirit as for path 1. At first sight the calculations in Eq. (3.71) and Eq. (3.73) appear quite lengthy and complicated. Note, however, that the result allows a straight-forward interpretation in terms of field operators (in the Schrödinger picture) which are carried along the interferometer paths due to the time-dependent displacement operator. Thus, if initially an atomic cloud is located at the origin, this simply means that the displacement operator accounts for the motion of the cloud along the interferometer paths. In order to find a way to more intuitively derive this result, we will approach the calculation of this section from a slightly different point of view in Sec. 3.4, which will eventually allow us to treat general interferometer geometries.

Matching condition and laser-atom interaction

So far we transformed the free Hamiltonian to the comoving frames, which has intro-duced the time-dependent displacement of the field operators along the classical trajec-tories. We will discuss the impact of this transformation on the interaction Hamiltonian further below but first, we turn to the initial phase and position of the field operator corresponding to path 2, which so far were completely arbitrary. This ambiguity will be fixed in the following by matching the trajectories at the remaining beam splitter at t_1. Indeed, when we substitute $\hat{\Psi}_j(\boldsymbol{r}) \rightarrow \mathrm{e}^{\mathrm{i}\phi_j(t)} \mathcal{D}_j(t) \hat{\Psi}_j(\boldsymbol{r})$ in Eq. (3.39), we can eliminate the exponential $\mathrm{e}^{\mathrm{i}\boldsymbol{k}\hat{\boldsymbol{r}}}$ by choosing the matching conditions

$$
\begin{aligned}
\boldsymbol{\chi}_2^r(t_1) &= \boldsymbol{\chi}_1^r(t_1) \\
\boldsymbol{\chi}_2^p(t_1) &= \boldsymbol{\chi}_1^p(t_1) + \hbar\boldsymbol{k} \, .
\end{aligned}
\tag{3.74}
$$

In addition to the matching of position and momentum, we eliminate any dependency of the beam splitter on a phase in App. C.3.1 by choosing ϕ_2 appropriately. After some algebra, this choice leads to

$$
\phi_2(t) = \varphi_{\mathrm{L}}(t_1) + \frac{1}{\hbar} \int_{t_\mathrm{i}}^{t} \mathrm{d}t' \, \overline{\mathscr{L}}_2(t') - \frac{1}{2\hbar} \left[\boldsymbol{\chi}_j^p(t) \boldsymbol{\chi}_j^r(t) - \boldsymbol{\chi}_1^p(t_\mathrm{i}) \boldsymbol{\chi}_1^r(t_\mathrm{i}) \right]
\tag{3.75}
$$

with the Lagrange function

$$
\overline{\mathscr{L}}_2(t) = \mathscr{L}_j(t) + \hbar\boldsymbol{k}\boldsymbol{\chi}_1^r(t)\delta(t - t_1)
\tag{3.76}
$$

where $j = 1$ for $t_\mathrm{i} \le t \le t_1$ and $j = 2$ for $t > t_1$. The interpretation of Eq. (3.75) is obvious. It is the phase acquired along the real physical path, that is, along path 1 from t_i to t_1 and along path 2 for later times. Thus, the matching conditions for position, momentum, and phase eliminate the dependency on the fictitious input port and replace it by the actual path. With these considerations the resulting beam-splitter Hamiltonian at t_1 simplifies to

$$
\hat{U}_{\mathcal{D}}^{\dagger} \hat{H}_{\mathrm{L}}(t) \hat{U}_{\mathcal{D}} = -\frac{\hbar\theta_1}{2}\delta(t - t_1) \int \mathrm{d}^3\boldsymbol{r} \left(\hat{\Psi}_2^{\dagger}(\boldsymbol{r}) \hat{\Psi}_1(\boldsymbol{r}) + \mathrm{H.c.} \right) ,
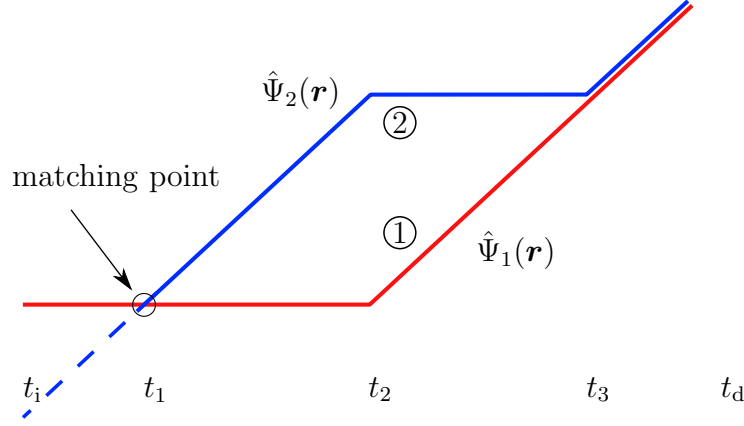\tag{3.77}
$$

Figure 3.3.: Visualization of the two paths of an MZ interferometer. After inter-
changing the π-pulse beam splitter with the adjacent external time-evolution
operator, the field operators describe the two interferometer paths rather than
the internal states. As a result, the transformation introduced in Sec. 3.3.5
corresponds to a change into the comoving frames carried along the two paths.
At t_1 the field operators are matched in order to eliminate any dependence on
the external degrees of freedom from the atom-laser interaction Hamiltonian.
The dashed line is referred to as fictitious input port as the occupation of $\hat{\Psi}_2(\boldsymbol{r})$
is zero until t_1.

which does neither transfer momentum nor imprint a phase. Finally, we mention that
the fictitious input port still remains present in the external Hamiltonian for $t < t_1$.
However, here only $\hat{\Psi}_1$ is occupied so that this fact is of no physical consequences.

Atom-atom interaction

At the end of this section we discuss the interaction Hamiltonian. Fortunately, this is a
straightforward exercise since due to the bilinear form of the interaction Hamiltonian,
the phase factors in Eqs. (3.71) and (3.73) cancel and one simply needs to replace
$\hat{\Psi}_j(\boldsymbol{r}) \to \mathcal{D}_j(t)\hat{\Psi}_j(\boldsymbol{r})$. Hence,

$$\hat{H}_{\mathrm{I}} = \int \mathrm{d}^3\boldsymbol{r} \left\{ \frac{g_1}{2}\hat{\Psi}_1^\dagger(\boldsymbol{r})^2\hat{\Psi}_1(\boldsymbol{r})^2 + \frac{g_2}{2}\hat{\Psi}_2^\dagger(\boldsymbol{r})^2\hat{\Psi}_2(\boldsymbol{r})^2 \right.$$
$$\left. + g_{12}[\mathcal{D}_1(t)\hat{\Psi}_1(\boldsymbol{r})]^\dagger \mathcal{D}_1(t)\hat{\Psi}_1(\boldsymbol{r})[\mathcal{D}_2(t)\hat{\Psi}_2(\boldsymbol{r})]^\dagger \mathcal{D}_2(t)\hat{\Psi}_2(\boldsymbol{r}) \right\}, \qquad (3.78)$$

where we used Eq. (C.8) to show that the displacement operators drop out of the first
two terms. The time-dependent relative displacement between the field operators in
the second line of Eq. (3.78) accounts for the separation of the clouds between t_1 and t_3.
Most remarkable is the fact that for a sufficiently small extension of the atomic clouds
they do not overlap most of the time. Furthermore, in the case of weak interactions,
distortion effects due to the dynamical separation of the atomic clouds are small and
the second line of Eq. (3.78) can be neglected so that the interaction Hamiltonian
becomes time independent. In fact, this approximation will be used in chapter 4 to
study two-mode squeezing.

Summary and discussion

When we substitute Eqs. (3.71) and (3.73) into Eq. (3.66), recall the full MZ sequence, Eq. (3.65), and combine the two displacement operators with the help of the composition rule, Eq. (A.10), we obtain the final result

$$\hat{U}^\dagger(t_\mathrm{d},t_\mathrm{i})\delta\hat{N}\hat{U}(t_\mathrm{d},t_\mathrm{i}) = -\mathrm{i}\int \mathrm{d}^3\boldsymbol{r}\,\hat{U}_\mathrm{MZ}^\dagger(t_3,t_\mathrm{i})\left\{\hat{\Psi}_1^\dagger(\boldsymbol{r})\mathcal{D}(\Delta\boldsymbol{\chi})\hat{\Psi}_2(\boldsymbol{r})\mathrm{e}^{\mathrm{i}\phi_\mathrm{MZ}} - \mathrm{H.c.}\right\}\hat{U}_\mathrm{MZ}(t_3,t_\mathrm{i}) \tag{3.79}$$

where $\Delta\boldsymbol{\chi} = \boldsymbol{\chi}_2(t_3) - \boldsymbol{\chi}_1(t_3)$ and the Mach-Zehnder phase reads

$$\phi_\mathrm{MZ} = \varphi_\mathrm{L} + \frac{1}{\hbar}\Delta S(t_3) - \frac{1}{2\hbar}\Delta\boldsymbol{\chi}^r(t_3)\left[\boldsymbol{\chi}_2^p(t_3) + \boldsymbol{\chi}_1^p(t_3)\right]. \tag{3.80}$$

The total laser phase abbreviates $\varphi_\mathrm{L} = \varphi_{\mathrm{L},1} - 2\varphi_{\mathrm{L},2} + \varphi_{\mathrm{L},3}$ and $\Delta S(t_3) = S_2(t_3) - S_1(t_3)$ is the classical action difference along the two paths. The remaining time evolution operator $\hat{U}_\mathrm{MZ}$ contains the reduced one-body Hamiltonians, the laser-atom interaction Hamiltonian at $t = t_1$ without momentum transfer and phase imprint as well as the interaction Hamiltonian, Eq. (3.78).

In summary, we provided a formalism in which the local atomic clouds along the paths are described from their comoving frames. Working in second quantization, we included particle-particle interaction into this framework, providing a natural generalization to Sec. 1.2. Indeed, in the limit of zero interactions, Eq. (3.80) reduces to Eq. (1.33). We stress that this formalism is exact also for arbitrary potentials as long as the delta-pulse approximation is valid. Describing atom interferometers from the comoving frames, a numerical simulation of the Gross-Pitaevskii equation becomes computationally less demanding when the simulation is performed on a grid of the size of the atomic clouds rather than the extent of the whole interferometer. However, it is important to mention that the theory is limited to interferometer geometries where exactly two paths are present, as for example in the MZ interferometer or in butterfly geometries. In the next section we will generalize this formalism to multi-path sequences and other diffraction schemes like Bragg diffraction or double-Bragg diffraction.

3.4.   More complex interferometer geometries

In the preceding section we discussed the MZ interferometer employing Raman diffraction. In this context we demonstrated how to relate the two field operators corresponding to the two internal states to the exactly two paths in an MZ interferometer. However, how do we for instance describe a multiple-path geometry? Even in an MZ interferometer with imperfect π pulse one in principle needs to take into account spurious branches. More fundamentally, how do we treat Bragg diffraction, where only one internal state is present during the whole interferometer sequence and the mapping between internal state and path breaks down? In this section we aim at a solution to this problem by introducing different field operators for every interferometer path. These will only satisfy approximate bosonic commutation relations but the conditions for an accurate approximation will generally turn out to be well satisfied.

3.4.1. Decomposing phase space

Now we turn to this problem more formally by decomposing phase space into small disjoint boxes $\Omega_j = \Omega_j^r \times \Omega_j^p$ of the same size, centered at $\boldsymbol{\chi}_j$ and labeled by the double index j for the momentum and position direction. Special importance will be assigned to $\Omega_0 = \Omega_0^r \times \Omega_0^p$, the volume around the origin in phase space. Furthermore, we define the operator

$$\hat{\Pi} = \int_{\Omega_0^r} \mathrm{d}^3\boldsymbol{r}\, |\boldsymbol{r}\rangle\langle\boldsymbol{r}| \int_{\Omega_0^p} \mathrm{d}^3\boldsymbol{p}\, |\boldsymbol{p}\rangle\langle\boldsymbol{p}| \,, \tag{3.81}$$

which at first sight might look like a projector on Ω_0 in phase space as it is the product of the respective position and momentum projectors. However, it is important to note that $\hat{\Pi}$ itself is not a projector. The reason for this is that a projection in momentum space alters the distribution in position space and vice versa, as described by Heisenberg's uncertainty principle. This is visualized in more detail in Fig. 3.4. Indeed, if $\hat{\Pi}$ was a projector, we could prepare states violating the uncertainty principle. Let us illuminate this effect from a slightly different angle by defining:
A state $|\psi\rangle$ is said to have *support* on Ω_0 if $\langle\boldsymbol{p}\,|\psi\rangle$ and $\langle\boldsymbol{r}\,|\psi\rangle$ are only different from zero for $\boldsymbol{p} \in \Omega_0^p$ and $\boldsymbol{r} \in \Omega_0^r$. If this is true, the application of Eq. (3.81) leaves the state invariant, since

$$\hat{\Pi}\,|\psi\rangle = \int_{\Omega_0^r} \mathrm{d}^3\boldsymbol{r}\, |\boldsymbol{r}\rangle\langle\boldsymbol{r}| \int \mathrm{d}^3\boldsymbol{p}\, |\boldsymbol{p}\rangle\langle\boldsymbol{p}\,|\psi\rangle = \int \mathrm{d}^3\boldsymbol{r}\, |\boldsymbol{r}\rangle\langle\boldsymbol{r}\,|\psi\rangle = |\psi\rangle \,. \tag{3.82}$$

As $\langle\boldsymbol{p}\,|\psi\rangle$ is zero outside of Ω_0^p, we extended the integral over the full momentum space and recalled the decomposition of unity $\int\mathrm{d}^3\boldsymbol{p}\, |\boldsymbol{p}\rangle\langle\boldsymbol{p}| = 1$. The same argument holds for the subsequent projection in position space. In contrast, if the state only differs from zero outside Ω_0^r and Ω_0^p, the action of $\hat{\Pi}$ on this state produces zero. Clearly, if $|\psi\rangle$ has support on Ω_0, it is also left invariant by $\hat{\Pi}^\dagger$. We now define the operator

$$\hat{\Pi}_j = \hat{D}_j\,\hat{\Pi}\,\hat{D}_j^\dagger \,, \tag{3.83}$$

which is the product of the position and momentum projector on Ω_j as discussed in App. C.3.2. The displacement operator on the right side first shifts the phase-space distribution from Ω_j to Ω_0, followed by the action of $\hat{\Pi}$, after which the state is displaced back to Ω_j. Clearly, a state with support on Ω_j stays invariant under the action of $\hat{\Pi}_j$ in the same spirit as realized in Eq. (3.82). Next, we define

$$|\psi_j\rangle = \hat{\Pi}_j\,|\psi\rangle \,. \tag{3.84}$$

The crucial insight is that *if* $|\psi_j\rangle$ has support on Ω_j the operator $\hat{\Pi}_j$ acts as a projector since

$$\hat{\Pi}_j^2\,|\psi\rangle = \hat{\Pi}_j\,|\psi_j\rangle = |\psi_j\rangle = \hat{\Pi}_j\,|\psi\rangle \,, \tag{3.85}$$

where we used Eq. (3.84) twice and Eq. (3.82). In the following we will show that if $\hat{\Pi}_j$ acts as a projector for all j on a given quantum state, we can introduce field operators for each path, which satisfy bosonic commutation relations on Ω_0.
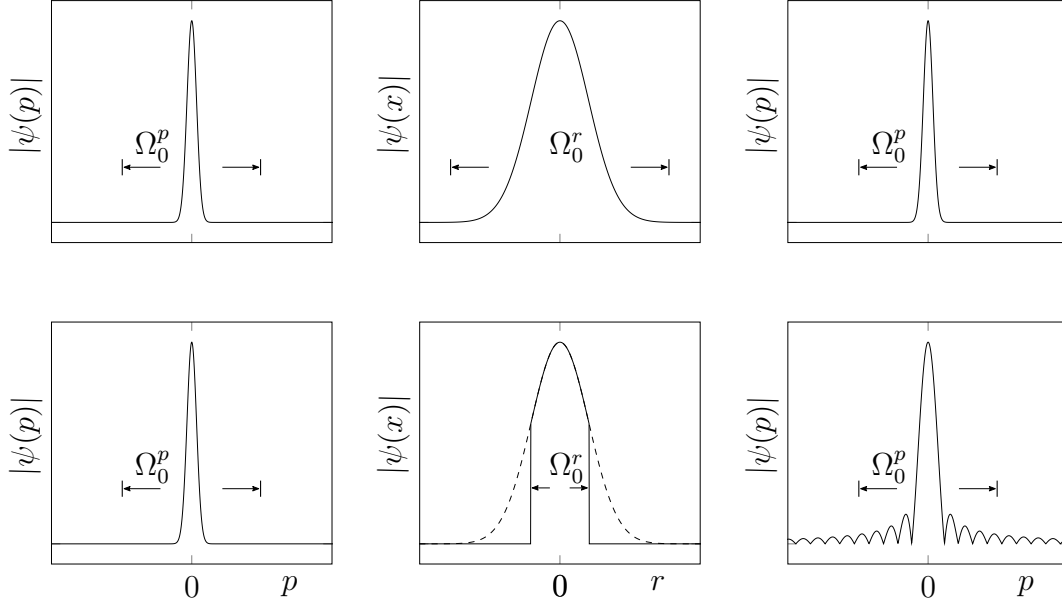
Figure 3.4.: Action of the operator $\hat{\Pi}$ on a quantum state. The crucial difference between the two rows is the different width of the box in position space. First row: The state has support on Ω_0^p as well as Ω_0^r, that is, the projection in momentum and subsequently in position space leaves the state invariant. Consequently, $\hat{\Pi}$ acts as a projector. Second row: The state has support inside Ω_0^p but the projection on Ω_0^r in position space cuts off the state (dashed line vs. solid line). After Fourier transforming, the momentum representation has changed with respect to the initial state. As the subsequent application of $\hat{\Pi}$ again alters the state, it does not act as a projector.

3.4.2. Path-dependent field operators

So far the discussion has been in first quantization. We are now confronted with the problem of how to transfer the insights we gained into second quantization. Since a field operator is associated with a phase-space distribution only by the many-particle state $|\Psi\rangle$, when we refer to the 'position- and momentum distribution of a field', we always implicitly mean the expectation values with respect to $|\Psi\rangle$

$$\langle \hat{\Psi}^\dagger(\boldsymbol{r})\hat{\Psi}(\boldsymbol{r})\rangle \quad \text{and} \quad \langle \hat{\Psi}^\dagger(\boldsymbol{p})\hat{\Psi}(\boldsymbol{p})\rangle . \tag{3.86}$$

We begin by decomposing unity in App. C.3.2 as

$$1 = \sum_j \hat{D}_j \, \hat{\Pi} \, \hat{D}_j^\dagger , \tag{3.87}$$

which we insert into the mode expansion of the field operator

$$\hat{\Psi}(\boldsymbol{r}) = \sum_n \langle \boldsymbol{r} \, | n \rangle \, \hat{a}_n = \sum_j \langle \boldsymbol{r} | \, \hat{D}_j \sum_n \hat{\Pi}\hat{D}_j^\dagger \, | n \rangle \, \hat{a}_n \equiv \sum_j \mathcal{D}_j \hat{\Psi}_j(\boldsymbol{r}) . \tag{3.88}$$

As before, we can multiply each field operator with an arbitrary phase, which we omit for more clarity in the expressions. The equation might as well be inverted

$$\hat{\Psi}_j(\boldsymbol{r}) = \sum_n \langle \boldsymbol{r} | \, \hat{\Pi} \hat{D}_j^\dagger \, | n \rangle \, \hat{a}_n = \int \mathrm{d}^3 \boldsymbol{r}' \, \langle \boldsymbol{r} | \, \hat{\Pi} \hat{D}_j^\dagger \, | \boldsymbol{r}' \rangle \, \hat{\Psi}(\boldsymbol{r}') = \Pi \mathcal{D}_j^\dagger \hat{\Psi}(\boldsymbol{r}) \, . \tag{3.89}$$

With these definitions we turn to the commutation relations of the new field operators. Using Eq. (3.89) and $[\hat{\Psi}(\boldsymbol{r}), \hat{\Psi}^\dagger(\boldsymbol{r}')] = \delta(\boldsymbol{r} - \boldsymbol{r}')$, it is straightforward to show that

$$\left[\hat{\Psi}_j(\boldsymbol{r}), \hat{\Psi}_l^\dagger(\boldsymbol{r}') \right] = \delta_{jl}^\Omega(\boldsymbol{r} - \boldsymbol{r}') \neq \delta(\boldsymbol{r} - \boldsymbol{r}')\delta_{jl} \tag{3.90}$$

with the incomplete delta function

$$\delta_{jl}^\Omega(\boldsymbol{r} - \boldsymbol{r}') = \langle \boldsymbol{r} | \, \hat{\Pi} \hat{D}_j^\dagger \hat{D}_l \hat{\Pi}^\dagger \, | \boldsymbol{r}' \rangle \, . \tag{3.91}$$

The commutation relations in Eq. (3.90) are not bosonic as expected. However, Eq. (3.91) should be thought of in a distributional sense. Given the function $f(\boldsymbol{r}) = \langle \boldsymbol{r} \, | f \rangle$ with support on Ω_0, we find

$$\int \mathrm{d}^3 \boldsymbol{r}' \, \delta_{jl}^\Omega(\boldsymbol{r} - \boldsymbol{r}') f(\boldsymbol{r}') = \langle \boldsymbol{r} | \, \hat{\Pi} \hat{D}_j^\dagger \hat{D}_l \hat{\Pi}^\dagger \, | f \rangle = f(\boldsymbol{r})\delta_{jl} \, , \tag{3.92}$$

where we recalled that $\hat{\Pi}^\dagger | f \rangle = | f \rangle$. The state only remains in Ω_0 if $j = l$, otherwise it becomes displaced to a different box in phase space and the subsequent action of $\hat{\Pi}$ yields zero. If f has support on the complement of Ω_0, Eq. (3.92) is zero.

Methodology

In the previous section we realized that the path-dependent field operators satisfy bosonic commutation relations with respect to the incomplete delta function. In this paragraph we will lay out a formalism based on this insight.

In the case of light-pulse interferometry, the field operator in momentum representation disintegrates into parts closely located around multiples of $\hbar k$. The momentum spread of these local atomic clouds can be estimated for a Bose-Einstein condensate trapped in a harmonic potential [142] as $\Delta p/\hbar k \sim 1/kR \ll 1$, where R is the initial Thomas-Fermi radius. Furthermore, the interaction energy converted into kinetic energy during the expansion after switching off the trap leads to only a slight change of this result [183]. In the same manner for large arm separation the local clouds with the same mean momentum never overlap in position space. As can be seen from the definition of the path-dependent field operators, Eq. (3.89), the displacement operators shift the local atomic clouds to the origin of momentum- and position space. As we will realize further below, this again corresponds to a transformation to the comoving frames. From the considerations made above we conclude that it is meaningful to assume that there exists a decomposition of phase space and path-dependent field operators at each instance of time so that $\hat{\Pi}$ acts as a projector on $\hat{\Psi}_j(\boldsymbol{r})$. For that reason the incomplete delta function defined in Eq. (3.91) will reduce to the usual delta function times Kronecker delta as we will see in the following calculations. In the comoving frames the time
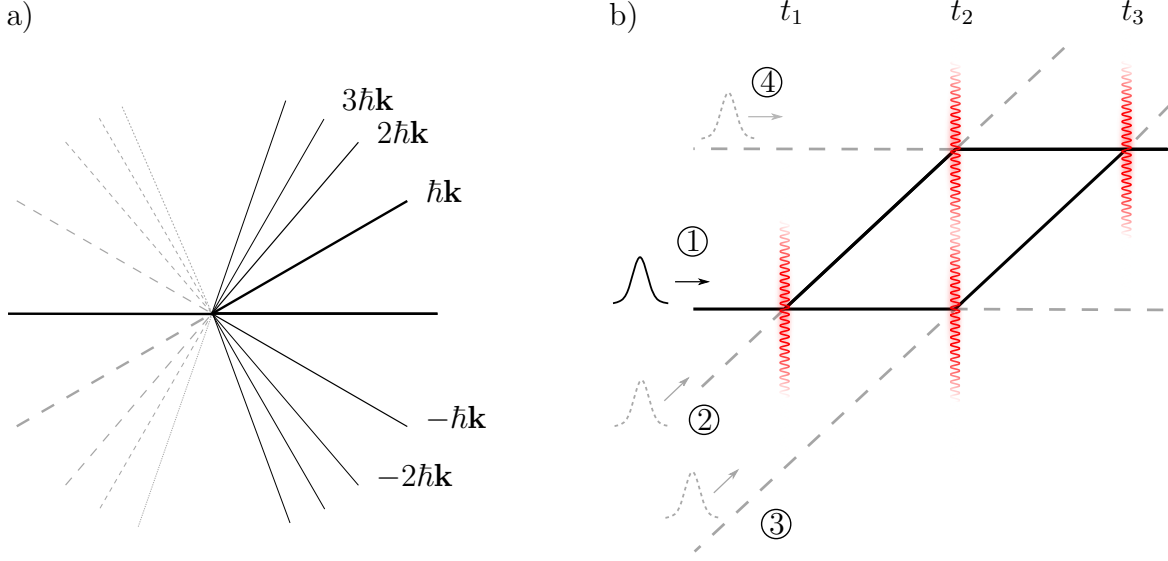
Figure 3.5.: Allocation of approximate bosonic field operators to each path. a) A laser
pulse drives transitions between branches separated by multiples of $\hbar\boldsymbol{k}$. For
sufficiently small momentum spread of the local clouds we can assign bosonic
field operators to each path. In this picture the laser pulses simply change the
population of the fields at the intersections of the paths. In the following we
will refer to the space-time point where one momentum branch is plit in many
as *vertex of an interferometer*. b) Description of an MZ interferometer as an
eight-port interferometer, where we take into account only the resonant paths.
Initially, all particles reside in path 1, illustrated by the solid density profile.
Over the course of the interferometer the laser pulses successively populate the
paths corresponding to the fictitious input ports.

evolution is governed by the free expansion of the cloud, only slightly distorted by the
residual (weak) potential and particle-particle interaction.

We now introduce a field operator for each interferometer path. As can be seen in
Fig. 3.5, we promote the interferometer to a multi-port geometry, the paths correspond
to the solutions of the classical Hamilton equations of motion with respect to the free
Hamiltonian. The laser pulses couple the paths and exchange population between
them. Every path which becomes populated by the laser pulse is interpreted as a
fictitious input port into which the vacuum is fed. For each laser pulse we will derive
matching conditions similar to Sec. 3.3.6 between the incoming populated field and the
vacuum of a new path in a way that no momentum is transferred from the perspective
of the comoving frames.

During a Bragg pulse the laser-atom interaction drives transitions between many paths.
In our formalism each corresponds to a path-dependent field operator. This is depicted
in Fig. 3.5.a. The case of a MZ interferometer, where in the lowest-order approximation
we only take into account the resonant paths, is illustrated in Fig. 3.5.b.

The formalism is based on the insight that the Gross-Pitaevskii equation can be de-

coupled when applied to a state with support only on clearly separated subsets of momentum space. This idea was originally exploited in the context of nonlinear fiber optics [204] and referred to as *slowly varying envelope approximation*. The application to Bose-Einstein condensates was pioneered by Trippenbach et al. [205] and was utilized to treat interaction effects during the cloud separation after a Kapitza-Dirac pulse in Refs. [195, 206]. In the present work this idea is formalized, generalized to second quantization, to include potentials and atom-light interaction, and to general interferometer geometries.

3.4.3. Dynamical evolution

Having defined new field operators, we now turn to the time evolution. In the following three paragraphs we subsequently discuss the free Hamiltonian, the interaction Hamiltonian, and the laser-atom interaction Hamiltonian.

Free Hamiltonian

In Eq. (3.88) we assigned a field operator to each trajectory and a displacement operator which initially shifts the boxes associated with each local atomic cloud to the origin of phase space. As the local wave packets move during the interferometer time (mainly in position space), the boxes around them do so as well. Representing the field operator as in Eq. (3.88), we will show in the following that the transformation to the comoving frame of each field operator correspond to a shift of the time-dependent position of the boxes to the center of Ω_0. Thus, we will be able to describe the whole time evolution within the interferometer from the perspective of Ω_0.
The free Hamiltonian is again given by

$$\hat{H}_{\mathrm{F}} = \int \mathrm{d}^3\boldsymbol{r}\, \hat{\Psi}^\dagger(\boldsymbol{r})\mathcal{H}(\boldsymbol{r})\hat{\Psi}(\boldsymbol{r})\,, \tag{3.93}$$

which we would like to replace by the reduced Hamiltonian, Eq. (3.63),

$$\hat{H}_{\mathrm{F}} \to \hat{H}_{\mathrm{R}} = \sum_j \int \mathrm{d}^3\boldsymbol{r}\, \hat{\Psi}_j^\dagger(\boldsymbol{r})\mathcal{H}_j^{\mathrm{R}}\hat{\Psi}_j(\boldsymbol{r}) \tag{3.94}$$

for each trajectory. The evolution with respect to this Hamiltonian is governed by dispersion effects and the influence of (small) harmonic as well as anharmonic contributions but the position of the center of the cloud will only slightly be modified. We now calculate the Heisenberg equations of motion with respect to Eq. (3.94)

$$\mathrm{i}\hbar\frac{\mathrm{d}}{\mathrm{d}t}\hat{\Psi}_j(\boldsymbol{r},t) = \left[\hat{\Psi}_j(\boldsymbol{r},t), \hat{H}_{\mathrm{R}}\right] = \sum_n \int \mathrm{d}^3\boldsymbol{r}'\, \delta_{jn}^\Omega(\boldsymbol{r}-\boldsymbol{r}')\mathcal{H}_n^{\mathrm{R}}\hat{\Psi}_n(\boldsymbol{r}',t)$$

$$= \mathcal{H}_j^{\mathrm{R}}\hat{\Psi}_j(\boldsymbol{r},t)\,. \tag{3.95}$$

Here, we used the commutation relation, Eq. (3.90), assumed that initially $\hat{\Psi}_n(\boldsymbol{r})$ has support on Ω_0 for all n and that this property is preserved during the time evolution

with respect to $\hat{\mathcal{H}}_n^{\mathrm{R}}$. In this case Eq. (3.95) is exact, however, for real systems this result will at all times be only approximately correct. The solution to Eq. (3.95) is

$$\hat{U}_{\mathrm{R}}^{\dagger}\hat{\Psi}_j(\boldsymbol{r})\hat{U}_{\mathrm{R}} = \mathcal{U}_{\mathrm{R},j}\hat{\Psi}_j(\boldsymbol{r})\,. \tag{3.96}$$

In order to perform the replacement $\hat{H}_{\mathrm{F}} \to \hat{H}_{\mathrm{R}}$ in the full time-evolution operator, we proceed along the lines of Eq. (3.59). We transform into the interaction picture with respect to $\hat{H}_{\mathrm{F}}$ and subsequently reverse it with respect to $\hat{H}_{\mathrm{R}}$. Defining as before $\hat{U}_{\mathcal{D}} = \hat{U}_{\mathrm{F}}\hat{U}_{\mathrm{R}}^{\dagger}$, we obtain

$$\hat{U}_{\mathcal{D}}^{\dagger}\hat{\Psi}(\boldsymbol{r})\hat{U}_{\mathcal{D}} = \hat{U}_{\mathrm{R}}\sum_j \mathcal{U}_{\mathrm{F}}\mathcal{D}_j\hat{\Psi}_j(\boldsymbol{r})\hat{U}_{\mathrm{R}}^{\dagger} = \sum_j \mathcal{U}_{\mathrm{F}}\mathcal{D}_j\mathcal{U}_{\mathrm{R},j}^{\dagger}\hat{\Psi}_j(\boldsymbol{r}) = \sum_j \mathrm{e}^{\mathrm{i}\phi_j(t)}\mathcal{D}_j(t)\hat{\Psi}_j(\boldsymbol{r})\,. \tag{3.97}$$

We first used the result of App. C.1.1 and recalled the definition of the new field operators, Eq. (3.88). In the second step we applied Eq. (1.26), which leads to time-dependent displacement operators. Also recall the abbreviation $\hat{D}(t) \equiv \hat{D}(\boldsymbol{\chi}(t))$. The trajectory is determined by the classical Hamilton equations of motion and the dynamical phase is related to the classical action along the path by

$$\phi_j(t) = \phi_j + \frac{1}{\hbar}\int_{t_{\mathrm{i}}}^t \mathrm{d}t'\, S_j(t') - \frac{1}{2\hbar}\left(\boldsymbol{\chi}_j^p(t)\boldsymbol{\chi}_j^r(t) - \boldsymbol{\chi}_j^p\boldsymbol{\chi}_j^r\right)\,, \tag{3.98}$$

where we again included an initial phase ϕ_j. Note again that variables without time argument are supposed to be evaluated at $t = t_{\mathrm{i}}$.

In summary we showed in this paragraph that if $\hat{\Psi}_j(\boldsymbol{r})$ has support on Ω_0 during the evolution with respect to $\hat{\mathcal{H}}_j^{\mathrm{R}}$, we simply need to replace

$$\hat{H}_{\mathrm{F}} \to \hat{H}_{\mathrm{R}} \tag{3.99}$$

and

$$\hat{U}_{\mathcal{D}}^{\dagger}\hat{\Psi}(\boldsymbol{r})\hat{U}_{\mathcal{D}} = \sum_j \mathrm{e}^{\mathrm{i}\phi_j(t)}\mathcal{D}_j(t)\hat{\Psi}_j(\boldsymbol{r})\,, \tag{3.100}$$

everywhere else in the calculation. By this replacement we effectively remove the main part of the time evolution from the interferometer, namely the motion of the atomic clouds along the interferometer trajectories. The residual motion is simply given by the time evolution inside the comoving frames.

Interaction Hamiltonian

So far we only considered the free Hamiltonian. Now we extend the ideas of the previous section to interacting systems and investigate which additional conditions we need to require on the state and the decomposition of phase space. Performing the transformation, Eq. (3.59), replaces

$$\hat{\Psi}(\boldsymbol{r}) \to \hat{U}_{\mathcal{D}}^{\dagger}\hat{\Psi}(\boldsymbol{r})\hat{U}_{\mathcal{D}} = \sum_j \mathrm{e}^{\mathrm{i}\phi_j(t)}\mathcal{D}_j(t)\hat{\Psi}_j(\boldsymbol{r}) \tag{3.101}$$

in the interaction Hamiltonian, Eq. (3.17),

$$\hat{H}_{\mathrm{I}} = \frac{g}{2} \int \mathrm{d}^3 r \, \hat{\Psi}^\dagger(\boldsymbol{r}) \hat{\Psi}^\dagger(\boldsymbol{r}) \hat{\Psi}(\boldsymbol{r}) \hat{\Psi}(\boldsymbol{r}) \,. \tag{3.102}$$

We show in App. C.3.3 that the equations of motion with respect to the transformed interaction Hamiltonian can be written as

$$\mathrm{i}\hbar \frac{\mathrm{d}}{\mathrm{d}t} \hat{\Psi}_j(\boldsymbol{r},t) = g \sum_{\mathrm{coupl.}} \mathrm{e}^{\mathrm{i}\phi_{jmlk}(t)} \left[\mathcal{D}_j^\dagger(t)\mathcal{D}_m(t)\hat{\Psi}_m(\boldsymbol{r},t) \right]^\dagger$$
$$\times \left[\mathcal{D}_j^\dagger(t)\mathcal{D}_l(t)\hat{\Psi}_l(\boldsymbol{r},t) \right] \left[\mathcal{D}_j^\dagger(t)\mathcal{D}_k(t)\hat{\Psi}_k(\boldsymbol{r},t) \right] \,, \tag{3.103}$$

where the phase is

$$\phi_{jmlk}(t) = \phi_l(t) + \phi_k(t) - \phi_j(t) - \phi_m(t) \,. \tag{3.104}$$

The sum in Eq. (3.103) runs over all indices in momentum space with

$$\Delta \boldsymbol{\chi}_{jmlk}^p(t) = \boldsymbol{\chi}_l^p(t) + \boldsymbol{\chi}_k^p(t) - \boldsymbol{\chi}_j^p(t) - \boldsymbol{\chi}_m^p(t) \cong 0 \tag{3.105}$$

and only takes into account terms with support on Ω_0^r. As shown in App. C.3.3 we need to impose a stronger condition on the momentum distributions of the field operators, namely they must have support on only a third of Ω_0^p. The relative displacement in Eq. (3.105) approximately connects the centers of the boxes in momentum space. We assume that three times the width of the momentum distribution displaced by this deviation still has support on Ω_0^p. If satisfied, Eq. (3.103) is exact and the field operators $\hat{\Psi}_j(\boldsymbol{r})$ remain supported on Ω_0. From the perspective of the comoving frames the separation of the atomic clouds (e.g. later originating from the interaction with a laser), enters the equation by the time-dependent displacement operators in the interaction Hamiltonian. It is important to note that the assumptions made above need to be carefully reviewed for each choice of a decomposition of phase space and interferometer geometry but the approximation is generally well suited for the experiments discussed in this work.

Laser-atom interaction

Finally, we turn to the last part of the Hamiltonian, the atom-light interaction. In this paragraph we investigate Bragg diffraction but other schemes, e.g. double Bragg diffraction do not pose any fundamental difficulties. After adiabatic elimination of the exited state, the effective laser-coupling Hamiltonian reads

$$\hat{H}_{\mathrm{L}} = -\hbar\Omega(t) \int \mathrm{d}^3 r \, \hat{\Psi}^\dagger(\boldsymbol{r}) \hat{\Psi}(\boldsymbol{r}) \, \mathrm{e}^{\mathrm{i}\boldsymbol{k}\boldsymbol{r} + \mathrm{i}\varphi_{\mathrm{L}}(t)} + \mathrm{H.c.} \,, \tag{3.106}$$

which was derived in Eq. (3.29). After performing transformation, Eq. (3.59), the equation of motion with respect to Eq. (3.106) is obtained as

$$\mathrm{i}\hbar \frac{\mathrm{d}}{\mathrm{d}t} \hat{\Psi}_m(\boldsymbol{r},t) = -\hbar\Omega(t) \sum_{n,j} \int \mathrm{d}^3 r' \, \delta_{mn}^\Omega(\boldsymbol{r} - \boldsymbol{r}') \, \hat{B}_{nj}(\boldsymbol{r}',t) \tag{3.107}$$

with the operator-valued function

$$\hat{B}_{nj}(\boldsymbol{r},t) = \mathcal{D}_n^\dagger(t) \left[e^{i\boldsymbol{k}\boldsymbol{r}+i\varphi_{\rm L}(t)} + {\rm H.c.} \right] \mathcal{D}_j(t) e^{i\phi_j(t)-i\phi_n(t)} \hat{\Psi}_j(\boldsymbol{r},t) . \qquad (3.108)$$

It remains to show that $\hat{B}_{nm}$ either has support on Ω_0 or on its complement. Consequently, δ_{jm}^Ω reduces to the product of a delta function and a Kronecker delta and the convolution in Eq. (3.107) only selects those terms supported on Ω_0. Thus, the final result is

$$i\hbar \frac{\rm d}{{\rm d}t} \hat{\Psi}_m(\boldsymbol{r},t) = -\hbar\Omega(t) \sum_{\rm coupl.} \mathcal{D}_m^\dagger(t) \left[e^{i\boldsymbol{k}\boldsymbol{r}+i\varphi_{\rm L}(t)} + {\rm H.c.} \right] \mathcal{D}_j(t) e^{i\phi_j(t)-i\phi_m(t)} \hat{\Psi}_j(\boldsymbol{r},t) .$$
$$(3.109)$$

The sum only runs over those j which correspond to coupled boxes in momentum space, defined by

$$\boldsymbol{\chi}_m^p - \boldsymbol{\chi}_j^p \pm \hbar\boldsymbol{k} \cong 0 \qquad (3.110)$$

and of course only takes into account the field operators with nonvanishing overlap in Ω_0^r. Again the approximate sign in Eq. (3.110) signifies that the momentum displacements only initially point to the center of the momentum boxes. Finally, we introduce the laser-atom interaction Hamiltonian which reproduces the equation of motion, Eq. (3.108), which reads

$$\hat{U}_{\mathcal{D}}^\dagger \hat{H}_{\rm L} \hat{U}_{\mathcal{D}} = -\hbar\Omega(t) \int {\rm d}^3\boldsymbol{r} \sum_{\rm coupl.} \hat{\Psi}_n^\dagger(\boldsymbol{r}) \mathcal{D}_n^\dagger(t) e^{i\boldsymbol{k}\boldsymbol{r}} \mathcal{D}_j(t) \hat{\Psi}_j(\boldsymbol{r}) \, e^{i[\phi_j(t)-\phi_n(t)+\varphi_{\rm L}(t)]} + {\rm H.c.} .$$
$$(3.111)$$

This result means that we simply have to insert the sum over path-dependent field operators, Eq. (3.100), into the laser-atom interaction Hamiltonian and then only have to take into account these terms which are coupled via the condition, Eq. (3.110).

3.4.4. Matching conditions

In this section we complete the discussion by introducing matching conditions for trajectory and phase in correspondence to Sec. 3.3.6. As mentioned before, we can include an arbitrary phase in Eq. (3.88) for each field operator. Thus, this definition leaves the initial conditions undetermined not only for $\boldsymbol{\chi}_j$ but also for ϕ_j for every fictitious input field. To fix this ambiguity, we impose the following matching conditions for adjacent momentum boxes

$$\boldsymbol{\chi}_n^p(t_1) - \boldsymbol{\chi}_j^p(t_1) - \hbar\boldsymbol{k} = 0$$
$$\boldsymbol{\chi}_n^r(t_1) - \boldsymbol{\chi}_j^r(t_1) = 0 , \qquad (3.112)$$

exemplary for a laser pulse starting at $t = t_1$. These conditions have the following meaning. In position space we match the center of the local clouds, in momentum space we match the mean momenta modulo $\hbar\boldsymbol{k}$, which is transferred by the laser pulse. For the phase we define

$$\phi_j(t_1) - \phi_n(t_1) + \varphi_{\rm L}(t_1) + \frac{1}{2}\boldsymbol{k}\boldsymbol{\chi}_j^r(t_1) = 0 . \qquad (3.113)$$

The procedure is completely equivalent to the discussion in Sec. 3.3.6. As explained in this section and App. C.3.1, $\boldsymbol{\chi}_j(t)$ and $\phi_j(t)$ attain the interpretation of trajectory and phase along the physical path of the interferometer. However, due to the finite pulse length, the matching conditions cannot completely eliminate the dependency on spatial- and time-dependent phase factors in the laser-atom interaction Hamiltonian in contrast to Sec. 3.3.6, where we invoked the delta-pulse approximation. Nevertheless, the Hamiltonian can be further simplified and used for numerical simulations. This will be discussed in Sec. 3.5.2.

3.4.5. Summary

In the previous sections we assigned approximate bosonic field operators to each path of an interferometer. After the slightly technical and lengthy derivations, the summary in this section is supposed to serve as a guide for a straightforward application of the formalism.

After decomposing phase space in rectangular boxes and transforming to the comoving frames, we require that $\hat{\Pi}$ acts as a projector on every field operator and that this attribute is kept during the entire evolution. The projector property of $\hat{\Pi}$ is guaranteed for small momentum and position width of the local atomic clouds compared to the width of the phase-space boxes and for sufficiently weak nonlinear potentials and interactions. Having checked the mentioned prerequisites, one replaces the free by the reduced Hamiltonian

$$\hat{H}_{\mathrm{F}} \to \hat{H}_{\mathrm{R}} \tag{3.114}$$

and everywhere else, including in the operator to be measured,

$$\hat{\Psi}(\boldsymbol{r}) \to \sum_j \mathrm{e}^{\mathrm{i}\phi_j(t)} \mathcal{D}_j(t)\hat{\Psi}_j(\boldsymbol{r})\,. \tag{3.115}$$

The displacement operators are defined with respect to the classical trajectories and $\phi_j(t)$ is related to the classical action by Eq. (3.98). In the particle-particle interaction and laser-atom interaction Hamiltonian we only keep coupled products of field operators defined by Eq. (3.105) and Eq. (3.110) and with nonvanishing overlap in position space. The field operators then satisfy bosonic commutation relations.

After defining matching conditions in order to eliminate the ambiguous initial conditions ϕ_j and $\boldsymbol{\chi}_j$ for each fictitious input port, the laser-atom Hamiltonian becomes independent of phase- and spatial-dependent factors at the beginning of each laser pulse and can therefore efficiently be implemented numerically or used as a starting point for the delta-pulse approximation. This will be discussed in more detail in following sections.

By the decomposition of phase space, we transformed the whole evolution within the interferometer to Ω_0, however, at the cost of having to solve an infinite hierarchy of coupled equations for the field operators. Since the coupling to higher-order momentum boxes is strongly suppressed, it will turn out to be sufficient to only take into account a few non-resonant branches.

3.5. Applications

After the rather formal derivation in the previous sections, we apply the formalism to a number of examples. In Sec. 3.5.1 we start by deriving the explicit form of the observables measured in an interferometer experiment. The Gross-Pitaevskii approximation allows to efficiently implement the formalism numerically in Sec. 3.5.2. In contrast, we further pursue the delta-pulse approximation analytically in Sec. 3.5.3 and 3.5.4. Finally, we apply the formalism to an MZ interferometer in Sec. 3.5.5.

3.5.1. Observables

The observable we seek to measure is the number of particles in a certain exit port of an interferometer. This is equivalent to the number of particles occupying an interferometer branch which corresponds to a field operator. Hence, the operator for e.g. path n is

$$\hat{\mathcal{O}} = \int \mathrm{d}^3 \boldsymbol{r} \, \hat{\Psi}^\dagger(\boldsymbol{r}) \mathcal{D}_n(t) \Pi \mathcal{D}_n^\dagger(t) \hat{\Psi}(\boldsymbol{r}) \,, \tag{3.116}$$

which reads after performing transformation, Eq. (3.59)

$$\hat{U}_\mathcal{D}^\dagger \hat{\mathcal{O}} \hat{U}_\mathcal{D} = \int \mathrm{d}^3 \boldsymbol{r} \, \hat{\Psi}_n^\dagger(\boldsymbol{r}) \hat{\Psi}_n(\boldsymbol{r}) \,. \tag{3.117}$$

3.5.2. Numerical simulation

In this section, we show how to implement the formalism numerically. For this task we return to the laser-atom interaction Hamiltonian, Eq. (3.111). First we merge the two displacement operators between the two field operators together with the exponential $\exp(\boldsymbol{kr})$ using the composition rule, Eq. (A.10). Second, for each time-dependent quantity $C(t)$ we introduce the notation

$$C(t) = C(t_1) + \delta C(t) \,. \tag{3.118}$$

With the help of the conditions Eq. (3.112) and Eq. (3.113) we match the trajectories at $t = t_1$ and find the result

$$\hat{D}_n^\dagger(t) \mathrm{e}^{\mathrm{i} \boldsymbol{k} \hat{\boldsymbol{r}}} \hat{D}_j(t) \, \mathrm{e}^{\mathrm{i}[\phi_j(t) - \phi_n(t) + \varphi_\mathrm{L}(t)]} = \hat{D} \left[\delta \boldsymbol{\chi}_j(t) - \delta \boldsymbol{\chi}_n(t) \right] \mathrm{e}^{\mathrm{i} \phi_{nj}(t)} \tag{3.119}$$

with the time-dependent phase

$$\phi_{nj}(t) = \frac{1}{2\hbar} \left[\delta \boldsymbol{\chi}_n(t)^\mathrm{T} \boldsymbol{\mathcal{J}} \boldsymbol{\chi}_n(t_1) - \delta \boldsymbol{\chi}_j(t)^\mathrm{T} \boldsymbol{\mathcal{J}} \boldsymbol{\chi}_j(t_1) + \delta \boldsymbol{\chi}_n(t)^\mathrm{T} \boldsymbol{\mathcal{J}} \delta \boldsymbol{\chi}_j(t) \right]$$
$$+ \delta \varphi_\mathrm{L}(t) - \delta \phi_n(t) + \delta \phi_j(t) \,. \tag{3.120}$$

It is important to stress that at $t = t_1$ Eq. (3.119) reduces to unity and Eq. (3.120) vanishes. Thus, the laser-atom interaction Hamiltonian does not contain any phase- and spatial-dependent factors anymore at this specific point of time. We already applied matching conditions in Sec. 3.3.6. Note that the discussion here is much more general

as we allow finite pulse lengths. Indeed, due to the time dependence of the displacement operators, perfect matching is only achieved at $t = t_1$ but the displacement at later times is small thanks to the extremely short laser-atom interaction time and it is caused only by the residual nonlinear potentials.

This insight is the main result of this chapter. Introducing path-dependent field operators has led us to a formalism which allows to remove trivial contributions to the motion, for example the linear motion originating from the laser pulses or the free fall in the gravitational field. This fact makes a numerically exact simulation of a light-pulse interferometer particularly simple as we detail in the following: After calculating the Heisenberg equations of motion for the field operators, we replace $\hat{\Psi}_n(\boldsymbol{r}, t) \rightarrow \langle \hat{\Psi}_n(\boldsymbol{r}, t) \rangle = \Psi_n(\boldsymbol{r}, t)$ in the spirit of the Gross-Pitaevskii approximation. Each order parameter evolves according to the respective reduced Hamiltonian. In the interaction Hamiltonian one needs to implement the time-dependent relative shifts of the order parameters induced by the displacement operators. In the laser-atom interaction Hamiltonian one chooses a certain number of paths one would like to take into account and truncates the hierarchy at this number. For Bragg diffraction in the deep Bragg regime it is often sufficient to take into account only three non-resonant paths of the momentum ladder [21].

Realizing that the relative displacements of the order parameters and the time-dependent phase factors during the laser pulse are extremely small, the numerical implementation forms a set of coupled Gross-Pitaevskii equations which can be simulated on a grid of the size of the atomic clouds rather than the extent of the interferometer. Interestingly, it is even sufficient to simulate the GPEs on a grid of the size of the initial atomic cloud when using the scaling approach described in Sec. 2.3.2. After outlining the numerical simulation, we return to analytical methods for the beam splitters in the following sections.

3.5.3. Delta-pulse approximation

In the previous sections we established the path-dependent formalism in its general form. Starting from this result, we will successively introduce approximations until we recover the description in its simplest form. We first adopt the delta-pulse approximation in the present section, particularize the discussion to linear gravitational fields in Sec. 3.5.4 and finally apply the results to an MZ interferometer in Sec. 3.5.5. In Sec. 3.4.3 we obtained the exact result

$$\hat{H}_{\mathrm{L}} = -\hbar\Omega(t) \int \mathrm{d}^3\boldsymbol{r} \sum_{\mathrm{coupl.}} \hat{\Psi}_n^\dagger(\boldsymbol{r}) \mathcal{D}_n^\dagger(t) \mathrm{e}^{\mathrm{i}\boldsymbol{k}\boldsymbol{r}} \mathcal{D}_j(t) \hat{\Psi}_j(\boldsymbol{r}) \, \mathrm{e}^{\mathrm{i}\phi_j(t) - \mathrm{i}\phi_n(t) + \mathrm{i}\varphi_{\mathrm{L}}(t)} + \mathrm{H.c.} \,, \quad (3.121)$$

which relies on the projector properties of $\hat{\bar{\Pi}}$. In this and the following section we derive the delta-pulse approximation in a rigorous manner. Suppose the laser is switched on at $t = t_1$. First, we express the time-dependent phase and the displacement operator

as

$$\begin{aligned}
\hat{D}_j(t)\mathrm{e}^{\mathrm{i}\phi_j(t)} &= \hat{\mathcal{U}}_\mathrm{F}(t,t_\mathrm{i})\hat{D}_j\hat{\mathcal{U}}_{\mathrm{R},j}^\dagger(t,t_\mathrm{i})\\
&= \hat{\mathcal{U}}_\mathrm{F}(t,t_1)\hat{\mathcal{U}}_\mathrm{F}(t_1,t_\mathrm{i})\hat{D}_j\hat{\mathcal{U}}_{\mathrm{R},j}^\dagger(t_1,t_\mathrm{i})\hat{\mathcal{U}}_{\mathrm{R},j}^\dagger(t,t_1)\\
&= \hat{\mathcal{U}}_\mathrm{F}(t,t_1)\hat{D}_j(t_1)\mathrm{e}^{\mathrm{i}\phi_j(t_1)}\hat{\mathcal{U}}_{\mathrm{R},j}^\dagger(t,t_1)
\end{aligned} \tag{3.122}$$

by making again use of Eq. (1.32). Therefore, the product in Eq. (3.121) can be cast in the form

$$\begin{aligned}
\hat{D}_n^\dagger(t)\mathrm{e}^{\mathrm{i}\boldsymbol{k}\hat{\boldsymbol{r}}}\hat{D}_j(t)\,\mathrm{e}^{\mathrm{i}\phi_j(t)-\mathrm{i}\phi_n(t)+\mathrm{i}\varphi_\mathrm{L}(t)} =& \hat{\mathcal{U}}_{\mathrm{R},n}(t,t_1)\hat{D}_n^\dagger(t_1)\hat{D}(\boldsymbol{\chi}_\mathrm{F}(t))\hat{D}_j(t_1)\hat{\mathcal{U}}_{\mathrm{R},j}^\dagger(t,t_1)\\
&\times \mathrm{e}^{\mathrm{i}\phi_j(t_1)-\mathrm{i}\phi_n(t_1)+\mathrm{i}\varphi_\mathrm{F}(t)+\mathrm{i}\varphi_\mathrm{L}(t)}
\end{aligned} \tag{3.123}$$

where we defined $\boldsymbol{\chi}_\mathrm{F}$ and φ_F implicitly via

$$\hat{\mathcal{U}}_\mathrm{F}^\dagger(t,t_1)\mathrm{e}^{\mathrm{i}\boldsymbol{k}\hat{\boldsymbol{r}}}\hat{\mathcal{U}}_\mathrm{F}(t,t_1) = \hat{D}(\boldsymbol{\chi}_\mathrm{F}(t))\mathrm{e}^{\mathrm{i}\varphi_\mathrm{F}(t)}\,. \tag{3.124}$$

Note that contrary to App. C.3.1, in this section $\boldsymbol{\chi}_\mathrm{F}$ is time dependent but as before $\boldsymbol{\chi}_\mathrm{F}(t_1) = (0,\hbar\boldsymbol{k})^\mathrm{T}$. Moreover, writing the product in Eq. (3.124) as a displacement operator times a phase factor, implicitly assumes a harmonic approximation to the free Hamiltonian during the laser pulse.

As was explained in Sec. 1.1.3, the first step in the delta-pulse approximation is the transformation into the interaction picture with respect to the external Hamiltonian. When we neglect atom-atom interactions during the laser pulse, this change of picture exactly removes the reduced time-evolution operators on the very left and right of the operator product in Eq. (3.123). Merging the three displacement operators by subsequent application of the composition rule, Eq. (A.10), and furthermore making again use of the matching conditions

$$\boldsymbol{\chi}_n(t_1) - \boldsymbol{\chi}_j(t_1) - \boldsymbol{\chi}_\mathrm{F}(t_1) = 0 \tag{3.125}$$

for the trajectory and

$$\phi_j(t_1) - \phi_n(t_1) + \varphi_\mathrm{L}(t_1) - \frac{1}{2\hbar}\boldsymbol{\chi}_\mathrm{F}^\mathrm{T}(t_1)\boldsymbol{\mathcal{J}}\boldsymbol{\chi}_j(t_1) = 0 \tag{3.126}$$

for the phase, we arrive at the final result of this section

$$\hat{H}_\mathrm{L}^\mathrm{I} = -\hbar\Omega(t)\int\mathrm{d}^3\boldsymbol{r}\sum_{\mathrm{coupl.}}\hat{\Psi}_n^\dagger(\boldsymbol{r})\mathcal{D}(\delta\boldsymbol{\chi}_\mathrm{F}(t))\hat{\Psi}_j(\boldsymbol{r})\,\mathrm{e}^{\mathrm{i}\varphi_{nj}(t)} + \mathrm{H.c.}\,. \tag{3.127}$$

In Eq. (3.127) we defined the residual time-dependent phase

$$\varphi_{nj}(t) = \frac{1}{2\hbar}[\boldsymbol{\chi}_n(t_1) + \boldsymbol{\chi}_j(t_1)]^\mathrm{T}\boldsymbol{\mathcal{J}}\delta\boldsymbol{\chi}_\mathrm{F}(t) + \delta\varphi_\mathrm{L}(t) + \varphi_\mathrm{F}(t) \tag{3.128}$$

where $\delta\varphi_\mathrm{L}(t)$ and $\delta\boldsymbol{\chi}_\mathrm{F}(t)$ are defined by Eq. (3.118). The Hamiltonian in Eq. (3.127) still is time dependent, therefore time-ordering in the time-evolution operator is still necessary. In the next section we further particularize the Hamiltonian to an interferometer in the linear gravitational field.

3.5.4. Interferometry in the linear gravitational field

In this section we turn to an MZ interferometer employing Bragg diffraction. For simplicity we assume a linear gravitational potential, corresponding to the free Hamiltonian

$$\hat{\mathcal{H}} = \frac{\hat{\boldsymbol{p}}^2}{2m} + mg\hat{z}\,, \tag{3.129}$$

and neglect interactions during the laser pulse. Next, we decompose phase space. The laser-atom interaction Hamiltonian induces transitions between multiples of $\hbar\boldsymbol{k}$ and we therefore choose the center of the momentum boxes around $\boldsymbol{\chi}_n^p = n\hbar\boldsymbol{k}$ as initial conditions. The values of the momenta at $t = t_1$ are

$$\begin{aligned}
\boldsymbol{\chi}_n^p(t_1) &= n\hbar\boldsymbol{k} - \boldsymbol{g}mt_1 \\
\boldsymbol{\chi}_j^p(t_1) &= j\hbar\boldsymbol{k} - \boldsymbol{g}mt_1
\end{aligned} \tag{3.130}$$

where $\boldsymbol{g} = (0,\,0,\,g)^{\mathrm{T}}$. With the help of the coupling conditions, Eq. (3.125), we conclude from Eq. (3.127) that

$$\hat{H}_{\mathrm{L}}^{\mathrm{I}} = -\hbar\Omega(t)\int \mathrm{d}^3\boldsymbol{r}\sum_n \hat{\Psi}_n^\dagger(\boldsymbol{r})\mathcal{D}(\delta\boldsymbol{\chi}_{\mathrm{F}}(t))\hat{\Psi}_{n-1}(\boldsymbol{r})\,\mathrm{e}^{\mathrm{i}\varphi_{n,n-1}(t)} + \mathrm{H.c.}\,. \tag{3.131}$$

For each momentum box we introduce several field operators corresponding to boxes in position space. Thus, Eq. (3.131) is individually valid at each vertex of the interferometer where the momentum branches are mixed.
Finally, we calculate

$$\varphi_{\mathrm{F}} = -\frac{1}{2}\boldsymbol{k}\boldsymbol{g}(t - t_1)^2 \tag{3.132}$$

and

$$\delta\boldsymbol{\chi}_{\mathrm{F}}^p(t) = 0 \quad \text{and} \quad \delta\boldsymbol{\chi}_{\mathrm{F}}^r(t) = -\frac{\hbar\boldsymbol{k}}{m}(t - t_1) \tag{3.133}$$

with the free Hamiltonian by comparing to Eq. (3.124) and come to the following expression for the phase

$$\varphi_{n,n-1}(t) = \omega_r(2n - 1)(t - t_1) - \frac{1}{2}\boldsymbol{k}\boldsymbol{g}(t^2 - t_1^2) + \delta\varphi_{\mathrm{L}}(t) \tag{3.134}$$

where we defined the *recoil frequency* $\omega_r = \hbar k^2/2m$. For resonance the laser phase $\varphi_{\mathrm{L}}(t) = \varphi_{\mathrm{L}} - \Delta\omega(t)t$ is chirped according to

$$\Delta\omega(t) = \omega_r + \alpha t\,. \tag{3.135}$$

For the choice $\alpha = -1/2\boldsymbol{k}\boldsymbol{g}$, any dependence on g vanishes and we find the final result with the resonant transition $n = 0 \leftrightarrow n = 1$

$$\hat{H}_{\mathrm{L}}^{\mathrm{I}} = -\hbar\Omega(t)\int \mathrm{d}^3\boldsymbol{r}\sum_n \left\{\hat{\Psi}_n^\dagger(\boldsymbol{r})\mathrm{e}^{\mathrm{i}\nu\tau}\mathrm{e}^{\mathrm{i}\omega_r 2(n-1)\tau}\hat{\Psi}_{n-1}(\boldsymbol{r}) + \hat{\Psi}_n^\dagger(\boldsymbol{r})\mathrm{e}^{-\mathrm{i}\nu\tau}\mathrm{e}^{-\mathrm{i}\omega_r 2n\tau}\hat{\Psi}_{n+1}(\boldsymbol{r})\right\} \tag{3.136}$$

where we introduced the abbreviation $\tau = (t - t_1)$. This result was already found in Ref. [21], where it was presented in first-quantized form. The operator $\hat{\nu} = \boldsymbol{k}\hat{\boldsymbol{p}}/m$ is

referred to as *velocity-selectivity* operator. It accounts for the Doppler shift due to the finite momentum spread of the state. Recall that the transformation to the comoving frames shifts the phase-space distribution of each local atomic cloud to the origin. Thus, the momentum distribution of each field operator is strongly bounded around zero and the effect of the velocity selectivity is small.

When we neglect $\hat{\nu}$ and all terms in Eq. (3.136) oscillating with nonzero multiples of ω_r we recover the effective two-level Hamiltonian

$$\hat{H}_{\mathrm{L}}^{\mathrm{I}} = -\hbar\Omega(t) \int \mathrm{d}^3\boldsymbol{r}\,\hat{\Psi}_1^\dagger(\boldsymbol{r})\hat{\Psi}_0^\dagger(\boldsymbol{r}) + \mathrm{H.c.} \qquad (3.137)$$

for an $SU(2)$ interferometer.

In order to take also into account nonresonant paths, the *method of averaging* can be employed, which was first introduced in Ref. [207] and reformulated in Refs. [21, 208]. With the help of this formalism one systematically derives effective time-independent Hamiltonians in powers of $\epsilon = \Omega/\omega_{\mathrm{r}} \approx 0.1$ [21], leaving for the moment aside the effect of the velocity selectivity. While preserving unitarity, as the expansion takes place in the exponent, it comes at the cost of still having to calculate matrix exponential functions. Even when computer algebra systems are employed, this becomes a hideous task as more and more higher-order branches are taken into account.

We analysed in detail how to cope with this problem in the case of single-Bragg diffraction, but we will only briefly discuss the results in the following. The simplest way is to perform a naive Dyson expansion. However, it diverges due to the appearance of secular terms already at second order. A possible way to overcome this problem is to first transform into the interaction picture with respect to the effective two-level system and then perform the Dyson expansion. In this case the secular terms describe a beating of the Rabi oscillations with a frequency of the order of $1/\omega_r$ which makes the expansion valid over several Rabi cycles. In fact, this leads to surprisingly concise terms which very accurately match the numerically exact solution but for an expansion to order ϵ^2 it is easily shown that one needs to go to fourth order in the Dyson expansion. At first sight, this seems to be an impossible endeavor due to the cumbersome expressions. However, it is important to note that in most integrals involved it is sufficient to only integrate the fast oscillating terms. This leads to a remarkably simple analytical formalism which should be applicable also to Raman, double-Bragg or further more exotic coupling schemes. A perturbative method that really is an expansion in powers of ϵ can presumably be obtained by renormalizing secular terms, see e.g. [209–211], but is left for further investigations.

For $\hat{\nu} \ll \Omega$ we additionally include the effects of velocity selectivity by Taylor expanding $\mathrm{e}^{\mathrm{i}\hat{\nu}t}$ e.g. to second order followed by the expansion outlined above. In the same spirit one can take into account the effects of inaccurate chirping (phases proportional to t^2 in the exponent) or harmonic potentials (phases including the position operator) [96]. However, it is important to mention that realistic laser pulses are smooth and in general not box shaped. Still, approaching the problem as described allows to derive general delta-pulse beam splitter, in which semianalytical functions that involve the general pulse shapes, enter as transition elements.

3.5.5. The Mach-Zehnder Interferometer

At the end of this section we apply the theory to an MZ interferometer. In order to focus on the main principles, we again restrict the consideration to a linear gravitational field and furthermore take only into account resonant momentum branches, that is, the laser-atom interaction Hamiltonian, Eq. (3.137), must be slightly generalized to the respective vertices of the interferometer as we will see further below. Supposing that initially all particles reside in $|1\rangle$, we introduce the decomposition of phase space and define the field operators

$$\hat{\Psi}(\boldsymbol{r}) = \sum_{j=1}^{4} e^{i\phi_j(t)} \mathcal{D}_j(t) \hat{\Psi}_j(\boldsymbol{r}) \tag{3.138}$$

according to Fig. 3.5. We consider the particle-number difference between the two exit ports, which is given by

$$\delta\hat{N} = \int d^3\boldsymbol{r} \left(\hat{\Psi}_4^\dagger(\boldsymbol{r})\hat{\Psi}_4(\boldsymbol{r}) - \hat{\Psi}_3^\dagger(\boldsymbol{r})\hat{\Psi}_3(\boldsymbol{r}) \right) \tag{3.139}$$

according to Sec. 3.5.1. Moreover, we assume weak interactions, either resultant from tuning the interaction strength by a Feshbach resonance or from waiting with the first laser pulse until the BEC has sufficiently expanded. In the case of repulsive interactions the local atomic clouds repel each other during the separation after the laser pulse and gain a small additional velocity. As we showed by a full 3D GPE simulation and by analytical methods in the Thomas-Fermi approximation, this velocity is extremely small, however, should be carefully taken into account for high-precision measurements. In the analytical approach one expands perturbations to the radial symmetric Thomas-Fermi profile into the complete set of *collective oscillations* [187]. The time-dependence then follows ordinary differential equations which allow analytical solutions in terms of hypergeometric functions.

We now address the laser-atom interaction Hamiltonian. Neglecting all spurious branches, the effect of velocity selectivity and the quadratic time dependence of the phase due to nonperfect chirping, we obtain from Eq. (3.136) the three laser-atom interaction Hamiltonians for $t = t_1, t_2$ and t_3

$$\hat{H}_{\rm L} = -\hbar\Omega_1\delta(t - t_1) \int d^3\boldsymbol{r}\, \hat{\Psi}_2^\dagger(\boldsymbol{r})\hat{\Psi}_1(\boldsymbol{r}) + \text{H.c.} \tag{3.140}$$

$$\hat{H}_{\rm L} = -\hbar\Omega_2\delta(t - t_2) \int d^3\boldsymbol{r} \left(\hat{\Psi}_4^\dagger(\boldsymbol{r})\hat{\Psi}_2(\boldsymbol{r}) + \hat{\Psi}_3^\dagger(\boldsymbol{r})\hat{\Psi}_1(\boldsymbol{r}) \right) + \text{H.c.} \tag{3.141}$$

$$\hat{H}_{\rm L} = -\hbar\Omega_3\delta(t - t_3) \int d^3\boldsymbol{r}\, \hat{\Psi}_3^\dagger(\boldsymbol{r}) e^{i\phi_{\rm MZ}} \mathcal{D}(\Delta\boldsymbol{\chi}) \hat{\Psi}_4(\boldsymbol{r}) + \text{H.c.}. \tag{3.142}$$

It is important to mention that Eq. (3.142) contains a displacement operator and the phase $\phi_{\rm MZ}$. This is because at the final vertex both incoming fields are occupied and there is no fictitious input port to eliminate this dependency. Relabeling the upper path with index u and the lower with b in order to avoid confusion with the labeling of the field operators, the phase and the relative displacement operator become

$$\phi_{\rm MZ} = \varphi_{\rm L} + \frac{1}{\hbar}\Delta S(t_3) - \frac{1}{2\hbar}\Delta\boldsymbol{\chi}^r \left[\boldsymbol{\chi}_{\rm u}^p(t_3) + \boldsymbol{\chi}_{\rm b}^p(t_3) \right] \tag{3.143}$$

and $\Delta\boldsymbol{\chi} = \boldsymbol{\chi}_{\mathrm{u}}(t_3) - \boldsymbol{\chi}_{\mathrm{b}}(t_3)$ in complete accordance with Sec. 3.3.6. The total laser phase is $\varphi_{\mathrm{L}} = \varphi_{\mathrm{L},1} - 2\varphi_{\mathrm{L},2} + \varphi_{\mathrm{L},3}$ and $\Delta S(t_3) = S_{\mathrm{u}}(t_3) - S_{\mathrm{b}}(t_3)$ as before. In Eq. (3.141) each pair, namely $\hat{\Psi}_1(\boldsymbol{r})$ and $\hat{\Psi}_4(\boldsymbol{r})$ as well as $\hat{\Psi}_2(\boldsymbol{r})$ and $\hat{\Psi}_3(\boldsymbol{r})$ correspond to the same momentum box but are defined on different position boxes. Consequently, they are treated as independent bosonic field operators.

Next, we need to calculate the action of the beam splitter operators on the observable. In Eq. (3.40) we already used beam-splitter transformations which contained a momentum displacement. The generalization to the displacement operator in Eq. (3.142) is straightforward, one simply replaces $\mathrm{e}^{\mathrm{i}\boldsymbol{k}\hat{\boldsymbol{r}}} \to \hat{D}(\Delta\boldsymbol{\chi})$. Thus, we conclude

$$\hat{U}^\dagger(t_{\mathrm{d}}, t_{\mathrm{i}})\hat{\mathcal{O}}\hat{U}(t_{\mathrm{d}}, t_{\mathrm{i}}) = -\mathrm{i}\int\mathrm{d}^3\boldsymbol{r}\,\hat{U}_{\mathrm{MZ}}^\dagger(t_3, t_{\mathrm{i}})\left\{\hat{\Psi}_1^\dagger(\boldsymbol{r})\mathrm{e}^{\mathrm{i}\phi_{\mathrm{MZ}}}\mathcal{D}(\Delta\boldsymbol{\chi})\hat{\Psi}_2(\boldsymbol{r}) - \mathrm{H.c.}\right\}\hat{U}_{\mathrm{MZ}}(t_3, t_{\mathrm{i}}),$$
(3.144)

where we additionally commuted the π-pulse according to Eq. (3.141) to the left in the interferometer sequence. Thus, $\hat{\Psi}_4(\boldsymbol{r}) \to \mathrm{i}\hat{\Psi}_2(\boldsymbol{r})$ and $\hat{\Psi}_3(\boldsymbol{r}) \to \mathrm{i}\hat{\Psi}_1(\boldsymbol{r})$ everywhere for times larger than t_2. The residual time-evolution operator then reads

$$\hat{U}_{\mathrm{MZ}}(t_{\mathrm{d}}, t_{\mathrm{i}}) = \hat{U}_{\mathrm{e}}(t_3, t_1)\hat{S}_{\pi/2}\hat{U}_{\mathrm{e}}(t_1, t_{\mathrm{i}})$$
(3.145)

where the beam splitter is with respect to Eq. (3.140) and the external Hamiltonian

$$\hat{H}_{\mathrm{e}}(t) = \hat{H}_{\mathrm{R}} + \hat{H}_{\mathrm{I}}(t)$$
(3.146)

is expressed in the comoving frames, consequently $\hat{\mathcal{H}}_{\mathrm{R}} = \hat{\boldsymbol{p}}^2/2m$ for all branches. Resorting to Hamiltonian, Eq. (3.17), we furthermore conclude

$$H_{\mathrm{I}} = \frac{g}{2}\int\mathrm{d}^3\boldsymbol{r}\,\hat{\Psi}_1^\dagger(\boldsymbol{r})\hat{\Psi}_1^\dagger(\boldsymbol{r})\hat{\Psi}_1(\boldsymbol{r})\hat{\Psi}_1(\boldsymbol{r})$$
(3.147)

for $t \in [t_{\mathrm{i}}, t_1]$ and

$$\hat{H}_{\mathrm{I}}(t) = \frac{g}{2}\int\mathrm{d}^3\boldsymbol{r}\,\left\{\hat{\Psi}_1^\dagger(\boldsymbol{r})^2\hat{\Psi}_1(\boldsymbol{r})^2 + \hat{\Psi}_2^\dagger(\boldsymbol{r})^2\hat{\Psi}_2(\boldsymbol{r})^2 + 4\hat{n}_1(\boldsymbol{r} - \boldsymbol{\chi}_{\mathrm{b}}^r(t))\,\hat{n}_2(\boldsymbol{r} - \boldsymbol{\chi}_{\mathrm{u}}^r(t))\right\}$$
(3.148)

for $t \in [t_1, t_3]$. In Eq. (3.148) we introduced the abbreviation $\hat{n}_j(\boldsymbol{r}) = \hat{\Psi}_j^\dagger(\boldsymbol{r})\hat{\Psi}_j(\boldsymbol{r})$. Note the factor 4 in Eq. (3.148) as opposed to the factor 2 in Eq. (3.78) in the case of two different internal states. Moreover, we disregarded in Eq. (3.147) and Eq. (3.148) unoccupied field operators. This assumes that initially even when including the thermal cloud and quantum fluctuations, the state remains well inside the initial phase-space box. The position displacements correspond to the two paths of the interferometer, namely

$$\boldsymbol{\chi}_{\mathrm{u}}^r(t) = \frac{\hbar\boldsymbol{k}}{m}(t - t_1)$$
$$\boldsymbol{\chi}_{\mathrm{b}}^r(t) = 0$$
(3.149)

for $t \in [t_1, t_2]$ and

$$\boldsymbol{\chi}_{\mathrm{u}}^r(t) = \frac{\hbar\boldsymbol{k}}{m}(t_2 - t_1)$$
$$\boldsymbol{\chi}_{\mathrm{b}}^r(t) = \frac{\hbar\boldsymbol{k}}{m}(t - t_2)$$
(3.150)

for $t \in [t_2, t_3]$, where we removed the contribution $-1/2gt^2$ from the free fall in the linear gravitational potential by redefining the integration variable in the interaction Hamiltonian.

It is worthwhile to note that the result in this section for Bragg diffraction is completely equivalent to the derivation for Raman diffraction in Sec. 3.3.6 apart from the factor 2 in the interaction Hamiltonian. Finally, we mention that one could also generalize the discussion to butterfly interferometers. Note, however, that one cannot completely eliminate the external degrees of freedom for this geometry in the case of an open interferometer since the displacement operators introduce a small relative shift after each loop. When simulated numerically in the GPE approximation, one simply displaces the order parameters at this instance of time.

3.6. Summary

At the end of this chapter we summarize the results. We started by presenting a method for the adiabatic elimination of ancillary states to obtain effective Hamiltonians for the laser-atom interaction in second quantization. By carefully separating various time scales, we arrived at a simple method which allows to treat a wide range of different coupling schemes. In this formalism the adiabatic elimination becomes straightforward. One only needs to evaluate a commutator.

After some calculations in order to get familiar with the method of second quantization, we introduced field operators for every path of an interferometer and showed under which conditions these fields become bosonic. We included the interaction Hamiltonian and laser-atom interaction Hamiltonian into the description and provided an intuitive interpretation of the formalism. Introducing path-dependent field operators corresponds to a transformation into the comoving frame of each interferometer path. In these frames the description of the interferometer becomes particularly simple as the whole evolution takes place within a small region around the center of phase space. This allows to perform a full simulation of an n-port interferometer e.g. within the Gross-Pitaevskii approximation with manageable computational effort for arbitrary long interferometer times. Furthermore, the kinetic phase resultant from the motion along different paths can be separated from those contributions stemming from the particle-particle interaction. Most remarkably, if certain conditions on the local atomic clouds are satisfied, the formalism is exact.

Finally we showed which approximations are necessary to recover the standard formalism in which the interaction with the laser is modelled by infinitely short pulses.

Chapter 4

Sensitivity and two-mode squeezing

With the advance of atom interferometry interest was also directed towards limits for the accuracy of phase measurements. As opposed to the *standard quantum limit* [212], Yurke soon identified the *Heisenberg scaling* as ultimate lower bound for fermionic particles [213] relying on the $SU(2)$ angular momentum algebra [214] in his proof. This result was generalized later to bosons in Ref. [215]. Since atoms, unlike photons, interact among each other, the nonlinear interaction Hamiltonian leads to a spread of the relative phase distribution between two separated samples. This phenomenon known as *phase diffusion* was conceived first by Leggett and Sols in Ref. [75], employing an approximate phase model for the Josephson Hamiltonian, see also Ref. [216] for a rigorous derivation of this approach. Lewenstein and You found phase diffusion within the $U(1)$ symmetry-breaking formalism for Bose-Einstein condensates [165, 217], which was reconciled later with the number-conserving approaches discussed in Sec. 2.2.2. This effect was also discovered in guided double-well interferometers [76, 218]; see also the comment [144] and reply [219]. Instead of viewing phase diffusion as detrimental to the accuracy of measurements, Kitagawa et al. [220] and Wineland et al. [221] introduced the notion of *spin squeezing* to even enhance the precision of phase measurements.

Spurred by these results, strong theoretical effort was further addressed to this field in the following years, either in order to reduce phase diffusion or to design experimental protocols to achieve strong spin squeezing. Apart from general theoretical considerations [222–225] the adiabatic splitting process of a BEC in a potential by ramping up a barrier was found to produce states with reduced particle fluctuations between the two wells [226–229] which can be enhanced by employing optimal control techniques [230]. In addition, the role of excited states during the splitting process was studied [231]. In Refs. [232–236] the impact of phase diffusion was investigated and possible schemes were developed to reduce its effect.

On the experimental side, reduced particle number fluctuations were shown in Ref. [237] and spin squeezing between two internal states was demonstrated by reducing the overlap of the wave functions [238], by tuning the interaction strength via a Feshbach resonance [239] and by creating entanglement with the help of spin-changing collisions [240].

It is often stated [63, 88] that effects of interaction can be neglected in light-pulse interferometers with Bose-Einstein condensates. Before the first laser pulse the BEC is

allowed to expand, which should sufficiently reduce mean-field interactions. However, as we will show in the present chapter, this assertion is wrong when the phase sensitivity for a measurement of the particle number at each exit port is considered. This will be shown in Sec. 4.2, where we calculate the sensitivity of an MZ interferometer as a function of the initial expansion period and the time of delta-kick collimation. We will find a dramatic deviation from the standard quantum limit.

4.1. Two-mode approximation

In order to calculate the phase sensitivity of an MZ interferometer, we need to introduce a few mathematical tools. In this section we first present an elegant derivation of the two-mode approximation and subsequently express all operators in terms of angular momentum operators [214].

In chapter 3 we already reduced the Mach-Zehnder sequence to

$$\hat{U}^\dagger(t_{\rm d}, t_{\rm i})\delta\hat{N}\hat{U}(t_{\rm d}, t_{\rm i}) = -{\rm i}\int {\rm d}^3\boldsymbol{r}\,\hat{U}_{\rm MZ}^\dagger(t_3, t_{\rm i})\left\{\hat{\Psi}_1^\dagger(\boldsymbol{r})\hat{\Psi}_2(\boldsymbol{r}){\rm e}^{{\rm i}\phi_{\rm MZ}} - {\rm H.c.}\right\}\hat{U}_{\rm MZ}(t_3, t_{\rm i}).$$
(4.1)

In the case of Raman diffraction the field operators label different internal states, while in the case of Bragg diffraction they correspond to different interferometer paths. In contrast to Eq. (3.79) and Eq. (3.144) no relative displacement operator appears in Eq. (4.1) since we restrict the discussion to a closed interferometer. As a result, the phase also reduces to

$$\phi_{\rm MZ} = \varphi_{\rm L} + \frac{1}{\hbar}\Delta S(t_3)$$
(4.2)

where we recalled the laser phase $\varphi_{\rm L} = \varphi_{\rm L,1} - 2\varphi_{\rm L,2} + \varphi_{\rm L,3}$ and $\Delta S(t_3) = S_2(t_3) - S_1(t_3)$ is the classical action difference along the two paths of the interferometer. The remaining MZ time-evolution operator reads

$$\hat{U}_{\rm MZ} = \hat{U}_{\rm e}(t_3, t_1)\hat{S}_{\pi/2}$$
(4.3)

where $\hat{U}_{\rm e}$ is the time-evolution operator associated with the external Hamiltonian in the comoving frames. This Hamiltonian is of the form

$$\hat{H}_{\rm e} = \hat{H}_{\rm R} + \frac{g}{2}\int {\rm d}^3\boldsymbol{r}\,\left\{\hat{\Psi}_1^\dagger(\boldsymbol{r})\hat{\Psi}_1^\dagger(\boldsymbol{r})\hat{\Psi}_1(\boldsymbol{r})\hat{\Psi}_1(\boldsymbol{r}) + \hat{\Psi}_2^\dagger(\boldsymbol{r})\hat{\Psi}_2^\dagger(\boldsymbol{r})\hat{\Psi}_2(\boldsymbol{r})\hat{\Psi}_2(\boldsymbol{r})\right\},$$
(4.4)

where we assumed $g_1 = g_2$, which is approximately true for Raman interferometry and exact for Bragg diffraction schemes where only one internal state is present. Furthermore, we assumed that the splitting time of the wave packets is much smaller than the total interferometer time, hence we neglect the term containing time-dependent displacement operators. As distortion effects on the local atomic clouds during this time are small for sufficiently weak interactions, Eq. (4.4) is a good approximation. Furthermore, for simplicity we will assume a linear gravitational potential, thus the reduced Hamiltonian is state- and path independent and is simply given by $\hat{\mathcal{H}}_{\rm R} = \hat{\boldsymbol{p}}^2/2m$. The restriction to an at most globally harmonic potential is important, otherwise in the

case of path-dependent potentials, mean-field effects appear during the whole interferometer time and one should resort to solving the Gross-Pitaevskii equation. By adding and subtracting the term $g \int \mathrm{d}^3 \boldsymbol{r}\, \hat{\Psi}_1^\dagger(\boldsymbol{r}) \hat{\Psi}_1(\boldsymbol{r}) \hat{\Psi}_2^\dagger(\boldsymbol{r}) \hat{\Psi}_2(\boldsymbol{r})$ in Eq. (4.4), we define

$$\hat{H}_{\mathrm{GP}} = \hat{H}_{\mathrm{R}} + \frac{g}{2} \int \mathrm{d}^3 \boldsymbol{r} \left\{ \hat{\Psi}_1^\dagger(\boldsymbol{r})^2 \hat{\Psi}_1(\boldsymbol{r})^2 + \hat{\Psi}_2^\dagger(\boldsymbol{r})^2 \hat{\Psi}_2(\boldsymbol{r})^2 + 2 \hat{\Psi}_1^\dagger(\boldsymbol{r}) \hat{\Psi}_1(\boldsymbol{r}) \hat{\Psi}_2^\dagger(\boldsymbol{r}) \hat{\Psi}_2(\boldsymbol{r}) \right\} . \tag{4.5}$$

As one can easily recognize, the Hamiltonian $\hat{H}_{\mathrm{GP}}$ commutes with the operator within the parenthesis in Eq. (4.1) as long as the reduced Hamiltonian $\hat{\mathcal{H}}_{\mathrm{R}}$ is path independent. Thus, in the interaction picture with respect to $\hat{H}_{\mathrm{GP}}$, the external Hamiltonian becomes

$$\hat{H}_{\mathrm{e}}^{\mathrm{I}} = g \int \mathrm{d}^3 \boldsymbol{r}\, \hat{U}_{\mathrm{GP}}^\dagger \hat{\Psi}_1^\dagger(\boldsymbol{r}) \hat{\Psi}_1(\boldsymbol{r}) \hat{\Psi}_2^\dagger(\boldsymbol{r}) \hat{\Psi}_2(\boldsymbol{r}) \hat{U}_{\mathrm{GP}} = g \int \mathrm{d}^3 \boldsymbol{r}\, |\phi_{\mathrm{GP}}(\boldsymbol{r}, t)|^4\, \hat{a}_1^\dagger \hat{a}_1 \hat{a}_2^\dagger \hat{a}_2 + \mathcal{O}(\sqrt{N}) . \tag{4.6}$$

In Sec. 2.2.2 we discussed the number-conserving approaches to Bose-Einstein condensation. To lowest order we replaced the Heisenberg field operator $\hat{\Psi}_j(\boldsymbol{r}, t) \approx \hat{a}_j \phi_{\mathrm{GP}}(\boldsymbol{r}, t)$, where $\hat{a}_j$ is time independent to this order and the mode function $\phi_{\mathrm{GP}}(\boldsymbol{r}, t)$ evolves according to the Gross-Pitaevskii equation. We furthermore assumed the same mode function for both interferometer paths. We suppose that all particles initially reside in the groundstate $|\psi\rangle = 1/\sqrt{N!}\, \hat{a}_1^{\dagger N} |0\rangle$. Applying a $\pi/2$ pulse to this state, we obtain

$$\hat{S}_{\pi/2} |\psi\rangle = \frac{1}{\sqrt{N! 2^N}} \left[\hat{a}_1^\dagger - \mathrm{i} \hat{a}_2^\dagger \right]^N |0\rangle , \tag{4.7}$$

which corresponds to a binomial distribution over the two paths of the interferometer with variance $\langle \delta \hat{N}^2 \rangle - \langle \delta \hat{N} \rangle^2 = \sqrt{N}$ when we expand the parenthesis. For that reason the nonlinear Hamiltonian, Eq. (4.6), induces a nontrivial dephasing. This effect will be discussed in more detail in Sec. 4.2. However, before that we need to introduce further theoretical tools which are particularly useful for the discussion of interferometers in the two-mode approximation.

Representation of states

Here, we provide possible ways to represent the general state for a two-mode system with N particles. Due to the exchange symmetry of the wave function, there are exactly $N + 1$ orthogonal states, which can be chosen as the eigenfunctions of the particle difference operator. These Dicke states [241] are defined as

$$|j, m\rangle \equiv \frac{1}{\sqrt{(j + m)!(j - m)!}} (\hat{a}_1^\dagger)^{j+m} (\hat{a}_2^\dagger)^{j-m} |0\rangle \tag{4.8}$$

where $j = N/2$ and $-j \leq m \leq j$. Equivalently, a state can be expanded in the overcomplete set of coherent spin states [242]

$$|\theta, \phi\rangle = \frac{1}{\sqrt{N!}} \left[\cos(\theta/2) \hat{a}_1^\dagger + \sin(\theta/2) \mathrm{e}^{-\mathrm{i}\phi} \hat{a}_2^\dagger \right]^N |0\rangle \tag{4.9}$$

with $\theta \in [0, \pi]$ and $\phi \in [0, 2\pi)$.

Angular momentum algebra

We now introduce the angular momentum operators [214]

$$
\begin{aligned}
\hat{L}_x &= \frac{1}{2}\left(\hat{a}_1^\dagger\hat{a}_2 + \hat{a}_2^\dagger\hat{a}_1\right) \\
\hat{L}_y &= \frac{i}{2}\left(\hat{a}_2^\dagger\hat{a}_1 - \hat{a}_1^\dagger\hat{a}_2\right) \\
\hat{L}_z &= \frac{1}{2}\left(\hat{a}_1^\dagger\hat{a}_1 - \hat{a}_2^\dagger\hat{a}_2\right) \;,
\end{aligned}
\tag{4.10}
$$

which satisfy the commutation relations $[L_i, L_j] = i\epsilon_{ijk}L_k$. The $N+1$ Dicke states are simultaneous eigenstates of $\hat{L}_z$ and $\hat{\boldsymbol{L}}^2 = \hat{L}_x^2 + \hat{L}_y^2 + \hat{L}_z^2$. A general state can be represented on a sphere by means of the Q function [243–245]

$$
Q(\theta, \phi) = \frac{N+1}{4\pi}\left|\langle\theta, \phi\,|\psi\rangle\right|^2 \;,
\tag{4.11}
$$

where θ is interpreted as polar angle and ϕ as azimuthal angle. Since every linear interferometer in the two-mode approximation can be represented by subsequent unitary transformations of the form

$$
\hat{S}_\theta^i = \exp\left\{-i\theta\hat{L}_i\right\}
\tag{4.12}
$$

with $i = (x, y, z)$, it is sometimes referred to as $SU(2)$ interferometer. The beam-splitter operators $\hat{S}_\theta^i$ rotate a state about the respective axis on the Bloch sphere. The explicit transformations are summarized in Ref. [214], we quote the result in App. D.1. Using these operators, we are now in the position to rewrite sequence, Eq. (4.1), as follows

$$
\begin{aligned}
-i\int d^3\boldsymbol{r}\left\{\hat{\Psi}_1^\dagger(\boldsymbol{r})\hat{\Psi}_2(\boldsymbol{r})e^{i\phi_{\mathrm{MZ}}} - \mathrm{H.c.}\right\} &= 2\sin(\phi_{\mathrm{MZ}})\hat{L}_x + 2\cos(\phi_{\mathrm{MZ}})\hat{L}_y \\
&= -2\hat{S}_{\phi_{\mathrm{MZ}}}^{z\dagger}\hat{S}_{-\pi/2}^{x\dagger}\hat{L}_z\hat{S}_{-\pi/2}^x\hat{S}_{\phi_{\mathrm{MZ}}}^z \;.
\end{aligned}
\tag{4.13}
$$

The time-evolution operator $\hat{U}_{\mathrm{MZ}}$ contains nonlinear interaction terms and cannot be represented by the beam splitters defined in Eq. (4.12). The question how this operator can be included in the description in terms of angular momentum operators will be addressed next.

Squeezing Hamiltonian

In the previous section we introduced angular momentum operators and expressed the MZ sequence in terms of these operators. We now turn to the nonlinear interaction Hamiltonian, Eq. (4.6). We start by noting that

$$
\hat{a}_1^\dagger\hat{a}_1\hat{a}_2^\dagger\hat{a}_2 = -\hat{L}_z^2 + \hat{N}^2/4 \;,
\tag{4.14}
$$

where the operator $\hat{N} = \hat{a}_1^\dagger\hat{a}_1 + \hat{a}_2^\dagger\hat{a}_2$ is merely a constant which can be disregarded since the total number of particles is fixed. Thus, the MZ time-evolution operator becomes

$$
\hat{U}_{\mathrm{MZ}} = \hat{S}_{\mathrm{sq}}(\xi)\hat{S}_{-\pi/2}^x
\tag{4.15}
$$

where we defined the *squeezing operator* [220]

$$\hat{S}_{\mathrm{sq}}(\xi) = \exp\left\{-\mathrm{i}2\xi\hat{L}_z^2\right\},\tag{4.16}$$

which is a function of the time-dependent squeezing parameter [236]

$$\dot{\xi}(t) = \frac{g}{2\hbar}\int \mathrm{d}^3\boldsymbol{r}\ |\phi_{\mathrm{GP}}(\boldsymbol{r},t)|^4 .\tag{4.17}$$

Hence, with these definitions the full time-evolution operator for an MZ interferometer reads

$$\hat{U} = \hat{S}_{-\pi/2}^x\ \hat{S}_{\phi_{\mathrm{MZ}}}^z\ \hat{U}_{\mathrm{MZ}}\tag{4.18}$$

and $\hat{U}_{\mathrm{MZ}}$ is given by Eq. (4.15). In the following we will calculate the phase sensitivity of the interferometer in the case of $\xi \neq 0$.

4.2. Interaction reduces sensitivity

In the preceding section we introduced the squeezing operator. In order to assess the effect of this operator on the accuracy of the phase $\Delta\phi$, we apply the formula [213]

$$\Delta\phi^2 = \frac{\Delta\hat{L}_z^2}{\left|\frac{\partial\langle\hat{L}_z\rangle}{\partial\phi}\right|^2}.\tag{4.19}$$

Here, $\hat{L}_z$ is the Heisenberg operator with respect to the time-evolution operator defined in Eq. (4.18) and the expectation values are understood to be taken with respect to the initial state $|j,j\rangle$. Equivalently, this can be written as

$$\Delta\phi^2 = \frac{\Delta\hat{L}_x^2}{\langle\hat{L}_y\rangle^2} + \cot^2(\phi_{\mathrm{MZ}})\frac{\Delta\hat{L}_y}{\langle\hat{L}_y\rangle^2},\tag{4.20}$$

where we used $\hat{S}_{-\pi/2}^x\ \hat{S}_{\phi_{\mathrm{MZ}}}^z$ to act on $\hat{L}_z$ and the expectation values are now taken with respect to the state $\hat{U}_{\mathrm{MZ}}|j,j\rangle = \hat{S}_{\mathrm{sq}}(\xi)|-\pi/2,0\rangle$. The exact solution, summarized in App. D.2, is furthermore approximated for $N \gg 1$, $N\xi^2 \ll 1$ and $N\xi > 1$ as

$$\Delta\phi \approx \sqrt{\frac{1}{N} + 4N\xi^2 + 8N^2\xi^4\cot^2(\phi_{\mathrm{MZ}})}\tag{4.21}$$

where $\Delta\phi$ denotes the phase sensitivity of the MZ interferometer. For $\xi = 0$ this uncertainty reduces to the *standard quantum limit* or *shot-noise limit*

$$\Delta\phi_{\mathrm{sql}} = \frac{1}{\sqrt{N}},\tag{4.22}$$

which reflects the aforementioned binomial distribution over the Dicke states. For finite interactions, however, $\Delta\phi$ is considerably larger than the standard quantum limit. To
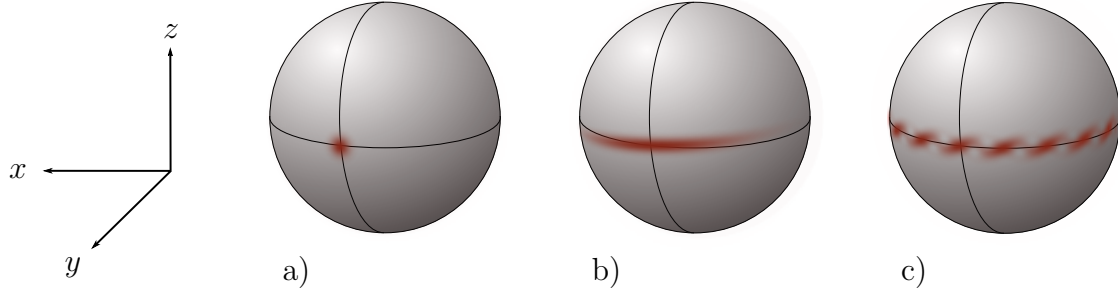
Figure 4.1.: Q function of a squeezed coherent spin state for $N = 600$ particles. a)
Coherent spin state: The Q function approaches a Gaussian distribution for
large particle numbers. b) Squeezed state: While the variance in z direction
stays invariant, $\Delta \hat{L}_x$ strongly increases. So does $\hat{L}_y$ as the state starts to bend
around the Bloch sphere. When appropriately rotated about the y axis, we can
decrease the particle-number fluctuations. c) Extremely squeezed state: As the
distribution has completely whirled around the sphere, it does not contain any
information about the phase anymore.

illustrate this effect, which is referred to as phase diffusion, we plot the Q function of
a squeezed coherent spin state in Fig. 4.1.

In the following we estimate the size of ξ for values comparable to the experimental
parameters of a QUANTUS II experiment and calculate the phase uncertainty. Obvi-
ously, Eq. (4.21) is minimal for the angle $\phi_{\mathrm{MZ}} = \phi_{\min} = \pi/2$, which will therefore be
fixed to this value in the present consideration. Invoking the Thomas-Fermi approxi-
mation and the scaling approach for an isotropic trap, Eq. (4.17) can be represented
as [233]

$$\xi = \frac{1}{7} \left(\frac{15 a_{\mathrm{s}}}{a_{\mathrm{ho}}} \right)^{\frac{2}{5}} N^{-\frac{3}{5}} \gamma \qquad (4.23)$$

where a_s is the s-wave scattering length, $a_{\mathrm{ho}} = \sqrt{\hbar/m\omega}$ the harmonic oscillator length,
ω the initial trap frequency and N the total number of particles. The time evolution
of the Gross-Pitaevskii wave function only appears in the factor

$$\gamma = \int_{t_1}^{t_3} \mathrm{d}t' \frac{\omega}{\lambda(t')^3} \qquad (4.24)$$

where t_1 and t_3 are the times of the first and last laser pulses after the release of
the Bose-Einstein condensate from the trap at $t = 0$. The scaling factor of the Bose-
Einstein condensate is determined by Eq. (2.27). The integral can in principle be solved
analytically, which leads to lengthy expressions in terms of hypergeometric functions.
But for a simple order-of-magnitude estimation we resort to a numerical solution.
The result is depicted in Fig. 4.2. We vary the time between release and delta-kick
collimation, while keeping the subsequent period until the first laser pulse constant at
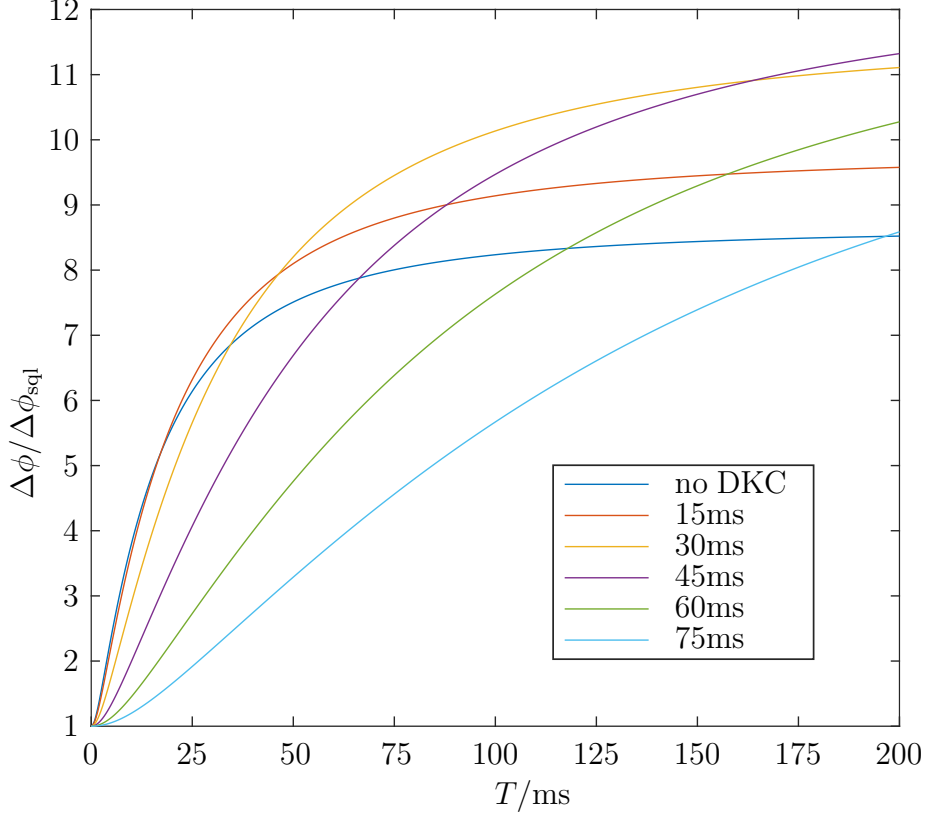20ms.

Figure 4.2.: Impact of phase diffusion on the accuracy of a phase measurement, when the particle-number difference operator is measured. In the figure each line corresponds to one choice for the expansion time before delta-kick collimation, while keeping the subsequent time until the first laser pulse constant at 20ms. The phase accuracy is then calculated according to Eq. (4.21) at the optimal angle $\phi_{\text{MZ}} = \phi_{\text{min}} = \pi/2$. It can clearly be seen from the figure that phase diffusion considerably affects the phase accuracy. For a given half interferometer time T there is a trade off since it is generally better to wait longer, which, however, implies longer experimental preparation times and larger atomic clouds. The numerical values are chosen for ^{87}Rb: $a_s = 100a_0$, where a_0 is the Bohr radius, the number of particles is $N = 10^6$ and the initial frequency of the trap is $\omega = 30$Hz.

We conclude that the influence of phase diffusion is important and non-negligible. If one does not wait long enough, until the density of the BEC has decreased (note the cubic scaling with $1/\lambda^3$ in Eq. (4.24)), one can easily find

$$\frac{\Delta\phi}{\Delta\phi_{\text{sql}}} \approx 10 \tag{4.25}$$

already at interferometer times of 100ms.

Overcoming phase diffusion

Is there a way to minimize or even remove the problem of phase diffusion? To answer this question, we slightly modify the total time-evolution operator, Eq. (4.18), by changing the angle of the last rotation about the x-axis

$$\hat{U} = \hat{S}^x_{-\theta} \, \hat{S}^z_{\phi_{\mathrm{MZ}}} \, \hat{S}_{\mathrm{sq}}(\xi) \, \hat{S}^x_{-\pi/2} \, .$$ (4.26)

Indeed, minimizing the phase uncertainty with respect to ϕ_{MZ} and θ yields as before $\phi_{\min} = \pi/2$ and

$$\theta_{\min} = \arctan\left(\frac{N}{2\langle \hat{L}_z \hat{L}_x + \hat{L}_x \hat{L}_z \rangle}\right) \approx -\arctan\left(\frac{1}{2N\xi}\right) \, .$$ (4.27)

When we again approximate this expression for $N \gg 1$, $N\xi^2 \ll 1$ and $N > 1$, we arrive at

$$\frac{\Delta\phi}{\Delta\phi_{\mathrm{sql}}} = \sqrt{1 + \frac{32}{3}\xi^6 N^4 + \dots} \, .$$ (4.28)

Due to the high power of ξ the phase accuracy deviates only extremely slowly from the standard quantum limit. However, since the minimal rotation angle, defined in Eq. (4.27), quickly approaches $\theta_{\min} = 0$, the contrast decreases as well. In fact

$$C \sim \frac{1}{2\xi N} \, ,$$ (4.29)

which quickly approaches zero. Thus, this method is only practical for extremely weak squeezing.

Is there another way to circumvent the problem of phase diffusion or even use it to enhance the performance of an interferometer? The most simple way in the case of Bragg diffraction is to reduce phase diffusion by switching off the interactions employing a Feshbach resonance [246, 247]. However, in Raman interferometry the resonances of both internal states cannot be addressed simultaneously.

On the other hand, one can in principle use squeezing to increase the sensitivity. Here, a squeezed state must be rotated appropriately *before* it is fed into the interferometer as input state. Then phase accuracy approximately becomes [220]

$$\frac{\Delta\phi}{\Delta\phi_{\mathrm{sql}}} = \sqrt{\frac{1}{4N^2\xi^2} + \frac{8}{3}\xi^4 N^2}$$ (4.30)

with the minimal value

$$\Delta\phi \propto \frac{1}{N^{\frac{5}{6}}} \, ,$$ (4.31)

which is close to the ultimate Heisenberg limit $\Delta\phi = 1/N$. However, it is important to note that due to the intrinsic multimode-structure of a Bose-Einstein condensate, one should include thermal and quantum fluctuations into the calculation. Using Bogoliubov theory, Sørensen and coworkers [248, 249] were not able to find a considerable deviation from the two-mode result. In a series of papers [250–254] it was shown with the

help of semiclassical field simulations that finite-temperature effects and spontaneous emission strongly limit the possible squeezing strength. Nevertheless, for ultracold temperatures and weak interactions it should still be possible to considerably surpass the shot-noise limit. Indeed, in the theoretical work [255, 256] the superposition of a BEC in two internal states was investigated within the truncated Wigner approach. Due to the slight difference of the scattering lengths, time-dependent density modulations occur during which the overlap between the condensates decreases, leading to strong squeezing.

Before we conclude this section, we want to comment on the Fisher information, a tool to assess the information stored in a probability distribution. It unfolds its power together with the Cramer-Rao bound [257, 258], which provides a lower bound for unbiased estimators after having specified the measurement observable. In Refs. [259, 260] the Fisher information was generalized to quantum observables, leading to an ultimate lower bound for unbiased estimators. Recently, the Fisher information was applied in the context of atom-light pulse interferometry for measurements of the gravitational acceleration in order to discuss the optimal observables to measure [261, 262].

4.3. Summary

In this chapter we described the effect of self interaction of a BEC on the accuracy of a phase measurement. Following the approach of Ref. [214] we first represented all beam splitters in terms of angular-momentum operators and presented an intuitive derivation of the spin-squeezing operator with the help of the number-conserving approaches to Bose-Einstein condensation. Next we investigated phase diffusion which we illustrated with the help of the Q function. Then we applied these concepts to a typical QUANTUS experiment, that is, for the case of a measurement of the number-difference operator between the two exit ports. We realized that phase diffusion considerably derogates the sensitivity of an interferometer even when the Bose-Einstein condensate is allowed to expand before the first laser pulse is applied. Finally, we commented upon possible methods to use spin squeezing to enhance the performance of an interferometer and briefly described existing concepts to relate the phase sensitivity to the measured observable.

Summary

The phenomenal advance in sensitivity of light-pulse atom interferometers over the last decades and expected further increase requires a thorough consideration of all the relevant influences to the phase measured in interferometers. This task needs particularly adapted and refined theoretical tools to consistently compare the magnitudes of relevant effects. In this thesis we achieved this goal by a perturbative approach valid for noninteracting particles. To obtain a simplified description of interferometry with interacting Bose-Einstein condensates, we derived a general second-quantized framework.

In chapter 1 we first reviewed a description of light-pulse atom interferometry in terms of comoving frames where one follows the atoms along each interferometer branch. In these frames where linear potentials including the laser-atom interaction vanish the evolution is solely determined by distortion effects of the wave-packet. We streamlined the transformation to these frames, which we obtained by mere operator algebra. We stress that the method is exact for the case of noninteracting particles and infinitely short laser pulses. Apart from being intuitive, the approach is particularly useful in the case of large and strongly varying anharmonic potentials, as for example present in a guided interferometer. Here, the transformation serves as a first step before the local harmonic approximation or before a subsequent numerical exact simulation.

In the second part of chapter 1 we presented a new method built on the insight that small effects are best assessed within a perturbative description. Mathematically, the approach combines the concept of path ordering known from quantum field theory with the Magnus expansion. In previous approaches one approximately solves for the interferometer trajectories generated by the full Hamiltonian including the perturbation. In contrast, our method is based on the trivial interferometer trajectories without including the perturbation so that approximate calculations of trajectories become superfluous. We mention that the method is valid for arbitrary anharmonic and time-dependent perturbations. In a number of examples we subsequently illuminated the mechanism of the formalism and generalized mitigation strategies for gravity gradients by including anharmonicities in the gravitational potential of the Earth and the influence of nearby mass sources. Future work could for example aim at a generalization to incorporate finite-time duration effects of laser pulses.

Bose-Einstein condensation is a fascinating phenomenon but mathematically sophisticated from a fundamental perspective. Chapter 2 serves as a review of the theoretical foundations of BEC and is addressed to both theorists and experimentalists who work in this field. We revisited the old question of the relative phase between two Bose-Einstein condensates and contrasted spontaneous symmetry-breaking with

number-conserving approaches. This helped us realize that the latter model is better suited for the application to light-pulse atom interferometers.

Employing Bose-Einstein condensates as high-flux coherent atom sources for matter-wave interferometry requires theoretical tools for a careful description of interaction effects. However, even within the mean-field approximation, analytic methods are unsatisfactory due to the lack of generality and accuracy. Thus, in chapter 3 we set up a framework in the language of second quantization which generalizes the comoving description to arbitrary interacting systems. Furthermore, the small momentum spread of ultracold BECs after magnetic lensing as well as the large arm separation allowed us to utilize a path-dependent description by assigning approximate bosonic field operators to each interferometer path.

In conclusion, chapter 3 should be regarded as a solid framework for future implementations of 3D numerical simulations of full multi-path interferometer experiments including fully resolved laser-atom interaction. The second-quantized approach not only reduces in the simplest approximation to a mean-field description in terms of a coupled system of Gross-Piatevskii equations but also offers possibility to include beyond mean-field effects like thermal and quantum fluctuations.

Additionally, the transformation to comoving frames does not only considerably reduce computational demands but also separates all phases resulting from the center-of-mass motion of the atoms along the interferometer branches. The subsequent simulation of the reduced dynamics in the comoving frames elucidates additional phases originating solely from particle-particle and laser-atom interaction.

The number-conserving point of view on matter-wave interferometry with Bose-Einstein condensates naturally results in a single-mode approximation for each interferometer path. Within this description we expressed the Hamiltonian for a two-path interferometer in terms of angular momentum operators [214] in chapter 4 and showed that phase diffusion considerably derogates the sensitivity of an interferometer even if the Bose-Einstein condensate is allowed to expand before the first laser pulse. We outlined some ideas to mitigate the effect of phase diffusion and in turn described existing concepts to enhance the performance utilizing particle-particle interactions. Experimental realization of these methods, however, seems to be highly ambitious in state-of-the-art light-pulse atom interferometers.

In summary, we considered some important aspects relevant for high-precision interferometry. For negligible particle-particle interaction we derived a powerful perturbative approach to calculate contrast and phase. In the case where interactions become relevant we set up a theoretical framework in second quantization which generalizes existing comoving descriptions.

Appendices

Appendix A

Displacement operators

In this appendix we first review some of the most important properties and identities of displacement operators. Second, we calculate the time derivative in the case of time-dependent arguments. Finally, we calculate the expectation value with respect to a general state which is invariant under a parity transformation.

General properties

Displacement operators are defined as

$$\hat{D}(\boldsymbol{\chi}) = e^{-\frac{i}{\hbar}\boldsymbol{\chi}^{\mathrm{T}}\boldsymbol{\mathcal{J}}\hat{\boldsymbol{\xi}}} \tag{A.1}$$

with the six-dimensional vector $\boldsymbol{\chi} = (\boldsymbol{\chi}^r, \boldsymbol{\chi}^p)^{\mathrm{T}}$, the phase-space vector operator $\hat{\boldsymbol{\xi}} = (\hat{\boldsymbol{r}}, \hat{\boldsymbol{p}})^{\mathrm{T}}$, and the symplectic matrix

$$\boldsymbol{\mathcal{J}} = \begin{pmatrix} 0 & \mathbb{1} \\ -\mathbb{1} & 0 \end{pmatrix} \tag{A.2}$$

where $\mathbb{1}$ is the three-dimensional identity matrix. With the help of the Baker–Campbell–Hausdorff formula, we write the displacement operators as the product of the three exponentials

$$\hat{D}(\boldsymbol{\chi}) = e^{\frac{i}{\hbar}(\boldsymbol{\chi}^p\hat{\boldsymbol{r}} - \boldsymbol{\chi}^r\hat{\boldsymbol{p}})} = e^{-\frac{i}{2\hbar}\boldsymbol{\chi}^p\boldsymbol{\chi}^r}\, e^{\frac{i}{\hbar}\boldsymbol{\chi}^p\hat{\boldsymbol{r}}}\, e^{-\frac{i}{\hbar}\boldsymbol{\chi}^r\hat{\boldsymbol{p}}} = e^{\frac{i}{2\hbar}\boldsymbol{\chi}^p\boldsymbol{\chi}^r}\, e^{-\frac{i}{\hbar}\boldsymbol{\chi}^r\hat{\boldsymbol{p}}}\, e^{\frac{i}{\hbar}\boldsymbol{\chi}^p\hat{\boldsymbol{r}}}\,. \tag{A.3}$$

In order to determine the action of a displacement operator on a quantum state in position representation, we first note that

$$e^{\frac{i}{\hbar}\boldsymbol{\chi}^p\hat{\boldsymbol{r}}}\,|\boldsymbol{p}\rangle = |\boldsymbol{p} + \boldsymbol{\chi}^p\rangle\,, \qquad e^{-\frac{i}{\hbar}\boldsymbol{\chi}^r\hat{\boldsymbol{p}}}\,|\boldsymbol{r}\rangle = |\boldsymbol{r} + \boldsymbol{\chi}^r\rangle \tag{A.4}$$

by inserting a complete set of momentum and position states. From Eq. (A.4) together with Eq. (A.3) we conclude

$$\hat{D}(\boldsymbol{\chi})\,|\boldsymbol{r}\rangle = e^{\frac{i}{2\hbar}\boldsymbol{\chi}^p\boldsymbol{\chi}^r}\, e^{\frac{i}{\hbar}\boldsymbol{\chi}^p\boldsymbol{r}}\,|\boldsymbol{r} + \boldsymbol{\chi}^r\rangle\,, \tag{A.5}$$

$$\hat{D}(\boldsymbol{\chi})\,|\boldsymbol{p}\rangle = e^{-\frac{i}{2\hbar}\boldsymbol{\chi}^p\boldsymbol{\chi}^r}\, e^{-\frac{i}{\hbar}\boldsymbol{\chi}^r\boldsymbol{p}}\,|\boldsymbol{p} + \boldsymbol{\chi}^p\rangle\,. \tag{A.6}$$

With the help of these expressions, it is easy to show that

$$\langle \boldsymbol{r}| \hat{D}(\boldsymbol{\chi}) |\boldsymbol{r}'\rangle = \mathrm{e}^{-\frac{\mathrm{i}}{2\hbar}\boldsymbol{\chi}^p\boldsymbol{\chi}^r} \, \mathrm{e}^{\frac{\mathrm{i}}{\hbar}\boldsymbol{\chi}^p\boldsymbol{r}} \, \delta(\boldsymbol{r} - \boldsymbol{r}' - \boldsymbol{\chi}^r) \tag{A.7}$$

and thus we obtain the action of a displacement operator on a quantum state in position representation as

$$\langle \boldsymbol{r}| \hat{D}(\boldsymbol{\chi}) |\psi\rangle = \mathrm{e}^{-\frac{\mathrm{i}}{2\hbar}\boldsymbol{\chi}^p\boldsymbol{\chi}^r} \, \mathrm{e}^{\frac{\mathrm{i}}{\hbar}\boldsymbol{\chi}^p\boldsymbol{r}} \, \psi\left(\boldsymbol{r} - \boldsymbol{\chi}^r\right) . \tag{A.8}$$

The inverse of a displacement operator is readily obtained as

$$\hat{D}^{-1}(\boldsymbol{\chi}) = \hat{D}^{\dagger}(\boldsymbol{\chi}) = \hat{D}(-\boldsymbol{\chi}) , \tag{A.9}$$

which we conclude from its exponential form.
The following important identities are proved in Ref. [86].
The *composition rule*

$$\hat{D}(\boldsymbol{\chi}_1)\hat{D}(\boldsymbol{\chi}_0) = \hat{D}(\boldsymbol{\chi}_1 + \boldsymbol{\chi}_0) \, \mathrm{e}^{-\frac{\mathrm{i}}{2\hbar}\boldsymbol{\chi}_1^{\mathrm{T}}\boldsymbol{\mathcal{J}}\boldsymbol{\chi}_0} \tag{A.10}$$

where

$$\boldsymbol{\chi}_1^{\mathrm{T}}\boldsymbol{\mathcal{J}}\boldsymbol{\chi}_0 = \boldsymbol{\chi}_1^r\boldsymbol{\chi}_0^p - \boldsymbol{\chi}_1^p\boldsymbol{\chi}_0^r . \tag{A.11}$$

The *sandwich rule*

$$\hat{D}(-\boldsymbol{\chi})\hat{D}(\boldsymbol{\chi}_0)\hat{D}(-\boldsymbol{\chi}) = \hat{D}(\boldsymbol{\chi}_0 - 2\boldsymbol{\chi}) , \tag{A.12}$$

the formula

$$\hat{D}^{\dagger}(\boldsymbol{\chi})\hat{D}(\boldsymbol{\chi}_0)\hat{D}(\boldsymbol{\chi}) = \hat{D}(\boldsymbol{\chi}_0) \, \mathrm{e}^{\frac{\mathrm{i}}{\hbar}\boldsymbol{\chi}^{\mathrm{T}}\boldsymbol{\mathcal{J}}\boldsymbol{\chi}_0} \tag{A.13}$$

as well as

$$\hat{D}^{\dagger}(\boldsymbol{\chi}) \, \hat{\boldsymbol{\xi}} \, \hat{D}(\boldsymbol{\chi}) = \hat{\boldsymbol{\xi}} + \boldsymbol{\chi} . \tag{A.14}$$

Derivative of $\hat{D}$

Suppose the argument of the displacement operator $\boldsymbol{\chi} = \boldsymbol{\chi}(t)$ is time dependent. The time derivative of the displacement operator is then calculated as

$$\mathrm{i}\hbar\frac{\mathrm{d}}{\mathrm{d}t}\hat{D} = \dot{\boldsymbol{\chi}}^{\mathrm{T}}\boldsymbol{\mathcal{J}}\left(\hat{\boldsymbol{\xi}} - \frac{1}{2}\boldsymbol{\chi}\right)\hat{D} . \tag{A.15}$$

The proof is straightforward. First, separate the operator according to Eq. (A.3). Second, take the derivative of each exponential individually and third, recombine the displacement operator by using Eq. (A.14).

Expectation value of a displacement operator

Suppose a state can be written as

$$|\psi\rangle = \hat{D}(\langle \hat{\boldsymbol{\xi}} \rangle)|\tilde{\psi}\rangle \tag{A.16}$$

where $\langle \hat{\boldsymbol{\xi}} \rangle$ is with respect to $|\psi\rangle$ and $|\tilde{\psi}\rangle$ is invariant under a parity transformation, meaning that $\hat{P}|\tilde{\psi}\rangle = |\tilde{\psi}\rangle$, where $\hat{P}$ is the parity operator. Since $\hat{P}^\dagger \hat{D} \hat{P} = \hat{D}^\dagger$, it is straightforward to show that the expectation value

$$\langle \tilde{\psi}|\hat{D}(\boldsymbol{\chi})|\tilde{\psi}\rangle = C \tag{A.17}$$

is real. Together with Eq. (A.13) we then find

$$\langle \psi| \, \hat{D}(\boldsymbol{\chi}) \, |\psi\rangle = C \, \mathrm{e}^{\frac{\mathrm{i}}{\hbar} \langle \hat{\boldsymbol{\xi}} \rangle^{\mathrm{T}} \boldsymbol{\mathcal{J}} \boldsymbol{\chi}} \,, \tag{A.18}$$

and identify C as the contrast. Note, however, that C is in general a complex quantity. For example an input state after magnetic lensing is still centered, that is, with zero momentum and position expectational value, but not parity invariant [89]. Thus, we obtain a complex expectation value of a displacement operator which additionally introduces phases.

Appendix B

Path-dependent perturbation theory

In this appendix we present supplementing material for the perturbative methods developed in Sec. 1.3. We first generalize the standard Magnus expansion in App. B.1 to a direct expansion of the overlap operator. Subsequently, we show in App. B.2 that the nested contour integrals over path-independent functions vanish. Finally, we Taylor expand the gravitational potential up to third order in the inverse of Earth's radius in App. B.3 and calculate explicitly the functions f needed for calculations in Sec. 1.3.

B.1. Magnus expansion of the overlap operator

In this appendix we generalize the standard Magnus expansion. The result will be a nonlinear integral equation for the exponent of the combined overlap operator, which must be solved perturbatively. In the derivation we will generalize the informal proof given in Ref. [263] for the standard Magnus expansion. We begin by defining

$$\hat{U}_1^\dagger(t, t_\mathrm{i})\hat{U}_2(t, t_\mathrm{i}) = \mathrm{e}^{\hat{\Omega}(t, t_\mathrm{i})} \tag{B.1}$$

in which we insert the general group property of a time-evolution operator

$$\hat{U}(t, t_\mathrm{i} - \delta t) = \hat{U}(t, t_\mathrm{i})\hat{U}(t_\mathrm{i}, t_\mathrm{i} - \delta t)\,, \tag{B.2}$$

resulting in

$$\mathrm{e}^{\hat{\Omega}(t, t_\mathrm{i} - \delta t)} \cong \mathrm{e}^{\frac{\mathrm{i}}{\hbar}\hat{H}_1(t_\mathrm{i})\delta t}\mathrm{e}^{\hat{\Omega}(t, t_\mathrm{i})}\mathrm{e}^{-\frac{\mathrm{i}}{\hbar}\hat{H}_2(t_\mathrm{i})\delta t} \tag{B.3}$$

to first order in δt. The three exponentials are now combined to one with the help of the Baker–Campbell–Hausdorff formula. For general operators X and Y the explicit form of the BCH series is enormously cumbersome but to linear order in one of the operators, say Y, the remarkable simple, explicit form can be derived [264]

$$\mathrm{e}^X\mathrm{e}^Y = \exp\left\{X + \sum_{k=0}^{\infty}(-1)^k\frac{B_k}{k!}\left[X, Y\right]_k + \mathcal{O}(Y^2)\right\}\,. \tag{B.4}$$

Here, $[.,.]_k$ is the usual nested commutator and B_k are the Bernoulli numbers [116] with

$$B_0 = 1,\ \ B_1 = -1/2,\ \ B_2 = 1/6,\ \ \dots. \tag{B.5}$$

To linear order in X, the right-hand side of Eq. (B.4) takes exactly the same form with $X \leftrightarrow Y$ but without the alternating sign $(-1)^k$. As a result, the combination of the product of three exponentials reads

$$
\mathrm{e}^Z \mathrm{e}^X \mathrm{e}^Y = \exp\left\{ X + \sum_{k=0}^{\infty} \frac{B_k}{k!} \left[X, Z + (-1)^k Y \right]_k + ... \right\} \tag{B.6}
$$

to linear order in Z and Y. Identifying $Z = \frac{\mathrm{i}}{\hbar}\hat{H}_1(t_\mathrm{i})\delta t$ and $Y = -\frac{\mathrm{i}}{\hbar}\hat{H}_2(t_\mathrm{i})\delta t$ as well as $X = \hat{\Omega}(t, t_\mathrm{i})$, we obtain

$$
\mathrm{e}^{\hat{\Omega}(t,t_\mathrm{i}-\delta t)} = \exp\left\{ \hat{\Omega}(t,t_\mathrm{i}) + \frac{\mathrm{i}}{\hbar} \sum_{k=0}^{\infty} \frac{B_k}{k!} \left[\hat{\Omega}(t,t_\mathrm{i}), \hat{H}_k(t_\mathrm{i}) \right]_k \delta t + \mathcal{O}(\delta t^2) \right\} \tag{B.7}
$$

with the abbreviation

$$
\hat{H}_k(t_\mathrm{i}) = \begin{cases} -\hat{H}_-(t_\mathrm{i}) & \text{for } k \text{ even} \\ \hat{H}_+(t_\mathrm{i}) & \text{for } k \text{ odd} \end{cases} \tag{B.8}
$$

where $\hat{H}_+ = \hat{H}_2 + \hat{H}_1$ and $\hat{H}_- = \hat{H}_2 - \hat{H}_1$. When we equate the exponents in Eq. (B.7), subtract $\hat{\Omega}(t, t_\mathrm{i})$, divide by δt and take the limit $\delta t \to 0$, we arrive at the differential equation

$$
\frac{\partial \hat{\Omega}(t,t_\mathrm{i})}{\partial t_\mathrm{i}} = -\frac{\mathrm{i}}{\hbar} \sum_{k=0}^{\infty} \frac{B_k}{k!} \left[\hat{\Omega}(t,t_\mathrm{i}), \hat{H}_k(t_\mathrm{i}) \right]_k \tag{B.9}
$$

with the initial condition $\hat{\Omega}(t_\mathrm{i}, t_\mathrm{i}) = 0$. This highly nonlinear equation can be formally integrated

$$
\hat{\Omega}(t,t_\mathrm{i}) = \frac{\mathrm{i}}{\hbar} \int_{t_\mathrm{i}}^{t} \mathrm{d}t' \sum_{k=0}^{\infty} \frac{B_k}{k!} \left[\hat{\Omega}(t,t'), \hat{H}_k(t') \right]_k \tag{B.10}
$$

and solved iteratively by the ansatz $\hat{\Omega} = \sum_{k=1}^{\infty} \epsilon^k \hat{\Omega}_k$ and $\hat{H}_k \to \epsilon \hat{H}_k$. With $\Omega_k = \mathrm{i}\phi_k$, the first three terms are

$$
\hat{\phi}_1(t_\mathrm{d}, t_\mathrm{i}) = -\frac{1}{\hbar} \int_{t_\mathrm{i}}^{t_\mathrm{d}} \mathrm{d}t_1 \, \hat{H}_-(t_1) \tag{B.11}
$$

$$
\hat{\phi}_2(t_\mathrm{d}, t_\mathrm{i}) = -\frac{\mathrm{i}}{2\hbar^2} \int_{t_\mathrm{i}}^{t_\mathrm{d}} \mathrm{d}t_1 \int_{t_1}^{t_\mathrm{d}} \mathrm{d}t_2 \, [\hat{H}_+(t_1), \hat{H}_-(t_2)] \tag{B.12}
$$

$$
\hat{\phi}_3(t_\mathrm{d}, t_\mathrm{i}) = \frac{1}{4\hbar^3} \int_{t_\mathrm{i}}^{t_\mathrm{d}} \mathrm{d}t_1 \int_{t_1}^{t_\mathrm{d}} \mathrm{d}t_2 \int_{t_2}^{t_\mathrm{d}} \mathrm{d}t_3 \Big\{ \; [\hat{H}_+(t_1), [\hat{H}_+(t_2), \hat{H}_-(t_3)]]
$$
$$
+ \frac{1}{3}[\hat{H}_-(t_2), [\hat{H}_-(t_3), \hat{H}_-(t_1)]]
$$
$$
+ \frac{1}{3}[\hat{H}_-(t_3), [\hat{H}_-(t_2), \hat{H}_-(t_1)]] \; \Big\}. \tag{B.13}
$$

In principle, higher-order terms can be calculated. However, just as in the standard Magnus expansion, the terms quickly become cumbersome. Note that in the derivation presented above the two Hamiltonians only appear in the form $\hat{H}_+$ and $\hat{H}_-$.

B.2. Integrals over path-independent functions

In this appendix we show that the nth-order nested contour integrals over a path-independent function vanish. Clearly, the integral

$$\int_\gamma \mathrm{d}t\, f(t) = 0 \tag{B.14}$$

if $f_1(t) = f_2(t)$ where the index on f denotes path 1 or 2 of the contour. We can easily convince ourselves by induction that this result is also true for the nth-oder nested integral. To this end, we define

$$h(t) \equiv \int_\gamma^t \mathrm{d}t'\, f(t') \tag{B.15}$$

and evaluate $h(t)$ on both parts of the contour. On γ_1 we find

$$h_1(t) = \int_{t_\mathrm{i}}^t \mathrm{d}t'\, f_1(t') \tag{B.16}$$

and on γ_2

$$h_2(t) = \int_{t_\mathrm{i}}^{t_\mathrm{d}} \mathrm{d}t'\, f_1(t') + \int_{t_\mathrm{d}}^t \mathrm{d}t'\, f_2(t') = \int_{t_\mathrm{i}}^t \mathrm{d}t'\, f_1(t') = h_1(t)\,, \tag{B.17}$$

where we made use of $f_1(t) = f_2(t)$. Thus, $h(t)$ is path independent. The path independence of higher-order integrals then follows simply by induction.

B.3. Phase and contrast in the gravitational potential

In this appendix we first expand the gravitational potential up to third order on the surface of the Earth and state the explicit values of the functions f for an MZ interferometer in this potential.

B.3.1. Expansion of the gravitational potential

The energy of a particle with mass m in the Newton gravitational potential reads

$$V(\boldsymbol{r}) = -G\frac{mM}{r} \tag{B.18}$$

where G is the gravitational constant and M the mass of the Earth. The origin of the coordinate system coincides with the center of the Earth. We can shift it to the surface by replacing $z \to z + R$ with the radius R of the Earth and subsequently Taylor expand about $\boldsymbol{r} = 0$ of the new coordinate system

$$V(\boldsymbol{r}) = mgz + \frac{1}{2}m\left[\frac{g}{R}(x^2 + y^2 - 2z^2) + \frac{g}{R^2}(2z^3 - 3zx^2 - 3zy^2) + ...\right]\,, \tag{B.19}$$

where we disregarded an irrelevant energy offset and identified the local acceleration $g = \frac{GM}{R^2} \cong 9.81 \mathrm{m/s}^2$. When we furthermore introduce the symmetric tensors $\Gamma_{ij}^{(1)}$ and $\Gamma_{ijk}^{(2)}$, we bring Eq. (B.19) to the form

$$V(\boldsymbol{r}) = mgz + \frac{1}{2}m \left[\Gamma_{ij}^{(1)} x_i x_j + \Gamma_{ijk}^{(2)} x_i x_j x_k + ... \right] \tag{B.20}$$

where repeated indices are summed over. The elements of the tensors are thus

$$\Gamma_{xx}^{(1)} = \Gamma_{yy}^{(1)} = \frac{g}{R} \tag{B.21}$$

and

$$\Gamma_{zz}^{(1)} = -2\frac{g}{R} \, . \tag{B.22}$$

All other components vanish and $\boldsymbol{\Gamma}^{(1)}$ is therefore diagonal. Furthermore,

$$\Gamma_{zzz}^{(2)} = 2\frac{g}{R^2} \, , \tag{B.23}$$

$$\Gamma_{xxz}^{(2)} = \Gamma_{xzx}^{(2)} = \Gamma_{zxx}^{(2)} = -\frac{g}{R^2} \tag{B.24}$$

and

$$\Gamma_{yyz}^{(2)} = \Gamma_{yzy}^{(2)} = \Gamma_{zyy}^{(2)} = -\frac{g}{R^2} \, . \tag{B.25}$$

All other components vanish and $\boldsymbol{\Gamma}^{(2)}$ is symmetric in all indices. With $\Gamma_{zjk}^{(2)} = (\boldsymbol{\Gamma}_z^{(2)})_{jk}$ we can also state it in matrix form as

$$\boldsymbol{\Gamma}_z^{(2)} = -\frac{g}{R^2} \begin{pmatrix} 1 & 0 & 0 \\ 0 & 1 & 0 \\ 0 & 0 & -2 \end{pmatrix} \, . \tag{B.26}$$

In Eq. (B.19) we expanded the gravitational potential in powers of R^{-1}, accordingly the ratio of the nth-order and the $(n+1)$th-order term in the expansion scales as

$$\frac{\Gamma^{(n+1)} l^{n+1}}{\Gamma^{(n)} l^n} \sim \frac{l}{R} \ll 1 \tag{B.27}$$

where l is a characteristic size of the interferometer. Consider for example an experiment in a 10m tower in the gravitational potential of the Earth. For $l = 10\mathrm{m}$ we find the extremely small value $l/R \sim 10^{-6}$ so that an expansion of the interferometer phase in terms of this parameter should be extremely accurate.

B.3.2. Corrections by the gravitational potential to second order with initial launching velocity

In the calculation of the influence of the gravitational field on an MZ interferometer to second order with closed unperturbed interferometer, the following integrals appear in Sec. 1.3.3. We include an initial velocity v_0 but set $z_0 = 0$ and $T_0 = 0$. We find the expressions

$$f_{\chi_p 1} = \oint dt\, z_c(t) = v_r T^2 \tag{B.28}$$

$$f_{\chi_r 1} = \oint dt\, z_c(t)t = v_r T^3 \tag{B.29}$$

$$f_{\varphi 1} = \oint dt\, z_c(t)^2 = -\frac{7}{6}g v_r T^4 + (2v_0 + v_r)v_r T^3 \tag{B.30}$$

$$f_{\varphi 2} = \oint dt\, z_c(t)^3 = \frac{31}{20}g^2 v_r T^6 - \frac{9}{4}g(2v_0 + v_r)v_r T^5 + \frac{1}{2}(7v_0^2 + 7v_0 v_r + 2v_r^2)v_r T^4 \tag{B.31}$$

$$f_{\varphi 3} = \int_{t_i}^{t_d} dt \int_t^{t_d} dt'\, z_{c+}(t)z_{c-}(t')(t - t') = \frac{31}{180}g v_r T^6 - \frac{1}{4}(2v_0 + v_r)v_r T^5 \tag{B.32}$$

$$f_{\chi_p 2} = f_{\varphi 1} \tag{B.33}$$

$$f_{\chi_p 3} = \int_{t_i}^{t_d} dt \int_t^{t_d} dt'\, z_{c-}(t')(t - t') = -\frac{7}{12}v_r T^4 \tag{B.34}$$

$$f_{\chi_r 2} = \oint dt\, z_c(t)^2 t = -\frac{3}{2}g v_r T^5 + \frac{7}{6}(2v_0 + v_r)v_r T^4 \tag{B.35}$$

$$f_{\chi_r 3} = \int_{t_i}^{t_d} dt \int_t^{t_d} dt'\, z_{c-}(t')(t - t')t = -\frac{1}{4}v_r T^5 \tag{B.36}$$

$$f_{A1} = f_{\chi_p 1} \tag{B.37}$$

$$f_{A2} = f_{\chi_r 1} \tag{B.38}$$

$$f_{A3} = \oint dt\, z_c(t)t^2 = \frac{7}{6}v_r T^4 \,. \tag{B.39}$$

Note that the definitions of the functions f stated above apply to completely general but closed interferometer geometries. Only after the second equal sign we particularized the calculation to an MZ sequence with initial velocity v_0.

B.3.3. Corrections by the gravitational potential to second order with initial launching velocity and open unperturbed interferometer

In this appendix we provide the expressions of the integrals needed for the calculation of the overlap operator of an open unperturbed interferometer under the influence of small harmonic and cubic contributions in the Hamiltonian. We consider an MZ interferometer with slightly modified momentum transfer in the second and third laser pulse, more specifically the recoil velocities are $\boldsymbol{v}_\mathrm{r} \to \boldsymbol{v}_\mathrm{r} + \Delta\boldsymbol{v}_\mathrm{r1}$ for the second and $\boldsymbol{v}_\mathrm{r} \to \boldsymbol{v}_\mathrm{r} + \Delta\boldsymbol{v}_\mathrm{r2}$ for the third laser pulse. As described in Sec. 1.3.4, we have to include the displacement $\Delta\boldsymbol{\chi}_0 \sim \boldsymbol{\Gamma}^{(1)}$ of the unperturbed interferometer into the classical trajectories, however, to the order considered here this is only necessary in Eq. (B.42) and Eq. (B.43), for the other expressions it is sufficient to chose the trajectories of the standard closed MZ interferometer. Note that we include an initial launching velocity $\boldsymbol{v}_0$ and employ the matrix notation defined in Eq. (1.133). The expressions are

$$\Delta\boldsymbol{\chi}_0^r = -2(\Delta\boldsymbol{v}_\mathrm{r2} - \Delta\boldsymbol{v}_\mathrm{r1})T \tag{B.40}$$

$$\Delta\boldsymbol{\chi}_0^p = m(\Delta\boldsymbol{v}_\mathrm{r2} - 2\Delta\boldsymbol{v}_\mathrm{r1}) \tag{B.41}$$

$$\Delta\boldsymbol{\chi}_1^r = \oint \mathrm{d}t\, \boldsymbol{\Gamma}^{(1)}\boldsymbol{r}_\mathrm{c}(t)t = \frac{1}{3}\boldsymbol{\Gamma}^{(1)}(3\boldsymbol{v}_\mathrm{r} - \Delta\boldsymbol{v}_\mathrm{r1} + 4\Delta\boldsymbol{v}_\mathrm{r2})T^3 \tag{B.42}$$

$$\Delta\boldsymbol{\chi}_1^p = -m \oint \mathrm{d}t\, \boldsymbol{\Gamma}^{(1)}\boldsymbol{r}_\mathrm{c}(t) = -m\boldsymbol{\Gamma}^{(1)}(\boldsymbol{v}_\mathrm{r} - \Delta\boldsymbol{v}_\mathrm{r1} + 2\Delta\boldsymbol{v}_\mathrm{r2})T^2 \tag{B.43}$$

$$\Delta\boldsymbol{\chi}_2^r = \frac{3}{2} \oint \mathrm{d}t\, \boldsymbol{r}_\mathrm{c}(t)^\mathrm{T}\boldsymbol{\Gamma}^{(2)}\boldsymbol{r}_\mathrm{c}(t)t = -\frac{9}{4}\boldsymbol{g}^\mathrm{T}\boldsymbol{\Gamma}^{(2)}\boldsymbol{v}_\mathrm{r}T^5 + \frac{7}{4}\boldsymbol{v}_\mathrm{r}^\mathrm{T}\boldsymbol{\Gamma}^{(2)}(2\boldsymbol{v}_0 + \boldsymbol{v}_\mathrm{r})T^4 \tag{B.44}$$

$$\Delta\boldsymbol{\chi}_2^p = -\frac{3}{2}m \oint \mathrm{d}t\, \boldsymbol{r}_\mathrm{c}(t)^\mathrm{T}\boldsymbol{\Gamma}^{(2)}\boldsymbol{r}_\mathrm{c}(t) = \frac{7}{4}m\boldsymbol{g}^\mathrm{T}\boldsymbol{\Gamma}^{(2)}\boldsymbol{v}_\mathrm{r}T^4 - \frac{3}{2}m\boldsymbol{v}_\mathrm{r}^\mathrm{T}\boldsymbol{\Gamma}^{(2)}(2\boldsymbol{v}_0 + \boldsymbol{v}_\mathrm{r})T^3 \tag{B.45}$$

$$\Delta\boldsymbol{\chi}_3^r = \int_{t_\mathrm{i}}^{t_\mathrm{d}}\mathrm{d}t \int_t^{t_\mathrm{d}}\mathrm{d}t'\, [\boldsymbol{\Gamma}^{(1)}]^2\boldsymbol{r}_{\mathrm{c}-}(t')(t - t')t = -\frac{1}{4}[\boldsymbol{\Gamma}^{(1)}]^2\boldsymbol{v}_\mathrm{r}T^5 \tag{B.46}$$

$$\Delta\boldsymbol{\chi}_3^p = -m \int_{t_\mathrm{i}}^{t_\mathrm{d}}\mathrm{d}t \int_t^{t_\mathrm{d}}\mathrm{d}t'\, [\boldsymbol{\Gamma}^{(1)}]^2\boldsymbol{r}_{\mathrm{c}-}(t')(t - t') = \frac{7}{12}m[\boldsymbol{\Gamma}^{(1)}]^2\boldsymbol{v}_\mathrm{r}T^4 \tag{B.47}$$

$$\boldsymbol{A}^{rr} = 3m \oint \mathrm{d}t\, \boldsymbol{\Gamma}^{(2)}\boldsymbol{r}_\mathrm{c}(t) = 3m\boldsymbol{\Gamma}^{(2)}\boldsymbol{v}_\mathrm{r}T^2 \tag{B.48}$$

$$\boldsymbol{A}^{rp} = 3 \oint \mathrm{d}t\, \boldsymbol{\Gamma}^{(2)}\boldsymbol{r}_\mathrm{c}(t)t = 3\boldsymbol{\Gamma}^{(2)}\boldsymbol{v}_\mathrm{r}T^3 \tag{B.49}$$

$$\boldsymbol{A}^{pp} = \frac{3}{m} \oint \mathrm{d}t\, \boldsymbol{\Gamma}^{(2)}\boldsymbol{r}_\mathrm{c}(t)t^2 = \frac{7}{2m}\boldsymbol{\Gamma}^{(2)}\boldsymbol{v}_\mathrm{r}T^4\,. \tag{B.50}$$

The expressions, Eq. (B.40) and Eq. (B.41), are valid for the MZ interferometer with slightly modified momentum transfer. The other equations are valid for arbitrary interferometer geometries, only after the second equal sign we particularized the calculation to the MZ interferometer.

Appendix C

Interferometer and second quantization

In this appendix we showcase the detailed calculations which lead to the results discussed in chapter 3. We start by collecting some important properties of first quantized operators acting on field operators in App. C.1. As an example we briefly consider displacement operators. In App. C.2 we provide supplementary material on adiabatic elimination for field operators and carefully discuss the different time scales of the problem. For the transformation to the comoving frames in Sec. 3.3 and Sec. 3.4 we prove some relevant properties in App. C.3.

C.1. First-quantized operators and field operators

In this section we introduce a compact notation for first-quantized operators which act on the space of mode functions. In this work we denote these operators without hat and write for instance

$$\mathcal{A}\hat{\Psi}(\boldsymbol{r}) \equiv \int \mathrm{d}^3\boldsymbol{r}' \, \langle \boldsymbol{r}| \, \hat{A} \, |\boldsymbol{r}'\rangle \, \hat{\Psi}(\boldsymbol{r}') \tag{C.1}$$

for the action of an operator $\hat{A}$ on a field operator.

C.1.1. Time-evolution with respect to a one-body Hamiltonian

We start by discussing how a field operator evolves with respect to the one-body Hamiltonian

$$\hat{H} = \int \mathrm{d}^3\boldsymbol{r} \, \hat{\Psi}^\dagger(\boldsymbol{r}) \mathcal{H}(t) \hat{\Psi}(\boldsymbol{r}) \, . \tag{C.2}$$

To this end, we calculate the Heisenberg equation of motion

$$\mathrm{i}\hbar \frac{\mathrm{d}}{\mathrm{d}t} \hat{\Psi}_\mathrm{H}(\boldsymbol{r}, t) = \int \mathrm{d}^3\boldsymbol{r}' \, \langle \boldsymbol{r}| \, \hat{\mathcal{H}}(t) \, |\boldsymbol{r}'\rangle \, \hat{\Psi}_\mathrm{H}(\boldsymbol{r}', t) \, , \tag{C.3}$$

where the index H denotes the Heisenberg picture with respect to Hamiltonian, Eq. (C.2). The equation admits the solution

$$\hat{\Psi}_{\mathrm{H}}(\boldsymbol{r}, t) = \int \mathrm{d}^3 \boldsymbol{r}' \, \langle \boldsymbol{r} | \hat{\mathcal{U}}(t, t_{\mathrm{i}}) | \boldsymbol{r}' \rangle \, \hat{\Psi}(\boldsymbol{r}') = \mathcal{U}(t, t_{\mathrm{i}}) \hat{\Psi}(\boldsymbol{r}) \tag{C.4}$$

with the first-quantized time-evolution operator

$$\hat{\mathcal{U}}(t, t_{\mathrm{i}}) = \mathcal{T} \exp \left\{ -\frac{\mathrm{i}}{\hbar} \int_{t_{\mathrm{i}}}^{t} \mathrm{d}t' \, \hat{\mathcal{H}}(t') \right\} . \tag{C.5}$$

For the proof simply substitute Eq. (C.4) into to the equation of motion, Eq. (C.3).

C.1.2. Displacement operators and second quantization

In the spirit of the definition Eq. (C.1), the action of a displacement operator on a field operator is denoted by

$$\mathcal{D}\hat{\Psi}(\boldsymbol{r}) = \int \mathrm{d}^3 \boldsymbol{r}' \, \langle \boldsymbol{r} | \hat{D} | \boldsymbol{r}' \rangle \, \hat{\Psi}(\boldsymbol{r}') = \mathrm{e}^{-\frac{\mathrm{i}}{2\hbar} \boldsymbol{\chi}^p \boldsymbol{\chi}^r} \, \mathrm{e}^{\frac{\mathrm{i}}{\hbar} \boldsymbol{\chi}^p \boldsymbol{r}} \, \hat{\Psi}(\boldsymbol{r} - \boldsymbol{\chi}^r) , \tag{C.6}$$

where we used Eq. (A.7). Similarly, the one-body Hamiltonian with respect to a displaced field operator might be written as

$$\begin{aligned} \hat{H} &= \int \mathrm{d}^3 \boldsymbol{r} \, \mathrm{d}^3 \boldsymbol{r}' \left[\mathcal{D}_1 \hat{\Psi}(\boldsymbol{r}) \right]^{\dagger} \langle \boldsymbol{r} | \hat{\mathcal{H}} | \boldsymbol{r}' \rangle \, \mathcal{D}_2 \hat{\Psi}(\boldsymbol{r}') \\ &= \int \mathrm{d}^3 \boldsymbol{r} \, \mathrm{d}^3 \boldsymbol{r}' \hat{\Psi}^{\dagger}(\boldsymbol{r}) \, \langle \boldsymbol{r} | \hat{D}_1^{\dagger} \hat{\mathcal{H}} \hat{D}_2 | \boldsymbol{r}' \rangle \, \hat{\Psi}(\boldsymbol{r}') \\ &= \int \mathrm{d}^3 \boldsymbol{r} \, \hat{\Psi}^{\dagger}(\boldsymbol{r}) \mathcal{D}_1^{\dagger} \mathcal{H} \mathcal{D}_2 \hat{\Psi}(\boldsymbol{r}) , \end{aligned} \tag{C.7}$$

where we again employed the definition, Eq. (C.1).
Finally, note that for general displacement operators we have the identity

$$\int \mathrm{d}^3 \boldsymbol{r} \left[\mathcal{D}_1 \hat{\Psi}(\boldsymbol{r}) \right]^{\dagger} \left[\mathcal{D}_2 \hat{\Psi}(\boldsymbol{r}) \right]^{\dagger} \mathcal{D}_3 \hat{\Psi}(\boldsymbol{r}) \mathcal{D}_4 \hat{\Psi}(\boldsymbol{r})$$
$$= \int \mathrm{d}^3 \boldsymbol{r} \, \hat{\Psi}^{\dagger}(\boldsymbol{r}) \left[\mathcal{D}_1^{\dagger} \mathcal{D}_2 \hat{\Psi}(\boldsymbol{r}) \right]^{\dagger} \mathcal{D}_1^{\dagger} \mathcal{D}_3 \hat{\Psi}(\boldsymbol{r}) \mathcal{D}_1^{\dagger} \mathcal{D}_4 \hat{\Psi}(\boldsymbol{r}) . \tag{C.8}$$

For the proof simply use Eq. (C.6) and redefine the integration variable.

C.2. Adiabatic elimination

In this appendix we derive the formulas of Eq. (3.22) and Eq. (3.23) presented in Sec. 3.2.3. In order to avoid the complications associated with the standard approach of adiabatic elimination, we use a more systematic formalism in which we explicitly manipulate the time-evolution operator rather than working with the equations of motion in the Heisenberg picture. This allows us to neglect two-body interactions and

one-body potentials in a more systematic way and in principle to extend the theory to higher-order contributions. In order to assess the complicated time evolution generated by Hamiltonian, Eq. (3.21), we first resort to a simplified version, e.g.

$$\hat{H}(t) = \hbar \int d^3\boldsymbol{r} \left(\lambda e^{i\Delta t} \hat{\Psi}_1^\dagger(\boldsymbol{r}) \hat{\Psi}_2(\boldsymbol{r}) + \text{H.c.} \right) \tag{C.9}$$

where λ is now merely a real constant and we assume $\lambda \ll \Delta$. It is important to recall that due to the explicit time dependence in Eq. (C.9), the time-evolution operator is *not*

$$\hat{U}(t,0) = \mathcal{T}\exp\left\{ -\frac{i}{\hbar} \int_0^t dt' \, \hat{H}(t') \right\} \neq \exp\left\{ \frac{\lambda}{\Delta}\left(1 - e^{i\Delta t}\right) \int d^3\boldsymbol{r} \, \hat{\Psi}_1^\dagger(\boldsymbol{r})\hat{\Psi}_2(\boldsymbol{r}) - \text{H.c.} \right\} \tag{C.10}$$

where we simply disregarded the time-ordering operator. Transforming a field operator into the Heisenberg picture with respect to the wrong time-evolution operator in Eq. (C.10) would lead to a power series in terms of $\frac{\lambda}{\Delta} \ll 1$ and transitions between the internal states would be suppressed by this factor. The correct result is of course obtained as follows. Derive the equations of motion in the Heisenberg picture and integrate them iteratively, that is,

$$\hat{\Psi}_1(\boldsymbol{r},t) = \hat{\Psi}_1(\boldsymbol{r}) - i\lambda \int_0^t dt' \, e^{i\Delta t'} \hat{\Psi}_2(\boldsymbol{r},t')$$

$$\hat{\Psi}_2(\boldsymbol{r},t) = \hat{\Psi}_2(\boldsymbol{r}) - i\lambda \int_0^t dt' \, e^{-i\Delta t'} \hat{\Psi}_1(\boldsymbol{r},t') \,, \tag{C.11}$$

resulting in, e.g. for $\hat{\Psi}_1(\boldsymbol{r})$,

$$\hat{\Psi}_1(\boldsymbol{r},t) = \hat{\Psi}_1(\boldsymbol{r}) - \frac{\lambda}{\Delta}\left(e^{i\Delta t} - 1\right)\hat{\Psi}_2(\boldsymbol{r}) + \left[\frac{\lambda^2}{\Delta^2}\left(e^{i\Delta t} - 1\right) - i\frac{\lambda^2}{\Delta}t\right]\hat{\Psi}_1(\boldsymbol{r}) + \dots . \tag{C.12}$$

Again, we observe powers of $\frac{\lambda}{\Delta} \ll 1$, but also the term $\frac{\lambda^2}{\Delta}t$. This term arises solely from the time-ordered structure of the time-evolution operator. Choosing the laser interaction time such that this term is of the order of unity shows that transitions between the internal states result from these secular terms. Before we transfer this insight to the full Hamiltonian, Eq. (3.21), we note that a general time-evolution operator with respect to a Hamiltonian $\hat{H}$ can be cast in the form

$$\hat{U}(t,t_i) = e^{-\hat{F}(t)}\hat{U}_{\text{eff}}(t,t_i)e^{\hat{F}(t_i)} \tag{C.13}$$

and we choose

$$i\hbar\frac{d}{dt}\hat{F}(t) + \hat{H}(t) = 0 \,. \tag{C.14}$$

In order to determine the explicit form of $\hat{H}_{\text{eff}}$, we solve Eq. (C.13) for $\hat{U}_{\text{eff}}$ and subsequently differentiate with respect to time on both sides. With the help of the derivative of the exponential map [265]

$$\frac{d}{dt}e^{\hat{F}(t)} = \frac{i}{\hbar}\sum_{j=0}^{\infty} \frac{1}{(j+1)!}\left[\hat{F}(t), \hat{H}(t)\right]_j e^{\hat{F}(t)} \tag{C.15}$$

where $[.,.]_j$ denotes the nested commutators, we conclude

$$\hat{H}_{\mathrm{eff}}(t) = \sum_{j=1}^{\infty} \frac{j}{(j+1)!} \left[\hat{F}(t), \hat{H}(t)\right]_j . \tag{C.16}$$

A similar identity was used in Ref. [208]. The result, Eq. (C.13), will now help us separate the two different scalings encountered in Eq. (C.12). To this end, we start from the full Hamiltonian

$$\hat{H} = \hat{H}_{\mathrm{e}} + \hat{H}_{\mathrm{L}} , \tag{C.17}$$

where we recall the laser-atom interaction Hamiltonian, Eq. (3.21),

$$\hat{H}_{\mathrm{L}} = \int \mathrm{d}^3\boldsymbol{r} \left(\sum_{j,k} \hbar\lambda_{jk}(\boldsymbol{r},t)\mathrm{e}^{\mathrm{i}\Delta_{jk}t}\hat{\Psi}_j^{\dagger}(\boldsymbol{r})\hat{\Psi}_k(\boldsymbol{r}) + \mathrm{H.c.}\right) \tag{C.18}$$

and the external Hamiltonian $\hat{H}_{\mathrm{e}}$ which includes one-body as well as two-body operators. When we transform into the interaction picture with respect to $\hat{H}_{\mathrm{e}}$ and subsequently separate the time-evolution operator according to Eq. (C.13), we arrive at

$$\hat{U}(t,t_{\mathrm{i}}) = \hat{U}_{\mathrm{e}}(t,t_{\mathrm{i}})\mathrm{e}^{-\hat{F}(t)}\hat{U}_{\mathrm{eff}}(t,t_{\mathrm{i}})\mathrm{e}^{\hat{F}(t_{\mathrm{i}})} \tag{C.19}$$

where $\hat{F}$ now solves the differential equation

$$\mathrm{i}\hbar\frac{\mathrm{d}}{\mathrm{d}t}\hat{F} + \hat{H}_{\mathrm{L}}^{\mathrm{e}} = 0 . \tag{C.20}$$

The superscript e denotes the interaction picture with respect to $\hat{H}_{\mathrm{e}}$. Consequently, the effective laser-atom interaction Hamiltonian reads

$$\hat{H}_{\mathrm{eff}}(t) = \sum_{j=1}^{\infty} \frac{j}{(j+1)!} \left[\hat{F}(t), \hat{H}_{\mathrm{L}}^{\mathrm{e}}(t)\right]_j . \tag{C.21}$$

An approximate solution to Eq. (C.20) is obtained by only integrating the rapidly oscillating exponential in Eq. (C.18), that is,

$$\hat{F}(t) = \int \mathrm{d}^3\boldsymbol{r} \left(\sum_{j,k} \frac{\lambda_{jk}(\boldsymbol{r},t)}{\Delta_{jk}}\mathrm{e}^{\mathrm{i}\Delta_{jk}t}\hat{\Psi}_j^{\mathrm{e}\dagger}(\boldsymbol{r},t)\hat{\Psi}_k^{\mathrm{e}}(\boldsymbol{r},t) - \mathrm{H.c.}\right) . \tag{C.22}$$

The quality of this approximation can be estimated by substituting Eq. (C.22) back into Eq. (C.20). This results in three contributions stemming from the time dependence of the exponential, of λ, and of the Heisenberg-picture field operators.

Derivative of the exponential

The derivative of the exponential $\mathrm{e}^{\mathrm{i}\Delta_{jk}t}$ simply removes Δ_{jk} in the denominator and therefore reverses the integration. The approximation, Eq. (C.22), is thus justified if the time derivative of the other terms is much smaller compared to $\hat{H}_{\mathrm{L}}^{\mathrm{e}}$.

Derivative of $\lambda(\boldsymbol{r}, t)$

The time dependence of λ, which oscillates of the order of the laser frequency differences $\Delta\omega$, leads to another contribution. This term thus scales as $\frac{\Delta\omega}{\Delta} \sim 10^{-7}$ when compared to $\hat{H}_{\mathrm{L}}^{\mathrm{e}}$. The rate of change of the overall modulation of the electric field due to the finite pulse length is about the same size.

Derivative of the interaction-picture field operators

The third contribution necessitates slightly more effort. It stems from the external motion of the atom during the laser pulse, i.e. from the derivative of the time-dependence of the field operators in the interaction picture. For the following analysis we approximate

$$\hat{H}_{\mathrm{e}} = \int \mathrm{d}^3 \boldsymbol{r}\, \hat{\Psi}^\dagger(\boldsymbol{r}) \mathcal{H} \hat{\Psi}(\boldsymbol{r}) \tag{C.23}$$

with the one-body Hamiltonian $\hat{\mathcal{H}} = \hat{\boldsymbol{p}}^2/2m + \hat{V}$, that is, we treat the particle-particle interaction as an effective mean-field potential. Recall that λ consists of the sum of terms of the form e^{ikz}. Thus, we obtain

$$\int \mathrm{d}^3 \boldsymbol{r}\, \hat{\Psi}_j^{\mathrm{e}\dagger}(\boldsymbol{r}, t) \mathrm{e}^{ikz} \hat{\Psi}_k^{\mathrm{e}}(\boldsymbol{r}, t) = \int \mathrm{d}^3 \boldsymbol{r}\, \mathrm{d}^3 \boldsymbol{r}' \hat{\Psi}_j^\dagger(\boldsymbol{r}) \langle \boldsymbol{r} | \mathrm{e}^{ik\hat{z}(t)} | \boldsymbol{r}' \rangle \hat{\Psi}_k(\boldsymbol{r}') \tag{C.24}$$

where $\hat{z}(t)$ is the position operator in the Heisenberg picture with respect to Hamiltonian, Eq. (C.23). We estimate its size as

$$z(t) \sim \frac{1}{m} \left[\Delta p + \hbar k + \nabla V(\Delta z) t \right] t \tag{C.25}$$

where $\hbar k$ is the momentum of the particle and Δp as well as Δz denote the momentum and position width of the state. Hence, the rate of change of Eq. (C.24) is of the order of $k \frac{\mathrm{d}}{\mathrm{d}t} z(t) \sim (k \Delta p + \hbar k^2 + k \nabla V(\Delta z) t)/m$. For $k \approx 10^7/\mathrm{m}$, the momentum width of a Bose-Einstein condensate, the gravitational potential $V = mg\hat{z}$ and a laser-interaction time of about $10^{-5}\mathrm{s}$ the rate of change is of the order of $10^4/\mathrm{s}$, therefore many orders of magnitude smaller than Δ. The contribution of the mean-field particle-particle interaction potential can be estimated to be even smaller. (Recall from chapter 2 that the density modulation of a Bose-Einstein condensate in a trap is very smooth and its spatial derivative becomes very small.)

In the discussion above we justified the approximate solution, Eq. (C.22). However, we need to calculate an infinite number of complicated nested commutators in Eq. (C.21). However, as we will show in the following, all commutators of order higher than one can be neglected. Before that, let us disregard the two exponentials $\mathrm{e}^{-\hat{F}(t)}$ and $\mathrm{e}^{\hat{F}(t_\mathrm{i})}$ in Eq. (C.19) since even their largest contribution is of the order of $\lambda/\Delta \ll 1$. Furthermore, we reverse the interaction picture with respect to $\hat{H}_{\mathrm{e}}$. As the approximate integration of Eq. (C.22) has left the interaction-picture field operators unaffected, we simply replace the Heisenberg by the Schrödinger picture field operators. We now compare the sizes of the terms in the expansion, Eq. (C.21). Since we assumed that only states in different manifolds couple, the operators in $\hat{H}_{\mathrm{L}}$ and $\hat{F}$ only contain products of field operators corresponding to different manifolds. As a result the terms in the

commutator $[\hat{F}, \hat{H}]$ oscillate only with a frequency comparable to the energy differences in one manifold. The size of the first-order commutator in the time-evolution operator thus scales as $\frac{\lambda^2}{\Delta} t \sim 1$. We are now left with the task to show that all contributions for $j > 1$ in Eq. (C.21) are negligible compared to the first. Indeed, depending on whether or not the rapidly oscillating terms cancel in the higher-order nested commutators, the jth contribution scales at most as $\frac{\lambda^{j+1}}{\Delta^j} t$. Using $t \sim \frac{\Delta}{\lambda^2}$ we estimate the size of the jth contribution to be smaller than $\left(\frac{\lambda}{\Delta}\right)^{j-1} \ll 1$.

In summary we found a very simple algorithm for the method of adiabatic elimination. Given a laser-atom interaction Hamiltonian, Eq. (C.18) simply define

$$\hat{F}(t) = \int d^3\boldsymbol{r} \left(\sum_{j,k} \frac{\lambda_{jk}(\boldsymbol{r}, t)}{\Delta_{jk}} e^{i\Delta_{jk}t} \hat{\Psi}_j^\dagger(\boldsymbol{r}) \hat{\Psi}_k(\boldsymbol{r}) - \text{H.c.} \right) \qquad (C.26)$$

and replace in

$$\hat{H} = \hat{H}_e + \hat{H}_L \qquad (C.27)$$

the laser-atom interaction Hamiltonian by

$$\hat{H}_L \rightarrow \hat{H}_L^{\text{eff}} = \frac{1}{2} \left[\hat{F}(t), \hat{H}_L(t) \right] . \qquad (C.28)$$

Remarkably, for a given atom-light interaction Hamiltonian we only need to calculate a commutator to obtain the effective coupling scheme. How the effective Hamiltonian arises from the commutator is shown in detail for the case of Bragg, double-Bragg and Raman scattering in Sec. 3.2.3.

C.3. Path-dependent field operators

In this section we state and prove identities needed in Sec. 3.3 and Sec. 3.4. We start with the derivation of matching conditions for the field operators during the laser pulse to eliminate fictitious input ports. After decomposing unity in Sec. C.3.2, we show in Sec. C.3.3 how to include the interaction Hamiltonian into the formalism presented in Sec. 3.3 and Sec. 3.4.

C.3.1. Elimination of the fictitious input ports from the calculation of the phase

In this appendix we derive matching conditions for the field operators. As a consequence the beam splitter will - at least in the delta-pulse approximation - only act on the internal degrees of freedom. After the transformation to the comoving frames, terms like

$$\int d^3\boldsymbol{r}\, \hat{\Psi}_n^\dagger(\boldsymbol{r}) \mathcal{D}_n^\dagger(t_1) e^{i\boldsymbol{k}\boldsymbol{r}} \mathcal{D}_j(t_1) \hat{\Psi}_j(\boldsymbol{r}) e^{i\varphi_L(t_1) - i\phi_n(t_1) + i\phi_j(t_1)} \overset{!}{=} \int d^3\boldsymbol{r}\, \hat{\Psi}_n^\dagger(\boldsymbol{r}) \hat{\Psi}_j(\boldsymbol{r}) \quad (C.29)$$

appear in the laser-atom interaction Hamiltonian for a laser pulse at $t = t_1$, where $\varphi_L(t_1)$ is the laser phase evaluated at t_1 and $\phi_j(t_1)$ and $\phi_n(t_1)$ are the phases accumulated along the interferometer paths. Supposing that $\hat{\Psi}_n(\boldsymbol{r})$ corresponds to a fictitious

input port, the aim of this section is to choose $\boldsymbol{\chi}_n(t_1)$ and $\phi_n(t_1)$ in a way that the equal sign in Eq. (C.29) is correct.

This is easily achieved for the choice

$$\boldsymbol{\chi}_{\mathrm{F}}(t_1) + \boldsymbol{\chi}_j(t_1) - \boldsymbol{\chi}_n(t_1) = 0 \tag{C.30}$$

$$\varphi_{\mathrm{L}}(t_1) - \phi_n(t_1) + \phi_j(t_1) - \frac{1}{2\hbar}\boldsymbol{\chi}_{\mathrm{F}}(t_1)^{\mathrm{T}}\boldsymbol{\mathcal{J}}\boldsymbol{\chi}_j(t_1) = 0 \tag{C.31}$$

by combining the product of the two displacement operators and the exponential $\exp(\mathrm{i}\boldsymbol{k}\hat{\boldsymbol{r}})$ with the help of the composition rule, Eq. (A.10), and we defined $\boldsymbol{\chi}_{\mathrm{F}}(t_1) = (0, \hbar\boldsymbol{k})^{\mathrm{T}}$. For $t > t_1$ the phase of the field operator corresponding to the fictitious input port is thus calculated with the help of Eq. (3.64)

$$\phi_n(t) = \phi_n(t_1) + \frac{1}{\hbar}\int_{t_1}^{t}\mathrm{d}t'\,\mathscr{L}_n(t') - \frac{1}{2\hbar}\left[\boldsymbol{\chi}_n^p(t)\boldsymbol{\chi}_n^r(t) - \boldsymbol{\chi}_n^p(t_1)\boldsymbol{\chi}_n^r(t_1)\right]$$

$$= \varphi_{\mathrm{L}}(t_1) + \frac{1}{\hbar}\int_{t_i}^{t_1}\mathrm{d}t'\,\mathscr{L}_j(t') + \frac{1}{\hbar}\int_{t_1}^{t}\mathrm{d}t'\,\mathscr{L}_n(t')$$

$$- \frac{1}{2\hbar}\left[\boldsymbol{\chi}_n^p(t)\boldsymbol{\chi}_n^r(t) - \boldsymbol{\chi}_j^p(t_i)\boldsymbol{\chi}_j^r(t_i)\right]$$

$$+ \frac{1}{2\hbar}\left[\boldsymbol{\chi}_n^p(t_1)\boldsymbol{\chi}_n^r(t_1) - \boldsymbol{\chi}_j^p(t_1)\boldsymbol{\chi}_j^r(t_1) - \boldsymbol{\chi}_{\mathrm{F}}(t_1)^{\mathrm{T}}\boldsymbol{\mathcal{J}}\boldsymbol{\chi}_j(t_1)\right] . \tag{C.32}$$

When we recall that $\boldsymbol{\chi}_{\mathrm{F}}^p = \hbar\boldsymbol{k}$ and $\boldsymbol{\chi}_{\mathrm{F}}^r = 0$, the last line in Eq. (C.32) becomes

$$\boldsymbol{\chi}_n^p(t_1)\boldsymbol{\chi}_n^r(t_1) - \boldsymbol{\chi}_j^p(t_1)\boldsymbol{\chi}_j^r(t_1) - \boldsymbol{\chi}_{\mathrm{F}}(t_1)^{\mathrm{T}}\boldsymbol{\mathcal{J}}\boldsymbol{\chi}_j(t_1) = 2\hbar\boldsymbol{k}\boldsymbol{\chi}_j^r(t_1) \tag{C.33}$$

by using again the matching condition, Eq. (C.30). Thus, we arrive at the rather simple expression

$$\phi_n(t) = \varphi_{\mathrm{L}}(t_1) + \frac{1}{\hbar}\int_{t_i}^{t}\mathrm{d}t'\,\overline{\mathscr{L}}_n(t') - \frac{1}{2\hbar}\left[\overline{\boldsymbol{\chi}}_n^p(t)\overline{\boldsymbol{\chi}}_n^r(t) - \boldsymbol{\chi}_j^p(t_i)\boldsymbol{\chi}_j^r(t_i)\right] . \tag{C.34}$$

The Lagrange function in Eq. (C.34) is

$$\overline{\mathscr{L}}_n(t) = \hbar\boldsymbol{k}\boldsymbol{\chi}_j^r(t)\delta(t - t_1) + \begin{cases} \mathscr{L}_j(t) & \text{for} \quad t_i \leq t < t_1 \\ \mathscr{L}_n(t) & \text{for} \quad t_1 \leq t \end{cases} \tag{C.35}$$

and

$$\overline{\boldsymbol{\chi}}_n(t) = \begin{cases} \boldsymbol{\chi}_j(t) & \text{for} \quad t_i \leq t \leq t_1 \\ \boldsymbol{\chi}_n(t) & \text{for} \quad t_1 < t \end{cases} . \tag{C.36}$$

The meaning of this remarkable result is the following: By choosing the initial phase $\phi_n(t_i)$ appropriately, the phase assigned to a field operator introduced at a fictitious input port is simply given by the phase accumulated along the actual physical path of the interferometer. At the laser pulse we need to collect the laser phase $\varphi_{\mathrm{L}}(t_1)$ with positive sign if the momentum transfer is positive. As shown in Fig. 3.5.a) a laser pulse populates many paths and one should consider also nonresonant paths. These fictitious input ports only couple to other fictitious paths. Thus, when taking into account higher-order paths, one needs to recursively repeat the path- and phase matching. The calculation above is then easily generalized. For a fictitious input port corresponding to a transfer between paths separated by $l\hbar\boldsymbol{k}$, the field operator collects l times the laser phase in Eq. (C.34) and $\hbar\boldsymbol{k} \rightarrow l\hbar\boldsymbol{k}$ in Eq. (C.35).

C.3.2. Properties of $\hat{\Pi}$

In this section we show how to represent unity as sum over products of position and momentum projectors. To this end, we decompose phase space into 6-dimensional boxes $\Omega_j = \Omega_{j_r}^r \times \Omega_{j_p}^p$ with the double index $j = (j_r, j_p)$. The displacement to the center of each box is determined by the phase-space vector $\boldsymbol{\chi}_j$. We now define the operator

$$\hat{\Pi} = \int_{\Omega_0^r} \mathrm{d}^3\boldsymbol{r}\, |\boldsymbol{r}\rangle\langle\boldsymbol{r}| \int_{\Omega_0^p} \mathrm{d}^3\boldsymbol{p}\, |\boldsymbol{p}\rangle\langle\boldsymbol{p}| \tag{C.37}$$

where Ω_0 is the set around the origin. Recognizing that

$$\begin{aligned}
\hat{D}_j \hat{\Pi} \hat{D}_j^\dagger &= \int_{\Omega_0^r} \mathrm{d}^3\boldsymbol{r}\, \hat{D}_j|\boldsymbol{r}\rangle\langle\boldsymbol{r}|\hat{D}_j^\dagger \int_{\Omega_0^p} \mathrm{d}^3\boldsymbol{p}\, \hat{D}_j|\boldsymbol{p}\rangle\langle\boldsymbol{p}|\hat{D}_j^\dagger \\
&= \int_{\Omega_0^r} \mathrm{d}^3\boldsymbol{r}\, |\boldsymbol{r} + \boldsymbol{\chi}_j^r\rangle\langle\boldsymbol{r} + \boldsymbol{\chi}_j^r| \int_{\Omega_0^p} \mathrm{d}^3\boldsymbol{p}\, |\boldsymbol{p} + \boldsymbol{\chi}_j^p\rangle\langle\boldsymbol{p} + \boldsymbol{\chi}_j^p|,
\end{aligned} \tag{C.38}$$

where we employed Eqs. (A.5) and (A.6), we find the decomposition of unity

$$\begin{aligned}
\sum_j \hat{D}_j \hat{\Pi} \hat{D}_j^\dagger &= \int_{\Omega_0^r} \mathrm{d}^3\boldsymbol{r} \sum_j |\boldsymbol{r} + \boldsymbol{\chi}_{j_r}^r\rangle\langle\boldsymbol{r} + \boldsymbol{\chi}_{j_r}^r| \int_{\Omega_0^p} \mathrm{d}^3\boldsymbol{p}|\boldsymbol{p} + \boldsymbol{\chi}_{j_p}^p\rangle\langle\boldsymbol{p} + \boldsymbol{\chi}_{j_p}^p| \\
&= \sum_j \int_{\Omega_{j_r}^r} \mathrm{d}^3\boldsymbol{r}|\boldsymbol{r}\rangle\langle\boldsymbol{r}| \int_{\Omega_{j_p}^p} \mathrm{d}^3\boldsymbol{p}|\boldsymbol{p}\rangle\langle\boldsymbol{p}| \\
&= 1\,.
\end{aligned} \tag{C.39}$$

This result is intuitively clear. The operator $\hat{\Pi}$ is simply the product of the unity operator expressed in momentum and position eigenstates for the subset of states with support on Ω_0. The unity for the full Hilbert space is then composed by the sum over all unity operators for states with support on Ω_j.

C.3.3. Simplifying the interaction Hamiltonian

In this appendix we investigate for which conditions we can extend the path-dependent interferometer formalism to particle-particle interaction. By applying Eq. (3.59), we need to replace

$$\hat{\Psi}(\boldsymbol{r}) \to \hat{U}_\mathcal{D}^\dagger \hat{\Psi}(\boldsymbol{r}) \hat{U}_\mathcal{D} = \sum_j \mathrm{e}^{\mathrm{i}\phi_j(t)} \mathcal{D}_j(t) \hat{\Psi}_j(\boldsymbol{r}) \tag{C.40}$$

in the interaction Hamiltonian, Eq. (3.17), for Bragg scattering

$$\hat{H}_\mathrm{I} = \frac{g}{2} \int \mathrm{d}^3\boldsymbol{r}\, \hat{\Psi}^\dagger(\boldsymbol{r})\hat{\Psi}^\dagger(\boldsymbol{r})\hat{\Psi}(\boldsymbol{r})\hat{\Psi}(\boldsymbol{r})\,. \tag{C.41}$$

Using Eq. (3.90), the equation of motion for the field operator $\hat{\Psi}_j(\boldsymbol{r})$ with respect to this Hamiltonian is obtained as

$$\mathrm{i}\hbar\frac{\mathrm{d}}{\mathrm{d}t}\hat{\Psi}_j(\boldsymbol{r},t) = g \sum_{n,m,l,k} \int \mathrm{d}^3\boldsymbol{r}'\, \delta_{jn}^\Omega(\boldsymbol{r} - \boldsymbol{r}')\hat{A}_{nmlk}(\boldsymbol{r}',t) \tag{C.42}$$

where

$$\hat{A}_{nmlk}(\boldsymbol{r}, t) \sim \mathrm{e}^{\mathrm{i}\phi_{nmlk}(t)} \left[\mathcal{D}_n^\dagger(t)\mathcal{D}_m(t)\hat{\Psi}_m(\boldsymbol{r}, t) \right]^\dagger \left[\mathcal{D}_n^\dagger(t)\mathcal{D}_l(t)\hat{\Psi}_l(\boldsymbol{r}, t) \right] \left[\mathcal{D}_n^\dagger(t)\mathcal{D}_k(t)\hat{\Psi}_k(\boldsymbol{r}, t) \right] , \tag{C.43}$$

and the phase is

$$\phi_{nmlk}(t) = \phi_l(t) + \phi_k(t) - \phi_n(t) - \phi_m(t) . \tag{C.44}$$

In the following we show that for a given choice (n, m, l, k) of indices, $\hat{A}_{nmlk}$ either has support on Ω_0 or on its complement. The convolution with δ_{jn}^Ω then exactly selects those indices corresponding to support on Ω_0. Recall again that we implicitly mean by 'position- and momentum distribution of a field' the expectation values, Eq. (3.86), with respect to the quantum state of the system.

For position space the argument is simple. Most of the time there is no overlap between the field operators due to the time-dependent relative displacement. During periods with nonvanishing overlap, $\hat{A}_{nmlk}$ either has support on Ω_0^r or on its complement if each field operator has support on Ω_0^r. The convolution with the incomplete delta function in Eq. (C.42) then only selects those tuples of indices (n, m, l, k) corresponding to support on Ω_0^r.

A similar argument holds for momentum space. Let us rewrite Eq. (C.43) as

$$\hat{A}_{nmlk}(\boldsymbol{r}, t) \sim \frac{1}{(2\pi\hbar)^{\frac{9}{2}}} \mathrm{e}^{\frac{\mathrm{i}}{\hbar}\Delta\boldsymbol{\chi}_{nmlk}^p(t)\boldsymbol{r}} \int \mathrm{d}^3\boldsymbol{p}_1 \mathrm{d}^3\boldsymbol{p}_2 \mathrm{d}^3\boldsymbol{p}_3 \, \mathrm{e}^{\mathrm{i}(\boldsymbol{p}_2+\boldsymbol{p}_3-\boldsymbol{p}_1)\boldsymbol{r}/\hbar} \, \hat{\Psi}_m^\dagger(\boldsymbol{p}_1, t)\hat{\Psi}_l(\boldsymbol{p}_2, t)\hat{\Psi}_k(\boldsymbol{p}_3, t) \tag{C.45}$$

where we defined

$$\Delta\boldsymbol{\chi}_{nmlk}^p(t) = \boldsymbol{\chi}_l^p(t) + \boldsymbol{\chi}_k^p(t) - \boldsymbol{\chi}_n^p(t) - \boldsymbol{\chi}_m^p(t) \tag{C.46}$$

and disregarded phase factors which are not important for this discussion. Next, we calculate the momentum distribution of $\hat{A}$ by a Fourier transformation as

$$\hat{A}_{nmlk}(\boldsymbol{p}, t) = \frac{1}{(2\pi\hbar)^3} \int \mathrm{d}^3\boldsymbol{p}_1 \mathrm{d}^3\boldsymbol{p}_2 \, \hat{\Psi}_m^\dagger(\boldsymbol{p}_1, t)\hat{\Psi}_l(\boldsymbol{p}_2, t)\hat{\Psi}_k(\boldsymbol{p}_1 - \boldsymbol{p}_2 - \Delta\boldsymbol{\chi}_{nmlk}^p(t) + \boldsymbol{p}, t) . \tag{C.47}$$

First we note that this expression is only different from zero for the indices with

$$\Delta\boldsymbol{\chi}_{nmlk}^p(t) \cong 0 \tag{C.48}$$

because otherwise the overlap in momentum space is zero. But due to the convolution integrals the momentum distribution is three times as wide as the one of each field [206]. In order to guarantee that $\hat{A}$ has support on Ω_0 for those indices satisfying Eq. (C.48) and vanishes otherwise, we additionally need to require that each field has support in momentum space on only a third of the width of Ω_0. This argument provides us with the condition

$$3\Delta p + |\Delta\boldsymbol{\chi}_{nmlk}^p| \ll \hbar k \tag{C.49}$$

where Δp is the width of the momentum distribution of a field operator and $\hbar k$ is the size of the momentum box. If true, $\hat{A}_{nmlk}$ remains supported on Ω_0^p.

The equation of motion with respect to the interaction Hamiltonian then reads

$$
\begin{aligned}
i\hbar\frac{\mathrm{d}}{\mathrm{d}t}\hat{\Psi}_j(\boldsymbol{r},t) =& g\sum_{\mathrm{coupl.}} e^{i\phi_{jmlk}(t)} \left[\mathcal{D}_j^\dagger(t)\mathcal{D}_m(t)\hat{\Psi}_m(\boldsymbol{r},t)\right]^\dagger \\
&\times \left[\mathcal{D}_j^\dagger(t)\mathcal{D}_l(t)\hat{\Psi}_l(\boldsymbol{r},t)\right]\left[\mathcal{D}_j^\dagger(t)\mathcal{D}_k(t)\hat{\Psi}_k(\boldsymbol{r},t)\right]
\end{aligned} \tag{C.50}
$$

where the coupled indices are defined by the condition

$$
\Delta\boldsymbol{\chi}_{jmlk}^p(t) \cong 0\,. \tag{C.51}
$$

In conclusion we showed that the path-dependent formalism for field operators is also capable of including interactions when the additional constraints on the momentum widths of the states are satisfied.

Appendix D

Sensitivity and two-mode squeezing

In this appendix we quote the results of Refs. [214, 220], which are needed for the calculations in chapter 4.

D.1. Transformation of angular momentum operators

We start by summarizing the transformations of the angular momentum operators with respect to the beam splitters

$$\hat{S}^i_\theta = \exp\left\{-\mathrm{i}\theta\hat{L}_i\right\}. \tag{D.1}$$

In Ref. [214] these are calculated as

$$\hat{S}^{x\dagger}_\theta \hat{L}_x \hat{S}^x_\theta = \hat{L}_x \tag{D.2}$$

$$\hat{S}^{x\dagger}_\theta \hat{L}_y \hat{S}^x_\theta = \cos(\theta)\hat{L}_y - \sin(\theta)\hat{L}_z \tag{D.3}$$

$$\hat{S}^{x\dagger}_\theta \hat{L}_z \hat{S}^x_\theta = \sin(\theta)\hat{L}_y + \cos(\theta)\hat{L}_z \tag{D.4}$$

$$\hat{S}^{y\dagger}_\theta \hat{L}_x \hat{S}^y_\theta = \cos(\theta)\hat{L}_x + \sin(\theta)\hat{L}_z \tag{D.5}$$

$$\hat{S}^{y\dagger}_\theta \hat{L}_y \hat{S}^y_\theta = \hat{L}_y \tag{D.6}$$

$$\hat{S}^{y\dagger}_\theta \hat{L}_z \hat{S}^y_\theta = -\sin(\theta)\hat{L}_x + \cos(\theta)\hat{L}_z \tag{D.7}$$

$$\hat{S}^{z\dagger}_\theta \hat{L}_x \hat{S}^z_\theta = \cos(\theta)\hat{L}_x - \sin(\theta)\hat{L}_y \tag{D.8}$$

$$\hat{S}^{z\dagger}_\theta \hat{L}_y \hat{S}^z_\theta = \sin(\theta)\hat{L}_x + \cos(\theta)\hat{L}_y \tag{D.9}$$

$$\hat{S}^{z\dagger}_\theta \hat{L}_z \hat{S}^z_\theta = \hat{L}_z. \tag{D.10}$$

These expressions are simply rotations and can equally be expressed in terms of rotation matrices [214].

D.2. Expectation values with respect to the squeezed state

In this section we provide the first and second moments of the angular momentum operators calculated with respect to

$$|\psi\rangle = \hat{S}_{\mathrm{sq}}(\xi)\,\hat{S}^x_{-\pi/2}\,|j,j\rangle\;. \tag{D.11}$$

Initially all particles occupy the ground state, which is subsequently rotated about the x axis and then subjected to the squeezing operator with parameter ξ. This results in [220]

$$\langle \hat{L}_x \rangle = 0 \tag{D.12}$$

$$\langle \hat{L}_y \rangle = \frac{N}{2}\cos\left(2\,\xi\right)^{N-1} \tag{D.13}$$

$$\langle \hat{L}_z \rangle = 0 \tag{D.14}$$

$$\Delta\hat{L}_x^2 = \frac{N}{8}(N+1) - \frac{N}{8}(N-1)\cos\left(4\,\xi\right)^{N-2} \tag{D.15}$$

$$\Delta\hat{L}_y^2 = \frac{N}{8}(N+1) + \frac{N}{8}(N-1)\cos\left(4\,\xi\right)^{N-2} - \frac{N^2}{4}\cos\left(2\,\xi\right)^{2N-2} \tag{D.16}$$

$$\Delta\hat{L}_z^2 = \frac{N}{4} \tag{D.17}$$

$$\langle \hat{L}_x\hat{L}_y + \hat{L}_y\hat{L}_x \rangle = 0 \tag{D.18}$$

$$\langle \hat{L}_x\hat{L}_z + \hat{L}_z\hat{L}_x \rangle = -\frac{N}{2}(N-1)\sin(2\xi)\cos(2\xi)^{N-2} \tag{D.19}$$

$$\langle \hat{L}_y\hat{L}_z + \hat{L}_z\hat{L}_y \rangle = 0\,. \tag{D.20}$$

These expressions are used in Sec. 4.2 to show how phase diffusion derogates the interferometer phase.

Bibliography

[1] L. de Broglie, *Waves and quanta*, Nature **112**, 540 (1923).

[2] A. Einstein, *Die Feldgleichungen der Gravitation*, Sitzungsberichte der Preussischen Akademie der Wissenschaften, 844 (1915).

[3] C. Davisson and L. H. Germer, *Diffraction of electrons by a crystal of nickel*, Phys. Rev. **30**, 705 (1927).

[4] I. Estermann and O. Stern, *Beugung von Molekularstrahlen*, Z. Phys. **61**, 95 (1930).

[5] D. P. Mitchell and P. N. Powers, *Bragg reflection of slow neutrons*, Phys. Rev. **50**, 486 (1936).

[6] H. Rauch, W. Treimer, and U. Bonse, *Test of a single crystal neutron interferometer*, Phys. Lett. **47**, 369 (1974).

[7] R. Colella, A. W. Overhauser, and S. A. Werner, *Observation of gravitationally induced quantum interference*, Phys. Rev. Lett. **34**, 1472 (1975).

[8] S. A. Werner, J. Staudenmann, and R. Colella, *Effect of Earth's rotation on the quantum mechanical phase of the neutron*, Phys. Rev. Lett. **42**, 1103 (1979).

[9] D. M. Greenberger, *The neutron interferometer as a device for illustrating the strange behavior of quantum systems*, Rev. Mod. Phys. **55**, 875 (1983).

[10] J. F. Clauser, *Ultra-high sensitivity accelerometers and gyroscopes using neutral atom matter-wave interferometry*, Physica B **151**, 262 (1988).

[11] O. Carnal and J. Mlynek, *Young's double-slit experiment with atoms: A simple atom interferometer*, Phys. Rev. Lett. **66**, 2689 (1991).

[12] C. Bordé, *Atomic interferometry with internal state labelling*, Phys. Lett. A **140**, 10 (1989).

[13] F. Riehle, T. Kisters, A. Witte, J. Helmcke, et al., *Optical Ramsey spectroscopy in a rotating frame: Sagnac effect in a matter-wave interferometer*, Phys. Rev. Lett. **67**, 177 (1991).

[14] M. Kasevich and S. Chu, *Atomic interferometry using stimulated Raman transitions*, Phys. Rev. Lett. **67**, 181 (1991).

[15] P. Berman, *Atom interferometry*, 1st ed. (Academic Press, San Diego, 1997).

[16] A. D. Cronin, J. Schmiedmayer, and D. E. Pritchard, *Optics and interferometry with atoms and molecules*, Rev. Mod. Phys. **81**, 1051 (2009).

[17] P. L. Gould, G. A. Ruff, and D. E. Pritchard, *Diffraction of atoms by light: The near-resonant Kapitza-Dirac effect*, Phys. Rev. Lett. **56**, 827 (1986).

[18] P. Martin, B. Oldaker, A. Miklich, and D. Pritchard, *Bragg scattering of atoms from a standing light wave*, Phys. Rev. Lett. **60**, 515 (1988).

[19] M. Kozuma, L. Deng, E. W. Hagley, J. Wen, et al., *Coherent splitting of Bose-Einstein condensed atoms with optically induced Bragg diffraction*, Phys. Rev. Lett. **82**, 871 (1999).

[20] Y. Torii, Y. Suzuki, M. Kozuma, T. Sugiura, et al., *Mach-Zehnder Bragg interferometer for a Bose-Einstein condensate*, Phys. Rev. A **61**, 041602 (2000).

[21] E. Giese, A. Roura, G. Tackmann, E. M. Rasel, et al., *Double Bragg diffraction: A tool for atom optics*, Phys. Rev. A **88**, 053608 (2013).

[22] T. L. Gustavson, P. Bouyer, and M. A. Kasevich, *Precision rotation measurements with an atom interferometer gyroscope*, Phys. Rev. Lett. **78**, 2046 (1997).

[23] B. Canuel, F. Leduc, D. Holleville, A. Gauguet, et al., *Six-axis inertial sensor using cold-atom interferometry*, Phys. Rev. Lett. **97**, 010402 (2006).

[24] P. Berg, S. Abend, G. Tackmann, C. Schubert, et al., *Composite-light-pulse technique for high-precision atom interferometry*, Phys. Rev. Lett. **114**, 063002 (2015).

[25] A. Peters, K. Y. Chung, and S. Chu, *Measurement of gravitational acceleration by dropping atoms*, Nature **400**, 849 (1999).

[26] J. E. Debs, P. A. Altin, T. H. Barter, D. Döring, et al., *Cold-atom gravimetry with a Bose-Einstein condensate*, Phys. Rev. A **84**, 033610 (2011).

[27] P. A. Altin, M. T. Johnsson, V. Negnevitsky, G. R. Dennis, et al., *Precision atomic gravimeter based on Bragg diffraction*, New J. Phys. **15**, 023009 (2013).

[28] T. Farah, C. Guerlin, A. Landragin, P. Bouyer, et al., *Underground operation at best sensitivity of the mobile LNE-SYRTE cold atom gravimeter*, Gyroscopy and Navigation **5**, 266 (2014).

[29] S. M. Dickerson, J. M. Hogan, A. Sugarbaker, D. M. S. Johnson, et al., *Multiaxis inertial sensing with long-time point source atom interferometry*, Phys. Rev. Lett. **111**, 083001 (2013).

[30] M. Hauth, C. Freier, V. Schkolnik, A. Senger, et al., *First gravity measurements using the mobile atom interferometer GAIN*, Appl. Phys. B **113**, 49 (2013).

[31] M. Snadden, J. McGuirk, P. Bouyer, K. Haritos, et al., *Measurement of the Earth's gravity gradient with an atom interferometer-based gravity gradiometer*, Phys. Rev. Lett. **81**, 971 (1998).

[32] O. Carraz, C. Siemes, L. Massotti, R. Haagmans, et al., *A spaceborne gravity gradiometer concept based on cold atom interferometers for measuring Earth's gravity field*, Microgravity Sci. Technol. **26**, 139 (2014).

[33] G. W. Biedermann, X. Wu, L. Deslauriers, S. Roy, et al., *Testing gravity with cold-atom interferometers*, Phys. Rev. A **91**, 033629 (2015).

[34] P. Asenbaum, C. Overstreet, T. Kovachy, D. D. Brown, et al., *Phase shift in an atom interferometer due to spacetime curvature across its wave function*, Phys. Rev. Lett. **118**, 183602 (2017).

[35] A. Bertoldi, G. Lamporesi, L. Cacciapuoti, M. de Angelis, et al., *Atom interferometry gravity-gradiometer for the determination of the Newtonian gravitational constant G*, Eur. Phys. J. D **40**, 271 (2006).

[36] J. B. Fixler, G. T. Foster, J. M. McGuirk, and M. A. Kasevich, *Atom interferometer measurement of the Newtonian constant of gravity*, Science **315**, 74 (2007).

[37] G. Lamporesi, A. Bertoldi, L. Cacciapuoti, M. Prevedelli, et al., *Determination of the Newtonian gravitational constant using atom interferometry*, Phys. Rev. Lett. **100**, 050801 (2008).

[38] G. Rosi, F. Sorrentino, L. Cacciapuoti, M. Prevedelli, et al., *Precision measurement of the Newtonian gravitational constant using cold atoms*, Nature **510**, 518 (2014).

[39] A. Wicht, J. M. Hensley, E. Sarajlic, and S. Chu, *A preliminary measurement of the fine-structure constant based on atom interferometry*, Phys. Scr. **102**, 82 (2002).

[40] R. Bouchendira, P. Cladé, S. Guellati-Khélifa, F. Nez, et al., *New determination of the fine-structure constant and test of the quantum electrodynamics*, Phys. Rev. Lett. **106**, 080801 (2011).

[41] R. Bouchendira, P. Cladé, S. Guellati-Khélifa, F. Nez, et al., *State of the art in the determination of the fine structure constant: Test of quantum electrodynamics and determination of $\hbar/M$*, Ann. Phys. **525**, 484 (2013).

[42] R. H. Parker, C. Yu, W. Zhong, B. Estey, et al., *Measurement of the fine-structure constant as a test of the standard model*, Science **360**, 191 (2018).

[43] E. Di Casola, S. Liberati, and S. Sonego, *Nonequivalence of equivalence principles*, Am. J. Phys. **83**, 39 (2015).

[44] D. Giulini, "Equivalence principle, quantum mechanics, and atom-interferometric tests", in *Quantum field theory and gravity: Conceptual and mathematical advances in the search for a unified framework*, edited by F. Finster, O. Müller, M. Nardmann, J. Tolksdorf, et al. (Springer Basel, Basel, 2012), p. 345.

[45] M. A. Hohensee, H. Müller, and R. B. Wiringa, *Equivalence principle and bound kinetic energy*, Phys. Rev. Lett. **111**, 151102 (2013).

[46] R. v. Eötvös, D. Pekár, and E. Fekete, *Beiträge zum Gesetze der Proportionalität von Trägheit und Gravität*, Ann. Phys. (Berl.) **373**, 11 (1922).

[47] S. Schlamminger, K.-Y. Choi, T. A. Wagner, J. H. Gundlach, et al., *Test of the equivalence principle using a rotating torsion balance*, Phys. Rev. Lett. **100**, 041101 (2008).

[48] J. G. Williams, S. G. Turyshev, and D. H. Boggs, *Progress in lunar laser ranging tests of relativistic gravity*, Phys. Rev. Lett. **93**, 261101 (2004).

[49] P. Touboul, G. Métris, M. Rodrigues, Y. André, et al., *MICROSCOPE Mission: First results of a space test of the equivalence principle*, Phys. Rev. Lett. **119**, 231101 (2017).

[50] F. Sorrentino, Q. Bodart, L. Cacciapuoti, Y.-H. Lien, et al., *Sensitivity limits of a Raman atom interferometer as a gravity gradiometer*, Phys. Rev. A **89**, 023607 (2014).

[51] J. M. McGuirk, G. T. Foster, J. B. Fixler, M. J. Snadden, et al., *Sensitive absolute-gravity gradiometry using atom interferometry*, Phys. Rev. A **65**, 033608 (2002).

[52] S. Fray, C. A. Diez, T. W. Hänsch, and M. Weitz, *Atomic interferometer with amplitude gratings of light and its applications to atom based tests of the equivalence principle*, Phys. Rev. Lett. **93**, 240404 (2004).

[53] A. Bonnin, N. Zahzam, Y. Bidel, and A. Bresson, *Simultaneous dual-species matter-wave accelerometer*, Phys. Rev. A **88**, 043615 (2013).

[54] L. Zhou, S. Long, B. Tang, X. Chen, et al., *Test of equivalence principle at 10^{-8} level by a dual-species double-diffraction Raman atom interferometer*, Phys. Rev. Lett. **115**, 013004 (2015).

[55] A. Bonnin, N. Zahzam, Y. Bidel, and A. Bresson, *Characterization of a simultaneous dual-species atom interferometer for a quantum test of the weak equivalence principle*, Phys. Rev. A. **92**, 023626 (2015).

[56] D. Schlippert, J. Hartwig, H. Albers, L. L. Richardson, et al., *Quantum test of the universality of free fall*, Phys. Rev. Lett. **112**, 203002 (2014).

[57] M. G. Tarallo, T. Mazzoni, N. Poli, D. V. Sutyrin, et al., *Test of Einstein equivalence principle for 0-spin and half-integer-spin atoms: Search for spin-gravity coupling effects*, Phys. Rev. Lett **113**, 023005 (2014).

[58] H. Müller, S.-w. Chiow, Q. Long, S. Herrmann, et al., *Atom interferometer with up to 24-photon-momentum-transfer beam splitters*, Phys. Rev. Lett. **100**, 180405 (2008).

[59] P. Cladé, S. Guellati-Khélifa, F. Nez, and F. Biraben, *Large momentum beam splitter using Bloch oscillations*, Phys. Rev. Lett. **102**, 240402 (2009).

[60] S.-w. Chiow, T. Kovachy, H.-C. Chien, and M. A. Kasevich, *$102\hbar k$ large area atom interferometers*, Phys. Rev. Lett. **107**, 130403 (2011).

[61] D. M. Greenberger, *Inadequacy of the usual Galilean transformation in quantum mechanics*, Phys. Rev. Lett **87**, 100405 (2001).

[62] J. Rudolph, W. Herr, C. Grzeschik, T. Sternke, et al., *A high-flux BEC source for mobile atom interferometers*, New J. Phys. **17**, 065001 (2015).

[63] S. Abend, M. Gebbe, M. Gersemann, H. Ahlers, et al., *Atom-chip fountain gravimeter*, Phys. Rev. Lett. **117**, 203003 (2016).

[64] *Der Fallturm Bremen*, `https://www.zarm.uni-bremen.de/fileadmin/user_upload/drop_tower/ZARM-Broschuere_Fallturm.pdf` (visited on 03/20/2019).

[65] R. Geiger, V. Ménoret, G. Stern, N. Zahzam, et al., *Detecting inertial effects with airborne matter-wave interferometry*, Nat. Commun. **2**, 1 (2011).

[66] T. van Zoest, N. Gaaloul, Y. Singh, H. Ahlers, et al., *Bose-Einstein condensation in microgravity*, Science **328**, 1540 (2010).

[67] H. Müntinga, H. Ahlers, M. Krutzik, A. Wenzlawski, et al., *Interferometry with Bose-Einstein condensates in microgravity*, Phys. Rev. Lett. **110**, 093602 (2013).

[68] D. Becker, M. D. Lachmann, S. T. Seidel, H. Ahlers, et al., *Space-borne Bose–Einstein condensation for precision interferometry*, Nature **562**, 391 (2018).

[69] J. Williams, S.-w. Chiow, N. Yu, and H. Müller, *Quantum test of the equivalence principle and space-time aboard the International Space Station*, New J. Phys. **18**, 025018 (2016).

[70] Cold atom lab, NASA, `https://coldatomlab.jpl.nasa.gov/` (visited on 02/20/2019).

[71] G. Tino, F. Sorrentino, D. Aguilera, B. Battelier, et al., *Precision gravity tests with atom interferometry in space*, Nucl. Phys. B **243**, 203 (2013).

[72] D. N. Aguilera, H. Ahlers, B. Battelier, A. Bawamia, et al., *STE-QUEST—test of the universality of free fall using cold atom interferometry*, Class. Quantum Grav. **31**, 159502 (2014).

[73] S. Chu, J. E. Bjorkholm, A. Ashkin, J. P. Gordon, et al., *Proposal for optically cooling atoms to temperatures of the order of 10^{-6} K*, Opt. Lett. **11**, 73 (1986).

[74] H. Ammann and N. Christensen, *Delta-kick cooling: A new method for cooling atoms*, Phys. Rev. Lett. **78**, 2088 (1997).

[75] A. J. Leggett and F. Sols, *On the concept of spontaneously broken gauge symmetry in condensed matter physics*, Found. Phys. **21**, 353 (1991).

[76] J. Javanainen and M. Wilkens, *Phase and phase diffusion of a split Bose-Einstein condensate*, Phys. Rev. Lett. **78**, 4675 (1997).

[77] P. Storey and C. Cohen-Tannoudji, *The Feynman path integral approach to atomic interferometry. A tutorial*, J. Phys. II France **4**, 1999 (1994).

[78] A. Peters, K. Y. Chung, and S. Chu, *High-precision gravity measurements using atom interferometry*, Metrologia **38**, 25 (2001).

[79] P. Wolf and P. Tourrenc, *Gravimetry using atom interferometers: Some systematic effects*, Phys. Lett. A **251**, 241 (1999).

[80] K. Bongs, R. Launay, and M. Kasevich, *High-order inertial phase shifts for time-domain atom interferometers*, Appl. Phys. B **84**, 599 (2006).

[81] C. Antoine and C. J. Bordé, *Quantum theory of atomic clocks and gravito-inertial sensors: An update*, J. Opt. B **5**, 199 (2003).

[82] C. J. Bordé, *Atomic clocks and inertial sensors*, Metrologia **39**, 435 (2002).

[83] C. J. Bordé, *Theoretical tools for atom optics and interferometry*, C. R. Acad. Sci. Paris **2**, 509 (2001).

[84]   C. Antoine and C. Bordé, *Exact phase shifts for atom interferometry*, Phys. Lett. A **306**, 277 (2003).

[85]   W. P. Schleich, D. M. Greenberger, and E. M. Rasel, *A representation-free description of the Kasevich–Chu interferometer: A resolution of the redshift controversy*, New J. Phys. **15**, 013007 (2013).

[86]   S. Kleinert, E. Kajari, A. Roura, and W. P. Schleich, *Representation-free description of light-pulse atom interferometry including non-inertial effects*, Phys. Rep. **605**, 1 (2015).

[87]   J. M. Hogan, D. Johnson, and M. A. Kasevich, *Light-pulse atom interferometry*, arXiv, atom–ph/0806.3261 (2008).

[88]   A. Roura, W. Zeller, and W. P. Schleich, *Overcoming loss of contrast in atom interferometry due to gravity gradients*, New J. Phys. **16**, 123012 (2014).

[89]   W. Zeller, *The impact of wave-packet dynamics in long-time atom interferometry*, Ph.D. thesis, Universität Ulm (2016).

[90]   A. Roura, *Gravitational redshift in quantum-clock interferometry*, arXiv, atom–ph/1810.06744 (2018).

[91]   E. Giese, S. Kleinert, M. Meister, V. Tamma, et al., "The interface of gravity and quantum mechanics illuminated by Wigner phase space", in *Atom interferometry, Proceedings of the International School of Physics*, 188th ed. (Italian Physical Society, IOS Press, 2014), p. 171.

[92]   W. Magnus, *On the exponential solution of differential equations for a linear operator*, Commun. Pure Appl. Math **7**, 649 (1954).

[93]   M. Scully and M. Zubairy, *Quantum optics*, 1st ed. (Cambridge University Press, Cambridge, 1997).

[94]   K. Moler, D. S. Weiss, M. Kasevich, and S. Chu, *Theoretical analysis of velocity-selective Raman transitions*, Phys. Rev. A **45**, 342 (1992).

[95]   A. Peters, *High precision gravity measurements using atom interferometry*, Ph.D. thesis, Stanford University (1998).

[96]   C. Antoine, *Matter wave beam splitters in gravito-inertial and trapping potentials: Generalized ttt scheme for atom interferometry*, Appl. Phys. B **84**, 585 (2006).

[97]   C. Antoine, *Rotating matter-wave beam splitters and consequences for atom gyrometers*, Phys. Rev. A **76**, 033609 (2007).

[98]   M. A. H. M. Jansen and K. A. H. van Leeuwen, *Initial wavefunction dependence on atom interferometry phases*, Appl. Phys. B **93**, 389 (2008).

[99]   R. Stoner, D. Butts, J. Kinast, and B. Timmons, *Analytical framework for dynamic light-pulse atom interferometry at short interrogation times*, J. Opt. Soc. Am. B **28**, 2418 (2011).

[100] E. Giese, *Mechanisms of matter-wave diffraction and their application to interferometers*, Fortschr. Phys. **63**, 337 (2015).

[101] X. Li, C.-G. Shao, and Z.-K. Hu, *Raman pulse duration effect in high-precision atom interferometry gravimeters*, J. Opt. Soc. Am. B **32**, 248 (2015).

[102] E. Giese, A. Friedrich, S. Abend, E. M. Rasel, et al., *Light shifts in atomic Bragg diffraction*, Phys. Rev. A **94**, 063619 (2016).

[103] A. Bertoldi, F. Minardi, and M. Prevedelli, *Phase shift in atom interferometers: Corrections for non-quadratic potentials and finite-duration laser pulses*, arXiv, quant–ph/1812.11890 (2018).

[104] M. Kasevich and S. Chu, *Measurement of the gravitational acceleration of an atom with a light-pulse atom interferometer*, Appl. Phys. B **54**, 321 (1992).

[105] B. Cheng, P. Gillot, S. Merlet, and F. Pereira Dos Santos, *Influence of chirping the Raman lasers in an atom gravimeter: Phase shifts due to the Raman light shift and to the finite speed of light*, Phys. Rev. A **92**, 063617 (2015).

[106] D. S. Weiss, B. C. Young, and S. Chn, *Precision measurement of $\hbar/M_{Cs}$ based on photon recoil using laser-cooled atoms and atomic interferometry*, Appl. Phys. B **59**, 217.

[107] J. Audretsch and K.-P. Marzlin, *Atom interferometry with arbitrary laser configurations: Exact phase shift for potentials including inertia and gravitation*, J. Phys. II France **4**, 2073 (1994).

[108] K.-P. Marzlin and J. Audretsch, *State independence in atom interferometry and insensitivity to acceleration and rotation*, Phys. Rev. A **53**, 312 (1996).

[109] I. Bialynicki-Birula and Z. Bialynicka-Birula, *Center-of-mass motion in the many-body theory of Bose-Einstein condensates*, Phys. Rev. A **65**, 063606 (2002).

[110] G. Nandi, R. Walser, E. Kajari, and W. P. Schleich, *Dropping cold quantum gases on Earth over long times and large distances*, Phys. Rev. A **76**, 063617 (2007).

[111] S. Dimopoulos, P. W. Graham, J. M. Hogan, and M. A. Kasevich, *General relativistic effects in atom interferometry*, Phys. Rev. D **78**, 042003 (2008).

[112] P. de Gennes, *Superconductivity of metals and alloys*, 1st ed. (CRC Press, Boca Raton, 1999).

[113] J. Schwinger, *Brownian motion of a quantum oscillator*, J. Math. Phys. **2**, 407 (1961).

[114] L. V. Keldysh, *Diagram technique for nonequilibrium processes*, JETP **20**, 1018 (1965).

[115] G. Stefanucci and R. van Leeuwen, *Nonequilibrium many-body theory of quantum systems: A modern introduction*, 1st ed. (Cambridge University Press, Cambridge, 2013).

[116] M. A. Abramowitz and I. A. Stegun, *Handbook of Mathematical Functions*, 1st ed. (Dover Publications, Mineola, 1965).

[117] A. M. Nobili, *Fundamental limitations to high-precision tests of the universality of free fall by dropping atoms*, Phys. Rev. A **93**, 023617 (2016).

[118] A. Roura, *Circumventing Heisenberg's uncertainty principle in atom interferometry tests of the equivalence principle*, Phys. Rev. Lett. **118**, 160401 (2017).

[119] Y. A. Neretin, *Lectures on Gaussian integral operators and classical groups*, EMS Series of Lectures in Mathematics (European Mathematical Society, Zürich, 2011).

[120] M. A. Kasevich, E. Riis, S. Chu, and R. G. DeVoe, *RF spectroscopy in an atomic fountain*, Phys. Rev. Lett. **63**, 612 (1989).

[121] A. Sugarbaker, S. M. Dickerson, J. M. Hogan, D. M. S. Johnson, et al., *Enhanced atom interferometer readout through the application of phase shear*, Phys. Rev. Lett. **111**, 113002 (2013).

[122] S.-Y. Lan, P.-C. Kuan, B. Estey, P. Haslinger, et al., *Influence of the coriolis force in atom interferometry*, Phys. Rev. Lett. **108**, 090402 (2012).

[123] G. D'Amico, G. Rosi, S. Zhan, L. Cacciapuoti, et al., *Canceling the gravity gradient phase shift in atom interferometry*, Phys. Rev. Lett. **119**, 253201 (2017).

[124] C. Overstreet, P. Asenbaum, T. Kovachy, R. Notermans, et al., *Effective inertial frame in an atom interferometric test of the equivalence principle*, Phys. Rev. Lett. **120**, 183604 (2018).

[125] S. Olivares, *Quantum optics in the phase space: A tutorial on Gaussian states*, Eur. Phys. J. **203**, 3 (2012).

[126] W. B. Case, *Wigner functions and Weyl transforms for pedestrians*, Am. J. Phys. **76**, 937 (2008).

[127] F. J. Narcowich and R. F. O'Connell, *Necessary and sufficient conditions for a phase-space function to be a Wigner distribution*, Phys. Rev. A **34**, 1 (1986).

[128] S. Bose, *Plancks Gesetz und Lichtquantenhypothese*, Z. Phys. **26**, 178 (1924).

[129] A. Einstein, *Quantentheorie des einatomigen idealen Gases*, Sitzungsberichte der Preussischen Akademie der Wissenschaften, 3 (1925).

[130] F. Dalfovo, S. Giorgini, L. P. Pitaevskii, and S. Stringari, *Theory of Bose-Einstein condensation in trapped gases*, Rev. Mod. Phys. **71**, 463 (1999).

[131] I. Bloch, J. Dalibard, and W. Zwerger, *Many-body physics with ultracold gases*, Rev. Mod. Phys. **80**, 885 (2008).

[132] M. H. Anderson, J. R. Ensher, M. R. Matthews, C. E. Wieman, et al., *Observation of Bose-Einstein condensation in a dilute atomic vapor*, Science **269**, 198 (1995).

[133] K. B. Davis, M. O. Mewes, M. R. Andrews, N. J. van Druten, et al., *Bose-Einstein condensation in a gas of sodium atoms*, Phys. Rev. Lett. **75**, 3969 (1995).

[134] W. Ketterle, *Nobel lecture: When atoms behave as waves: Bose-Einstein condensation and the atom laser*, Rev. Mod. Phys. **74**, 1131 (2002).

[135] E. A. Cornell and C. E. Wieman, *Nobel Lecture: Bose-Einstein condensation in a dilute gas, the first 70 years and some recent experiments*, Rev. Mod. Phys. **74**, 875 (2002).

[136] S. Inouye, M. R. Andrews, J. Stenger, H.-J. Miesner, et al., *Observation of Feshbach resonances in a Bose–Einstein condensate*, Nature **392**, 151 (1998).

[137] J. Denschlag, J. E. Simsarian, D. L. Feder, C. W. Clark, et al., *Generating solitons by phase engineering of a Bose-Einstein condensate*, Science **287**, 98 (2000).

[138] M. R. Matthews, B. P. Anderson, P. C. Haljan, D. S. Hall, et al., *Vortices in a Bose-Einstein condensate*, Phys. Rev. Lett. **83**, 2498 (1999).

[139] O. Penrose and L. Onsager, *Bose-Einstein condensation and liquid helium*, Phys. Rev. **104**, 576 (1956).

[140] C. N. Yang, *Concept of off-diagonal long-range order and the quantum phases of liquid He and of superconductors*, Rev. Mod. Phys. **34**, 694 (1962).

[141] C. Pethick and H. Smith, *Bose-Einstein condensation in dilute gases*, 1st ed. (Cambridge University Press, Cambridge, 2002).

[142] L. P. Pitaevskii and S. Stringari, *Bose-Einstein condensation and superfluidity*, 1st ed. (Oxford University Press, Oxford, 2016).

[143] P. W. Anderson, "Measurement in quantum theory and the problem of complex systems", in *The Lesson of Quantum Theory*, Vol. 35 (Elsevier, 1986), p. 615.

[144] A. J. Leggett and F. Sols, *Comment on "phase and phase diffusion of a split Bose-Einstein condensate"*, Phys. Rev. Lett. **81**, 1344 (1998).

[145] J. Javanainen and S. M. Yoo, *Quantum phase of a Bose-Einstein condensate with an arbitrary number of atoms*, Phys. Rev. Lett. **76**, 161 (1996).

[146] Y. Castin and J. Dalibard, *Relative phase of two Bose-Einstein condensates*, Phys. Rev. A **55**, 4330 (1997).

[147] N. N. Bogoliubov, *Lectures on quantum statistics*, 1st ed., Vol. 2 (Gordon and Breach, New York, 1970).

[148] N. N. Bogoliubov, *On the theory of superfluidity*, J. Phys. (USSR) **11**, 23 (1947).

[149] M. Ueda, *Fundamentals and new frontiers of Bose-Einstein condensation*, 1st ed. (World Scientific Publishing Co. Pte. Ltd, Singapore, 2010).

[150] L. P. Pitaevskii, *Vortex lines in an imperfect Bose gas*, JETP **13**, 451 (1961).

[151] E. P. Gross, *Structure of a quantized vortex in boson systems*, Nuovo Cimento, 454 (1961).

[152] N. P. Proukakis and B. Jackson, *Finite-temperature models of Bose–Einstein condensation*, J. Phys. B: At. Mol. Opt. Phys. **41**, 203002 (2008).

[153] A. L. Fetter, *Nonuniform states of an imperfect Bose gas*, Ann. Phys. **70**, 67 (1972).

[154] A. Fetter and J. Walecka, *Quantum theory of many-particle systems*, Dover Books on Physics (Dover Publications, Mineola, 2003).

[155] T. Köhler and K. Burnett, *Microscopic quantum dynamics approach to the dilute condensed Bose gas*, Phys. Rev. A **65**, 033601 (2002).

[156] S. A. Morgan, *A gapless theory of Bose-Einstein condensation in dilute gases at finite temperature*, J. Phys. B: At. Mol. Opt. Phys. **33**, 3847 (2000).

[157] D. A. W. Hutchinson, E. Zaremba, and A. Griffin, *Finite temperature excitations of a trapped Bose gas*, Phys. Rev. Lett. **78**, 1842 (1997).

[158] E. Zaremba, T. Nikuni, and A. Griffin, *Dynamics of trapped Bose gases at finite temperatures*, J. Low Temp. Phys. **116**, 69.

[159] A. Griffin, T. Nikuni, and E. Zaremba, *Bose-condensed gases at finite temperatures*, 1st ed. (Cambridge University Press, Cambridge, 2009).

[160] Y. Kagan and B. V. Svistunov, *Evolution of correlation properties and appearance of broken symmetry in the process of Bose-Einstein condensation*, Phys. Rev. Lett. **79**, 3331 (1997).

[161] M. J. Davis, S. A. Morgan, and K. Burnett, *Simulations of Bose fields at finite temperature*, Phys. Rev. Lett. **87**, 160402 (2001).

[162] P. B. Blakie and M. J. Davis, *Projected Gross-Pitaevskii equation for harmonically confined Bose gases at finite temperature*, Phys. Rev. A **72**, 063608 (2005).

[163] M. Brewczyk, M. Gajda, and K. Rzażewski, *Classical fields approximation for bosons at nonzero temperatures*, J. Phys. B: At. Mol. Opt. Phys. **40**, R1 (2007).

[164] M. J. Steel, M. K. Olsen, L. I. Plimak, P. D. Drummond, et al., *Dynamical quantum noise in trapped Bose-Einstein condensates*, Phys. Rev. A **58**, 4824 (1998).

[165] M. Lewenstein and L. You, *Quantum phase diffusion of a Bose-Einstein condensate*, Phys. Rev. Lett. **77**, 3489 (1996).

[166] A. J. Leggett, *Bose-Einstein condensation in the alkali gases: Some fundamental concepts*, Rev. Mod. Phys. **73**, 307 (2001).

[167] Y. Castin and R. Dum, *Low-temperature Bose-Einstein condensates in time-dependent traps: Beyond the $U(1)$ symmetry-breaking approach*, Phys. Rev. A **57**, 3008 (1998).

[168] C. W. Gardiner, *Particle-number-conserving Bogoliubov method which demonstrates the validity of the time-dependent Gross-Pitaevskii equation for a highly condensed Bose gas*, Phys. Rev. A **56**, 1414 (1997).

[169] S. A. Gardiner and S. A. Morgan, *Number-conserving approach to a minimal self-consistent treatment of condensate and noncondensate dynamics in a degenerate Bose gas*, Phys. Rev. A **75**, 043621 (2007).

[170] T. P. Billam, P. Mason, and S. A. Gardiner, *Second-order number-conserving description of nonequilibrium dynamics in finite-temperature Bose-Einstein condensates*, Phys. Rev. A **87**, 033628 (2013).

[171] P. Mason and S. A. Gardiner, *Number-conserving approaches to n-component Bose-Einstein condensates*, Phys. Rev. A **89**, 043617 (2014).

[172] J. Dziarmaga and K. Sacha, *Bogoliubov theory of a Bose-Einstein condensate in the particle representation*, Phys. Rev. A **67**, 033608 (2003).

[173] J. Dziarmaga and K. Sacha, *N-particle Bogoliubov vacuum state*, Laser Phys. **16**, 1134 (2006).

[174] S. A. Gardiner and T. P. Billam, "Number-conserving approaches for atomic Bose-Einstein condensates: An overview", in *Quantum gases. Finite temperatures and non-equilibrium dynamics*, 1st ed. (Imperial College Press, London, 2013), p. 133.

[175] E. H. Lieb, R. Seiringer, and J. Yngvason, *Justification of c-number substitutions in bosonic Hamiltonians*, Phys. Rev. Lett. **94**, 080401 (2005).

[176] E. H. Lieb, R. Seiringer, and J. Yngvason, *Bose-Einstein condensation and spontaneous symmetry breaking*, Rep. Math. Phys. **59**, 389 (2007).

[177] V. I. Yukalov, *Bose-Einstein condensation and gauge symmetry breaking*, Laser Phys. Lett. **4**, 632 (2007).

[178] V. I. Yukalov, *Basics of Bose-Einstein condensation*, Physics Part. Nucl. **42**, 460 (2011).

[179] M. Gajda and K. R., *Fluctuations of Bose-Einstein condensate*, Phys. Rev. Lett. **78**, 2686 (1997).

[180] Y. Castin and R. Dum, *Bose-Einstein condensates in time dependent traps*, Phys. Rev. Lett. **77**, 5315 (1996).

[181] Y. Kagan, E. L. Surkov, and G. V. Shlyapnikov, *Evolution of a Bose-condensed gas under variations of the confining potential*, Phys. Rev. A **54**, R1753 (1996).

[182] Y. Kagan, E. L. Surkov, and G. V. Shlyapnikov, *Evolution of a Bose gas in anisotropic time-dependent traps*, Phys. Rev. A **55**, R18 (1997).

[183] M. Meister, S. Arnold, D. Moll, M. Eckart, et al., "Efficient description of Bose–Einstein condensates in time-dependent rotating traps", in, 66th ed., Advances In Atomic, Molecular, and Optical Physics (Academic Press, 2017), p. 75.

[184] J. F. Dobson, *Harmonic-potential theorem: Implications for approximate many-body theories*, Phys. Rev. Lett. **73**, 2244 (1994).

[185] Y. Japha and Y. B. Band, *Motion of a condensate in a shaken and vibrating harmonic trap*, J. Phys. B: At. Mol. Opt. Phys. **35**, 2383 (2002).

[186] H. Ott, J. Fortágh, and C. Zimmermann, *Dynamics of a Bose–Einstein condensate in an anharmonic trap*, J. Phys. B: At. Mol. Opt. Phys. **36**, 2817 (2003).

[187] S. Stringari, *Collective excitations of a trapped Bose-condensed gas*, Phys. Rev. Lett. **77**, 2360 (1996).

[188] V. M. Perez-Garcia, H. Michinel, J. I. Cirac, M. Lewenstein, et al., *Low energy excitations of a Bose-Einstein condensate: A time-dependent variational analysis*, Phys. Rev. Lett. **77**, 5320 (1996).

[189] Y. Castin and R. Dum, *Instability and depletion of an excited Bose-Einstein condensate in a trap*, Phys. Rev. Lett. **79**, 3553 (1997).

[190] P. A. M. Dirac, *The quantum theory of the emission and absorption of radiation*, Proceedings of the Royal Society of London. Series A **114**, 767 (1927).

[191] V. Z. Fock, *Konfigurationsraum und zweite Quantelung*, Z. Phys. **75**, 622 (1932).

[192] J. A. Stickney, D. Z. Anderson, and A. A. Zozulya, *Increasing the coherence time of Bose-Einstein-condensate interferometers with optical control of dynamics*, Phys. Rev. A **75**, 063603 (2007).

[193] J. A. Stickney, R. P. Kafle, D. Z. Anderson, and A. A. Zozulya, *Theoretical analysis of a single- and double-reflection atom interferometer in a weakly confining magnetic trap*, Phys. Rev. A **77**, 043604 (2008).

[194] A. O. Jamison, B. Plotkin-Swing, and S. Gupta, *Advances in precision contrast interferometry with Yb Bose-Einstein condensates*, Phys. Rev. A **90**, 063606 (2014).

[195] T. He and P. Niu, *Multimode Kapitza-Dirac interferometer on Bose-Einstein condensates with atomic interactions*, Phys. Lett. A **381**, 1087 (2017).

[196] R. Jannin, P. Cladé, and S. Guellati-Khelifa, *Phase shift due to atom-atom interactions in a light-pulse atom interferometer*, Phys. Rev. A **92**, 013616 (2015).

[197] W. Schleich, *Quantum optics in phase space*, 1st ed. (Wiley-VCH, Berlin, 2001).

[198] W. L. Bragg, *The diffraction of short electromagnetic waves by a crystal*, Scientia **23**, 153 (1929).

[199] P. Martin, B. Oldaker, A. Miklich, and D. Pritchard, *Bragg scattering of atoms from a standing light wave*, Phys. Rev. Lett. **60**, 515 (1988).

[200] D. A. Steck, *Rubidium 87 D line data, (revision 2.1.5, 13 January 2015)*, `http://steck.us/alkalidata` (visited on 12/09/2018).

[201] D. A. Steck, *Quantum and atom optics, (revision 0.12.5, 26 January 2019)*, `http://steck.us/teaching` (visited on 02/09/2019).

[202] H. Ahlers, H. Müntinga, A. Wenzlawski, M. Krutzik, et al., *Double-Bragg interferometry*, Phys. Rev. Lett. **116**, 173601 (2016).

[203] C. V. Raman, *A new radiation*, Indian J. Phys. **2**, 387 (1928).

[204] G. P. Agrawal, *Nonlinear fiber optics*, 5th ed. (Academic press, Oxford, 2013).

[205] M. Trippenbach, Y. B. Band, M. Edwards, M. Doery, et al., *Coherence properties of an atom laser*, New J. Phys. **33**, 47 (2000).

[206] A. O. Jamison, J. N. Kutz, and S. Gupta, *Atomic interactions in precision interferometry using Bose-Einstein condensates*, Phys. Rev. A **84**, 043643 (2011).

[207] N. N. Bogoliubov and Y. A. Mitropolsky, *Asymptotic methods in the theory of non-linear oscillations*, 1st ed. (Hindustan Publishing, Delhi, 1961).

[208] P. Kling, *Theory of the free-electron laser: From classical to quantum*, Ph.D. thesis, Universität Ulm (2017).

[209] I. L. Egusquiza, *Beyond adiabatic elimination: Systematic expansions*, arXiv, quant–ph/1309.0628 (2013).

[210] S. Iso, H. Ohta, and T. Suyama, *Secular terms in Dyson series to all orders of perturbation*, Progr. Theor. Exp. Phys. **2018**, 083A01 (2018).

[211]   M. Sanz, E. Solano, and Í. L. Egusquiza, "Beyond adiabatic elimination: Effective Hamiltonians and singular perturbation", in *Applications+ Practical Conceptualization+ Mathematics= fruitful Innovation* (Springer, 2016), p. 127.

[212]   M. O. Scully and J. P. Dowling, *Quantum-noise limits to matter-wave interferometry*, Phys. Rev. A **48**, 3186 (1993).

[213]   B. Yurke, *Input states for enhancement of fermion interferometer sensitivity*, Phys. Rev. Lett. **56**, 1515 (1986).

[214]   B. Yurke, S. L. McCall, and J. R. Klauder, *SU(2) and SU(1, 1) interferometers*, Phys. Rev. A **33**, 4033 (1986).

[215]   J. P. Dowling, *Correlated input-port, matter-wave interferometer: Quantum noise limits to the atom-laser gyroscope*, Phys. Rev. A **57**, 4736 (1998).

[216]   J. R. Anglin, P. Drummond, and A. Smerzi, *Exact quantum phase model for mesoscopic Josephson junctions*, Phys. Rev. A **64**, 063605 (2001).

[217]   A. Imamoḡlu, M. Lewenstein, and L. You, *Inhibition of coherence in trapped Bose-Einstein condensates*, Phys. Rev. Lett. **78**, 2511 (1997).

[218]   E. M. Wright, D. F. Walls, and J. C. Garrison, *Collapses and revivals of Bose-Einstein condensates formed in small atomic samples*, Phys. Rev. Lett. **77**, 2158 (1996).

[219]   J. Javanainen and M. Wilkens, *Javanainen and Wilkens reply*, Phys. Rev. Lett. **81**, 1345 (1998).

[220]   M. Kitagawa and M. Ueda, *Squeezed spin states*, Phys. Rev. A. **47**, 5138 (1993).

[221]   D. J. Wineland, J. J. Bollinger, W. M. Itano, and D. J. Heinzen, *Squeezed atomic states and projection noise in spectroscopy*, Phys. Rev. A **50**, 67 (1994).

[222]   J. Javanainen and M. Y. Ivanov, *Splitting a trap containing a Bose-Einstein condensate: Atom number fluctuations*, Phys. Rev. A **60**, 2351 (1999).

[223]   L. Pezzé, L. A. Collins, A. Smerzi, G. P. Berman, et al., *Sub-shot-noise phase sensitivity with a Bose-Einstein condensate Mach-Zehnder interferometer*, Phys. Rev. A **72**, 050801 (2005).

[224]   C. Bodet, J. Estève, M. K. Oberthaler, and T. Gasenzer, *Two-mode Bose gas: Beyond classical squeezing*, Phys. Rev. A **81**, 063605 (2010).

[225]   E. O. Ilo-Okeke and A. A. Zozulya, *Atomic population distribution in the output ports of cold-atom interferometers with optical splitting and recombination*, Phys. Rev. A **82**, 053603 (2010).

[226]   C. Menotti, J. R. Anglin, J. I. Cirac, and P. Zoller, *Dynamic splitting of a Bose-Einstein condensate*, Phys. Rev. A **63**, 023601 (2001).

[227]   U. V. Poulsen and K. Mølmer, *Quantum beam splitter for atoms*, Phys. Rev. A **65**, 033613 (2002).

[228]   M. Jääskeläinen, W. Zhang, and P. Meystre, *Limits to phase resolution in matter-wave interferometry*, Phys. Rev. A **70**, 063612 (2004).

[229] L. Pezzé, A. Smerzi, G. P. Berman, A. R. Bishop, et al., *Dephasing and breakdown of adiabaticity in the splitting of Bose–Einstein condensates*, New J. Phys. **7**, 85 (2005).

[230] J. Grond, J. Schmiedmayer, and U. Hohenester, *Shaking the condensates: Optimal number squeezing in the dynamic splitting of a Bose–Einstein condensate*, Physica E **42**, 432 (2010).

[231] A. I. Streltsov, O. E. Alon, and L. S. Cederbaum, *Role of excited states in the splitting of a trapped interacting Bose-Einstein condensate by a time-dependent barrier*, Phys. Rev. Lett. **99**, 030402 (2007).

[232] G. J. Milburn, J. Corney, E. M. Wright, and D. F. Walls, *Quantum dynamics of an atomic Bose-Einstein condensate in a double-well potential*, Phys. Rev. A **55**, 4318 (1997).

[233] A. Sinatra and Y. Castin, *Binary mixtures of Bose-Einstein condensates: Phase dynamics and spatial dynamics*, Eur. Phys. J. D **8**, 319 (2000).

[234] E. Boukobza, M. Chuchem, D. Cohen, and A. Vardi, *Phase-diffusion dynamics in weakly coupled Bose-Einstein condensates*, Phys. Rev. Lett. **102**, 180403 (2009).

[235] J. Grond, U. Hohenester, I. Mazets, and J. Schmiedmayer, *Atom interferometry with trapped Bose–Einstein condensates: Impact of atom–atom interactions*, New J. Phys. **12**, 065036 (2010).

[236] A. Fallon, R. H. Leonard, and C. A. Sackett, *Estimation of phase diffusion rates in a condensate interferometer using the Gross–Pitaevskii equation*, J. Phys. B: At. Mol. Opt. Phys. **48**, 205301 (2015).

[237] T. Berrada, S. van Frank, R. Bücker, T. Schumm, et al., *Integrated Mach–Zehnder interferometer for Bose–Einstein condensates*, Nat. Commun. **4**, 1 (2013).

[238] M. F. Riedel, P. Böhi, Y. Li, T. W. Hänsch, et al., *Atom-chip-based generation of entanglement for quantum metrology*, Nature **464**, 1170 (2010).

[239] C. Gross, T. Zibold, E. Nicklas, J. Estève, et al., *Nonlinear atom interferometer surpasses classical precision limit*, Nature **464**, 1165 (2010).

[240] K. Lange, J. Peise, B. Lücke, I. Kruse, et al., *Entanglement between two spatially separated atomic modes*, Science **360**, 416 (2018).

[241] R. H. Dicke, *Coherence in spontaneous radiation processes*, Phys. Rev. **93**, 99 (1954).

[242] J. M. Radcliffe, *Some properties of coherent spin states*, J. Phys. A **4**, 313 (1971).

[243] E. H. Lieb, *Proof of an entropy conjecture of Wehrl*, Commun. Math. Phys. **62**, 35 (1978).

[244] C. T. Lee, *Q representation of the atomic coherent states and the origin of fluctuations in superfluorescence*, Phys. Rev. A **30**, 3308 (1984).

[245] R. Gilmore, C. M. Bowden, and L. M. Narducci, *Classical-quantum correspondence for multilevel systems*, Phys. Rev. A **12**, 1019 (1975).

[246] M. Fattori, C. D'Errico, G. Roati, M. Zaccanti, et al., *Atom interferometry with a weakly interacting Bose-Einstein condensate*, Phys. Rev. Lett. **100**, 080405 (2008).

[247] M. Gustavsson, E. Haller, M. J. Mark, J. G. Danzl, et al., *Control of interaction-induced dephasing of Bloch oscillations*, Phys. Rev. Lett. **100**, 080404 (2008).

[248] A. Søndberg Sørensen, *Bogoliubov theory of entanglement in a Bose-Einstein condensate*, Phys. Rev. A **65**, 043610 (2002).

[249] A. Sørensen, L.-M. Duan, J. I. Cirac, and P. Zoller, *Many-particle entanglement with Bose-Einstein condensates*, Nature **409**, 63 (2001).

[250] Y. Li, Y. Castin, and A. Sinatra, *Optimum spin squeezing in Bose-Einstein condensates with particle losses*, Phys. Rev. Lett. **100**, 210401 (2008).

[251] A. Sinatra, Y. Castin, and E. Witkowska, *Coherence time of a Bose-Einstein condensate*, Phys. Rev. A. **80**, 033614 (2009).

[252] A. Sinatra, E. Witkowska, J.-C. Dornstetter, Y. Li, et al., *Limit of spin squeezing in finite-temperature Bose-Einstein condensates*, Phys. Rev. Lett. **107**, 060404 (2011).

[253] A. Sinatra, J.-C. Dornstetter, and Y. Castin, *Spin squeezing in Bose-Einstein condensates: Limits imposed by decoherence and non-zero temperature*, Front. Phys. **7**, 86 (2012).

[254] A. Sinatra, Y. Castin, and E. Witkowska, *Limit of spin squeezing in trapped Bose-Einstein condensates*, New J. Phys. **102**, 40001 (2013).

[255] S. A. Haine, J. Lau, R. P. Anderson, and M. T. Johnsson, *Self-induced spatial dynamics to enhance spin squeezing via one-axis twisting in a two-component Bose-Einstein condensate*, Phys. Rev. A **90**, 023613 (2014).

[256] S. A. Haine and M. T. Johnsson, *Dynamic scheme for generating number squeezing in Bose-Einstein condensates through nonlinear interactions*, Phys. Rev. A **80**, 023611 (2009).

[257] H. Cramer, *Mathematical methods of statistics*, 1st ed. (Princeton University Press, Princeton, 1946).

[258] C. R. Rao, *Information and the accuracy attainable in the estimation of statistical parameters*, Bulletin of the Calcutta Mathematical Society **37**, 81 (1945).

[259] C. W. Helstrom, *Minimum mean squared error of estimates in quantum statistics*, Phys. Lett. **25A**, 101 (1967).

[260] S. L. Braunstein and C. M. Caves, *Statistical distance and the geometry of quantum states*, Phys. Rev. Lett. **72**, 3439 (1994).

[261] M. Kritsotakis, S. S. Szigeti, J. A. Dunningham, and S. A. Haine, *Optimal matter-wave gravimetry*, Phys. Rev. A **98**, 023629 (2018).

[262] S. Kleinert, *Relativity, states and quantum evolutions in atom interferometry*, Ph.D. thesis, Universität Ulm (2019).

[263] S. Blanes, F. Casas, J. A. Oteo, and J. Ros, *A pedagogical approach to the Magnus expansion*, Eur. J. Phys. **31**, 907 (2010).

[264] S. Klarsfeld and J. A. Oteo, *The Baker-Campbell-Hausdorff formula and the convergence of the Magnus expansion*, J. Phys. A **22**, 4565 (1989).

[265] R. M. Wilcox, *Exponential operators and parameter differentiation in quantum physics*, J. Math. Phys. **8**, 962 (1967).

Acknowledgement